

NIMS Monographs

Hiroaki Isago

Optical Spectra of Phthalocyanines and Related Compounds

A Guide for Beginners



National Institute for
Materials Science



Springer

NIMS Monographs

Series editor

Naoki OHASHI

Editorial board

Takahito OHMURA

Yoshitaka TATEYAMA

Takashi TANIGUCHI

Kazuya TERABE

Masanobu NAITO

Nobutaka HANAGATA

Kenjiro MIYANO

The NIMS Monographs are published by the National Institute for Materials Science (NIMS), a leading public research institute in materials science in Japan, in collaboration with Springer. The series present research results achieved by NIMS researchers through their studies on materials science as well as current scientific and technological trends in those research fields.

These monographs provide readers up-to-date and comprehensive knowledge about fundamental theories and principles of materials science as well as practical technological knowledge about materials synthesis and applications.

With their practical case studies the monographs in this series will be particularly useful to newcomers to the field of materials science and to scientists and engineers working in universities, industrial research laboratories, and public research institutes. These monographs will be also available for textbooks for graduate students.

National Institute for Materials Science

<http://www.nims.go.jp/>

More information about this series at <http://www.springer.com/series/11599>

Hiroaki Isago

Optical Spectra of Phthalocyanines and Related Compounds

A Guide for Beginners

Hiroaki Isago
National Institute for Materials Science
Tsukuba
Japan

ISSN 2197-8891 ISSN 2197-9502 (electronic)
NIMS Monographs
ISBN 978-4-431-55101-0 ISBN 978-4-431-55102-7 (eBook)
DOI 10.1007/978-4-431-55102-7

Library of Congress Control Number: 2015939422

Springer Tokyo Heidelberg New York Dordrecht London

© National Institute for Materials Science, Japan. Published by Springer Japan 2015

This work is subject to copyright. All rights are reserved by the National Institute for Materials Science, Japan (NIMS), whether the whole or part of the material is concerned, specifically the rights of translation, reprinting, reuse of illustrations, recitation, broadcasting, reproduction on microfilms, or in any other physical way, and transmission or information storage and retrieval, electronic adaptation, computer software, or by similar or dissimilar methodology now known or hereafter developed. Exempted from this legal reservation are brief excerpts in connection with reviews or scholarly analysis or material supplied specifically for the purpose of being entered and executed on a computer system, for exclusive use by the purchaser of the work. Duplication of this publication or parts thereof is permitted only under the provisions of applicable copyright laws and applicable treaties, and permission for use must always be obtained from NIMS. Violations are liable to prosecution under the respective copyright laws and treaties.

The use of general descriptive names, registered names, trademarks, service marks, etc. in this publication does not imply, even in the absence of a specific statement, that such names are exempt from the relevant protective laws and regulations and therefore free for general use.

While the advice and information in this book are believed to be true and accurate at the date of publication, neither the authors nor the editors nor the publisher can accept any legal responsibility for any errors or omissions that may be made. NIMS and the publisher make no warranty, express or implied, with respect to the material contained herein.

Printed on acid-free paper

Springer Japan KK is part of Springer Science+Business Media (www.springer.com)

Preface

Phthalocyanines, since their accidental discovery in 1928, have established themselves as industrial commodities, especially as blue and green pigments of incomparable excellence. Nowadays, they enjoy a variety of industrial and medical applications as well as their use as colorants, where optical absorption and/or emission phenomena by the macrocyclic dyestuffs underlie the mechanisms.

A considerable number of scientists, engineers, and students may have been involved in work with phthalocyanines. During the course of their study, they may have tried to characterize their compounds, which can be either novel or known, or to monitor their reactions by means of optical spectroscopy. Some unfortunate investigators must have seen spectra quite different from prototypical ones that are displayed in textbooks. These compounds are tricky because they can be involved in colorful chemistry including molecular aggregation, electron transfer, and acid–base equilibria. They are prone to aggregation at a higher concentration, which gives rise to drastic spectral changes. Meanwhile, at a lower concentration, some portion can be consumed to produce another species (which could be protonated, oxidized, reduced, demetalated, or degraded) through a reaction (or reactions) with a trace amount of impurities in the solvents used for the spectral measurement. This is because their molar extinction coefficients are very large (on the order of $10^5 \text{ M}^{-1} \text{ cm}^{-1}$), so measurements have to be taken at a very low concentration around 10^{-6} M . This implies that reproducibility of spectral measurements might be poor unless their concentrations are accurately controlled. Thus, spectra of phthalocyanines behave like the sea god Proteus under various conditions and hence sometimes can be very misleading. Therefore, some novice investigators (including the author himself in his youth) may have been embarrassed by the deceptive behavior of phthalocyanines and could have, in the worst cases, given up their research.

This book is aimed not merely at reviewing the optical spectra of phthalocyanines and related compounds, but also at helping such people, particularly beginners, to understand the optical spectra of those macrocyclic dyes by showing some examples of their prototypical spectra and their variations in several situations. For the purpose of deepening the understanding of spectra of the macrocyclic

compounds, the book also provides an introduction to a theoretical background of their spectra as graphically as possible and without mathematization for readers who are weak in mathematics just like the author himself.

It is hoped that this book will be of help to such phthalocyanine beginners who are exhausted by the mischief of the macrocyclic witches.

Acknowledgments

I am grateful to those who supported me throughout the preparation of this work. Prof. Nagao Kobayashi (Tohoku University, Japan) kindly allowed me to use the absorption spectral data of the copper complex of tetraazaporphyrin derivative and encouraged me. Prof. Tebello Nyokong (Rhodes University, South Africa) and Prof. Martin J. Stillman (University of Western Ontario, Canada) were so generous as to permit me to use their unpublished results on the absorption and MCD spectra of ruthenium complexes of phthalocyanine, which have not been published elsewhere. Ms. Harumi Fujita (NIMS) made rigorous efforts to take beautiful photographs of fluorescence from phosphorous phthalocyanine. Many organizations and publishers, including, in alphabetical order, the American Chemical Society, the Chemical Society of Japan, Elsevier, the International Commission on Illumination, PhotochemCAD, the Royal Society of Chemistry, John Wiley & Sons, and World Scientific, permitted me to reuse their materials free of charge. I would like to thank the many chemists who sent me offprints/reprints of their excellent works. I also appreciate the technical and clerical support by the staffs of Springer Japan and of the Scientific Information Office (NIMS). Finally, I have to present my special thanks to Dr. Akiyuki Matsushita (NIMS; the leader of the research group that I belong to) and to Reiko Isago, my wife, for their generous patience as I spent so much time for this work.

Contents

1	Introduction	1
1.1	How Do We See a Color?	1
1.1.1	No Light, No Color	1
1.1.2	How to See a Color	2
1.1.3	Why Does a Molecule Absorb Light?	5
1.1.4	Electronic Transitions and Molecular Orbitals.	7
1.2	Phthalocyanines as Functional Dyes	10
1.2.1	Traditional Dyes and Functional Dyes.	10
1.2.2	What Are Phthalocyanines?	11
1.2.3	Use of Phthalocyanines in Industry	13
1.2.4	Application in Medical Fields	16
	References.	18
2	“Prototypical” Optical Absorption Spectra of Phthalocyanines and Their Theoretical Background	21
2.1	Prototypical Absorption Spectra of Phthalocyanines in Solutions	22
2.1.1	Prototypical Spectra of Phthalocyanines	22
2.1.2	Comparison with Spectra of Similar Tetrapyrrole Macrocycles.	23
2.2	Molecular Orbital Models of Porphyrins and Phthalocyanines	25
2.2.1	Selection Rule in Optical Absorption (Optical Absorption = Generation of Vector)	25
2.2.2	Perimeter Model.	26
2.2.3	Graphical Description of Molecular Orbitals.	28
2.2.4	“Descent-in-Symmetry” Model	29
2.2.5	How to Use Character Tables (for Group Theory).	30
2.2.6	Gouterman’s “Four-Orbital” Model.	32
2.2.7	Why Are the Spectra of Phthalocyanines Different from Those of Porphyrins in Spite of Their Similar Structures?	33
2.2.8	Degeneracy of Excited States and Magnetic Circular Dichroism (MCD) Spectroscopy	34

2.2.9	Assignment of Phthalocyanine Spectra by MCD Spectroscopy	37
2.2.10	Computational Molecular Orbital Calculations	39
	References	39
3	Real Optical Absorption Spectra Observed in Laboratories	41
3.1	Are All Phthalocyanines Blue?.	41
3.2	Factors Affecting Absorption Spectra of Phthalocyanines.	43
3.2.1	Effects of Metal Ion(s) in the Cavity of the Macrocycle and Axial Ligands on the Metal	43
3.2.2	Effects of Peripheral Substituents	56
3.2.3	Effects of Ring Expansion, Contraction, and Symmetry Lowering	61
3.2.4	Interaction Between Chromophores.	66
3.2.5	Effects of Acid-Base Equilibria Involving Phthalocyanine Macrocycle	79
3.2.6	Electron Transfer Reactions Involving Phthalocyanine Macrocycle	82
3.2.7	Solvent Effects	89
3.3	Spectra of Related Macrocyclic Compounds.	96
3.3.1	Subphthalocyanines	96
3.3.2	Superphthalocyanines.	96
3.3.3	Tetrabenzocorrolazines (Tetrabenzotriazacorroles)	98
3.4	Absorption Spectra in Solid State	99
	References	100
4	Optical Emission Spectra of Phthalocyanines	107
4.1	Fluorescence: Optical Emission from the Lowest Singlet Excited States	107
4.1.1	How Does an Excited Molecule Emit Light?.	107
4.1.2	Appearance of Fluorescence Spectra	110
4.1.3	Fluorescence Quantum Yield	113
4.1.4	Effects of Interactions Between Fluorophores	119
4.1.5	Misleading Impurity Emission (Importance of Measuring the Excitation Spectra)	121
4.2	Other Emission Phenomena	123
4.2.1	Phosphorescence	123
4.2.2	Delayed Fluorescence (DF)	126
4.2.3	Emission at Approximately 1270 nm.	128
4.2.4	Emission from Upper Excited States	128
4.2.5	Electrochemiluminescence (or Electrogenerated Chemiluminescence; ECL).	129
	References	131

Chapter 1

Introduction

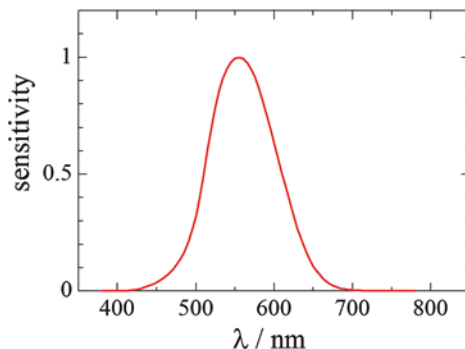
1.1 How Do We See a Color?

1.1.1 No Light, No Color

We cannot see color without light. Even though we have an apple in front of our eyes, we cannot recognize its color in the dark. We can tell its shape and size by the feel, but cannot tell if it is red, green, or yellow in the dark or when we close our eyes. Thus, light is essential for us to recognize the colors of objects. A color of an object is a visual impression perceived by an observer under light. Thus, the color stimulus is caused by light from the object.

What is “light”? As the readers know well, “light” is an electromagnetic wave, like X-rays and microwaves, but with wavelengths different from them. Although we can define it in various ways, according to the classical expression that “light allows us to feel brightness”, we may define “light” to denote electromagnetic waves of wavelengths that are visible to us. We have many opportunities to see white light in our daily life. This is because sunlight is white light. However, many people know, from their childhood, that sunlight is composed of various colored rays (red, orange, yellow, green, blue, indigo, and violet (memorized as Read Out Your Good Book In Verse) in the order of decreasing wavelength); a rainbow of seven colors that appears in the sky following rain or solar light is split by a prism into rays of various colors. These colored rays are electromagnetic waves of wavelengths in the range of 380–780 nm (Fig. 1.1) and are referred to as “visible light”. The sensitivities of our eyes to light above 690 nm and below 420 nm are less than 1 % of the maximum (555 nm). In some cases, electromagnetic waves with wavelengths slightly shorter than violet light (ultraviolet rays; UV rays) and those with wavelengths slightly longer than red light (near-infrared rays; NIR rays) can be included in the definition of light, although these are invisible to human eyes.

Fig. 1.1 Spectral luminous efficiency curve for photopic vision. The curve is reproduced using data from “CIE 1931 standard colorimetric observer” (© CIE—International Commission on Illumination) with permission



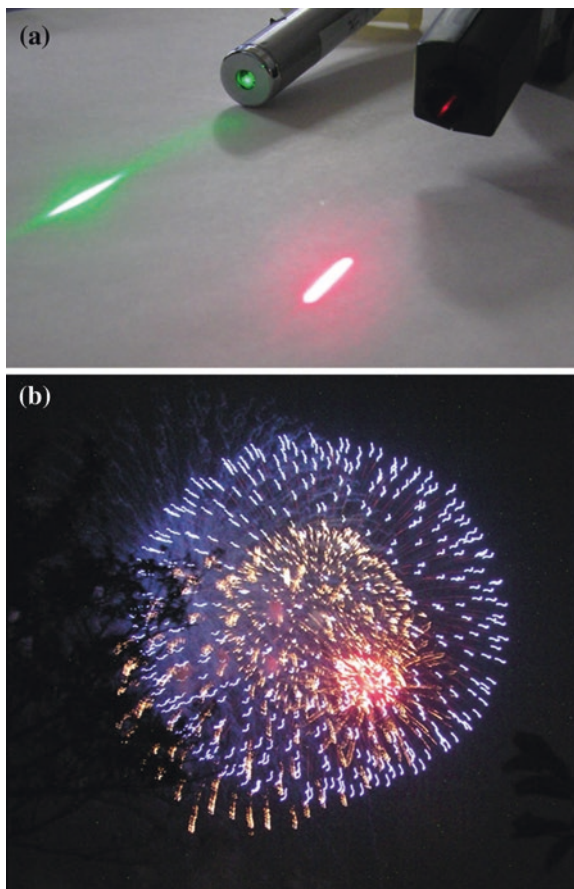
In this monograph, we will refer to rays that are visible to human eye as “visible light” and those including UV and NIR rays as simply “light” to avoid unnecessary confusion.

1.1.2 How to See a Color

When we recognize the color of an object, there are roughly two possibilities of stimulation of our eyes. The first case involves direct detection of the light emitted from the object, which is referred to as a “self-luminous color”. A typical example of the self-luminous color is a laser beam. Figure 1.2a shows a photograph of green and red laser pointers emitting 532 and 650 nm beams, respectively. Another but more familiar example may be fireworks, in which pyrotechnic compounds (generally containing metal elements) glow in various colors (Fig. 1.2b). The optical emission occurs when the thermally excited pyrotechnic metal element returns to its ground state; the color observed depends on the element included.

How do we see the color of nonluminous objects such as an apple? It is evident that an apple does not emit light because it cannot be seen in the dark. Therefore, we can recognize its color only by stimulation with light from a light source (e.g., the sun or a fluorescent lamp) that is reflected at the surface of the object (or passed through a transparent sheet such as cellophane). Let us consider an organic dye that exhibits a blue color. Figure 1.3 shows the color of an ethanolic solution containing methylene blue (structure shown in the same figure) and graphs presenting how the solution is transparent against visible light (broken line). The vertical axis represents the transmittance of light [i.e., the ratio of the transmitted light intensity (I) to the incident light intensity (I_0)]. However, as the physical quantity, transmittance, does not have any physical meaning, this graph is generally represented using another physical quantity, “absorbance”, which is proportional to the optical path length and the concentration of the light-absorbing species. The “transmittance” is converted to absorbance using the following convention: $\text{Absorbance} = -\log_{10} (I/I_0)$. That is, when the incident light passes through the solution without loss (i.e., $I = I_0$) at a given wavelength, absorbance = 0. In

Fig. 1.2 Photographs of **a** laser pointers emitting *green* (532 nm) and *red* (650 nm) beams and **b** Lake Teganuma fireworks display (August 3, 2013). *Source* NIMS eSciDoc—IMEJI. © Hiroaki Isago with CC-BY-NC 3.0 license



contrast, when 10 % of the incident light passes through the solution, the absorbance becomes unity. A graph that displays the absorbance of light at a given wavelength (vertical axis) as a function of the wavelength of light (horizontal axis) is referred to as an “optical absorption spectrum” (solid line in the figure). It should be noted that some authors prefer citing optical absorption spectra on an energy scale (inversely proportional to wavelength) to recording on a wavelength scale because the quantity “wavelength” has no physical meaning. Nevertheless, the majority of absorption spectra have been reported with this convention because conventional spectrometers are designed to record spectra in the form of “absorbance vs wavelength” by default. The absorption spectrum (solid line) of methylene blue clearly indicates that this compound is not transparent against light of approximately 650 nm, whereas it is transparent in the other spectral range (note that ethanol is transparent throughout the whole spectral range in this figure). As is evident from Fig. 1.2, a light ray of 650 nm is red. That is, methylene blue has the characteristic of strongly absorbing red light and transmitting light of other colors.

Fig. 1.3 Optical absorption spectra of ethanolic solution containing methylene blue (photograph provided in inset figure) on an absorbance scale (*solid line*) and a transmittance scale (*dashed line*). The molecular structure of the dye is shown at the *top*. Source NIMS eSciDoc—IMEJI. © Hiroaki Isago with CC-BY-NC 3.0 license

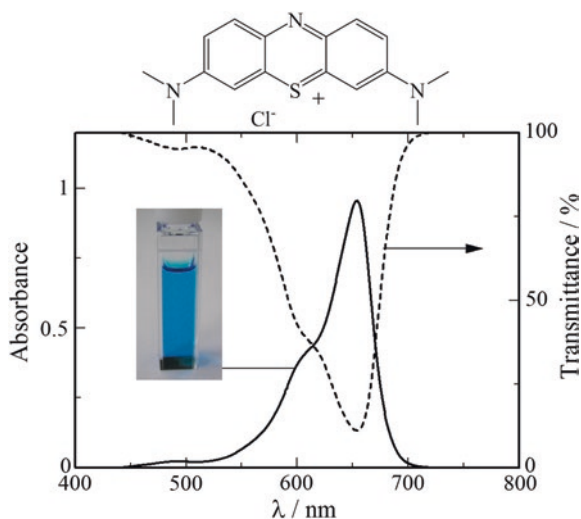
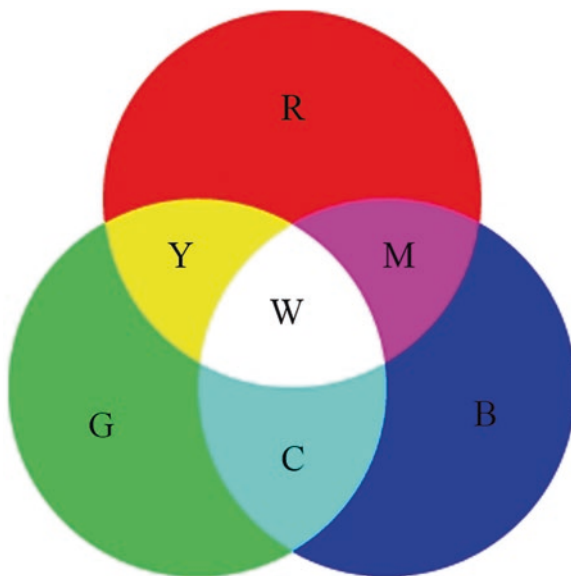
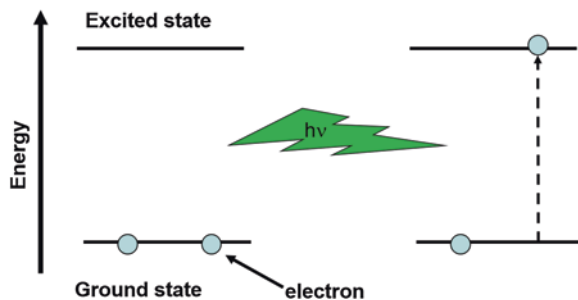


Fig. 1.4 Three primary colors of light (R, G, and B stand for red, green, and blue, respectively). The colors produced, Y, M, C, and W, stand for yellow, magenta, cyan, and white, respectively



As mentioned above, white light is an assembly of rays of all colors. In particular, red, green, and blue are known as the three primary colors of light; hence, any color can be reproduced by appropriately mixing them (Fig. 1.4). Therefore, the removal of red light from white light through absorption by an object will make that object cyan colored (area “C” in Fig. 1.4). What is important in this subsection is that methylene blue appears blue not because it has a blue color but because it strongly absorbs red light. Likewise, objects absorbing blue and green light appear yellow and magenta, respectively. Such color expressions are referred to as “non-self-luminous object colors”.

Fig. 1.5 Schematic diagram of the ground (before photoirradiation; *left*) and excited (upon photoirradiation; *right*) states of a dye molecule



1.1.3 Why Does a Molecule Absorb Light?

As mentioned above, fireworks make use of optical emission phenomena that occur when thermally excited pyrotechnic metal elements return to their ground state. Optical absorption is its reverse process, that is, light is absorbed when a molecule is excited from the ground state to higher energy states. Let us consider what happens when a molecule is irradiated with light. As light is an electromagnetic wave, its propagation is accompanied by a change in electric and magnetic fields. As a molecule has many electrons (even a carbon atom has 6 electrons) and electrons have a negative charge, they are directly affected, in particular, by the electric field. It should be noted that dye molecules (at most, 1 nm in diameter) are generally much smaller than the wavelength of visible light (380–780 nm); hence, we may assume that the light has an equal effect on the whole molecule. When a molecule is subjected to an electromagnetic wave, its electrons vibrate in accordance with the wavelength (and hence frequency) of the wave. However, at a specific wavelength/frequency peculiar to the compound, the electrons are rigorously shaken and their distribution is significantly changed to such an extent that an electric dipole is generated (this phenomenon is referred to as resonance). In other words, a molecule absorbs light when it is excited to higher energy states by the electromagnetic wave with its electron distribution rearranged in such a way that an electric dipole is generated in the molecule. Thus, since a molecule absorbs light in accordance with transitions from the ground state to excited states (Fig. 1.5), an optical absorption spectrum is also referred to as an “electronic absorption spectrum”. Each compound has a resonant wavelength/frequency for each electronic excitation (normally a compound has more than one electronically excited state). For methylene blue mentioned above, “650 nm” is its resonant wavelength for its lowest excitation. As the resonant wavelength depends on the structure of the compound, it is not surprising that some compounds can absorb light of wavelengths just above that of red light (NIR rays) or just below that of blue light (UV rays).¹ Therefore, some scientists refer to an “optical absorption spectrum” as a “UV-VIS (visible)-NIR absorption spectrum”. To avoid unnecessary confusion, “optical absorption spectrum” will be used throughout this monograph.

¹All compounds, including the simplest molecules, e.g., H₂, absorb UV-rays.

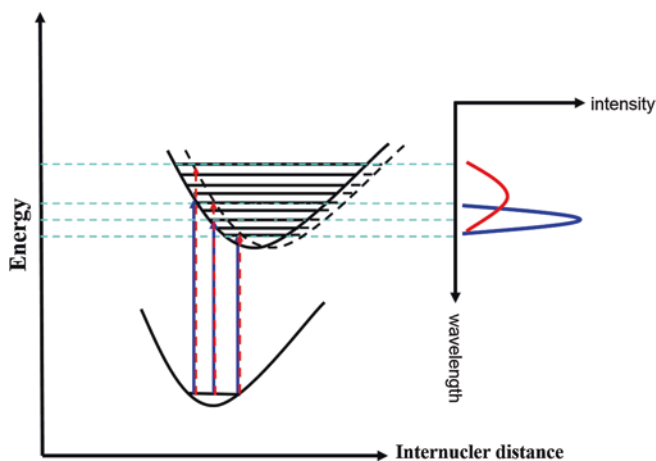
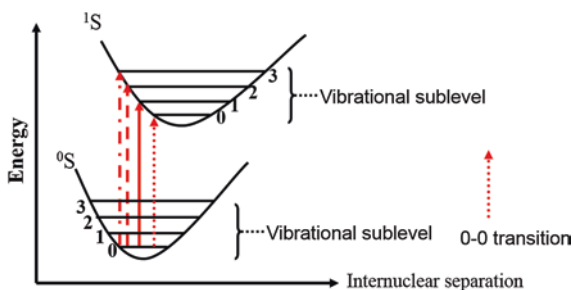


Fig. 1.6 Schematic diagram of photoexcitation of a dye molecule as a function of internuclear distance within the molecule. The excited states with insignificant structural distortion and with significant distortion are shown by *solid black* and *dashed black lines*, and the corresponding transitions (the observed spectrum) are shown in *blue* and *red* by the *arrows (curves)*, respectively. Source NIMS eSciDoc—IMEJI. © Hiroaki Isago with CC-BY-NC 3.0 license

Careful readers may have found that the absorption spectrum in Fig. 1.3 has a certain bandwidth but is not a line spectrum, unlike atomic spectra, although it has been stated above that each species has a “specific resonant wavelength/frequency”. This is because all the molecules in the ground state are vibrating around their equilibrium internuclear distance; hence, the compound can be regarded as a mixture of isomers of essentially the same structure but with slightly different bond lengths and/or angles at a certain moment. The “isomer” that has an equilibrium internuclear distance should have the largest population, and the isomers with a larger deviation from the equilibrium configuration, a smaller population. Moreover, as a general tendency, the structure of an excited molecule is different from that in the ground state (longer bonding distances, distorted angles, etc.) owing to more antibonding characteristics in the excited states (Sect. 1.1.4). Electronic transitions occur within femtoseconds (10^{-15} s); meanwhile, changes in interatomic configuration in the molecule are negligible (Franck-Condon principle).² Molecules in the lowest sublevel (each electronic state has a number of sublevels based on vibration, rotation, etc.) in the ground state are promoted to the corresponding sublevels in the excited state in accordance with their deviation from the equilibrium distance (Fig. 1.6). Therefore, as “each species has a specific resonant

²The lifetimes of excited states are not so long and rapidly relax to the ground state. Some molecules quickly return to the ground state by emitting light (fluorescence), some transfer their energy to the neighboring molecules, such as solvent molecules, without optical emission (non-radiative relaxation), and others return to the ground state through a spin-forbidden lower excited state (triplet state) without or with optical emission (phosphorescence), as is described in Chap. 4.

Fig. 1.7 Transitions from the lowest vibrational sublevel in the ground state to higher sublevels in the excited states. The dotted line stands for a transition between the lowest levels (0–0 transitions).
 Source NIMS eSciDoc—IMEJI. © Hiroaki Isago with CC-BY-NC 3.0 license



wavelength”, the observed spectrum is a superposition of spectra of all the “isomers”, and hence, has a certain width. It should also be noted that the magnitude of the bandwidth is related to the significance of structural distortion in the excited state. Figure 1.6 illustrates schematic diagrams of photoexcitation of a dye molecule when its structural change between the ground and excited states is small (excited states are shown in solid black lines) and large (dashed black lines). When the distortion is insignificant, the number of possible states involved in the excitation is small (blue arrows); hence, the spectral band (blue spectrum) becomes narrower. In contrast, in the case of significant distortion, the number of possible states involved (red arrows) becomes larger; hence, the band width is larger (red).

Some intense absorption bands have one or more subsidiary bands at their blue flank. For example, the absorption spectrum of methylene blue shows another band at approximately 610 nm as a shoulder in addition to the main band at approximately 650 nm. This structure is attributed to vibronic transitions from the lowest vibrational sublevel in the ground state to the second sublevel in the excited state (i.e., red solid arrow in Fig. 1.7) [1]. This is also seen in fluorescence spectra (Sect. 4.1.1).

1.1.4 Electronic Transitions and Molecular Orbitals

What kind of electrons in a molecule is involved in such optical absorption? Visible light can promote electrons only in the outermost shell of the molecule, such as those in π -orbitals in aromatic compounds or d-orbitals in transition metal compounds, to the lowest excited states. Promotion of much inner electrons requires as high an energy as that of X-rays. As many readers know, ethylene gas is colorless. This is because ethylene molecules (Fig. 1.8a) absorb only UV rays (lowest excitation peak wavelength (λ_{\max}): 188 nm [1]) and hence are transparent in the visible spectral range. 1,3-Butadiene (Fig. 1.8b) is colorless for the same reason (λ_{\max} , 217 nm [2]). In contrast, β -carotene (Fig. 1.8c), which is contained in pumpkins, spinach, and carrots, shows an orange color because it absorbs bluish-violet light (λ_{\max} , 477 nm). In all three compounds, a single bond and a double bond appear alternately.³ What makes β -carotene alone colored?

³Such compounds are referred to as alternant hydrocarbons.

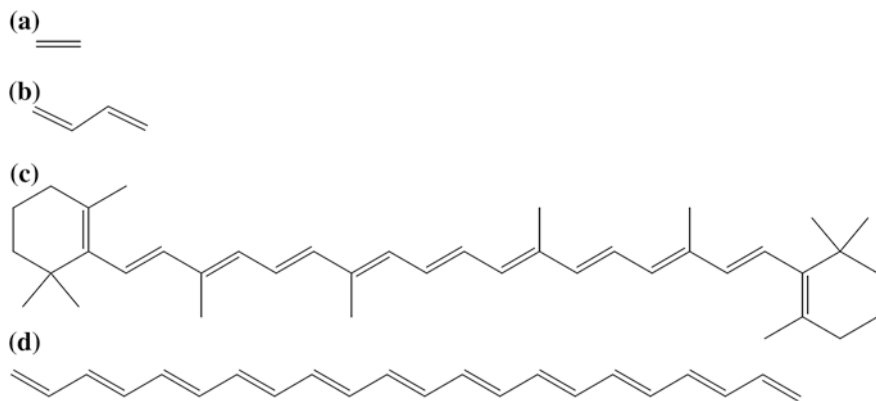


Fig. 1.8 Molecular structures of alternant hydrocarbons: **a** ethylene, **b** 1,3-butadiene, **c** β -carotene, **d** 1,3,5,7,9,11,13,15,17,19-eicosadecaene

In Sect. 1.1.3, it was stated that optical absorption involves a change in the electron distribution in the molecule upon photoirradiation. If some useful data to determine both the energy level of a dye molecule and electron distribution within the molecule are available, those would be helpful for us to describe the electronic transitions of dye molecules. Fortunately, molecular orbitals (MOs) play this role. The wording “molecular orbital” may remind us of something like an orbit of planets or a trajectory of comets, but molecular orbitals display distributions of one electron within the molecule in a specific energy level. In other words, a molecular orbital is a map that tells us where and with what probability we are to find the electron within the molecule rather than a “railway” for the electron.

A molecular orbital is spread over the entire molecule. However, quite often, it is approximated as a linear combination of atomic orbitals of all the constituent atoms. In particular, as π electrons generally have much higher energy than σ electrons, they are separable and only π electrons may be considered. Therefore, molecular orbitals of an ethylene molecule, for example, can be described as $c_1\phi_1 + c_2\phi_2$, where ϕ_1 and ϕ_2 denote atomic π (p_z)⁴ orbitals of the first and second carbon atoms, respectively, and c_1 and c_2 stand for their coefficients (the sum of their squares must be unity because the probability of finding the electron in the whole molecule is unity). Molecular (π) orbitals of ethylene calculated using MOPAC software are shown in Fig. 1.9a. As one ethylene molecule has two π electrons, it has two π orbitals. The blue and red clouds stand for coefficients of the MOs but with different phases (i.e., when blue ones respond to a positive sign, the red ones respond to a negative sign). As the magnitude of the square of the coefficients is proportional to the probability to find the electron in the region, a large cloud may be taken to indicate a high electron density within the orbital. The MO of lower energy (-17.48 eV) shows large clouds (in both red and blue)

⁴The molecular plane of ethylene is taken as the x,y-plane.

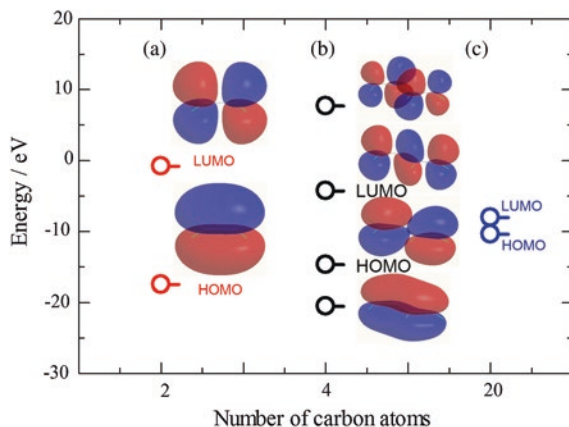


Fig. 1.9 Schematic diagrams of π MOs of **a** ethylene, **b** 1,3-dibutadiene, and **c** 1,3,5,7,9,11,13,15,17,19-eicosadecaene, and their energy levels (red circles ethylene; black 1,3-butadiene; blue 1,3,5,7,9,11,13,15,17,19-eicosadecaene) obtained by MOPAC calculation. Only HOMO and LUMO levels are shown with respect to 1,3,5,7,9,11,13,15,17,19-eicosadecaene. Source NIMS eSciDoc—IMEJI. © Hiroaki Isago with CC-BY-NC 3.0 license

between the two carbon atoms (Fig. 1.9a bottom). This indicates that electrons are likely to be present in this region with high probability. Therefore, the presence of electrons in this MO will increase the electron density between the carbon atoms; hence, this MO will greatly contribute to the bonding of the molecule. In contrast, another MO (Fig. 1.9a top), with higher energy (-0.78 eV) has no cloud between the carbon atoms, as if there were a wall⁵ to partition them off, indicating that electrons are unlikely to be present between them. Therefore, the presence of electrons in this MO will destabilize their bonding. The former MO is referred to as a “bonding orbital”, while its counterpart is an “antibonding orbital”. As one orbital accepts up to two electrons, the lower orbital is occupied by the two π electrons in the ground state; hence, the upper orbital is empty (unoccupied). The lower and upper MOs are called HOMO (highest occupied molecular orbital) and LUMO (lowest unoccupied molecular orbital), respectively. In 1,3-butadiene, which has four π electrons, the two lowest orbitals are occupied; hence, the second-lowest and the second-highest MOs are HOMO and LUMO, respectively (Fig. 1.9b). 1,3,5,7,9,11,13,15,17,19-Eicosadecaene (Fig. 1.8d; λ_{\max} , 447 nm [3]), which has the same length of the sequence of alternant single and double bonds as that of β -carotene, has 20 π electrons; hence, likewise, the 10th lowest and 10th highest MOs are HOMO and LUMO, respectively (Fig. 1.9c). Interestingly, the HOMO level increases and the LUMO level decreases with increasing length of the alternant hydrocarbon system. This is understandable because, for example, the HOMO of 1,3-butadiene has a nodal plane between the second and third atoms (2nd lowest in Fig. 1.9b) unlike that of ethylene, which has no nodal plane

⁵The “wall” is referred to as a nodal plane.

between the carbon atoms (Fig. 1.9a bottom). Likewise, the 1,3-butadiene LUMO is more stable than the ethylene LUMO because it has no nodal plane between the second and third atoms.⁶ Thus, the HOMO-LUMO energy gap becomes smaller for a longer polyene, allowing electronic excitation with lower energy (light of longer wavelengths). This is the reason why β -carotene alone looks colored whereas neither ethylene nor 1,3-butadiene do. As methylene blue also has an extended π -conjugation system, as shown in Fig. 1.3, it is excited with light of longer wavelengths (approximately 650 nm).

1.2 Phthalocyanines as Functional Dyes

1.2.1 Traditional Dyes and Functional Dyes

The term “dye(s)⁷” has been used for “compounds absorbing (and/or emitting) visible light”. Dyes originally had limited use as colorants for fabrics and their ornaments, cosmetics, food, and paintings; thereby, stability of the color quality is requested. In this meaning, the well-known phthalocyanines that are commonly used as colorants in industry are excellent dyes because of their robust thermal, chemical, and photochemical stability.⁸ On the other hand, phthalocyanines used as colorants in industry are generally believed to be highly stable because they are mostly used in solid state owing to their poor solubility in common solvents. In solid states, dye molecules are so close to each other that exciton coupling occurs between the chromophores, which significantly shortens lifetime of the excited state of the dye molecules (Sect. 4.1.4). However, in recent decades, apart from the use as colorants, they enjoy a variety of industrial and medical applications, where dyes are required to change their colors in accordance with an external stimulus or properties unrelated to their colors (e.g., their light-absorbing/emitting properties themselves) play more crucial roles. Phthalocyanines are typical dyestuffs used for such purposes (Fig. 1.10), as exemplified later (Sects. 1.2.3 and 1.2.4). From this viewpoint, the light absorbed/emitted by the “dye” molecules need not be visible. Therefore, we may need to expand the definition of dyes to materials that absorb

⁶It should be noted that a π MO of a higher energy level has a larger number of nodal planes that partition off the π clouds between the carbon atoms.

⁷There is another term, “pigment”, for similar compounds that are water-insoluble (in contrast, “dyes” have been used for water-soluble compounds). We do not distinguish between them in this monograph because there is little need to do so for our purposes. Hereafter, all colored compounds will be referred to as “dyes” whether they are water-soluble or not.

⁸However, it should be noted that phthalocyanines are not necessarily highly stable, in particular in their photochemistry. Nowadays, a number of soluble phthalocyanines are known and many of them have been found to undergo photodegradation in the presence of molecular oxygen [e.g., 4 and references cited herein]. This is because some phthalocyanines are capable of generating singlet oxygen upon photoirradiation (Sect. 1.2.4.1), which gives rise to degradation of the photosensitizers themselves.

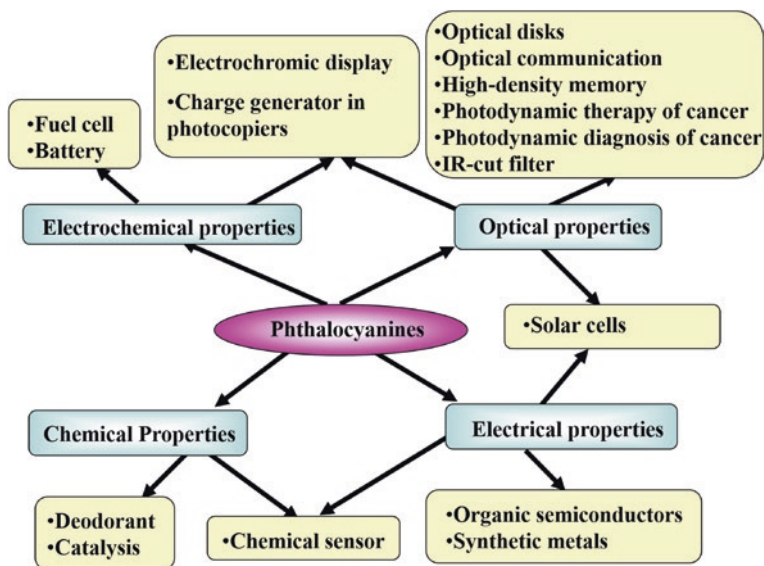


Fig. 1.10 Uses of phthalocyanines in industry and medicine. Source NIMS eSciDoc—IMEJI. © Hiroaki Isago with CC-BY-NC 3.0 license

and/or emit light (including UV and NIR rays). Unlike the traditional dyes where permanence of their colors is required, such new dyes are referred to as “functional dyes” [5].

1.2.2 What Are Phthalocyanines?

Phthalocyanine [whether unsubstituted (Fig. 1.11a) or substituted (Fig. 1.11b)] and their metal complexes (Fig. 1.11c) have an extended π -conjugation system, which is similar to those of porphyrin (Fig. 1.11d, e) and related macrocyclic compounds (porphyrinoids) that play vital roles in biological systems (for example, chlorophylls, heme, cobalamin (vitamin B₁₂), etc.). Actually, phthalocyanines are members of the porphyrinoid family in which all four methyne groups at the meso positions are replaced by nitrogen, and four benzene rings are fused to the periphery of the four pyrrole rings. Hence, phthalocyanine can be renamed “tetraazatetrabenzoporphyrin”.

“Phthalocyanine” is originally the name of a specific compound (Fig. 1.11a). However, nowadays, it represents all its family members (i.e., unsubstituted and substituted phthalocyanines and their metal complexes) at the same time. This could give rise to a serious misunderstanding; hence, we may need to define what “phthalocyanine” stands for to avoid unnecessary confusion. Hereafter, “phthalocyanines (in the plural form)” will be used as a general term referring to members

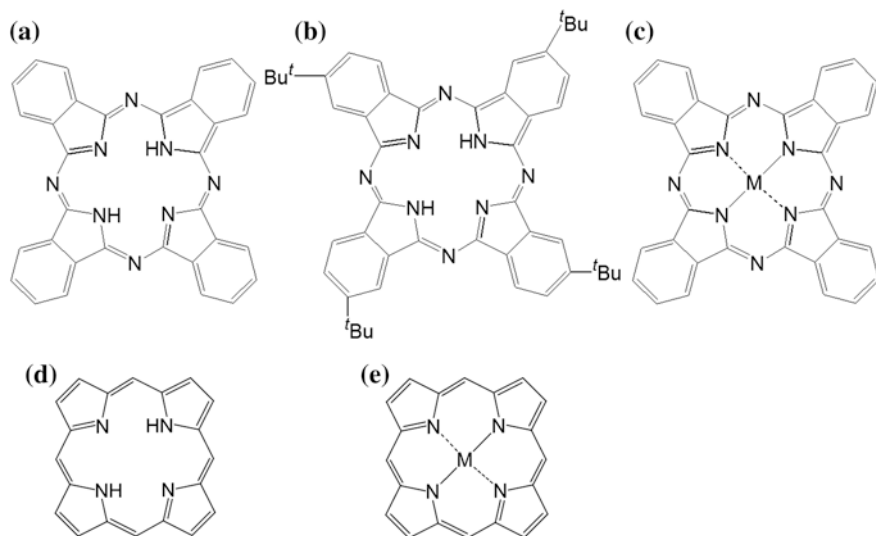


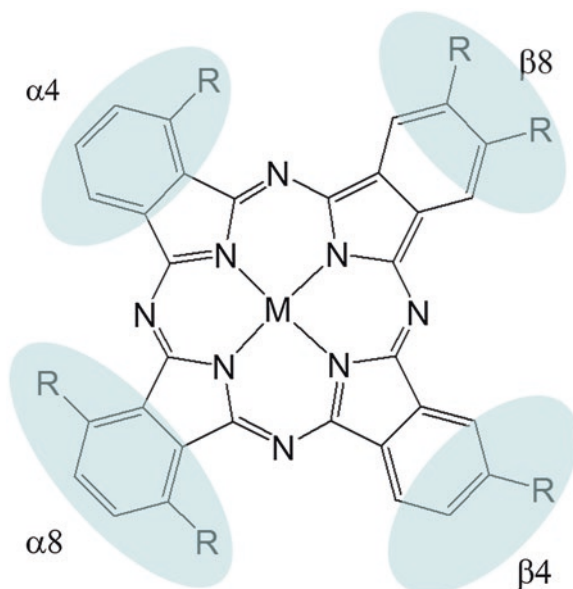
Fig. 1.11 Molecular structures of **a** unsubstituted phthalocyanine (H_2pc), **b** tetra(*tert*-butyl)phthalocyanine as an example of substituted phthalocyanines (of four regioisomers determined from the mutual positions of the four substituent groups, only one is shown here: the other three are shown in Figs. 2.1, 3.16, and 4.5 although their central elements are different), **c** a metal complex of H_2pc ($[M(pc)]$), where M denotes a divalent metal ion, such as copper(II), **d** unsubstituted porphyrin, and **e** its metal complex (M denotes a divalent metal ion)

of the “phthalocyanine family”. The “phthalocyanine(s)” as a general term is quite frequently abbreviated as “Pc(s)”. Let us follow this convention to represent metal-free phthalocyanines as $H_2Pc(s)$ when we do not need or do not desire to specify types or numbers of substituents on the periphery of the macrocycle. On the other hand, when we must refer to the specific compound (Fig. 1.11a), H_2pc will be employed, where pc denotes the dianion of the unsubstituted phthalocyanine (i.e., the doubly deprotonated form in Fig. 1.11a; $C_{32}H_{16}N_8^{2-}$). When we need to specify the type and/or numbers of peripheral substituents for a peculiar compound, they will be appropriately represented as, for example, H_2tbp ⁹ for tetra (*tert*-butyl)phthalocyanine or graphically illustrated (as in Fig. 1.11b). To specify the positions and number of substituents, the following conventions, “ $\alpha 4$ ”, “ $\alpha 8$ ”, “ $\beta 4$ ”,¹⁰ and “ $\beta 8$ ” (Fig. 1.12), which have been generally accepted, will be employed throughout this work.

⁹The abbreviation will be defined when it first appears.

¹⁰Careful readers may be concerned that the tetrasubstituted phthalocyanines are mixtures of four regioisomers, as determined from the positions of the substituents. This is true (see also Fig. 1.11b and the relevant caption). However, it is not important in most cases as mentioned in Sect. 2.1.1.

Fig. 1.12 Positions and numbers of substituents on the periphery of phthalocyanines and conventions to present them in this work



Likewise, their metal complexes will be referred to as $[M(\text{Pc})]$, where M is a divalent metal cation (for example, $[\text{Zn}(\text{Pc})]$ or $[\text{Co}(\text{Pc})]$ ¹¹) when there is no need to specify substituents. Normally, Pc ligands are dianions (i.e., $\text{Pc}(2-)$) in their metal complexes; hence, the oxidation state is not shown unless otherwise noted (e.g., $\text{Pc}(3-)$ and $\text{Pc}(-)$ stand for one-electron-reduced and oxidized species, respectively).

1.2.3 Use of Phthalocyanines in Industry

Phthalocyanines generally show an intense blue or green color, and they have been widely used as colorants: coloring of blue jeans and ornamental coating on Shinkansen Super Express train in Japan, for example. This is because they strongly absorb light in the range of 650–800 nm (their spectral details will be described in Chaps. 2 and 3). In recent decades, phthalocyanines enjoy a variety of industrial and medical applications [6–8], such as nonlinear optics [9], optical data storage [10, 11], solar cells [12–14], charge-generating materials for photocopiers and laser printers [15], electrochromic displays [16, 17], photosensitizers for solar cells [18], water splitting for fuel cells [19, 20], photocatalysts [21], photodynamic therapy (PDT) of tumors [22–25], photodynamic antimicrobial therapy

¹¹When a metal ion is trivalent, the complex is represented as $[M(\text{Pc})\text{X}]$, where X denotes a mono-anionic axial ligand. Likewise, $[M(\text{Pc})\text{X}_2]$ is for a complex of tetravalent cations.

(PACT) [26], fluorescence diagnosis of tumors [23–25], semiconductors [27], and synthetic metals [28] (Fig. 1.10). Some examples of applications involving phthalocyanines in industry and medicine are briefly described below.

1.2.3.1 Application to Optical Data Storage

Phthalocyanines are used for the storage and retrieval of data on optical disks, such as compact disk-recordable (CD-R), DVD, and Blu-ray disks [10, 11]. Figure 1.13a shows a schematic diagram of CD-R, which is composed of a transparent substrate (e.g., polycarbonate), a recording layer made of organic dye (where phthalocyanines are used), a metal reflective layer, and a protective resin layer. The recording layer is prepared on the substrate by spin-coating from a solution containing the dyes and solvent that does not dissolve the substrate (e.g., alcohols or aliphatic hydrocarbons). The storage of data is carried out by forming pits in the recording layer (Fig. 1.13b) through the use of a laser beam (generally around 780 nm for CD-R). The laser source emits an intense light beam that is focused onto the surface. The intense energy is absorbed by the dye molecules, and a small, localized region heats up and significantly changes its reflective properties [29]. The written information is retrieved by scanning the surface of the optical disk with a laser beam of the same wavelength but of a constant output power level that does not heat the data surface beyond its thermal writing threshold. The “reading beam” is reflected back as it is emitted from the laser to the

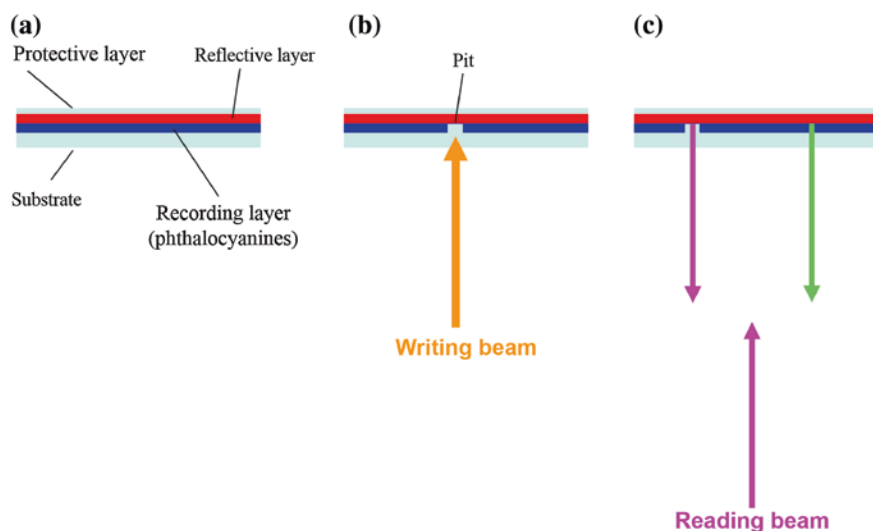


Fig. 1.13 Schematic diagrams of optical data storage and retrieval on CD-R: **a** initial state, **b** data storage, **c** data retrieval. *Source* NIMS eSciDoc—IMEJI. © Hiroaki Isago with CC-BY-NC 3.0 license

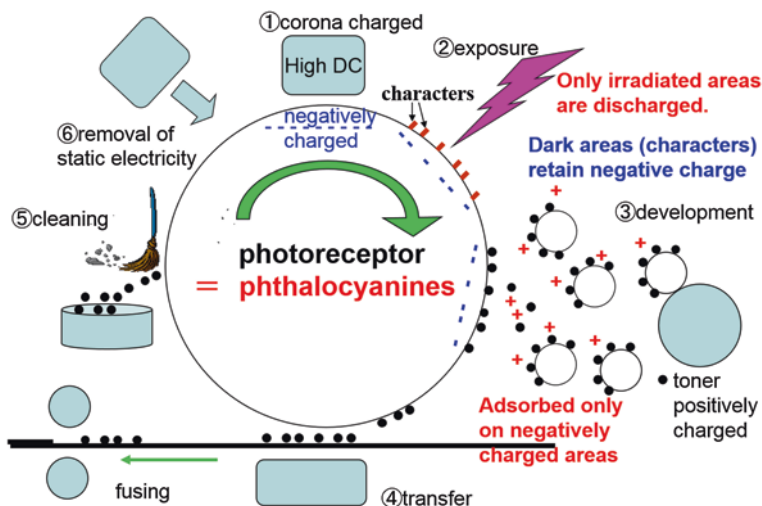


Fig. 1.14 Schematic diagram of the mechanism of a photocopier. *Source* NIMS eSciDoc—IMEJI. © Hiroaki Isago with CC-BY-NC 3.0 license

(metal) reflective layer in the “written” areas, but by way of the recording layer in the “blank” areas (Fig. 1.13c). Thus, the recorded data are retrieved as a sequence of such differences.

1.2.3.2 Application to Electronic Photograph

First of all, it should be noted that charge separation can be achieved by using dyes and light. When the dye is photoirradiated, an electron in its HOMO is excited (Fig. 1.5) to the LUMO with a hole generation in the HOMO. This mechanism is essentially the same as that for semiconductors where electrons are excited from the valence band to the conduction band. They will be rapidly recombined (i.e., the dye will return to the ground state). However, the positive and negative charges are separable in the presence of an appropriate neighboring electron acceptor by receiving an excited electron.¹² For example, the first step in photosynthesis in plants involves this phenomenon, where chlorophyll, or other similar macrocyclic compounds, plays the role as the dye. This phenomenon is applicable to water-splitting for fuel cells (artificial photosynthesis) [30] or degradation of pollutants in industrial wastewater (photocatalysis: The hole and excited electron can be used to oxidize and reduce another molecule in the vicinity of the dye, respectively) [21].

How many of us know that we are always using phthalocyanines in our office (other than CD-R)? Figure 1.14 illustrates how photocopiers work. Readers who have seen the inside of their photocopiers or laser printers may have seen

¹²Note that the electron transfer cannot occur in the ground state.

something like a drum in it. Phthalocyanines are contained in the drum as photoreceptors. A number of phthalocyanines are known as p-type organic semiconductors [12–14]. They behave essentially as insulators in the dark but become conductors upon photoirradiation, in line with the aforementioned charge generation mechanism. Let us assume that we are about to make a photocopy of a document. Firstly, the drum is negatively corona-charged in the dark by applying a high DC voltage to the photoreceptor (step 1 in Fig. 1.14). In the next step, the drum is exposed to light. As phthalocyanines will be positively charged upon irradiation and the drum has already been negatively charged, only the areas exposed to light will be discharged. The characters in your document prevent the light from reaching the surface of the photoreceptor; hence, the dark areas retain their negative charge (step 2). Pigmented powder (called toner) particles, which are made of colorant and plastic resin and are mixed with and positively charged by magnetized carrier beads, adhere to the negatively charged image (step 3). The powder image is transferred from the drum (photoreceptor) onto paper by bringing the paper into contact with the toner (step 4). The toner comprising the image is melted by heat and then fixed on the paper (fusing process). Thus, the document has been duplicated. The drum is then cleaned by removing residual toner particles (step 5) and residual static electricity (step 6) from the photoreceptor returns it to the initial state. Readers interested in more details on photocopiers should visit the relevant web site [30].

Essentially the same charge separation process underlies the mechanism of organic photovoltaic cell composed of p-n junction of organic semiconductors, where phthalocyanines and appropriate electron-withdrawing material play a role as the photoreceptor (p-type semiconductor). As photo-excited electrons in the photoreceptor are transferred to the neighboring n-type semiconductor layer through the p-n junction, charge separation is achieved and causes electromotive force. Since Tan reported a power conversion efficiency of approximately 1 % by means of a prototypical organic photovoltaic cell where copper phthalocyanine ([Cu(pc)]) and a perylene derivative as the photoreceptor (i.e., p-type semiconductor) and electron acceptor (i.e., n-type semiconductor), respectively [31], a remarkable development has been accomplished by using phthalocyanines and related macrocyclic compounds. Readers who are interested in this field should be referred to recent excellent reviews [12–14].

1.2.4 Application in Medical Fields

1.2.4.1 Photosensitization of Singlet Oxygen for Photodynamic Cancer Therapy

Molecular oxygen has two low-lying excited singlet states, $^1\Delta_g$ and $^1\Sigma_g$, respectively 7880 and 13,125 cm^{-1} above the triplet ground state [32, 33]. Their molecular structures are essentially the same as that of triplet oxygen ($^3\text{O}_2$) that we normally breathe, but only their spin states are different. Because of a much

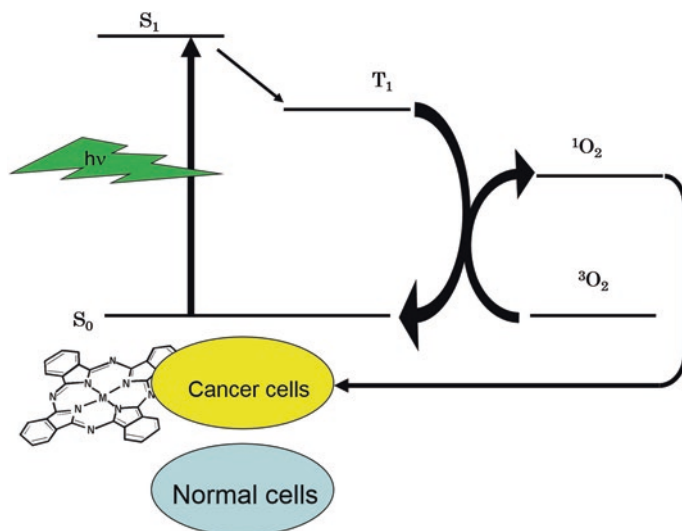


Fig. 1.15 Schematic diagram of putative mechanism proposed for photodynamic therapy of tumors. *Source* NIMS eSciDoc—IMEJI. © Hiroaki Isago with CC-BY-NC 3.0 license

shorter lifetime of the higher state ($^1\Sigma_g$) than that of the lower one ($^1\Delta_g$), and hence its little contribution to chemistry, hereafter, molecular oxygen in the $^1\Delta_g$ state alone will be referred to as just “singlet oxygen” or “ 1O_2 ”. Although it is difficult to directly excite 3O_2 to generate 1O_2 , photoexcited dye molecules can generate 1O_2 through energy transfer from the dye molecule to a neighboring 3O_2 (Fig. 1.15). It should be noted that dye molecules in the triplet excited state more effectively contribute to the photochemical reaction than those in the singlet excited state because of their much longer lifetime in the former state (also refer to Sects. 4.2.2 and 4.2.3). Singlet oxygen (1O_2) is known as one of the reactive oxygen species and is much more harmful than 3O_2 . Membrane damage induced by the attack of 1O_2 on the lipid or protein moieties can be highly deleterious. On the other hand, efforts have been made to apply the photosensitization of this toxic species to cancer therapy (photodynamic therapy; PDT) [22–25] and blood sterilization (photodynamic antimicrobial chemotherapy; PACT) [26].

PDT is performed by the following process [22]. Firstly, the sensitizer (dye) is administered (orally, topically, or intravenously) and is allowed to equilibrate for some appropriate duration so that maximum tumor/normal tissue differentiation is achieved. Secondly, the tumor is directly irradiated by using light such as lasers and fiber optics. Finally, the 1O_2 generated by the photoexcited dye molecules causes tumor cell destruction. As the photosensitizers have been selectively accumulated on the tumor tissues, normal cells are preferentially less susceptible to damage.

Phthalocyanines are considered promising candidates for such purposes (and also for photodynamic diagnosis (PDD), as mentioned later) because of their

intense optical absorption ($\epsilon \sim 10^5 \text{ M}^{-1}\text{cm}^{-1}$) in the red region of the visible spectrum or near-infrared region. This is because the use of light of longer wavelengths takes advantage of the increase in the penetration depth of the exciting light. Moreover, the absorption spectra of various chromophores present in tissues define the optical therapeutic window. Oxy- and deoxyhemoglobin, cytochromes, and melanin strongly absorb light of wavelengths below 600 nm. In addition, absorption by water owing to its harmonic vibration is significant above 1400 nm [22, 24]. Therefore, photosensitizers are required to absorb light in the spectral range of 600–1400 nm. Dyes with absorption peaks at wavelengths above 700 nm are preferable because their use at least doubles the penetration depth [22, 24].

1.2.4.2 Fluorescence Imaging for Tumor Diagnosis

With respect to the photoexcited dye molecules, attention in PDT has mostly been focused on the energy transfer from the photosensitizer to the neighboring molecular oxygen. However, some portions of the excited molecules can return to the ground state by emitting energy in the form of fluorescence (Chap. 4). Therefore, by employing some appropriate fluorescent dyes and by monitoring radiation from the excited photosensitizer, it should be possible to extract lesion areas from mixtures of normal and tumor tissues, as a function of the concentration of fluorophores. This concept provides a background for photodynamic diagnosis (PDD) or fluorescence diagnosis (FD) [23–25]. As is the case for PDT, phthalocyanines are again promising candidates because of their intense fluorescence with high efficiency in the optical therapeutic window as well as their strong optical absorption in the same spectral range (Chap. 4).

Thus, optical absorption is an important process in various industrial and medical applications of phthalocyanines as well as in the use as colorants. In the following chapter, typical absorption spectra of phthalocyanines and their theoretical background will be described.

References

1. G.N. Lewis, O. Goldschmidt, T. Magel, J. Bigeleise, *J. Am. Chem. Soc.* **65**, 1150–1154 (1943)
2. L.C. Jones, L.W. Taylor, *Anal. Chem.* **27**, 228–237 (1955)
3. F. Sondeheimer, D.A. Ben-Efrain, R. Wolovsky, *J. Am. Chem. Soc.* **83**, 1675–1681 (1961)
4. H. Isago, K. Miura, M. Kanesato, *J. Photochem. Photobiol. Sect. A*, **197**, 313–320 (2008)
5. S.-H. Kim (ed.), *Functional Dyes* (Elsevier, Amsterdam, 2006)
6. R. Hirohashi, K. Sakamoto, E. Okumura (eds.), *Phthalocyanines as Functional Dyes (in Japanese)* (IPC, Tokyo, 2004)
7. C.C. Leznoff, A.B.P. Lever (eds.), *Phthalocyanines: Properties and Applications*, vol 1–4. (VCH, New York, 1989–1996)
8. F.H. Moser, A.L. Thomas, *The Phthalocyanines*, vol I and II. (CRC Press, Boca Raton, 1983)
9. J.S. Shirk, J.R. Lindle, F.J. Bartoli, M.E. Boyle, *J. Phys. Chem.* **96**, 5847–5852 (1992)
10. R. Ao, L. Kummerl, D. Haarer, *Adv. Mater.* **7**, 495–499 (1995)

11. H. Mustroph, M. Stollenwerk, V. Bressau, *Angew. Chem. Int. Ed.* **45**, 2016–2035 (2006)
12. M.V. Martinez-Diaz, G. de la Torre, T. Torres, *Chem. Commun.* **46**, 7090–7108 (2010)
13. G. de la Torre, C.G. Claessens, T. Torres, *Chem. Commun.* **20**, 2000–2015 (2007)
14. M.G. Waltera, A.B. Rudineb, C.C. Wamser, J. Porphyrins Phthalocyanines **14**, 759–792 (2010)
15. K.-Y. Low, *Chem. Rev.* **93**, 449–486 (1993)
16. M.M. Nicholson, *Ind. Eng. Chem. Prod. Res. Dev.* **21**, 261–266 (1982)
17. C.-L. Lin, C.-C. Lee, K.-C. Ho, *J. Electroanal. Chem.* **524–525**, 81–89 (2002)
18. A. Hagfeldt, G. Boschloo, L. Sun, L. Kloo, H. Pettersson, *Chem. Rev.* **110**, 6595–6663 (2010)
19. D. Gust, T.A. Moore, A.L. Moore, *Acc. Chem. Res.* **42**, 1890–1898 (2009)
20. M.R. Wasielewski, *Chem. Rev.* **92**, 435–461 (1992)
21. Z. Wang, W. Mao, H. Chen, F. Zhang, X. Fan, G. Qian, *Catal. Commun.* **7**, 518–522 (2006)
22. R. Bonnett, *Chem. Soc. Rev.* **24**, 19–33 (1995)
23. K. Plaetzer, B. Krammer, J. Berlanda, F. Berr, T. Kiesslich, *Lasers Med. Sci.* **24**, 259–268 (2009)
24. S. Andersson-Engels, J. Johansson, S. Svanberg, K. Svanberg, *Anal. Chem.* **62**, 19A–27A (1990)
25. V.B. Loschenov, V.I. Konov, A.M. Prokhorov, *Laser Phys.* **10**, 1188–1207 (2000)
26. M. Wainwright, *J. Antimicrob. Chemother.* **42**, 13–28 (1998)
27. P. Turek, P. Petit, J.J. Andre, R. Evan, B. Boudjema, G. Guillaud, M. Maitrot, *J. Am. Chem. Soc.* **109**, 5119–5122 (1987)
28. T. Inabe, H. Tajima, *Chem. Rev.* **104**, 5503–5533 (2004)
29. A.H.M. Holtslag, E.R. MaCord, G.H. Werumeus Buning, *Jpn. J. Appl. Phys.* **31**, 484–493 (1992)
30. <http://www.xerox.com/innovation/chester-carlson-xerography/enlu.html>
31. C.W. Tang, *Appl. Phys. Lett.* **48**, 183–185 (1986)
32. M.C. DeRosa, R.J. Crutchley, *Coord. Chem. Rev.* **233–234**, 351–371 (2002)
33. C. Schweitzer, R. Schmidt, *Chem. Rev.* **103**, 1685–1757 (2003)

Chapter 2

“Prototypical” Optical Absorption Spectra of Phthalocyanines and Their Theoretical Background

In this chapter, the theoretical background of optical absorption spectra of phthalocyanines is described on the basis of their molecular orbitals (MOs). Note that because we attempted to describe the theoretical background without extreme mathematicization but as graphically as possible, some accuracy may have been sacrificed for comprehensibility. It is not our main purpose in this chapter to chronologically trace the progress of theoretical studies on phthalocyanines (and porphyrins); hence, some important milestone studies have been omitted. Readers interested in quantitative derivation should refer to the original papers. In this monograph, attention will be mostly focused on spectral properties in the solution phase. Exciton coupling between chromophores, which will be described in Sect. 3.2.4, is enhanced in the solid state; hence, the spectra are significantly broadened and become less structured. In the vapor phase, the molecules may be far apart; however, most of the phthalocyanines are involatile at room temperature and atmospheric pressure. Hence, as spectral measurements need to be carried out at considerably higher temperatures, the observed spectra may be rather broad as vibrational modes are highly activated. In solutions (regardless of their being organic or inorganic), phthalocyanines have quite a large molecular extinction coefficient at their most intense absorption band (on the order of $10^5 \text{ M}^{-1}\text{cm}^{-1}$), spectra of adequate quality are obtained from very dilute solutions (10^{-6} M), where the dye molecules are far apart (however, this depends on the compound and some compounds can form dimers or higher aggregates even in this concentration range as will be discussed in Sect. 3.2.4). It is true that interactions with solvent molecules need to be taken into consideration; however, the solvent effect is generally negligible unless the solvent used induces or takes part in certain chemical reactions with the phthalocyanines of interest (Sect. 3.2.7).

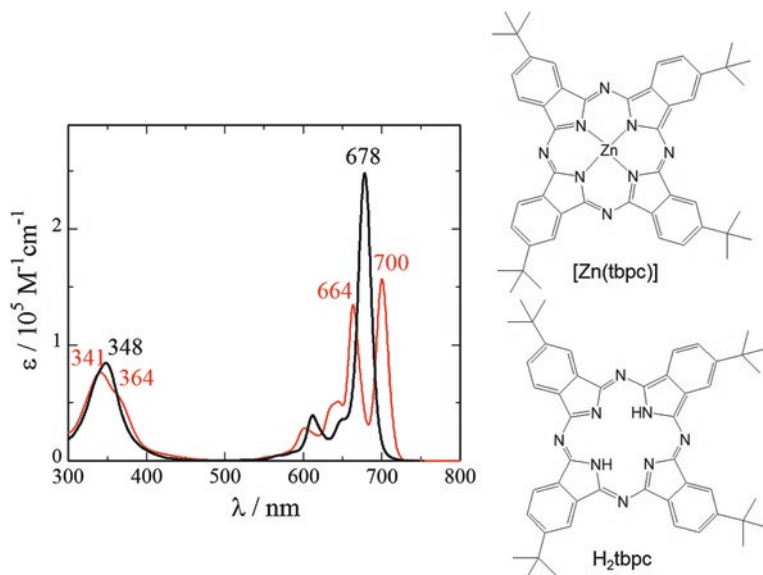


Fig. 2.1 Optical absorption spectra of [Zn(tbpc)] (black solid line) and H₂tbpc (red broken line) in chloroform. Only one regioisomer is shown for each compound

2.1 Prototypical Absorption Spectra of Phthalocyanines in Solutions

2.1.1 Prototypical Spectra of Phthalocyanines

Figure 2.1 shows the optical absorption spectra of zinc- and metal-free phthalocyanines in chloroform, represented as [Zn(tbpc)]¹ and H₂tbpc, respectively. The macrocycles are substituted by four *tert*-butyl (^tBu) groups to make them highly soluble in common organic solvents (particularly nonaromatic solvents, which are transparent in a wide spectral range). This substituent is very useful because it markedly improves the solubility of phthalocyanines in common organic solvents with negligible changes in their electronic structures and hence has been quite frequently used for spectroscopic investigation of phthalocyanines.²

The spectrum of [Zn(tbpc)] is typical of metallated phthalocyanines. It is characterized by (1) the appearance of an intense ($\log \epsilon = \text{ca. } 5$) absorption band at

¹The “tbpc” is the abbreviation of tetra(*tert*-butyl)phthalocyaninate dianion (Sect. 1.2.2).

²Careful readers may be concerned that the tetrasubstituted phthalocyanines are mixtures of four regioisomers, as determined from the positions of the substituents. This is true. However, it is not important in most cases. One research group has successfully separated four regioisomers of tetrasubstituted phthalocyanines using an HPLC technique; however, they have determined that the difference in their spectral properties is negligible [1].

approximately 670 nm [generally termed the Q band (Sect. 2.1.2)] associated with some less intense ($\log \epsilon = \text{ca. } 4$) satellites at its blue flank (600–650 nm), (2) the appearance of a less intense but broad band at approximately 350 nm (generally called the Soret or B band), and (3) transparency in the other spectral regions (spectral windows). The spectral feature of H_2tbpc , apart from the splitting of the Soret and Q bands into two bands having nearly the same intensity instead of a single band observed for $[\text{Zn}(\text{tbpc})]$,³ is essentially similar to that of $[\text{Zn}(\text{tbpc})]$. Thus, both species absorb red light intensely and are transparent in the other spectral regions (400–600 nm and >750 nm). This is the reason why phthalocyanines show an intense blue color, as discussed in Sect. 1.1.2.

The spectral band widths for the two species are quite narrow (484 cm^{-1} for $[\text{Zn}(\text{tbpc})]$, 357 (for the 700 nm band) and 408 cm^{-1} (for the 664 nm band) for H_2tbpc) as compared with that for methylene blue (1233 cm^{-1} ; Fig. 1.3). This suggests that their molecular structures are more rigid than that of methylene blue and their structures in the lowest excited state do not markedly differ from those in the ground state (Sect. 1.1.5).

Before considering the origin of the absorption bands, let us compare the spectra of phthalocyanines with those of the other dyes that have a similar cyclic tetrapyrrole skeleton.

2.1.2 Comparison with Spectra of Similar Tetrapyrrole Macrocycles

Figure 2.2 (left) shows the optical absorption spectra of metal complexes of the phthalocyanine derivative (Pc^4 ; $[\text{Cu}(\text{tbpc})]$), tetraazaporphyrin derivative (TAP), tetraphenylporphyrin (TPP), and tetrabenzoporphyrin derivative (TBP) as well as metal-free chlorin e6 (their structures are shown in Fig. 2.2 (right)). All the spectra are plotted with their most intense band normalized. The spectra of TPP and Pc are markedly different in spite of the similarity in their tetrapyrrole skeletons. The TPP spectrum shows an intense band at approximately 400 nm and very weak bands at approximately 550 nm, which are generally termed the Soret and Q bands, respectively. On the other hand, the spectrum of Pc, which is typical of metal complexes of phthalocyanines (Sect. 2.1.1), shows the most intense band at approximately 670 nm and much less intense band at approximately 350 nm. This difference cannot be attributed to the expansion of the π -conjugation system at the four fused benzo groups in Pc. Ring expansion from TPP to TBP (Fig. 2.2 (right)) gives rise to a slight shift at the Soret-band position.⁵ Comparison between these four similar macrocycles has shown that TAP and TBP can be considered to be structural intermediates

³The split Soret and Q bands of H_2tbpc are attributed to the symmetry-lowering effect based on the presence of imino protons in the cavity, as described in Sect. 2.2.9.

⁴In this subsection, as the central elements do not play a crucial role, they are not specified in the abbreviations of the macrocyclic compounds.

⁵The peripheral substituents are omitted for clarity in this discussion.

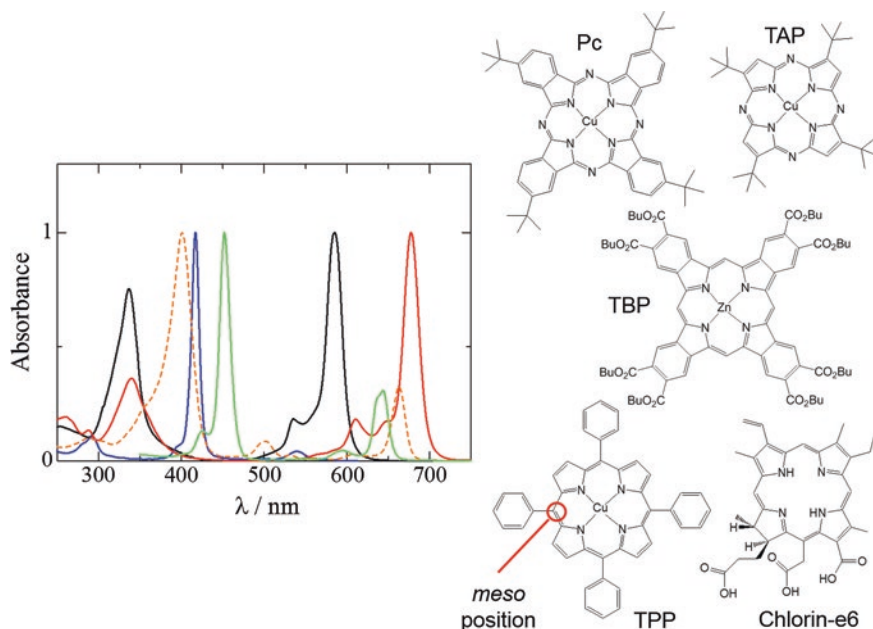


Fig. 2.2 Optical absorption spectra of Pc in dichloromethane (*red solid line*), TPP in dichloromethane (*blue solid line*), TAP in dichloromethane (*black solid line*), TBP in DMF (*green solid line*) [2], and chlorin e6 in ethanol (*orange broken line*) [3]. The spectra of TBP (*right*) and chlorin e6 (*left*) were redrawn from digital data available at the web site of “PhotochemCAD” (<http://omlc.ogi.edu/spectra/PhotochemCAD/index.html>) with permission. Source for the other species NIMS eSciDoc—IMEJI. © Hiroaki Isago with CC-BY-NC 3.0 license

between TPP and Pc. Substitution of the phenyl-substituted methyne (C-phenyl) groups at “*meso*-positions” (see TPP for the *meso*-position) in TPP with nitrogen atoms generates TAP, fusion of benzo groups to the periphery of the four pyrrole rings generates TBP, and both generate Pc. Interestingly, the spectral characteristics of TAP and TBP are also intermediate of those of the other two. In the case of TBP, upon fusion of a benzo group to the periphery of each of the pyrrole ring, the Soret band is slightly shifted, as mentioned above; however, a new band appears at approximately 630 nm, which resembles the Q band in the Pc spectrum. On the other hand, the modification of TPP to TAP brings about a significantly increased Q band intensity and caused a large blue-shift in the Soret-band position. Thus, it seems that the introduction of nitrogen atoms into the innermost 16-membered ring has greater effects on the electronic structure of the macrocycle than the fusion of benzene rings to the periphery of the pyrrole rings. It is noteworthy that chlorin e6 shows a spectrum similar (Fig. 2.2 (left)) to that of the TPP derivative notwithstanding the disruption of the π conjugation system at the peripheral ethylene bridge.⁶

⁶In contrast, disruption of the π -conjugation system in the innermost 16-membered ring of phthalocyaninate leads to the disappearance of the characteristic Q band (one or more broad bands are observed in the 400–500 nm region, instead) [4].

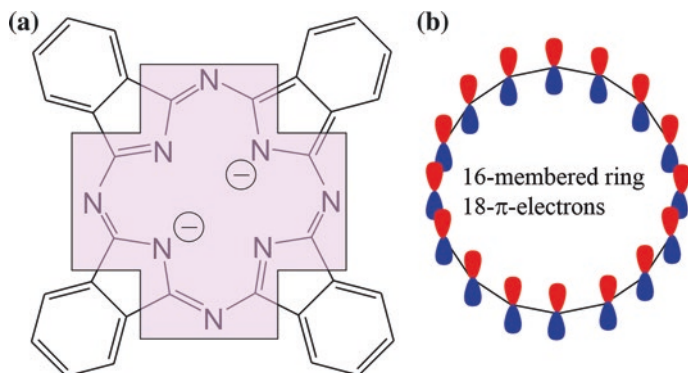


Fig. 2.3 **a** Innermost 16-membered ring in a phthalocyanine molecule and **b** dianion of ideal cyclic polyene, $C_{16}H_{16}^{2-}$ as starting model. *Source* NIMS eSciDoc-IMEJI. © Hiroaki Isago with CC-BY-NC 3.0 license

Therefore, to understand the optical absorption spectra and electronic structure of phthalocyanines, we may assume that (1) the same method applied to porphyrins can also be applied to phthalocyanines, (2) the innermost 16-membered ring should be the starting point (Fig. 2.3a), and (3) introduction of nitrogen atoms into the 16-membered ring and fusion of benzene rings play crucial roles in determining the balance in intensity between the Soret and Q bands.

In the following subsection, some representative MO models will be discussed to better understand the electronic structures of porphyrins, phthalocyanines, and other related macrocycles that exhibit the absorption spectra as shown in Fig. 2.2.

2.2 Molecular Orbital Models of Porphyrins and Phthalocyanines

2.2.1 Selection Rule in Optical Absorption (*Optical Absorption = Generation of Vector*)

Before considering MO models, it may be feasible to consider a selection rule dictating that the transition from the ground state to a given excited state involves optical absorption. In Chap. 1, it has been briefly mentioned that when a dye molecule is excited via optical absorption, the distribution of electrons changes in the molecule, which generates an electric dipole. That is, the molecule cannot be excited via optical absorption to higher states unless the transition involves generation of an electric dipole moment. Thus, absorption of light is equal to generation of a vector. Keeping this in mind, apparently complex phenomena, such as configuration interaction (Sect. 2.2.6) and exciton coupling (Sect. 3.2.4.2), may be understood more easily.

2.2.2 Perimeter Model

To understand optical absorption spectra and the electronic structures of porphyrins and related macrocyclic compounds, Simpson has proposed a simple “free-electron” model, in which 18 π -electrons are circulating along the periphery of the innermost 16-membered ring [5]. Note that two excess electrons of the macrocyclic ligand (in metal complexes, porphyrins and phthalocyanines may be regarded as dianions) in addition to the 16 π -electrons from each atom of the innermost 16-membered ring (Fig. 2.3a) are included in this model. Therefore, the dianion of an ideal 16-membered alternant cyclic polyene, $C_{16}H_{16}^{2-}$, has aromaticity according to Hückel’s “ $4n + 2$ ” rule. We use this as the starting model (Fig. 2.3b).

Let us consider the motion of a free electron circulating along the periphery of a 16-membered ring as a function of angle, ϕ (Fig. 2.4a). The k value is taken as positive when the electron is circulating clockwise and negative when it is circulating counterclockwise. The wave function Ψ_k for the electron with an angular momentum of k is represented by the following differential equations (Eqs. 2.1 and 2.2), where m , E_k , and \hbar denote the mass and energy of the electron, and the Planck constant, respectively.

$$\frac{\partial^2 \Psi_k}{\partial \phi^2} = -\frac{2mE_k}{\hbar^2} \Psi_k; \quad E_k = k^2(\hbar^2/2m) \quad (2.1)$$

$$\frac{\hbar}{i} \frac{\partial \Psi_{\pm k}}{\partial \phi} = \pm k \hbar \Psi_{\pm k} \quad (2.2)$$

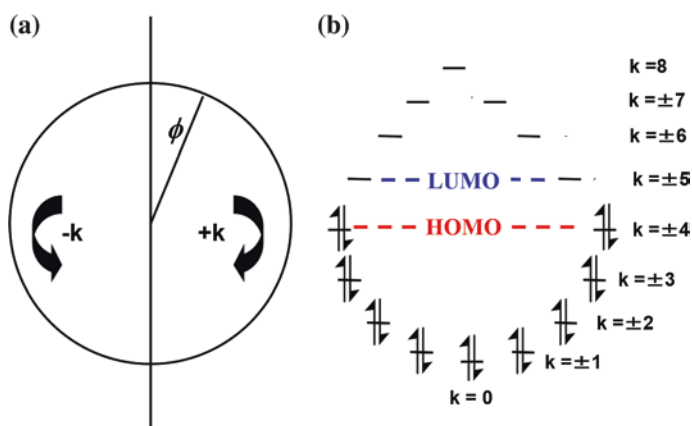


Fig. 2.4 **a** Perimeter model: a free electron circulating along the periphery of the 16-membered ring with an angular momentum of k (clockwise) and $-k$ (counterclockwise) and **b** energy levels of wave functions (MOs) for electrons with various k values. Source NIMS eSciDoc—IMEJI. © Hiroaki Isago with CC-BY-NC 3.0 license

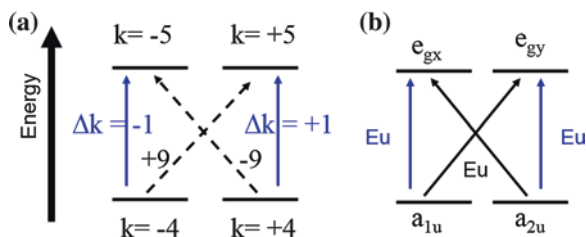


Fig. 2.5 Schematic diagrams of electronic transitions from HOMO to LUMO (straight transitions are shown as *blue arrows* and cross transitions as *black arrows*) in the perimeter model (a) and those of the “descent-in-symmetry” model (b). The *solid and broken arrows* denote allowed and forbidden transitions, respectively

The solution is given in a complex form as (Eq. 2.3).

$$\Psi_{\pm k} = \frac{1}{\sqrt{2}} \exp(\pm ik\phi); \quad (k = 0, 1, 2, \dots, 7, 8) \quad (2.3)$$

As each wave function has the same value for ϕ and $\phi + 2\pi$, (i.e., $\Psi(\phi) = \Psi(\phi + 2\pi)$), k must be an integer. As the energy of Ψ_k (E_k) is proportional to the square of k values and each orbital accepts up to two electrons, the orbitals with $k = 0, \pm 1, \pm 2, \pm 3$, and ± 4 are occupied by electrons in the ground state. Thus, $\Psi_{\pm 4}$ and $\Psi_{\pm 5}$ are the HOMOs and LUMOs,⁷ respectively (Fig. 2.4b). Note that the orbitals $\Psi_{\pm k}$ are degenerate because they are at the same energy level, only the direction of circulation is different. Therefore, there are four possible transitions from the HOMOs to the LUMOs. One set includes straight transitions (Ψ_{+4} to Ψ_{+5} and Ψ_{-4} to Ψ_{-5}) and another set includes cross transitions (Ψ_{+4} to Ψ_{-5} and Ψ_{-4} to Ψ_{+5}). The change in k during the transition is ± 1 in the straight transitions whereas it is ± 9 in the cross transitions (Fig. 2.5a). Of these two sets of transitions, only the former one is allowed because these transitions involve the generation of an electric dipole moment, as shown below.

Let us assume that the 16-membered ring is located parallel to the x,y -plane. Consequently, the wave functions consist of atomic p_z orbitals, which are perpendicular to the molecular plane. Cartesian coordinates (x, y) are presented using polar coordinates (r, ϕ) as ($r\cos\phi, r\sin\phi$). When the dipole moment is generated along the x -axis, the Cartesian coordinate x is presented as a function of ϕ (Eq. 2.4).

$$x = r \cos \phi = \frac{1}{2} \{ \exp(i\phi) + \exp(-i\phi) \} \quad (2.4)$$

As optical absorption occurs only when an electric dipole is generated, the following integral must be non-zero through the transition from Ψ_k to Ψ_n (Eq. 2.5).

$$\int_0^{2\pi} \Psi_k r \Psi_n^* d\phi = \int_0^{2\pi} \{ \exp(+ik\phi) x \exp(-in\phi) \} d\phi \quad (2.5)$$

⁷Refer to Sect. 1.1.4 for the definitions of HOMO and LUMO.

As x is represented by Eqs. 2.4 and 2.5 includes the following two integral calculations (Eq. 2.6), either of which must be non-zero.

$$\int_0^{2\pi} [\exp\{(+k + 1 - n)i\phi\}]d\phi + \int_0^{2\pi} [\exp\{(+k - 1 - n)i\phi\}]d\phi \neq 0 \quad (2.6)$$

Therefore, the change in k (Δk ; i.e., $n - k$) through the transition must be ± 1 . Similarly, the change in k caused by the generation of an electric dipole moment along the y -axis must also be ± 1 . However, it is determined that another set of transition values ($\Delta k = \pm 9$) are forbidden. This successfully explains the appearance of a very intense Soret band ($\Delta k = \pm 1$) and a very weak Q band ($\Delta k = \pm 9$) in the spectra of porphyrins (Fig. 2.2). The large change in Δk (± 9) for the Q band has also been evidenced by a magnetic circular dichroism study (Sect. 2.2.8). However, the energy profile (i.e., which of the two sets of transitions requires a higher energy?) cannot be explained by this model.

2.2.3 Graphical Description of Molecular Orbitals

As the wave functions described above include imaginary parts, they are not suitable for graphical representation of the MOs. Linear combination of a set of Ψ_{+k} and Ψ_{-k} can represent them in a form of trigonometric functions (Eq. 2.7).

$$\frac{\Psi_{+k} + \Psi_{-k}}{\sqrt{2}} = \cos(k\phi); \quad \frac{\Psi_{+k} - \Psi_{-k}}{\sqrt{2}i} = \sin(k\phi) \quad (2.7)$$

Figure 2.6 shows some examples of wave functions with only their phase taken into consideration. When $k = 0$, all the atomic p_z orbitals have the same phase (i.e., the same color⁸); hence, the wave function Ψ_0 has no nodal plane.⁹ When $k = \pm 1$, the phase (sign) of the wave function is inversed at the 0th and 8th atoms for the sine form and at the 4th and 12th atoms for the cosine counterpart; hence, there is one nodal plane. Similarly, wave functions with $k = \pm 2$ have two nodal planes. Thus, the number of nodal planes increases with increasing absolute value of k . Readers may have determined that the two wave functions $\Psi_{\pm k}$ are identical upon appropriate rotation (for example, in the case of $k = \pm 1$, $\sin\phi$ is equivalent to $\cos\phi$ upon clockwise rotation by 90°). This is because they are degenerate. Note that the linear combination of $\Psi_{\pm 8}$ similarly produces sine and cosine forms, but only one wave function (the cosine form in this case) makes sense because all the 16 atoms are located on nodes in its counterpart. What is most important in this discussion is that

⁸Even though there seems to be no red or blue color between neighboring atoms, it may be assumed that a considerable amount of π -cloud is present when the atoms have the same sign (color).

⁹Note that a nodal plane is present on the molecular plane (because of the nature of the p_z orbital) but this is not taken into account here.

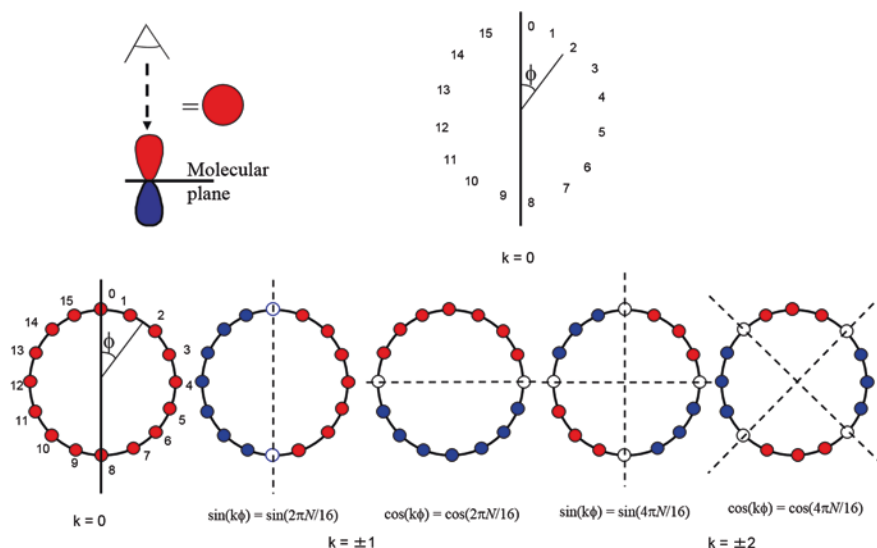


Fig. 2.6 Graphical illustrations of the lowest five π MOs ($k = 0, \pm 1, \pm 2$) based on perimeter model. The *red and blue closed circles* denote the phases of the MOs (the positive and negative signs are denoted by *red and blue circles*, respectively). Only the signs of the wave function are shown; hence, the size of the circles does not represent the amplitude of the coefficient). *Source* NIMS eSciDoc—IMEJI. © Hiroaki Isago with CC-BY-NC 3.0 license

both the HOMOs ($\Psi_{\pm 4}$) and LUMOs ($\Psi_{\pm 5}$) are degenerate in an ideal 16-membered cyclic polyene belonging to the D_{16h} point group (in group theory), as shown in Fig. 2.7 (top). In this symmetry, the HOMOs and LUMOs are both degenerate and belong to the following irreducible representations, e_{4u} and e_{5g} , respectively.

2.2.4 “Descent-in-Symmetry” Model

Neither porphyrins nor phthalocyanines actually belong to D_{16h} because of the presence of the nitrogen atoms and the four peripheral C_2H_2 bridges. These modifications decrease the symmetry of the parent 16-membered cyclic polyene, D_{16h} , to D_{4h} , which corresponds to the actual molecular symmetry point group of a common porphyrin [6]. Therefore, the perimeter model requires further modifications. Following the decrease in the symmetry, the degeneracy is lifted for the HOMOs (a_{1u} and a_{2u} ; Fig. 2.7 bottom), whereas it is maintained for the LUMOs (e_g). The a_{1u} HOMO is characterized by the presence of nodes at all the *meso*-positions and pyrrole nitrogen atoms. However, the a_{2u} counterpart has a large amplitude at the same positions and has nodes between these positions. The a_{2u} orbital is stabilized owing to the presence of the high electron density at atoms of large electronegativity (nitrogen) whereas the a_{1u} orbital is stabilized by a strong bonding interaction between the innermost 16-membered alternant polyene and the peripheral ethylene

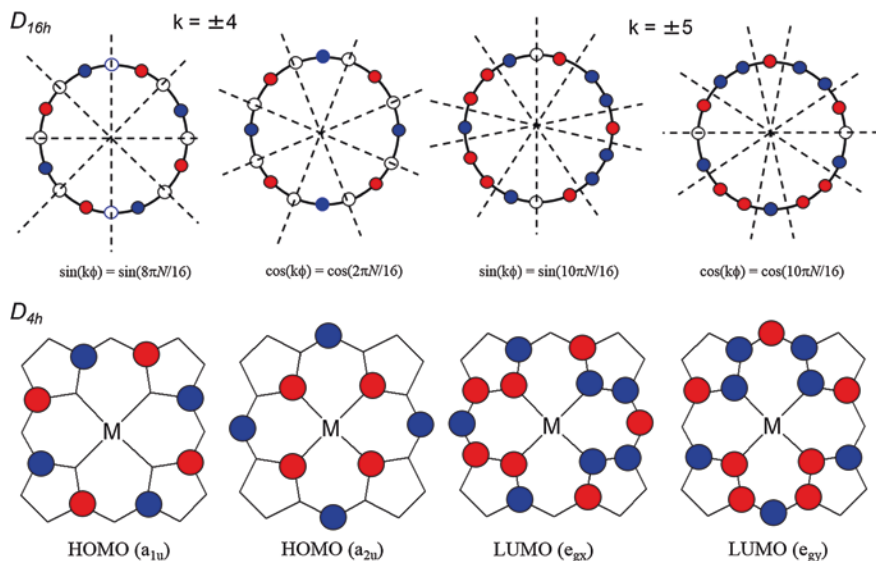


Fig. 2.7 Graphical illustrations of HOMO ($k = \pm 4$) and LUMO ($k = \pm 5$) based on perimeter model (top) and descent-in-symmetry model (bottom). The red and blue closed circles denote phases of the MOs (the positive and negative signs are denoted by red and blue circles respectively). Only the signs of the wave function are shown; hence, the size of the circles does not represent the amplitude of the coefficients). Source NIMS eSciDoc—IMEJI. © Hiroaki Isago with CC-BY-NC 3.0 license

moieties.¹⁰ In the case of porphyrins, these two effects are even; hence, the two orbitals are still nearly degenerate (accidental degeneracy).

The four HOMO-LUMO transitions under the D_{4h} symmetry are shown in Fig. 2.5b. In this modified model, the $a_{2u} \rightarrow e_g$ transition has a symmetry of E_u ($A_{2u} \times E_g = E_u$ ¹¹) and the $a_{1u} \rightarrow e_g$ transition also has the same symmetry ($A_{1u} \times E_g = E_u$; Sect. 2.2.5). The problem with this model is that both the transitions are allowed (x,y -polarized); hence, the weak Q band in the spectrum of porphyrin cannot be explained.

2.2.5 How to Use Character Tables (for Group Theory)

The purpose of this discussion is not to explain the group theory but how to determine when an electronic transition of interest is allowed or forbidden using only a character table. At the end of Sect. 2.2.4, it has been demonstrated that the $a_{1u} \rightarrow e_g$

¹⁰Note that all the ethylene moieties are isolated from the innermost 16-membered ring in a_{2u} by nodes.

¹¹In general, irreducible representations starting with a capital letter stand for a “state”, whereas those starting with a small letter represent MOs.

transition is allowed (x,y -polarized). It is easy to determine an allowed transition using this table and some basic mathematical operations. Therefore, readers who are already familiar with this method may skip this subsection.

Readers are reminded that optical absorption (i.e., allowed electronic transition) is equal to the generation of a vector. Let us consider whether an electron transition from the Ψ_k orbital to Ψ_n is allowed or forbidden. For this transition to be allowed, the integral expression (Eq. 2.8, where r denotes the electric dipole moment) must be non-zero. Therefore, the triple product of Ψ_k , r (which is a radius vector), and Ψ_n must include a totally symmetric irreducible representation (which has all characters = +1; e.g., A_{1g} in D_{4h} ; see Table 2.1). Assume that Ψ_k and Ψ_n belong to the irreducible representations a_{2u} and e_g , respectively. As the direct product of A_{2u} and E_g makes E_u (see the bottom row of Table 2.1), the irreducible representation of r must also be E_u to generate the A_{1g} representation as the result of the triple product (Table 2.2). As the E_u representation transforms (x, y) as shown in the rightmost column of the character table, this transition is allowed and x/y -polarized. However, a transition from a_{2u} to b_{1g} is determined to be forbidden because their direct product makes B_{2u} (Table 2.2), which cannot transform to any of x, y, z . Similarly, the $e_u \rightarrow e_u$ transition is also forbidden.

$$\int_{-\infty}^{\infty} \Psi_k r \Psi_n^* dv \neq 0 \quad (2.8)$$

Tables 2.1 and 2.3 show the character tables for the point groups D_{4h} and D_{2h} , to which the actual metallated and metal-free Pcs belong, respectively. Attention should be paid to the rightmost column, where basis functions of each irreducible representation are given. It has been determined that, of the ten irreducible representations (given in the leftmost column) in D_{4h} , only A_{2u} and E_u have a linear basis function ((x, y) and z , respectively). Similarly in D_{2h} , only B_{1u} (z), B_{2u} (y), and B_{3u} (x) have a linear basis function. Thus, r must belong to the irreducible

Table 2.1 Character table for D_{4h} point group

	E	$2C_4$	C_2	$2C'_2$	$2C''_2$	i	$2S_4$	σ_h	$2\sigma_v$	$2\sigma_d$	
A_{1g}	1	1	1	1	1	1	1	1	1	1	$x^2 + y^2, z^2$
A_{2g}	1	1	1	-1	-1	1	1	1	-1	-1	Rz
B_{1g}	1	-1	1	1	-1	1	-1	1	1	-1	$x^2 - y^2$
B_{2g}	1	-1	1	-1	1	1	-1	1	-1	1	xy
E_g	2	0	-2	0	0	2	0	-2	0	0	(Rx, Ry), (xz, yz)
A_{1u}	1	1	1	1	1	-1	-1	-1	-1	-1	
A_{2u}	1	1	1	-1	-1	-1	-1	-1	1	1	z
B_{1u}	1	-1	1	1	-1	-1	1	-1	-1	1	
B_{2u}	1	-1	1	-1	1	-1	1	-1	1	-1	
E_u	2	0	-2	0	0	-2	0	2	0	0	(x, y)
$A_{2u} \times E_g$	1×2	1×0	$1 \times (-2)$	-1×0	-1×0	-1×2	-1×0	$-1 \times (-2)$	1×0	1×0	
E_g	= 2	= 0	= -2	= 0	= 0	= -2	= 0	= 2	= 0	= 0	

Table 2.2 Product table for D_{4h} point group

	A_{1g}	A_{2g}	B_{1g}	B_{2g}	E_g		A_{1u}	A_{2u}	B_{1u}	B_{2u}	E_u
A_{1g}	A_{1g}	A_{2g}	B_{1g}	B_{2g}	E_g		A_{1u}	A_{2u}	B_{1u}	B_{2u}	E_u
A_{2g}	A_{2g}	A_{1g}	B_{2g}	B_{1g}	E_g		A_{2u}	A_{1u}	B_{2u}	B_{1u}	E_u
B_{1g}	B_{1g}	B_{2g}	A_{1g}	A_{2g}	E_g		B_{1u}	B_{2u}	A_{1u}	A_{2u}	E_u
B_{2g}	B_{2g}	B_{1g}	A_{2g}	A_{1g}	E_g		B_{2u}	B_{1u}	A_{2u}	A_{1u}	E_u
E_g	E_g	E_g	E_g	E_g	$A_{1g}+A_{2g}+B_{1g}+B_{2g}$		E_u	E_u	E_u	E_u	$A_{1u}+A_{2u}+B_{1u}+B_{2u}$
A_{1u}	A_{1u}	A_{2u}	B_{1u}	B_{2u}	E_u		A_{1g}	A_{2g}	B_{1g}	B_{2g}	E_g
A_{2u}	A_{2u}	A_{1u}	B_{2u}	B_{1u}	E_u		A_{2g}	A_{1g}	B_{2g}	B_{1g}	E_g
B_{1u}	B_{1u}	B_{2u}	A_{1u}	A_{2u}	E_u		B_{1g}	B_{2g}	A_{1g}	A_{2g}	E_g
B_{2u}	B_{2u}	B_{1u}	A_{2u}	A_{1u}	E_u		B_{2g}	B_{1g}	A_{2g}	A_{1g}	E_g
E_u	E_u	E_u	E_u	E_u	$A_{1u}+A_{2u}+B_{1u}+B_{2u}$		E_g	E_g	E_g	E_g	$A_{1g}+A_{2g}+B_{1g}+B_{2g}$

Table 2.3 Character table for D_{2h} point group

	E	$C_2(z)$	$C_2(y)$	$C_2(x)$	I	$\sigma(xy)$	$\sigma(xz)$	$\sigma(yz)$	Linear, rotations quadratic
A_g	1	1	1	1	1	1	1	1	x^2, y^2, z^2
B_{1g}	1	1	-1	-1	1	1	-1	-1	Rz, xy
B_{2g}	1	-1	1	-1	1	-1	1	-1	Ry, xz
B_{3g}	1	-1	-1	1	1	-1	-1	1	Rx, yz
A_u	1	1	1	1	-1	-1	-1	-1	
B_{1u}	1	1	-1	-1	-1	-1	1	1	z
B_{2u}	1	-1	1	-1	-1	1	-1	1	y
B_{3u}	1	-1	-1	1	-1	1	1	-1	x

representation(s) that transform as (the translations) x , y , z , as shown in the character tables when the transition involves optical absorption.

2.2.6 Gouterman’s “Four-Orbital” Model

Gouterman and coworkers have introduced the concept of “configuration interaction” between the two types of transition involving the doubly degenerate LUMO and two nearly degenerate HOMOs (hence, the four-orbital model) to explain the spectra of porphyrins [7–9]. Before considering this model, it should be again remembered that optical absorption is equal to the generation of a vector (an electric dipole moment). The “ x , y -polarized degenerate excited state” means that the x -polarized (the generated dipole is parallel to the x -axis) and y -polarized excited states are at exactly the same energy level. As stated in Sect. 2.2.4, both the $a_{1u} \rightarrow e_g$ and $a_{2u} \rightarrow e_g$ transitions belong to the same symmetry, E_u . The “same irreducible representation” means that these electric dipole moments generated through the transitions have the same direction. Therefore, the conventional

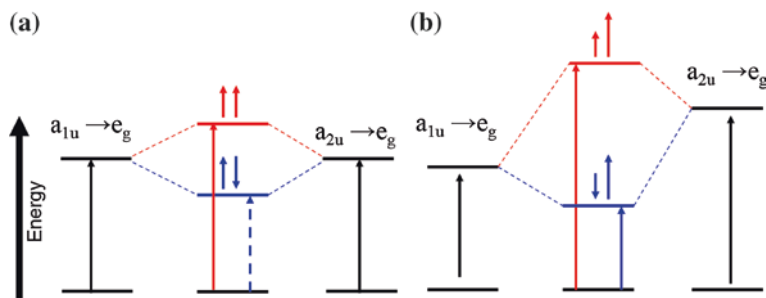


Fig. 2.8 Schematic diagrams of the four-orbital model for (a) porphyrins in which a_{1u} and a_{2u} orbitals are nearly degenerate and (b) phthalocyanines in which a_{2u} orbital is stabilized relative to a_{1u} counterpart. The energy scales are arbitrary

additivity rule for vectors may be applied to the dipole moments (i.e., they are enhanced when they are parallel and cancelled when they are antiparallel). In particular, the x -polarized $a_{2u} \rightarrow e_g$ and the x -polarized $a_{1u} \rightarrow e_g$ transitions have essentially the same energy (similar to the y -polarized transitions), because the a_{1u} and a_{2u} orbitals are nearly degenerate, and the two vectors strongly interact with each other.

Figure 2.8 shows schematic illustrations of the configuration interaction between the two types of transition. When the two dipole moments are parallel, the resultant energy level is higher than that of a single transition because of electric repulsion between the dipoles. The intensity increases because the two vectors are constructive. However, when they are antiparallel, the excited state is stabilized owing to electric attraction, but the spectral intensity is significantly reduced because the dipole moments have disappeared (cancelled by each other). This model predicts the appearance of an intense (Soret) band at a high energy and a very weak (Q) band at a low energy, as observed in the actual spectra of porphyrins (Fig. 2.2; blue solid line).¹²

2.2.7 Why Are the Spectra of Phthalocyanines Different from Those of Porphyrins in Spite of Their Similar Structures?

Figure 2.3 shows the absorption spectra of porphyrin (TPP) and the related macrocycles. The ring expansion (TBP) and substitution of *meso*-carbon atoms with nitrogen atoms (TAP) results in a significant increase in the intensity of the Q

¹²This description is rather qualitative and oversimplified. The MO wave function shown in Figs. 2.7 and 2.8 are converted by linear combinations of their complex forms (Eq. 2.7). Readers who are interested in strict, quantitative derivation should refer to the original papers [6–9].

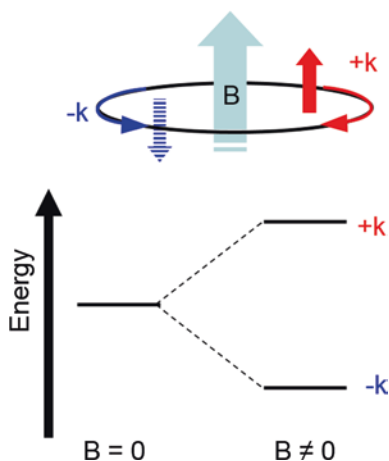
band. This demonstrates that these modifications upset the balance of energy level between the occupied frontier orbitals (a_{1u} and a_{2u}). For example, substitution of *meso*-carbon with nitrogen significantly stabilizes the a_{2u} orbital relative to the a_{1u} counterpart (Sect. 2.2.4). Consequently, as their transition energy is no longer the same ($a_{1u} \rightarrow e_g < a_{2u} \rightarrow e_g$), the electric dipole moment of the lower excited state is not completely cancelled. Fusion of the benzo groups to the periphery of TAP also enhances the energy imbalance so that the Q band is intensified.

2.2.8 Degeneracy of Excited States and Magnetic Circular Dichroism (MCD) Spectroscopy

In the free-electron model, the degenerate orbitals have been demonstrated as pairs of orbitals with the same angular momentum but with different circulation directions (that is, clockwise ($+k$) and counterclockwise ($-k$) circulation). The two orbitals have the same energy, which depends on k^2 alone, in the absence of a magnetic field. The circulation of the electron is equal to the ring current of the opposite direction (that is, clockwise circulation = counterclockwise ring current), generating an upside magnetic moment (Fig. 2.9). Likewise, the counterclockwise circulation generates a downside magnetic moment of the same magnitude. Once an external magnetic field is applied perpendicularly to the molecular plane, the two orbitals are no longer equivalent in energy level and the degeneracy is lifted owing to the Zeeman effect to a much smaller extent than to the symmetry-lowering effects.

MCD spectroscopy is a powerful tool for investigating the electronic structure of molecules with high symmetry, such as porphyrins or phthalocyanines, because it provides valuable information on their degenerate states. MCD spectra can be measured using a conventional circular dichroism (CD) spectrometer that can be

Fig. 2.9 Schematic illustration of degeneracy of MOs (in free-electron model) in the absence of external magnetic field and its disruption upon application of external magnetic field.
Source NIMS eSciDoc—IMEJL. © Hiroaki Isago with CC-BY-NC 3.0 license



equipped with an electromagnet or even a permanent magnet in its sample compartment. The magnetic field is oriented parallel to the optical propagation (that is, in the Faraday arrangement). In this orientation, only transitions between states with different angular magnetic quantum numbers (ΔJ) of unity can absorb light. Absorption of left circularly polarized (lcp) and right circularly polarized (rcp) light is associated with transitions of $\Delta J = +1$ and -1 , respectively (Fig. 2.10) [10–12]. The differential absorption between lcp and rcp light, ΔA_{L-R} , is recorded as the MCD spectrum and is characterized by three terms; Faraday A, B, and C terms (Eq. 2.9), where B is the strength of the magnetic field (T), cl is the product of the concentration of the molecule (M) and optical path length (cm), and kT is the product of the Boltzmann constant and temperature (K).

$$\Delta A_{L-R} = 152.5Bcl[A + (B + (C/kT))] \quad (2.9)$$

The Faraday A term is observed when the ground state is nondegenerate whereas the excited state is degenerate in the transition. The degenerate transition is split into two transitions which are very similar in energy and during which lcp light and rcp light are absorbed. Hence, the observed CD spectrum is sharp and it appears that the first-order derivative curve of the absorption spectrum was recorded (Fig. 2.10, top).

The Faraday B term appears irrespective of whether the transition is degenerate or nondegenerate (Fig. 2.10, middle). Therefore, when neither the ground state nor the excited state is degenerate for transitions in molecules of lower symmetry (e.g., H₂Pc; see Sect. 2.2.9), the MCD spectrum is completely dominated by B terms. The B terms arise owing to the mixing between excited states that are linked by a magnetic transition moment, which is induced by the applied magnetic field. The intensity of B terms increases in inverse proportion to the energy separation between the states. The spectrum relevant to the transitions must be a “zero-sum game”.

The Faraday C term (C/kT in Eq. 2.9) is observed only when the ground state is degenerate and the excited state is nondegenerate (Fig. 2.10, bottom). They are temperature-dependent because of the Boltzmann distribution between the split ground states induced by the magnetic field. Therefore, the C terms are Gaussian-shaped as is the case of B terms. However, degeneracy of ground states is not very common in phthalocyanines or related macrocycles because of the Jahn-Teller effect [13–15]. Hence, the C term is not taken up in this monograph.

MCD spectroscopy also provides information regarding the change in magnetic dipole moment through the observed transitions [16, 17]. The optical absorption and MCD spectra of some porphyrins and related macrocycles are shown in Fig. 2.11. The Q band observed for the Sb^V complex (cation) of octaethylporphyrin in the absorption spectrum is weaker than the Soret band (dotted line) commonly observed for normal porphyrins (e.g., TPP in Fig. 2.2) [18]. Nevertheless, the associated MCD spectrum has a comparable intensity. The free-electron model predicts that the Soret band is allowed and hence shows a small change in orbital angular momentum ($\Delta k = \pm 1$). In contrast, the Q-transition is forbidden but has a large $\Delta k (\pm 9)$, which is related to the magnetic moment in the excited state.

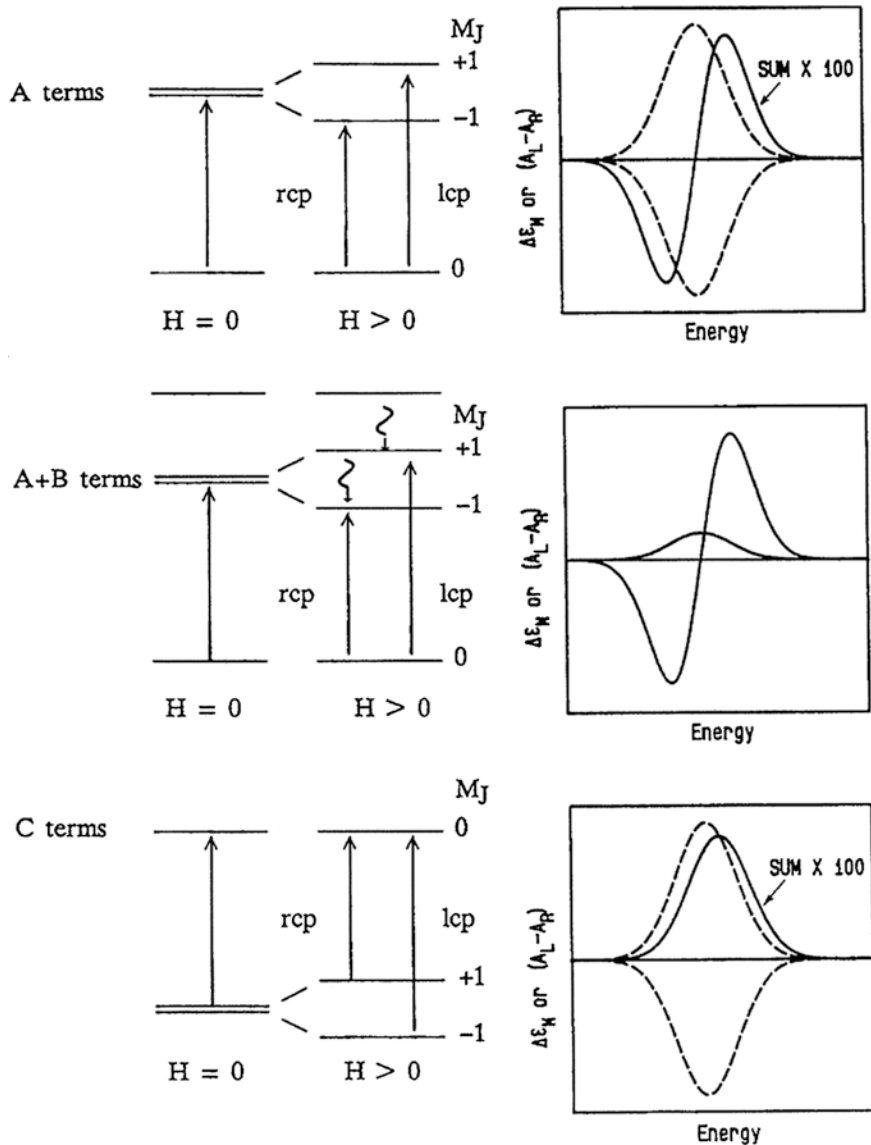
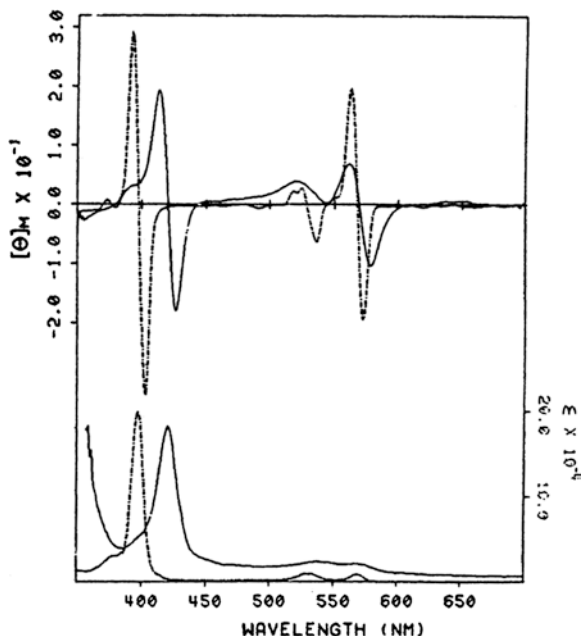


Fig. 2.10 Origin of the Faraday A, B, and C terms observed in MCD spectra. The *dashed curves* represent the absorbance of left and right circularly polarized light. "H", which stands for the magnitude of the external magnetic field, corresponds to "B" in the text. Reprinted from Ref. [12], Copyright 2003, with permission from Elsevier

Fig. 2.11 MCD (*top*) and optical absorption spectra of purified reduced +CO P-420 at pH 7.4 (*solid lines*) and (dihydroxo) (octaethylporphyrinato) antimony(V) chloride (*broken lines*) in dichloromethane. Reprinted with the permission from Ref. [18]. Copyright 1977 American Chemical Society



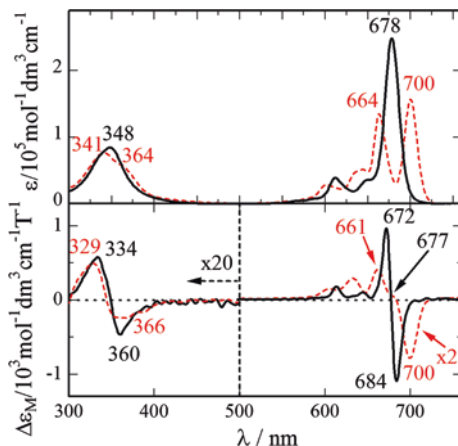
2.2.9 Assignment of Phthalocyanine Spectra by MCD Spectroscopy

Using MCD spectroscopy, we can unambiguously assign each band observed in Fig. 2.1. The spectra of $[\text{Zn}(\text{tbp})]$ and H_2tbp will be discussed as examples of degenerate and nondegenerate transitions, respectively.

The optical absorption and MCD spectra of $[\text{Zn}(\text{tbp})]$ are shown in Fig. 2.12 as black solid lines, where a distinct S-shaped curve is observed in the 650–700 nm spectral range with its center at essentially the same wavelength as that of the absorption maximum (678 nm). On this basis, we may assume that the MCD spectrum in this spectral region is dominated by a Faraday A term and hence this transition is degenerate. A similar S-shaped sigmoid curve is observed in the MCD spectrum at approximately 348 nm, indicating that this transition is also degenerate.¹³ Using MCD spectroscopy, we found that the 678- and 348-nm bands are unambiguously assigned as the Q and Soret bands, respectively, as is predicted from the four-orbital model. The weak satellites at the blue flank of the Q band are

¹³For some compounds, e.g., $[\text{Zn}(\text{pc})]$, $[\text{Mg}(\text{pc})]$, $[\text{Li}_2(\text{pc})]$ [19–21], and some As^{V} and Sb^{V} derivatives [22–24], a similar absorption band in the spectral region has been reported but they are considered as an overlap of two bands (B1/B2 bands) on the basis of MCD spectra (Sect. 3.2.2.1).

Fig. 2.12 Optical absorption (top) and MCD spectra of [Zn(tbpc)] (bottom), (black solid lines) and H₂tbpc (red broken lines) in chloroform solution. The absorption spectra are identical to those in Fig 2.1



attributed to vibronic progression (Sect. 1.1.3) associated with the Q band.¹⁴ These bands are nondegenerate as determined from the MCD spectrum in the same spectral region, which is dominated by B terms.

Absorption and MCD spectra of H₂tbpc are shown in Fig. 2.12, where no Faraday A term is observed under each band and only Faraday B terms are observed in the MCD spectrum as a Gaussian-shaped signal that appears similar to absorption bands. This indicates that H₂tbpc does not have any degenerate excited state because of its low molecular symmetry (D_{2h}). Owing to the presence of the imino protons in the cavity (Fig. 2.2), the e_g orbitals that are degenerate in D_{4h} symmetry are split into b_{2g} and b_{3g} in D_{2h} symmetry (note that the molecular plane is again taken as the xy -plane).¹⁵ Using this convention, the low and high transitions are y - ($A_u \times B_{2g} = B_{2u}$) and x -polarized ($A_u \times B_{3g} = B_{3u}$) and are hence no longer degenerate. It is not easy to determine the practical interpretations of B terms.

Careful readers may have determined that the sign of the MCD spectra in the Q-region changes from negative to positive with increasing energy (i.e., from longer to shorter wavelengths) for both A and B terms. This sequence makes sense and is observed when the energy gap between the two lowest unoccupied π -MOs (that is, adjacent LUMOs) is smaller than that between the two highest occupied π -MOs (adjacent HOMOs) [16, 17]. Readers who are interested in this issue are

¹⁴With respect to the second vibronic band (612 nm), Mack and Stillman have suggested the presence of an additional nondegenerate electronic (n - π) transition in this spectral region due to the lack of the corresponding band in the fluorescence spectrum [25].

¹⁵The convention employed for D_{2h} here is different from that of the global standard, which recommends taking the z -axis (principal axis) in the D_{2h} point group so that it passes through as many atoms as possible (i.e., the z -axis is parallel to the phthalocyanine molecular plane). This is the reason why some studies have shown that the split LUMOs belong to b_{1g} and b_{2g} . However, strictly following the standard convention might lead to unnecessary confusion in comparison with [Zn(Pc)] (D_{4h}), where the z -axis must be its C_4 axis and hence is perpendicular to the molecular plane. Therefore, the z -axis for H₂Pc has been taken similarly for easier comparison with [Zn(Pc)].

referred to Michl's original reports. This is common for porphyrins, phthalocyanines, and their related macrocyclic compounds because their LUMOs are doubly degenerate or nearly degenerate, whereas their adjacent HOMOs are separated in energy as is expected from the four-orbital model.

2.2.10 Computational Molecular Orbital Calculations

It is not our purpose in this chapter to discuss the electronic structures of phthalocyanines and related macrocycles on the basis of computational molecular orbital calculation. However, it should be mentioned that some findings are available from computational works alone. In particular, the following two findings are quite important for description of optical spectra of phthalocyanines.

First, the Q band is assigned as essentially a pure HOMO-LUMO transition (i.e., $a_{1u} \rightarrow e_g$ for $[M(\text{Pc})]$, and $a_u \rightarrow b_{2g}$ and $a_u \rightarrow b_{3g}$ for H_2Pc). Although the Q band transition is a mixture of $a_{1u} \rightarrow e_g$ and $a_{2u} \rightarrow e_g$ according to the four-orbital model, a large stabilizing effect of nitrogen substitution on the a_{2u} orbital as against a_{1u} significantly reduces the contribution of the a_{2u} orbital to the Q-transition [9–12, 26].

Second, three absorption bands (B, N, and L bands in the order of increasing energy) appear in the higher-energy spectral region (the so-called Soret region), and are mixtures of more than one degenerate electronic transitions [8, 10–12]. The bands of higher energy (N and L) cannot be observed in organic solvents because they are hidden owing to intense absorption by the solvents used. Their presence has been determined in the spectra of As^{V} and Sb^{V} complexes that have significantly redshifted the Q and Soret bands [22–24].

References

1. M. Sommerauer, C. Rager, M. Hanack, *J. Am. Chem. Soc.* **118**, 10085–10093 (1996)
2. O.S. Finikova, A.V. Cheprakov, I.P. Beletskaya, P.J. Carroll, S.A. Vinogradov, *J. Org. Chem.* **69**, 522–535 (2004)
3. E.S. Nyman, P.H. Hynninen, *J. Photochem. Photobiol. B Biol.* **73**, 1–28 (2004)
4. C. Ercolani, A.M. Paoletti, G. Pannesi, G. Rossi, A. Chiesi-Villa, C. Rizzoni, *J. Chem. Soc. Dalton Trans.* 1971–1977 (1990)
5. W.T. Simpson, *J. Chem. Phys.* **17**, 1218–1221 (1949)
6. A. Ceulemans, W. Oldenhof, C. Görrler-Walrand, L.G. Vanquickenborne, *J. Am. Chem. Soc.* **108**, 1155–1163 (1986)
7. M. Gouterman, *J. Mol. Spectrosc.* **6**, 138–163 (1961)
8. M. Gouterman, G.H. Wagniere, L.C. Snyder, *J. Mol. Spectrosc.* **11**, 108–127 (1963)
9. C. Weiss, H. Kobayashi, M. Gouterman, *J. Mol. Spectrosc.* **16**, 415–450 (1965)
10. M.J. Stillman, T. Nyokong, in *Phthalocyanines: Properties and Applications*, vol. 1, ed. by C.C. Leznoff, A.B.P. Lever (VCH, New York, 1989), p. 133
11. J. Mack, M.J. Stillman, in *Porphyrin Handbook*, vol. 16, ed. by K.M. Kadish, K.M. Smith, R. Guilard (Elsevier Science, USA, 2003), pp. 43–116

12. J. Mack, M.J. Stillman, *Coord. Chem. Rev.* **219–221**, 993–1032 (2001)
13. J. Mack, M.J. Stillman, *J. Am. Chem. Soc.* **116**, 1292–1304 (1994)
14. J. Mack, S. Kirkby, E. Ough, M.J. Stillman, *Inorg. Chem.* **31**, 1717–1719 (1991)
15. J. Mack, M.J. Stillman, *Inorg. Chem.* **36**, 413–425 (1997)
16. J. Michl, *J. Am. Chem. Soc.* **100**, 6801–6811 (1978)
17. J. Michl, *Tetrahedron* **40**, 3845–3934 (1984)
18. J.H. Dawson, J.R. Trudell, G. Barth, R.E. Linder, E. Bunnenberg, C. Djerassi, M. Gouterman, C.R. Connell, P. Sayer, *J. Am. Chem. Soc.* **99**, 641–642 (1977)
19. E. Ough, T. Nyokong, K.A.M. Creber, M.J. Stillman, *Inorg. Chem.* **27**, 2724–2732 (1988)
20. M.J. Stillman, A.J. Thomson, *J. Chem. Soc. Faraday Trans. II*(70), 805–814 (1974)
21. T.C. VanCott, J.L. Rose, G.C. Misener, B.E. Williamson, A.E. Schrimph, M.E. Boyle, P.N. Schatz, *J. Phys. Chem.* **93**, 2999–3011 (1989)
22. H. Isago, Y. Kagaya, *Inorg. Chem.* **51**, 8447–8454 (2012)
23. H. Isago, Y. Kagaya, *J. Porphyrins Phthalocyanines* **13**, 382–389 (2009)
24. H. Isago, Y. Kagaya, H. Fujita, T. Sugimori, *Dyes Pigm* **88**, 187–194 (2010)
25. J. Mack, M.J. Stillman, *J. Phys. Chem.* **99**, 7935–7945 (1995)
26. N. Kobayashi, H. Konami, in *Phthalocyanines: Properties and Applications*, vol. 4, ed. by C.C. Leznoff, A.B.P. Lever (VCH, New York, 1996), p. 343

Chapter 3

Real Optical Absorption Spectra Observed in Laboratories

3.1 Are All Phthalocyanines Blue?

As described in Chaps. 1 and 2, phthalocyanine derivatives and related macrocyclic compounds generally show an intense blue color because they intensely absorb red light (650–700 nm; $\log(\epsilon/M^{-1} \text{ cm}^{-1}) = \text{ca. } 5$) while they are transparent in the other visible region (window region), as shown in Fig. 2.1. Some of them absorb violet light (380–420 nm; $\log(\epsilon) = \text{ca. } 4$) as well; hence, they may show a green color. In any case, the appearance of the main band in the 650–700 nm region and the essential transparency in the other region dictate their color. Then, do phthalocyanines always show a blue/green color? Figure 3.1a shows a photograph of dichloromethane solutions containing phthalocyanine derivatives (tppc) that have the same peripheral substituents (Fig. 3.1b; R = 2,6-dimethylphenoxy) [1]. The leftmost (I) and the next (II) compounds show a blue color, as is the case for conventional phthalocyanines. However, the rightmost compound (III) shows a yellowish green color. Moreover, the second rightmost one (IV) is amber-colored. Let us consider what causes this difference. Figure 3.2 shows the absorption spectra of the four phthalocyanine derivatives I–IV in dichloromethane solutions. Those of metal-free (green line) and copper (blue line) derivatives are essentially the same as those of *tert*-butyl-substituted analogues [Figs. 2.1 and 2.2 (red line)]. Both compounds have intense optical absorption in the 650–700 nm region (Q-band) and at the same time, they are essentially transparent in the 400–600 nm region and above 750 nm. This is why the two phthalocyanines show an intense blue color (Sect. 2.1.1). On the other hand, compound III is amber-colored and compound IV shows an opaque green color. The appearance of a yellowish color for the two antimony derivatives is due to the presence of an extra absorption band¹ in the 400–500 nm region, where

¹The appearance of such an intense band in this spectral region is unusual. The origin of this band is discussed in Sect. 3.2.2.1.

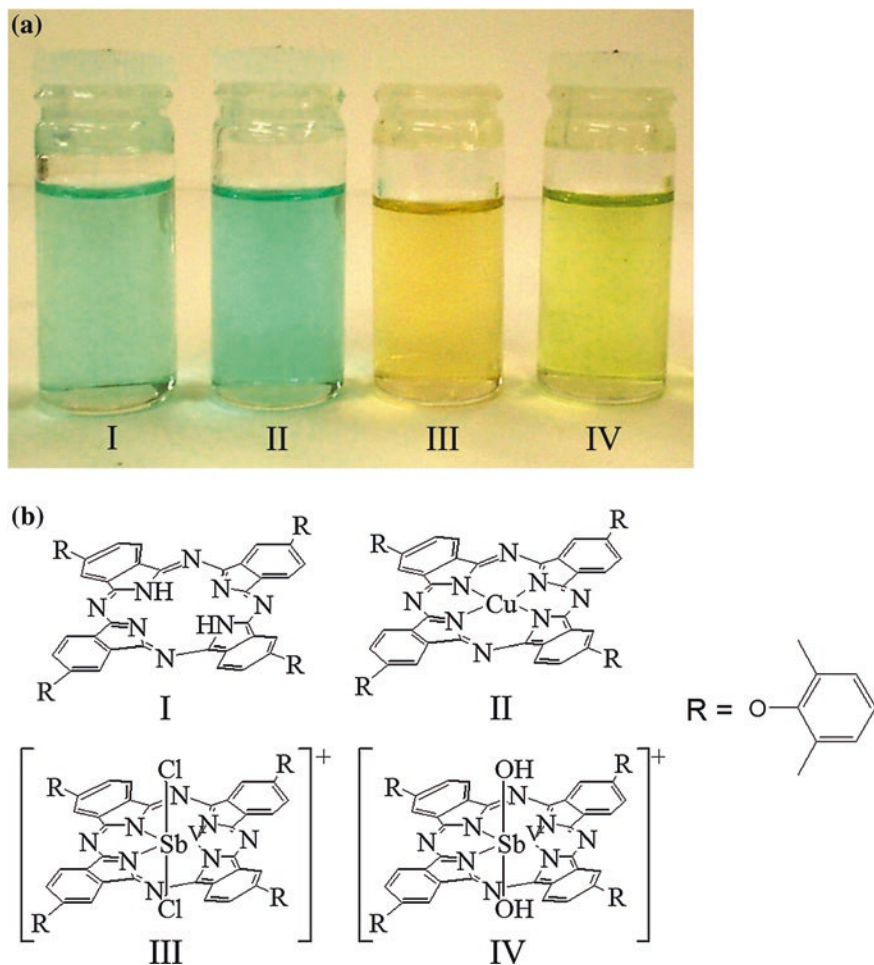


Fig. 3.1 a Color of phthalocyanine (tppc) derivatives I–IV in dichloromethane solutions and b molecular structures of the compounds. The counter anions of compounds III and IV are SbCl_4^- and PF_6^- , respectively. Reprinted from ref. [1], Copyright 2011, with permission from Elsevier

normal phthalocyanines are transparent. In addition, attention should be paid to the Q-band positions for the Sb^{V} complexes, which are located at a significantly red-shifted position.² Because of the very low sensitivity of our eyes to light above 700 nm (Fig. 1.1), the broad extra band in the 400–500 nm region, where our eyes are more sensitive, dominates the colors of the compounds. Thus, the optical absorption spectra of phthalocyanines can vary depending on the nature of the

²Although it is generally known that the Q-band position of phthalocyanines does not strongly depend on the metal ion in the cavity of the macrocycle (Sect. 3.2.1), the presence of a pnicogen can give rise to a significant redshift of the Q-band [2–11].

metal ion in the cavity, the axial ligands on the metal and the peripheral substituents. In this chapter, we discuss not only the internal factors (nature of the central element or peripheral substituents) that affect the absorption spectra of phthalocyanines, but also the external factors, including oxidation/reduction, acid-base equilibrium, solvent effects, and exciton coupling, by citing as many examples as possible.

3.2 Factors Affecting Absorption Spectra of Phthalocyanines

3.2.1 Effects of Metal Ion(s) in the Cavity of the Macrocyclic and Axial Ligands on the Metal

As phthalocyanines are useful dyestuffs and form metal complexes with essentially all the metal elements in the periodic table, optical absorption spectra have been reported for a large number of metal complexes [12–14]. The optical absorption spectra of metal complexes, apart from some exceptions, do not strongly depend on the metal ion in the cavity of the macrocyclic ligand. They basically look like the spectra of Zn^{II} (Fig. 2.1) or Cu^{II} (Fig. 2.2) complexes, although some additional weak bands can be observed for some metal derivatives as shown later. The spectra of metal complexes composed of more than one macrocyclic ligand in the vicinity, which are bound through the central metal itself or the axial ligand on the metal, are discussed elsewhere (Sect. 3.2.4). An exceptional spectrum has been reported for the Mo^{III} complex, which does not exhibit a characteristic Q-band [15].³ Table 3.1 shows optical absorption spectral data for various metal complexes, in which data for mostly unsubstituted and *tert*-butyl-substituted derivatives are given to underline the effects of the central element and axial ligands⁴ (if any) [16–81].

Table 3.1 reveals that metal complexes of unsubstituted phthalocyanine (i.e., those ligating pc^{2-}) have a Q-band in the range of 650–690 nm (mostly around 670 nm). However, some are known to have a Q-band at an unusual position; the Q-bands of Ir^{III} [16] and Ru^{II} [17] derivatives appear at a much shorter wavelength. In contrast, Bi^{III} [2, 3], Sb^{III} [6, 18], Sb^{V} [4, 5], As^{III} [9], As^{V} [9], Pb^{II} [19], Mn^{III} [20], and W^{V} [21]⁵ derivatives show their Q-band at a much longer wavelength. In particular, the large redshifts reported for pnictogen derivatives are noteworthy. These complexes are known to be cationic species⁶ in which the oxidation

³Little structural deformation of the macrocyclic ligand has been found in its crystal structure.

⁴Effects of peripheral substituents on the absorption spectra are discussed in Sect. 4.2.2.

⁵The width of the Q-band is large. Only the absorption maximum wavelength is reported in the literature.

⁶For the Bi^{III} derivatives, the dissociation of axial ligands in solutions has been suggested from electrochemical data [2, 3].

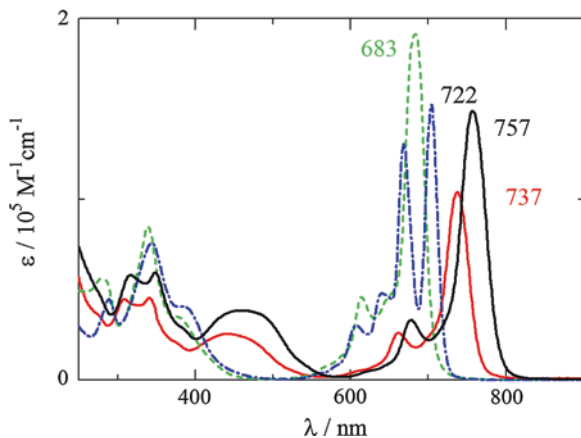


Fig. 3.2 Optical absorption spectra of compounds I (blue dot-dashed line), II (green broken line), III (red solid line), and IV (black solid line). Reprinted from Ref. [1], Copyright 2011, with permission from Elsevier

Table 3.1 Effects of central element on absorption spectra of phthalocyanine derivatives

M ^a	R ^b	P ^c	L ^d	Solvent ^e	λ/nm ^f	Ref.
H ₂				CLN	699Q, 664Q	[16]
Al ^{III}			F ⁻ x2	DCM	662Q, 633, 596, 365, 340, 280	[17]
Ag ^{II}				CLN	677Q, 649, 611, 348	[18]
Ag ^{II}				DCB	685Q, 618, 386, 356	[19]
Ag ^{III}		β4		DCB	722Q, 647, 424, 361: electro-oxidized	[19]
As ^{III}	^t Bu	β4		DCM	767Q; I ₃ salt; not isolated	[9]
As ^V	^t Bu	β4	F ⁻ x2	DCM	727Q, 695sh, 652, 393, 324, 300; PF ₆ ⁻ salt	[9]
As ^V	^t Bu	β4	Cl ⁻ x2	DCM	736Q, 702sh, 666; counter anion unknown	[9]
As ^V	^t Bu	β4	Br ⁻ x2	DCM	737Q, 707sh, 663; counter anion unknown	[9]
Au ^{II}				CLN	662, 633, 601, 348	[20]
Be ^{II}				CLN	692, 681.5, 655, 630.5, 614, 591, 570	[21]
Bi ^{III}			Br ⁻	DMSO	716Q, 645, 415sh, 343	[2, 3]
Bi ^{III}			Cl ⁻	DMSO	716Q, 645, 415sh, 344	[2, 3]
Cd ^{II}				DMSO	677Q, 612, 340	[22]
Co ^I				DMSO	702Q, 669, 640, 533, 432, 387, 320, 293	[23]
Co ^{II}				DMSO	657Q, 596, 327, 298, 270	[23]
Co ^{III}				DMSO	673Q, 607, 427, 352, 284	[23]

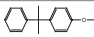
(continued)

Table 3.1 (continued)

M ^a	R ^b	P ^c	L ^d	Solvent ^e	λ /nm ^f	Ref.
Co ^{III}			CN ⁻ x2	DCM	665Q, 636sh, 601, 416, 392sh, 340, 325sh, 272	[24]
Co ^{III}			OH ⁻ x2	DCM	663Q, 630sh, 596, 550sh, 350sh, 335, 295, 265	[25]
Co ^{III}			F ⁻ x2	DCM	663Q, 630sh, 596, 550sh, 340, 285	[25]
Co ^{III}			Cl ⁻ x2	DCM	663Q, 630sh, 596, 550sh, 445sh, 395, 335, 285sh, 275, 270	[25]
Co ^{III}			Br ⁻ x2	DCM	663Q, 630sh, 596, 520, 430, 400, 330, 285	[25]
Cr ^{II}			py x2	PY	687Q, 632, 560, 525, 500, 345	[26]
Cr ^{III}			OH ⁻	CB	689Q, 621, 502, 347	[26]
Cr ^{III}			H ₂ O x2	MeOH	676Q, 610, 502, 477, 344	[26]
Cr ^{III}			F ⁻ x2	DCM	1123, 940, 826, 668Q, 603, 460, 358, 339, and some more weak bands	[27]
Cr ^{III}			Cl ⁻ x2	DCM	1188, 987, 867, 678Q, 611, 485, 405, 369, 344, 305, and some more weak bands	[27]
Cr ^{III}			Br ⁻ x2	DCM	1211, 1005, 883, 683Q, 615, 493, 429, 372, 344, 317, and some more weak bands	[27]
Cr ^{III}			I ⁻ x2	DCM	1244, 1029, 901, 688Q, 621, 501, 472, 400, 383, 345, and some more weak bands	[27]
Cu ^{II}				CLN	678Q, 648, 611, 588, 567, 526, 510, 350	[20, 22]
Er ^{III}			dbm	CLF	679Q, 336; similar spectra were reported for Sm, Eu, Gd, Tb, Dy, Ho, Tm, and Y analogues	[28]
Fe ^I			py	PY	800, 50, 565, 500, 360, 230: electro-reduced	[29]
Fe ^{II}				DCB	820, 758, 654Q, 448sh, 329	[23]
Fe ^{II}			CN ⁻ x2	DCM	664Q, 602, 426, 394, 210	[30, 31]
Fe ^{II}			py x2	DCM	651Q, 591, 412, 328	[30, 31]
Fe ^{II}			Mepy x2	DCM	652Q, 592, 413, 331	[30, 31]
Fe ^{II}			im x2	DCM	657Q, 596, 423, 339	[30, 31]
Fe ^{II}			Meim x2	DCM	658Q, 597, 423, 338	[30, 31]
Fe ^{II}			pip x2	DCM	659Q, 598, 425, 340	[30, 31]
Fe ^{II}			NH ₃ x2	DCM	661Q, 601, 425, 332	[30, 31]

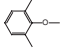
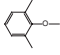
(continued)

Table 3.1 (continued)

M ^a	R ^b	P ^c	L ^d	Solvent ^e	λ/nm^f	Ref.
Fe ^{II}			CO/NH ₃	DCM	659Q, 596, 363, 317, 288	[30, 31]
Fe ^{III}			CN ⁻ x2	DCM	780, 686Q, 645, 613, 601, 550, 541, 513, 445, 429, 407, 394, 346, 317, 298, 273, 260	[30, 31]
Ga ^{III}			Cl ⁻	PY	684Q	[32]
Ge ^{II}				PY	655Q, 602, 445, 330	[33]
Ge ^{IV}			OR ⁻ x2 ^g	CYHX	668Q, 353, 343, 330sh	[34]
Hf ^{IV}			F ⁻ x3	DCM	676Q, 645sh, 613, 562, 345, 286	[35]
Hg ^{II}			CH ₃	BZ	721, 654, 440, 342, 285: Hg-binuclear complex	[36]
Hg ^{II}			CH ₃	THF	724Q Hg-binuclear complex	[37]
In ^{III}			ONO ⁻ x2 <i>cis</i>	DCM	683Q, 649sh, 615, 587sh, 362sh, 348, 247	[38]
In ^{III}			F ⁻ x2 <i>cis</i>	DCM	680Q, 649sh, 617, 571sh, 357, 336sh, 287, 245; likewise for L = Cl ⁻ , CN ⁻ , HCOO ⁻	[39]
Ir ^I				^t PrOH	633Q, 606, 578, 538, 391, 311, 286sh, 265sh	[40]
Ir ^{III}			Cl ⁻ x2	DCM	641Q, 617sh, 581, 543sh, 478, 413, 339, 303, 281	[41]
Ir ^{III}			Br ⁻ x2	DCM	642Q, 581, 485, 415, 375, 303, 281, 249	[41]
Ir ^{III}			I ⁻ x2	DCM	644Q, 581, 437, 420sh, 308, 279	[41]
Ir ^{III}			OH ⁻ x2	DCM	638Q, 579, 412, 308, 267	[41]
K ^I				EtOH	670Q, 596	[42]
Li ^I				DMA	667Q, 641, 604, 370, 332	[16]
Li ^I			CN ⁻ x2	DMSO	665Q, 636, 600, 378, 326: Li ₂ (pc)	[16]
Li ^I				DCM	665Q, 601, 376, 329, 268: Li(^t Bu ₄ N)(pc)	[15]
Li ^I				PY	667Q, 645sh, 638sh, 605, 442, 385, 327: HLi(pc)	[43]
Lu ^{III}			CH ₃ CO ₂ ⁻	DCB	672Q, 606, 344	[44, 45]
Mg ^{II}			H ₂ O x2	DCM	670Q, 642, 606, 345, 282	[46]
Mg ^{II}				DMSO	672Q, 607, 345	[22]
Mg ^{II}				CLN	678Q, 611.5	[22]
Mn ^{II}			(CH ₃ CH ₂) ₃ N x2	DMF	916, 862, 671Q, 641sh, 581sh, 380, 332	[47]
Mn ^{II}			CN ⁻ x2	DCM	894, 754, 672Q, 634, 615, 560, 498, 439, 391, 346sh, 326, 278, and some more weak shoulders	[48]
Mn ^{III}			CN ⁻ x2	DCM	807, 657Q, 629sh, 597, 547, 482, 450, 393, 383, 333sh, 313, and some more weak shoulders	[48]

(continued)

Table 3.1 (continued)

M ^a	R ^b	P ^c	L ^d	Solvent ^e	λ/nm^f	Ref.
Mn ^{III}			O ₂ ⁻	DMA	705Q, 678sh, 634, 495, 417, 355, 295	[49]
Mn ^{III}			OH ⁻	DMA	717Q, 646, 503.5, 359	[49]
Mn ^{III}	^t Bu	β 4	CH ₃ CO ₂ ⁻	DMF	1311, 1200, 1074, 716Q, 682sh, 645, 497, 420sh, 368	[47]
Mo ^{II}			CN ⁻ x2	AC	667Q, 606	[50]
Mo ^{III}			Br ⁻ x2	DCM	1401, 1161, 695, 631, 592, 535, 498, 351, 267: no Q-band-like absorption band	[15]
Mo ^{IV}			O ²⁻	TCB	703Q, 643	[51]
Mo ^{IV}			O ²⁻	PY	710Q, 652	[51]
Mo ^{IV}			?	DMSO	670s, 640, 605, 385, 330: electro-reduced	[52]
Mo ^V			O ²⁻ /OH ⁻	DMSO	690Q, 660, 625, 340	[52]
Mo ^V			O ²⁻ /OH ⁻	DCB	700s, 660, 633	[52]
Nd ^{III}			CH ₃ CO ₂ ⁻	DCB	673Q, 610, 344	[44, 45]
Ni ^{II}				CLN	670Q, 642, 603, 580	[16]
Os ^{II}			CO/py	CLF	632Q, 575	[53]
Os ^{II}			py x2	CLF	616Q, 563, 460, 436, 416, 369, 308	[54]
Os ^{II}			CN ⁻ x2	DCM	612Q, 564sh, 484, 456, 441, 430, 389, 338, and many other weak shoulders	[55]
Os ^{II}			Cl ⁻ x2	DCM	618Q, 572sh, 522, 489, 454, 416, 397, 325, and many other weak shoulders	[55]
Os ^{III}			Cl ⁻ x2	DCM	634Q, 578sh, 472, 431, 407, 326, 305sh, and many other weak shoulders	[56]
P ^V	^t Bu	β 4	O ²⁻ /OH ⁻	CLF	680Q, 615, 350	[57]
P ^V		β 4	O ²⁻ /OH ⁻	EtOH	683Q, 614, 390, 347, 292	[59]
P ^V		β 4	OH ⁻ x2	EtOH	707Q, 636, 410, 341, 299	[59]
P ^V			OH ⁻ x2	PY	669Q, 640, 602, 353	[58]
P ^V	^t Bu	β 4	OH ⁻ x2	PY	677Q, 648, 609, 353	[58]
P ^V	ⁿ BuO	α 8	CH ₃ O ⁻ x2	DCM	889Q (Fig)	[10]
Pb ^{II}				DMSO	702Q, 632.5, 336	[22]
Pb ^{II}				CLN	714Q, 664, 430, 342	[60]
Pd ^{II}				CLN	660.5Q, 633, 595, 576.5, 557, 347	[61]
Pt ^{II}				CLN	652Q, 624, 588, 564.5, 545	[21]
Re ^{III}			F ⁻ x2	DCM	1048, 709sh, 667Q, 641, 606, 368sh, 339, 271, and many shoulders	[52]

(continued)

Table 3.1 (continued)

M ^a	R ^b	P ^c	L ^d	Solvent ^e	λ/nm^f	Ref.
Re ^V			N ³⁻	CLN	700Q, 630, 364	[63]
Rh ^I				^t PrOH	645Q, 617sh, 585, 455, 439, 333	[40]
Rh ^{II}			py x2	DMF	661Q, 632, 598, 372, 326	[64]
Rh ^{III}			OH ⁻ x2	DCM	649Q, 625sh, 588, 345, 327sh, 291 and many other shoulders; likewise for derivatives of L=Cl ⁻ , Br ⁻ , I ⁻ , N ₃ ⁻ , CN ⁻ , NCO ⁻ , SCN ⁻ , SeCN ⁻	[65]
Rh ^{III}			L x2 ^h	AN	ca. 650Q, and many other weak shoulders in 250–500 nm	[66]
Ru ^{II}			py x2	DCM	622Q, 567, 375, 315	[67]
Ru ^{II}			dmf x2	DMF	622Q, 568, 382, 312	[67]
Ru ^{II}			CO/dmso	DCM	645Q, 583, 344, 293	[67]
Ru ^{II}			CO/dmf	DCM	638Q, 575, 344, 291	[68]
Ru ^{II}			pyrazine x2	CB	641Q, 587, 442, 376sh, 314, 268	[68]
Sb ^{III}				DCM	754Q, 677, 385, 347, 286; I ₃ ⁻ salt; not isolated	[69]
Sb ^{III}	^t Bu	β 4		DCM	762Q, 723sh, 683, 397, 353, 285; I ₃ ⁻ salt	[6]
Sb ^{III}				EtOH	729Q, 660, 381, 338, 257; not isolated	[7]
Sb ^V			F ⁻ x2	DCM	719Q, 691sh, 648, 402sh, 375, 328, 302, 269; PF ₆ ⁻ salt	[70]
Sb ^V			Cl ⁻ x2	DCM	726Q, 693sh, 652, 403sh, 374, 350, 328, 308, 279; PF ₆ ⁻ salt	[4]
Sb ^V	^t Bu	β 4	Cl ⁻ x2	DCM	739Q, 703sh, 663, 433.5sh, 402.5, 350.5, 312; ClO ₄ ⁻ salt	[5]
Sb ^V			Br ⁻ x2	DCM	729Q, 370; PF ₆ ⁻ salt	[71]
Sb ^V			OH ⁻ x2	DCM	710Q, 681, 639, 371, 347, 304, 275; PF ₆ ⁻ salt	[69]
Si ^{IV}			Cl ⁻ x2	PY	699Q, 627, 367, 314	[72]
Si ^{IV}			OH ⁻ x2	PY	671Q, 641.5, 604	[72]
Si ^{IV}			OH ⁻ x2	BZ	672Q, 642, 605, 355	[72]
Si ^{IV}			OR ⁻ x2 ⁱ	BZ	668.5Q, 638, 604, 353, 330sh,	[72]
Si ^{IV}			OR ⁻ x2 ^j	CYHX	665Q, 351, 341, 331sh	[34]
Sn ^{II}				EtOH	682, 616, 359, 302, 238	[60]
Sn ^{IV}			F ⁻ x2	CLN	700Q, 669.5sh, 631, 359.5	[73]
Sn ^{IV}			Cl ⁻ x2	CLN	702.5Q, 672.5, 632, 364	[73]
Sn ^{IV}			Cl ⁻ x2	CLN	701Q, 630, 363	[22]
Sn ^{IV}			Br ⁻ x2	CLN	705.5Q, 677.5, 635.5, 369.5	[73]
Sn ^{IV}			I ⁻ x2	CLN	710Q, 677.5sh, 639, 369	[73]
Th ^{IV}			acac x2	BN	684Q, 617, 353	[74]
Ti ^{IV}			O ²⁻	CLN	698Q, 630	[22]

(continued)

Table 3.1 (continued)

M ^a	R ^b	P ^c	L ^d	Solvent ^e	λ/nm^f	Ref.
Tl ^I				DCM	694Q, 667sh, 629, 585, 352, 337sh, 292	[75]
Tl ^{III}			ONO ⁻ x2 <i>cis</i>	DCM	690Q, 654sh, 621, 575, 361, 345, 288	[75]
U ^{IV}			acac x2	BN	689Q, 620, 351	[74]
V ^{IV}			O ²⁻	CLN	700Q, 631	[22]
V ^{IV}			O ²⁻	DMSO	685Q, 618.5, 346.5, 290	[22]
W ^{IV}	^t Bu	β 4	O ²⁻	TOL	725sh, 674.5Q, 611sh, 356.5	[76]
W ^V			N ³⁻	CLN	751Q, 699.5, 673.5, 359.5: broad Q-band	[76]
W ^V	^t Bu		N ³⁻	TOL	745Q, 677, 365; broad Q-band	[76]
Y ^{III}			Ph ₃ PO/Cl ⁻ /py <i>cis</i>	DCM	671Q, 606, 342, 283, 240	[77]
Zn ^{II}				CLN	672Q	[78]
Zn ^{II}			CN ⁻	DMA	669Q, 386, 331, 274	[79]
Zn ^{II}				DSMO	672Q, 607,345	[23]
Zn ^{II}			F ⁻	DCM	667Q, 633, 603, 425sh, 365sh, 335, 275	[17]
Zn ^{II}				DMF	667Q, 602, 335	[80]
Zr ^{IV}			Cl ⁻ x2	DCM	692Q, 660sh, 625, 350, 271	[81]
Zr ^{IV}			Cl ⁻ x3	DCM	680Q, 647sh, 613, 585, 342	[81]
Zr ^{IV}			F ⁻ x3	DCM	Numerous data are not provided (essentially the same as those of Hf ^{IV} analogue)	[35]

^aCentral element^bPeripheral substituent (basically, the macrocyclic ligand has no substituent unless otherwise noted)^cPositions and numbers of the substituents (β 4 means that each isoindole unit has one substituent at the β position (see Fig. 1.12 for the meaning of β 4 and α 8))^dAxial ligands and their number (when the number is more than one, two of them take a trans conformation unless otherwise noted); the uncommon abbreviations represent the following ligands: *acac* acetylacetonate (2,4-pentanedionate); *dbm* 1,3-diphenyl-1,3-propanedionate; *dmf* N,N-dimethylformamide (coordinated DMF); *dms* dimethylsulfoxide; *im* imidazole; *Meim* methylimidazole; *Mepy* methylpyridine; *pip* piperidine; *py* pyridine^eThe uncommon abbreviations represent the following solvents: *AC* acetone; *AN* acetonitrile; *BN* benzonitrile; *BZ* benzene; *CB* chlorobenzene; *CLF* chloroform; *CLN* 1-chloronaphthalene; *CYHX* cyclohexane; *DCB* 1,2-dichlorobenzene; *DCM* dichloromethane; *DMA* dimethylacetamide; *iPrOH* isopropyl alcohol (2-propanol); *PY* pyridine; *TCB* 1,2,4-trichlorobenzene; *TOL* toluene^fThe "Q" and "sh" after the figures denote the Q-band peak wavelength and shoulder absorption, respectively^g(L x2) = (H₂O x2), (Cl⁻/CH₃OH), (Br⁻/CH₃OH), (I⁻/CH₃OH)^hR = SiCH₃(OSi(CH₃)₃)₂ⁱR = Si(Si(CH₃)₃)(CH₃)₂^jR = SiCH₃(OSiMe₃)₂

number of the metal ion and the total negative charges of the surrounding ligands are not cancelled. This can be because the innermost 16-membered ring is directly affected by the residual positive charge. On the other hand, there is no clear correlation between the oxidation number of the central metal ion and the Q-band position. For example, with respect to $[\text{Fe}(\text{pc})(\text{CN})_2]^{-/2-}$, the Q-band of the Fe^{III} derivative appears at a longer wavelength (685 nm) than the Fe^{II} counterpart (677 nm) [24]. In contrast, the Sb^{III} complex has its Q-band at a longer wavelength (762 nm [6]) than the corresponding Sb^{V} analog ligating two chloride ions as axial ligands (739 nm [5]). Furthermore, the Q-bands of cobalt derivatives appear in the following order: Co^{I} (702 nm) > Co^{III} (673 nm) > Co^{II} (657 nm) [23].

The effects of axial ligands on absorption spectra are generally small unless they bridge more than one chromophore (Sect. 3.2.4.2) or the axial ligands themselves have a sufficiently large transition dipole moment [82], as mentioned later. In particular, the effects on the Q-band position are small; for example, the Q-band of $[\text{Co}(\text{pc})\text{L}_2]^-$ (where $\text{L} = \text{F}^-$, Cl^- , Br^- , OH^- , or CN^-) complexes appears in the range of 663–665 nm [24, 25]. Complexes of Cr^{III} , $[\text{Cr}(\text{pc})\text{L}_2]^-$ ($\text{L} = \text{F}^-$, Cl^- , Br^- , or I^-), show a relatively large dependence, but the magnitude of the shifts is at most $100\text{--}400\text{ cm}^{-1}$ (5–6 nm) [27]. This is also the case for complexes of the main group elements; small shifts are observed for $[\text{Sn}(\text{pc})\text{L}_2]$ (Table 3.1; $\text{L} = \text{F}^-$, Cl^- , Br^- , or I^-) [73]. In contrast, P^{V} derivatives are subject to a large dependence on axial ligands. Q-band positions are normal for $[\text{P}(\text{tbpc})(\text{O})(\text{OH})]$ and are typical of those of zinc and copper complexes [57]. Unsubstituted and octasubstituted analogues show essentially the same spectra [58].⁷ On the other hand, P^{V} derivatives bearing two methoxy groups as axial ligands have a significantly redshifted (by ca. 1900 cm^{-1}) Q-band [10, 11]. Note that the chromophores in the former species are neutral while those in the latter two are cationic. This difference can give rise to the shift of the Q-band. This speculation is further supported by recent work on P^{V} derivatives with 2,6-dimethylphenoxy groups as peripheral substituents (see Fig. 3.1b), $[\text{P}(\text{tppc})(\text{OH})(\text{O})]$ [59]. The Q-band of this compound appears at a normal wavelength (683 nm) in an ethanolic solution, whereas it is significantly redshifted (707 nm) upon protonation (Fig. 3.3a). The appearance of a Faraday A-term in the magnetic circular dichroism (MCD) spectrum (Fig. 3.3b) indicates that the C_4 symmetry is maintained throughout the protonation; hence, one of the two axial ligands has accepted the proton but not at a meso nitrogen atom.⁸ It is also noteworthy that cationic As^{V} , Sb^{V} , and Bi^{III} derivatives show a significantly redshifted Q-band.

As an exceptional example, it has been reported that the Ti^{IV} complex bearing a biphenyldioxy group as an axial (apical) ligand, which is transparent in the visible

⁷Although the authors of Ref. [58] have identified their compounds as $[\text{P}(\text{Pc})(\text{OH})_2]\text{OH}$ in their report, a neutral composition is considered more likely on the basis of experimental lines of evidence provided in the later report [57]. Note that both papers reported the same tetra-*tert*-butyl derivative.

⁸Protonation at meso nitrogen atom(s) gives rise to a significant redshift and splitting of the Q-band (Sect. 3.2.5.2).

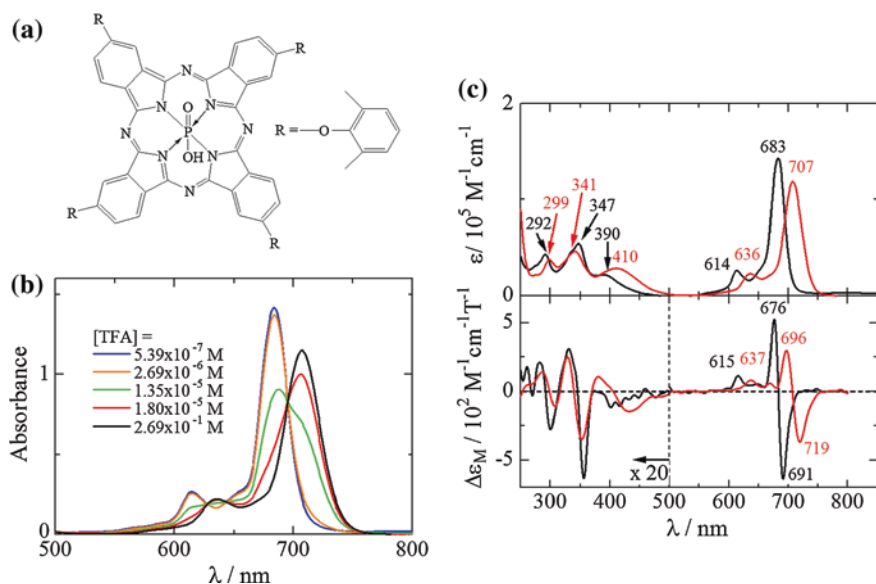
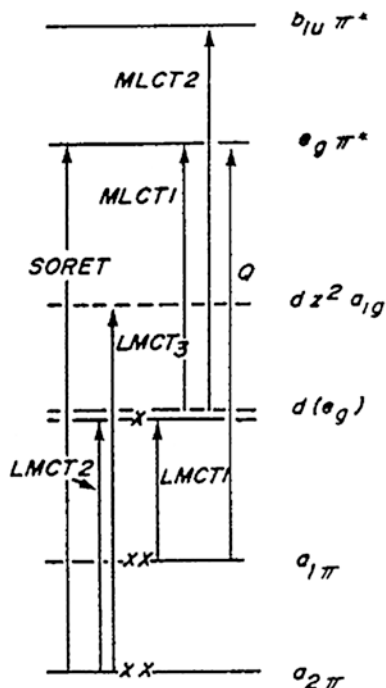


Fig. 3.3 **a** Structure of [P(tppc)(O)(OH)], **b** optical absorption spectra of ethanolic solutions containing [P(tppc)(O)(OH)] in the presence of various concentrations of TFA (trifluoroacetic acid), and **c** optical absorption (*top*) and MCD (*bottom*) spectra of [P(tppc)(O)(OH)] in EtOH (*black*) and those of [P(tppc)(OH)₂]⁺ in EtOH containing TFA. Reproduced from Ref. [59], Copyright 2013, with permission from World Scientific Publishing Company

region, shows split Q-bands [82]. This splitting has been attributed to the lifting of the degeneracy of the Q-band owing to the difference in magnitude of the interaction between the transition dipole moment of the biphenyldioxy group and either of the degenerate Q-band transition dipole moments.

The effects of a central metal ion or axial ligands on the absorption spectra are more clearly seen in the “window” spectral region rather than the Q-band or Soret-band regions. In Sect. 2.1.1, it has been stated that the optical absorption spectra of Zn^{II} complexes may be regarded as prototypical. This is because a Zn^{II} ion has a closed shell; hence, its d electrons (orbitals) do not contribute to electronic transitions, allowing us to observe only π - π^* transitions. Mg^{II} complexes also exhibit prototypical absorption spectra for the same reason. Even though the metal ion has an open shell, their spectra are close to prototype unless they are redox-inactive (e.g., Cu^{II} or Ni^{II}). With respect to complexes of redox-active transition metal ions, electronic transitions from an occupied (or singly occupied) d orbital to π^* orbitals in the macrocyclic ligand (MLCT, *metal to ligand charge transfer*) and those from an occupied π orbital to empty (or singly occupied) d orbitals (LMCT; *ligand to metal charge transfer*) can be observed (Fig. 3.4) [47]. Therefore, complexes of redox-active transition metal ions, such as those of chromium, manganese, iron, cobalt, ruthenium, and rhodium, can show one or more extra absorption bands in addition to the prototypical spectrum (i.e., in the 400–600 nm region and/or above the Q-band position, which are the “window” regions for complexes of closed-shell metals). In particular, complexes absorbing light in the range of

Fig. 3.4 Scheme of energy levels in a typical metallophthalocyanine, showing the origin of the various LMCT, MLCT, Q, and Soret bands discussed in the text. Reprinted from Ref. [47], Copyright 1981, with permission from the American Chemical Society



450–600 nm can appear more yellowish or reddish, because our eyes are the most sensitive to light of 555 nm wavelength (Fig. 1.1). Note that such complexes can show a nonblue color owing to the presence of such a charge-transfer band if, in particular, their Q-band is considerably redshifted for some reasons (i.e., owing to the effects of peripheral substituents or something else). As d orbitals of the central metal are deeply involved in such CT bands, the characteristics of its axial ligand(s) (i.e., as a σ -donor, π -donor, or π -acceptor) on the metal ion, which contribute little to the Q-band position (π - π^* transition), may give rise to large effects on the position and/or intensity of the CT bands. As an example, low-spin Fe^{II} complexes, $[\text{Fe}(\text{pc})\text{L}_2]$ (where L denotes an axial ligand as shown below), show an extra band in the spectral range of 400–450 nm (Fig. 3.5 [30]). The position of the extra band depends on the basicity (as a σ -donor) of the axial ligand and tends to red shift in the order of increasing basicity (Table 3.1; [30]); $\text{L} = \text{CN}^- < \text{methyl imidazole} < \text{piperidine} < \text{imidazole} < \text{pyridine} < \text{methyl pyridine} < \text{CO/NH}_3$. This band has been assigned as an MLCT band from degenerate $d(e_g)$ (d_{xz} and d_{yz}) orbitals to a nondegenerate π^* orbital (Fig. 3.6) on the basis of MCD study [i.e., the appearance of the Faraday A-term in the same spectral range (Fig. 3.5)] and electrochemical determination of their oxidation (metal-centered) and reduction (where the macrocyclic ligand is involved) potentials⁹ [30]. In the

⁹The MLCT transition can be understood as the simultaneous occurrence of metal-centered oxidation, Fe^{II} to Fe^{III} , and ligand-centered reduction, pc^{2-} to pc^{3-} . In contrast, LMCT can be understood as the simultaneous occurrence of metal-centered reduction and ligand-centered oxidation [47].

Fig. 3.5 Optical absorption (*top*) and MCD (*bottom*) spectra of the Fe^{II} phthalocyanine complex [Fe(pc)(NH₃)₂] in DMSO at room temperature. Reproduced from Ref. [23] with permission from The Royal Society of Chemistry

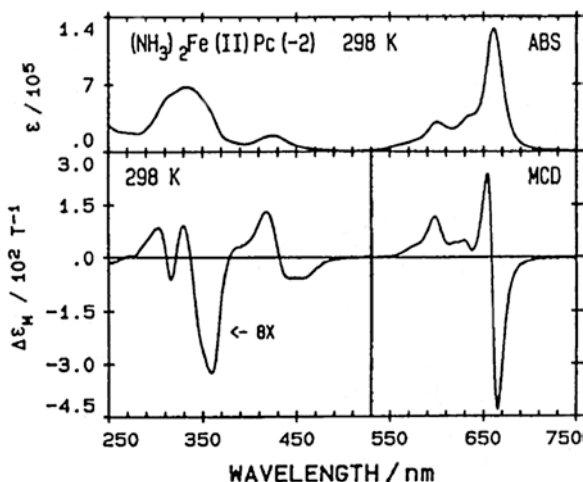
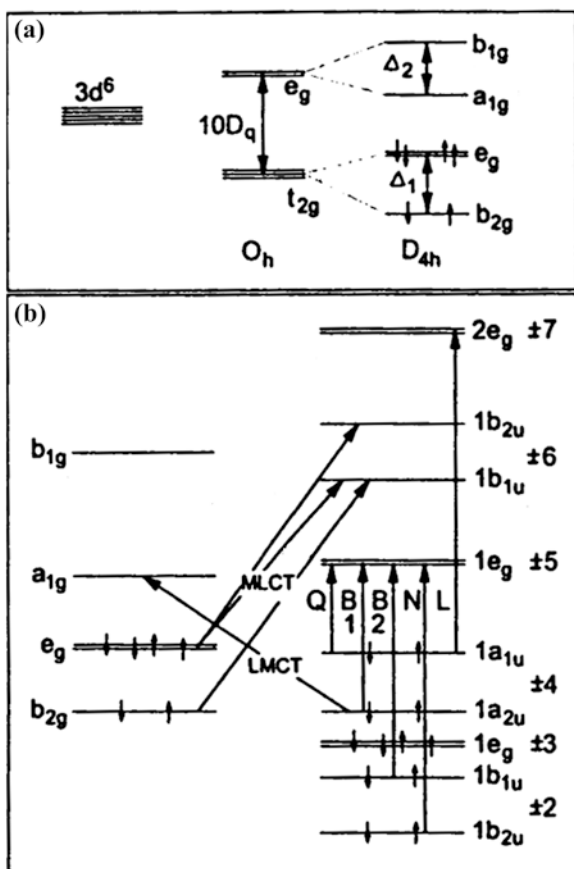


Fig. 3.6 Scheme of energy levels in a low-spin Fe^{II}-phthalocyanine, showing the origin of the various LMCT, MLCT, Q, and Soret bands discussed in the text. Reproduced from Ref. [23] with permission from The Royal Society of Chemistry



Fe^{III} derivative, as one electron has been removed from the degenerate $d(e_g)$ orbitals, electronic transitions from low-lying π orbitals (for example, a_{1u} and a_{2u}) to the $d(e_g)$ orbitals are allowed. Therefore, many more absorption bands are observed for the Fe^{III} complex and its spectrum is relatively complicated [31]. Although much less common, the position of a CT band can be very close to that of the Q-band or Soret band. In this case, their shape can depend on the nature of the axial ligand(s) on the central metal. As an example, the absorption spectra of the Ru^{II} complexes $[\text{Ru}(\text{pc})(\text{piperidine})_2]$ and $[\text{Ru}(\text{pc})(\text{CO})(\text{dmf})]$, where dmf denotes dimethylformamide (DMF) as a ligand (Fig. 3.7), are significantly affected by the axial ligands [12, 83]. In the absorption spectrum of the piperidine derivative, its Q-band is considerably broadened. The MCD spectrum in the same spectral region shows an unsymmetrical Faraday A-term, suggesting the presence of a negative Faraday B-term of comparable intensity, and hence the presence of another absorption band (which is considered as a CT band, although not clearly assigned yet). Another extra band is observed at approximately 350 nm, which may also be a CT band [12]. In contrast, the Q-band of the other complex ligating carbonyl is relatively well isolated from the other bands, indicating that the carbonyl ligation has given rise to a significant shift of the CT band away from the Q-band. Although the presence of a CT band in the Soret region is unclear in the absorption spectrum, an intense Faraday B-term, which is uncommon for the other (normal) metal complexes, is seen at approximately 350 nm, indicating the

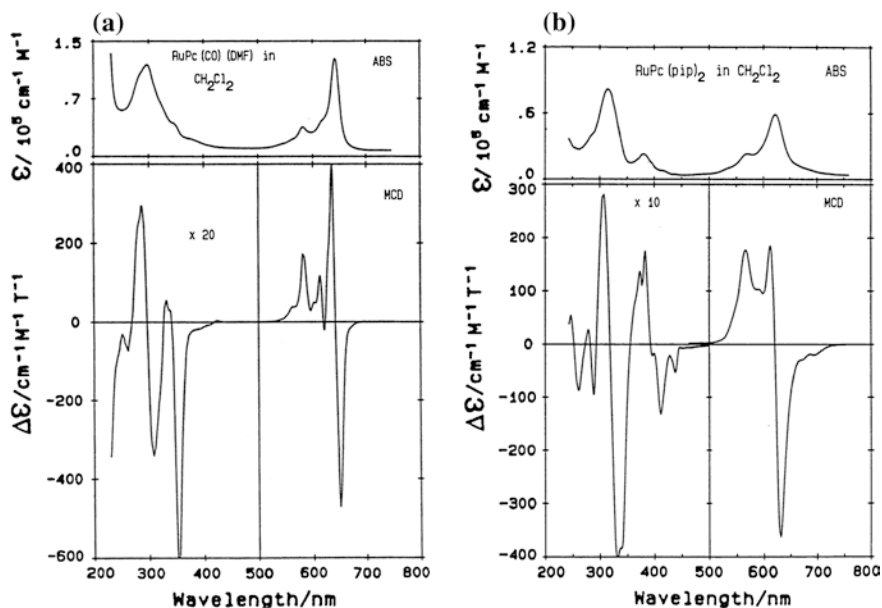
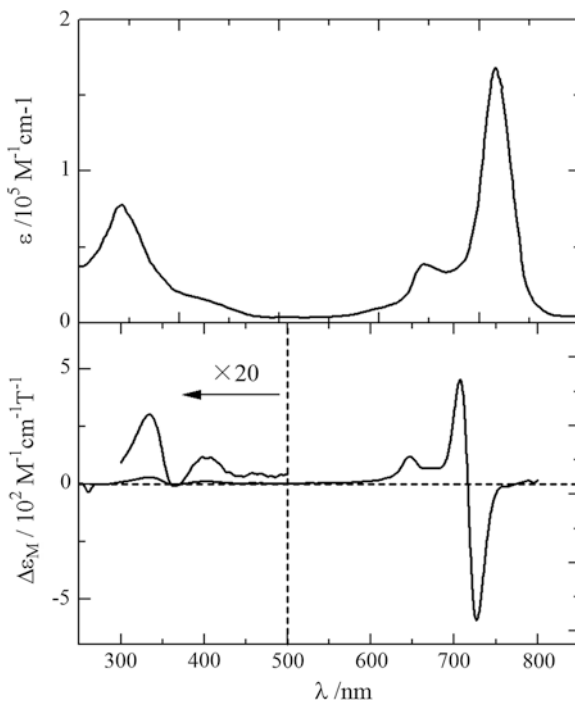


Fig. 3.7 **a** Optical absorption (*top*) and MCD (*bottom*) spectra of $[\text{Ru}(\text{pc})(\text{CO})(\text{dmf})]$ and **b** those of $[\text{Ru}(\text{pc})(\text{piperidine})_2]$ in dichloromethane. Unpublished results of T. Nyokong (Rhodes University, South Africa) and Martin J. Stillman (University of Western Ontario, Canada) and reproduced with their permission

Fig. 3.8 Optical absorption (*top*) and MCD (*bottom*) spectra of [Bi(pc)Br] in DMF. Reprinted from Ref. [3], Copyright 1994, with permission from the Chemical Society of Japan



presence of the CT band in this region. Thus, the absorption spectra of these Ru^{II} complexes are dominated by CT absorption bands as well as the π - π^* transition (e.g., Q- and Soret bands), and hence are subject to strong effects of axial ligands.

Complexes of main group elements with a lower oxidation state (Tl^I [75], Sn^{II} [60], Ge^{II} [33], Pb^{II} [41], As^{III} [9], Sb^{III} [6, 8], and Bi^{III} [2, 3]) have an extra band at a red flank of their Soret band, with comparable intensity (Fig. 3.8). Their spectra are dissimilar to those of the same elements but with a higher oxidation state,¹⁰ which show a prototypical spectrum (except for the significant red shift of absorption bands for As^V [9] and Sb^V derivatives [1, 4, 5, 18]). The appearance of an additional band near the Soret band is also known for porphyrin derivatives of the same elements with a lower oxidation state [84, 85], which are referred to as “hyper porphyrins”. For these hyper porphyrins, the extra band is assigned as a transition from a lone pair (p_z ; a_{2u}) orbital of the central element to the π^* orbital (e_g) of the macrocyclic ligand (i.e., an MLCT band in character) [84, 85]. Unlike the MLCT band of the hyper porphyrins, the extra bands observed for phthalocyanine derivatives are considerably broadened and not well isolated from their Soret bands. Assuming that this assignment can also be applied to the corresponding phthalocyanine derivatives, such a transition must be doubly degenerate, as is the case for Soret and Q-band transitions. Nevertheless, MCD studies on Sb^{III} [6] and

¹⁰Derivatives of lead and bismuth with a higher oxidation state are unknown.

Bi^{III} [3] have not provided convincing experimental evidence to prove the degeneracy of the transition. No clear assignment of this extra band has been given.

Some transition metal derivatives (for example, Cr^{III} , Mn^{II} , Mn^{III} , Cu^{II} , etc.) are known to show a very weak absorption band, which is attributed to a triplet-multiplet transition [47], although such bands are generally very weak. Note that a German group has reported a Mo^{III} complex that shows an absorption spectrum dominated by intense triplet-multiplet transitions [15], as briefly mentioned above.

3.2.2 Effects of Peripheral Substituents

A number of phthalocyanines and related macrocyclic compounds with various substituents on the periphery have been synthesized so far from the viewpoints of improving their solubility in common organic solvents or water and tuning of their physical properties, such as the wavelength of maximum optical absorption or the redox potentials of the macrocycle [86]. Spectral data of many substituted phthalocyanines have been reported by Luk'yanets [87] and Kobayashi and Fukuda [14]. However, because of their different solubilities in common organic solvents depending on the substituents and the different purposes of syntheses, their spectra have been reported for different metal complexes or in different solvents. To underline the effects of substituent groups on the optical absorption spectrum of the macrocyclic dyes (particularly the position of their Q-band), spectral data for complexes of the same metal element measured in the same solvents have been extracted and are shown in Table 3.2 [88–115]. In this table, “ $\alpha 4$ ”, “ $\alpha 8$ ”, “ $\beta 4$ ”, and “ $\beta 8$ ” denote the positions and numbers of the peripheral substituents on an

Table 3.2 Effects of peripheral substituents on the Q-band position

M^{a}	R^{b}	P^{c}	solvent ^d	$\lambda_{\text{max}}(\text{Q})/\text{nm}^{\text{e}}$	Ref.
Zn			PY	672	[22]
			CLN	672	[78]
			THF	665.5	[88, 89]
			DCM	671 ^f	[79]
			DMF	667	[80]
	tBu	$\beta 4$	CLF	678	[90]
			TOL	677	[90]
			BZ	678	[91, 92]
	Ph	$\beta 4$	CB	694	[93, 94]
			CLN	698	[93, 94]
	NO_2	$\beta 4$	THF	671.0	[95]
			THF	669.2	[95]
	CH_3O	$\beta 4$	CB	680	[96, 97]
			CB	707	[96, 97]

(continued)

Table 3.2 (continued)

M ^a	R ^b	P ^c	solvent ^d	$\lambda_{\max}(\text{Q})/\text{nm}^e$	Ref.	
	ⁿ BuO	$\beta 4$	THF	674.5	[89, 95]	
		$\beta 8$	THF	671.5	[89]	
		$\alpha 4$	THF	696	[89, 95]	
		$\alpha 8$	PY	758	[89, 95]	
	PhO	$\beta 4$	CB	681	[98, 99]	
		$\alpha 4$	CB	694	[98, 99]	
	PhS	$\beta 4$	CB	692	[98, 99]	
		$\alpha 4$	TCB	715	[98, 99]	
	Ph SO ₂	$\beta 4$	THF	676.7	[95]	
		$\alpha 4$	THF	664.0	[95]	
	CN	$\beta 8$	DMF	687	[100]	
		$\beta 8$	DMF	694	[80]	
	Co	^t BuC \equiv C–	$\beta 8$	DCM	711	[101]
				PY	658	[102]
			DCM	665	[83, 103]	
			CLN	670	[61]	
			DMSO	657	[23]	
^t Bu		$\beta 4$	PY	662	[102]	
NO ₂		$\beta 4$	PY	677	[102]	
		$\beta 4$	CLN	691	[104, 105]	
		$\alpha 4$	CLN	670	[104, 105]	
		$\alpha 4$	DMSO	654	[85]	
MeO		$\beta 8$	PY	655	[102]	
^t BuC \equiv C		$\beta 8$	DCM	701	[101]	
Cu		H		CLN	678	[78]
				DMF	668	[106]
	^t Bu	$\beta 4$	CLN	684	[107]	
		$\beta 4$	NB	683	[107]	
		$\beta 4$	TOL	677	[107]	
		$\beta 4$	DMSO	675	[107]	
		$\beta 4$	PN	671	[91, 92]	
	Ph	$\beta 4$	CB	691	[93, 94]	
		$\beta 4$	CLN	695	[93, 94]	
	Cl	$\beta 4$	CLN	679	[108]	
		$\alpha 4$	CLN	690	[108]	
		$\alpha 8$	CLN	705	[108]	
	CF ₃ S	$\beta 4$	CB	679	[109, 110]	
		$\alpha 4$	CB	682	[109, 110]	
		$\beta 8$	CB	687	[109, 110]	

(continued)

Table 3.2 (continued)

M ^a	R ^b	P ^c	solvent ^d	$\lambda_{\max}(\text{Q})/\text{nm}^e$	Ref.
	CF ₃ SO ₂	β 4	CB	682	[109, 110]
	NO ₂	α 4	CLN	680	[104, 105]
		α 4	DMF	666	[93, 94]
	(CH ₃) ₂ N	β 4	DMF	730	[111, 112]
		α 4	DMF	778	[111, 112]
	MeO	β 4	CB	678	[85]
		α 4	CB	702	[85]
	PhO	β 4	CB	678	[98, 99]
		α 4	CB	694	[98, 99]
	PhS	β 4	CB	692	[98, 99]
		α 4	CB	718	[98, 99]
	CN	β 8	DMF	686	[100]
	SO ₃ Na	β 4	DMF	666	[113]
	(CH ₃) ₂ NSO ₂	β 4	DMF	671	[114, 115]
		α 4	DMF	662	[114, 115]

^aCentral element

^bPeripheral substituent (basically, the macrocyclic ligand has no substituent unless otherwise noted)

^cPositions and numbers of the substituents (e.g., β 4 means that each isoindole unit has one substituent at the β position; see Fig. 1.12)

^dThe uncommon abbreviations represent the following solvents: *BZ* benzene; *CB* chlorobenzene; *CLF* chloroform; *CLN* 1-chloronaphthalene; *DCM* dichloromethane; *NB* nitrobenzene; *PN* *n*-pentane; *PY* pyridine; *TCB* 1,2,4-trichlorobenzene; *TOL* toluene

^eQ-band peak wavelength

^fThe central metal ion ligates an imidazole molecule as an axial ligand

isoindole moiety (Fig. 1.12). Unlike octasubstituted phthalocyanines, which are single isomers, tetrasubstituted derivatives are mixtures of four regioisomers on the basis of the positions of the substituents. However, we may assume that they are single isomers because the difference in spectra between the isomers is generally very small [116].

3.2.2.1 Electronic Effects

Table 3.2 shows the following trends: (1) electron-donating substituents generally more or less give rise to the redshift of the Q-band; (2) electron-withdrawing substituents generally have little effect on the position of the Q-band unless their

π -electrons or lone-pair electrons take part in the expansion of the π -conjugation system of the macrocycle; (3) substituents of which π -electrons or lone-pair electrons contribute to the expansion of the π -conjugation system of the macrocycle give rise to a significant redshift of the Q-band; (4) the effects of a given substituent at the α position are generally much greater than those of the same group at the β position; (5) the effects of substituents are not always additive.

There is no clear correlation between the Q-band position and the common parameter, such as Hammett's sigma (σ) values. For example, although that of the 2, 2-dimethylbutynyl ($t\text{BuC} \equiv \text{C}-$) group is close to zero at the β -position [101], it gives rise to a large redshift (by ca. $100 \text{ cm}^{-1}/\text{group}$) of the Q-band [117, 118]. In contrast, although $-\text{SO}_2\text{N}(\text{CH}_3)_2$ is a strong electron-withdrawing group, it has little effect on the Q-band position regardless of whether it is located at the α or β position [114, 115]. Therefore, mesomeric effects seem greater than inductive effects (either electron-donating or electron-withdrawing).

In particular, the presence of substituents capable of contributing to the π -conjugation system of the macrocycle at α positions gives rise to a significant redshift of the Q-band [119]. A redshift of the Q-band driven by the $-\text{N}(\text{CH}_3)_2$ group at the α position, which is greater than that of the same group at the β -position, is interpreted in terms of the participation of lone-pair electrons of the nitrogen atoms in the π -system of the macrocycle [119]. A phenyl group at the α position is known to give rise to the redshift of the Q-band (692 nm in chloroform; nickel derivative), whereas the shift is much smaller (675 nm in the same solvent) when the dihedral angle between the phthalocyanine macrocycle and the phenyl group is close to 90° [120]. It is rather surprising that the Q-band position of the tetranitro-derivative, which has substituents at α positions, is essentially the same as that of the unsubstituted derivative; hence, the magnitude of the shift is smaller than that of the β -isomer. Morley et al. [119] have reported, on the basis of their molecular orbital calculation, that the $-\text{NO}_2$ groups at α positions are not coplanar with the macrocycle. They have suggested that the presence of the coplanar $-\text{NO}_2$ group would give rise to a redshift of the Q-band by 8 nm per group.

When one macrocycle has more than one substituent, it is of interest if their effects on the Q-band position are additive. In some cases, such as *tert*-butyl [121] and alkynyl groups [117, 118], their effects can be additive. However, this is not always true, particularly when substituents are at α positions. Kobayashi and coworkers have exemplified the nonlinearity of substituent effects on the Q-band position of a number of *n*-butoxy-substituted phthalocyanines [89].

On the other hand, substituent effects on the Soret band are considered less significant than those on the Q-band [89]. However, unlike the Q-band, which is composed of an essentially pure HOMO-LUMO¹¹ transition, the Soret band is a mixture of more than one degenerate $\pi-\pi^*$ transition (see Sect. 2.2.10). Therefore, it is difficult to say that the effects of substituents on the absorption bands in the Soret region have been sufficiently investigated. Recently, the

¹¹Refer to Sect. 1.1.4 for the definition of HOMO and LUMO.

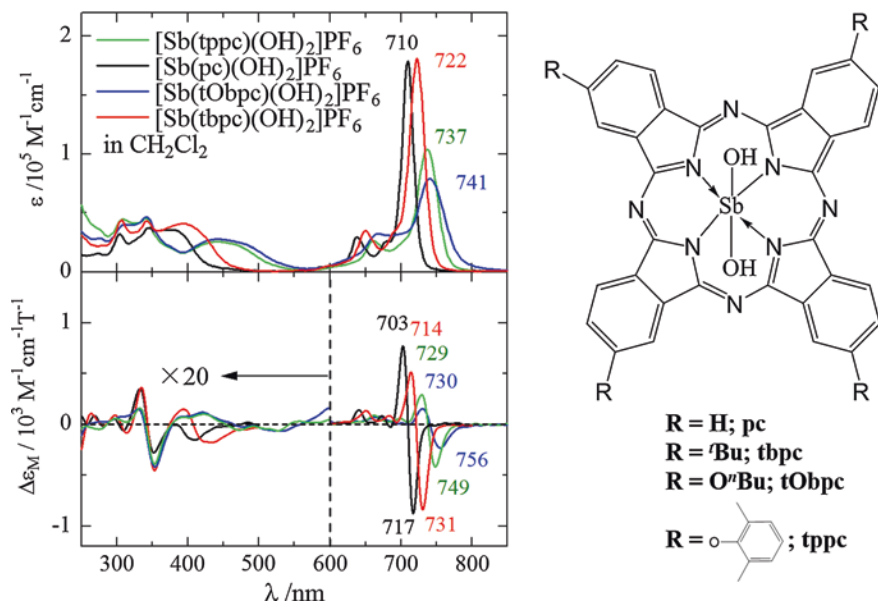


Fig. 3.9 Optical absorption (*top*) and MCD (*bottom*) spectra of Sb^V complexes of β -tetra-substituted and unsubstituted phthalocyanines bearing hydroxides as their axial ligands in dichloromethane. Reprinted from Ref. [1], Copyright 2011, with permission from Elsevier

author's group has reported a significantly large redshift of absorption bands in the Soret region [1]. Figure 3.9 shows the optical absorption and MCD spectra of Sb^V complexes of tetra- β -substituted (including unsubstituted) phthalocyanines bearing the same axial ligands (OH). Attention should be paid to the broad band that appears in the spectra (400–550 nm) of the *n*-butoxy (tObpc)- and 2,6-dimethylphenoxy (tppc)-substituted derivatives, which is not observed for *tert*-butyl-substituted (tbpc) or unsubstituted (pc) analogues. In contrast, a similar broad band that appears in the spectra (350–450 nm) of the latter two derivatives is not observed for the former two. Interestingly, the peak position of the broad band is redshifted in the order of H < *tert*-butyl < 2,6-dimethylphenoxy \approx *n*-butoxy, as is the case for the Q-band position. On the basis of the solvent dependence of this band and the similarity of the corresponding MCD spectra (Fig. 3.9, bottom) as well as the substituent-dependent redshift [1], these bands have been assigned as being of the same origin (B1/B2). Note that the broad band observed for the amber-colored phthalocyanines mentioned above (Fig. 3.2) has been likewise assigned [1]. It is also noteworthy that the absorption bands at approximately 300 and 350 nm, which involve degenerate transition(s),¹² are minimally affected by the peripheral substituents. These bands are tentatively assigned as degenerate N and L bands, which have been theoretically predicted [69], in order of ascending energy. It is

¹²A sharp Faraday A-term is observed in each corresponding MCD spectrum.

noteworthy that these degenerate transitions of higher energy are not normally observed in common organic solvents, although the presence of such bands in this spectral region is expected from theoretical works (Sect. 2.2.10). This is because these bands are generally hidden in an intense absorption of UV rays by the solvents used. Nevertheless, the significant redshift of the absorption bands of Sb^{V} complexes allows us to see them in common solvents.

3.2.2.2 Steric Effects

Cook and coworkers synthesized two metal-free phthalocyanines that are substituted by eight long unbranched $-(\text{CH}_2)_4\text{CH}_3$ and branched $-(\text{CH}_2)_2\text{CH}(\text{CH}_3)_2$ alkyl chains (at α positions), and compared their crystal structures and optical absorption spectra [122]. They found that the former macrocycle is essentially planar whereas the latter one is considerably distorted from planarity and is saddle-shaped. The Q-band positions of the latter (731 and 701 nm in THF) were slightly redshifted as compared with those of the former (728 and 696 nm) in the same solvent. When the neighboring two isoindole moieties were substituted by bulky groups, the macrocycle was distorted from planarity to reduce the steric hindrance between the substituents. Thus, the distortion of the macrocyclic ligand can have an effect on the absorption spectrum. Later, Kobayashi et al. synthesized a more significantly distorted metal-free phthalocyanine by introducing eight phenyl groups into the α positions [123]. Metal complexes of the distorted phthalocyanine had a significantly redshifted (by ca. 1500 cm^{-1}) Q-band [124]. However, in this case, as the dihedral angle between the phenyl group and the macrocycle was ca. 45° [123], participation of the phenyl groups in the π -conjugation system of the macrocycle can contribute to the redshift. Therefore, the large redshift of the Q-band can be due to both effects.

3.2.3 Effects of Ring Expansion, Contraction, and Symmetry Lowering

3.2.3.1 Effects of Ring Expansion and Contraction

Expansion of the π -conjugation system by fusing benzo groups on the periphery of the macrocycle and its contraction by removing them give rise to a significant redshift and blue shift of the Q-band position, respectively. We have learned in the previous chapter that the Q-band of the phthalocyanine derivative appears at a longer wavelength than that of the tetraazaporphyrin analogue (Sect. 2.1.2¹³).

¹³Note that the fusion of benzo groups to the periphery of TAP derivatives (i.e., ring expansion from TAP to Pc) contributes not only to the expansion of the π -conjugation system but also to enhancing the imbalance between the two highest occupied frontier orbitals (a_{1u} and a_{2u}). See Sect. 2.2.7.

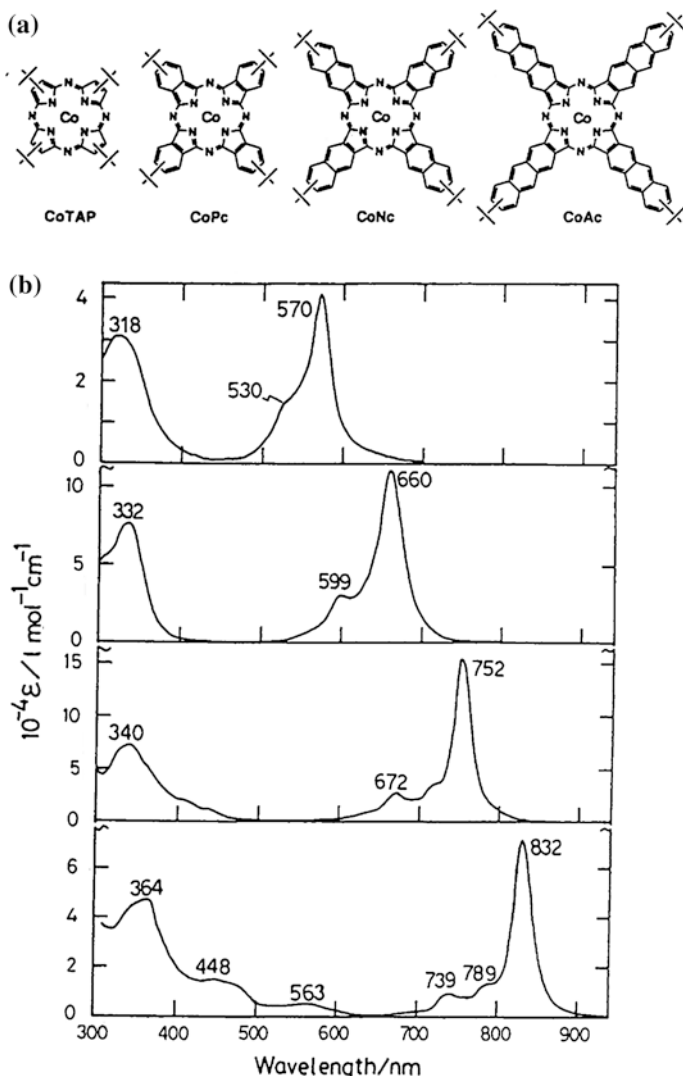
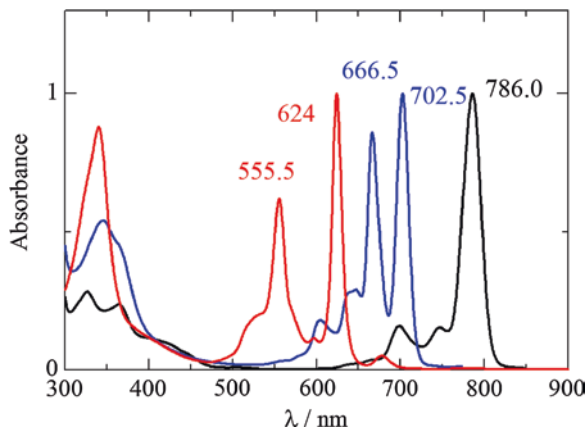


Fig. 3.10 **a** Structures of Co^{II} derivatives of tetraazaporphyrin (CoTAP), phthalocyanine (CoPc), naphthalocyanine (CoNc), and anthracyanine (CoAc), which all have four *tert*-butyl groups on their periphery to improve their solubility in common organic solvents, and **b** their optical absorption spectra in pyridine. Reprinted from Ref. [125], Copyright 1993, with permission from Elsevier

Kobayashi and coworkers reported the optical absorption and MCD spectra of Co^{II} complexes of tetra-*tert*-butyl-substituted tetraazaporphyrin (TAP), phthalocyanine (Pc), naphthalocyanine (Nc), and anthracocyanine (Ac) (Fig. 3.10a–d, respectively) [124]. All the compounds show a single Q-band (and a Faraday A-term in the spectral range) because of their C_4 symmetry with the peak position redshifted

Fig. 3.11 Optical absorption spectra of metal-free tetraazaporphyrin (*red*), phthalocyanine (*blue*), and naphthalocyanine (*black*) in 1,2-dichlorobenzene. Note that all the macrocycles have four *tert*-butyl groups on their periphery to improve their solubility in common organic solvents. H. Isago and H. Fujita, unpublished results



in order of the size of the macrocyclic ligand (TAP (570 nm in pyridine) < Pc (660) < Nc (752) < Ac (832)). In contrast, the spectra of their metal-free derivatives are dependent on the macrocycle size. The spectra of H₂TAP and H₂Pc show twin peaks due to symmetry lowering because of the presence of imino protons in the cavity (Sect. 2.2.9), whereas that of H₂Nc shows a single peak (Fig. 3.11), although the center of the Q-bands is redshifted with an increase in the size of the macrocycle in common with their Co^{II} complexes. The magnitude of the splitting of the Q-bands (i.e., Q_x and Q_y bands) decreases with increasing size of the macrocycle, i.e., H₂TAP (1976 cm⁻¹ in 1,2-dichlorobenzene) > H₂Pc (769 cm⁻¹) > H₂Nc (≈0 cm⁻¹). Kobayashi et al. have reported that the absorption spectrum of H₂Ac is similar to that of H₂Nc in pyridine, although the former peak position is redshifted as compared with the latter by 1110 cm⁻¹ [125]. Thus, it seems that the symmetry-lowering effect of the imino proton becomes less significant as the π-conjugation system of the macrocycle is expanded.

3.2.3.2 Effects of Symmetry Lowering

When the expansion of the π-conjugation system is not concentric (Fig. 3.12 left), the optical absorption spectra of the macrocycles show split Q-bands (Fig. 3.12 right) unless they have C₄ symmetry [88, 127]. This is easily interpreted in terms of the lifting of degeneracy of the LUMO (e_g under D_{4h} symmetry) upon symmetry lowering of the π-conjugation system. Interestingly, the absorption spectrum of compound **2**, which is a structural intermediate between the phthalocyanine (ZnPc in Fig. 3.12 left) and naphthalocyanine (ZnNc) derivatives, shows a single Q-band despite its C_{2v} symmetry (and hence the absence of a degenerate electronic transition) with an intermediate intensity between the two derivatives and with its peak position at an intermediate wavelength between the two (Fig. 3.12 right). A similar phenomenon has been reported for a structural intermediate

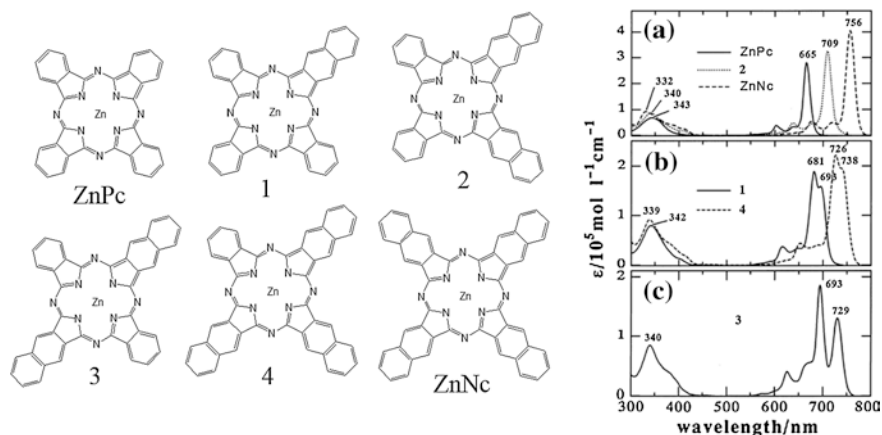


Fig. 3.12 Molecular structures of zinc complexes of phthalocyanine (*ZnPc*), naphthalocyanine (*ZnNc*), and four nonsymmetrically benzo-substituted phthalocyanines (1 benzo[*b*]phthalocyanine; 2 dibenzo[*b,k*]phthalocyanine; 3 dibenzo[*b,t*]phthalocyanine; 4 tribenzo[*b,k,t*]phthalocyanine) and their optical absorption spectra in THF. Reprinted from Ref. [88], Copyright 1992, with permission from the Chemical Society of Japan

between phthalocyanine and tetraazaporphyrin derivatives (Sect. 3.2.3.3) [128]. The findings with respect to the structural intermediates may appear inexplicable, but the splitting of the Q-band (or its absence) owing to the expansion of the π -conjugation system and the magnitude of the splitting can be interpreted without exception using symmetry-adapted perturbation (SAP) theory [127, 129]. As SAP theory is not discussed in this monograph, interested readers should refer to the original articles [127], which are visually enjoyable although readers need at least a basic knowledge of group theory. The theoretical absorption spectra of various metallated and metal-free phthalocyanines and their ring-expanded or ring-contracted derivatives have been predicted on the basis of computational molecular orbital calculations within the framework of the PPP approximation [129]. It seems that the calculated spectra qualitatively reproduce the experimental spectra.

3.2.3.3 Accidental Degeneracy and Pseudo Faraday A-Term in MCD Spectrum

As stated in Sects. 3.2.3.1 and 3.2.3.2, some macrocycles of C_2 symmetry (e.g., H_2Nc , compound 2 in Fig. 3.12 left) show a single Q-band despite the lack of C_4 symmetry. It may be of interest if the transition can be degenerate or not, although any electronic transition cannot be degenerate under C_2 symmetry in a strict sense. Figure 3.13a (bottom) shows the optical absorption spectra of Cu^{II} complexes of phthalocyanine and tetraazaporphyrin derivatives ($CuBoPc$ and $CuTAP$, respectively) as well as their structural intermediate 1 (Fig. 3.13b). Compound 1 shows a

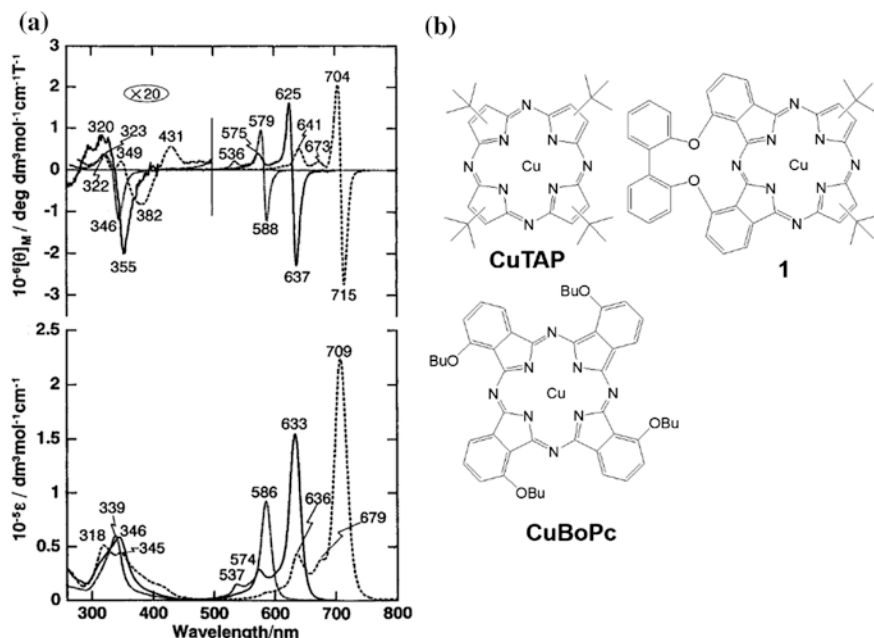


Fig. 3.13 a Optical absorption (*bottom*) and MCD (*top*) spectra of **b** CuTAP, CuBoPc, and their structural intermediate **1** in chloroform. Reprinted from Ref. [128], Copyright 1999, with permission from the American Chemical Society

single Q-band in common with the TAP and Pc derivatives, the macrocycles of which have C_4 symmetry. The peak intensity is intermediate between those of the other two, and its peak position is also located midway between the two. Surprisingly, its MCD spectrum (Fig. 3.13a; top) in the Q-region shows an *s*-shaped curve with its center at the absorption peak wavelength [128] as if the transition was degenerate despite its C_{2v} symmetry. This is also the case for the structural intermediate between Zn^{II} complexes of phthalocyanine and naphthalocyanine derivatives [130].¹⁴ Note that the MCD spectrum of metal-free naphthalocyanine (Fig. 3.10c) in the same solvent shows an *s*-shaped curve with its center at the absorption maximum wavelength [126]. Computational MO calculations predict the presence of two nondegenerate electronic transitions around the Q-region [128–130] with their separation much smaller ($100\text{--}300\text{ cm}^{-1}$) than the band widths of normal Q-bands. Therefore, the two transitions are essentially degenerate (accidental degeneracy); hence, such transitions can show a derivative-shaped curve such as that of a Faraday A-term as a result of an overlap of two B-terms of opposite sign (*pseudo*-A-term). Generally, the intensity of Faraday B-terms is

¹⁴It has been mentioned in Sect. 3.2.3.2 that the appearance of a single Q-band for the structural intermediate of the phthalocyanine and naphthalocyanine derivatives (compound **2** in Fig. 3.12 right) was predicted using SAP theory.

smaller than that of the A-term; however, in this case, the B-terms gain their intensity from the small energy gap between the two states.¹⁵ Thus, even though the molecular symmetry is lower,¹⁶ *pseudo-A* terms can be observed in MCD spectra when the magnitude of the splitting between the LUMO and the next LUMO is sufficiently small.

3.2.4 Interaction Between Chromophores

When two or more macrocycles are close to each other, regardless of whether they are chemically bonded or not, the observed optical absorption spectra, particularly in the Q-band region, are generally different from the superposition of the spectra of the monomers. The spectral changes can be due to the interaction between the transition dipole moments of each chromophore (when the distance between the macrocycles is larger than the van der Waals distance of 3.4 Å) or due to the overlapping of their π -conjugation systems (when the distance <3.4 Å).

3.2.4.1 Spectral Changes Associated with Molecular Aggregation

Before discussing the interaction between chromophores, it should first be noted that the optical absorption spectrum of phthalocyanines can be dependent on their concentration. Chemists working with phthalocyanines may often encounter such a phenomenon in their laboratories. The deviation of the spectrum from the “prototypical” monomer spectrum significantly depends on how the macrocycles are aligned, as described in the next subsection (Sect. 3.2.4.2). Figure 3.14 shows the optical absorption spectra of the Co^{II} complex of octakis(3,3-dimethyl-1-butynyl) phthalocyanine (Fig. 3.14 right), which is highly soluble in common organic solvents, in dichloromethane solutions at various concentrations [101]. Although this compound shows a prototypical Q-band in a very dilute solution (ca. 10^{-6} M), the apparent Q-band intensity decreases with increasing concentration, and a new absorption band appears at the blue flank of the Q-band. The inset of Fig. 3.14 clearly indicates that the Q-band intensity does not obey Lambert-Beer’s law. Such a phenomenon is common in the solution chemistry of phthalocyanines [101, 117, 131–133] and has been interpreted in terms of molecular aggregation, that is, the formation of dimers, trimers, or aggregates of higher order.¹⁷ Some

¹⁵As mentioned in Sect. 2.2.8, the intensity of B-terms is larger as the two excited states are closer in energy.

¹⁶States can be degenerate when the molecular symmetry is not lower than C_3 .

¹⁷Only monomers and dimers contribute to the absorption spectra (Fig. 3.14) within this concentration range because sharp isosbestic points are seen in the spectral changes; hence, the two species are in equilibrium.

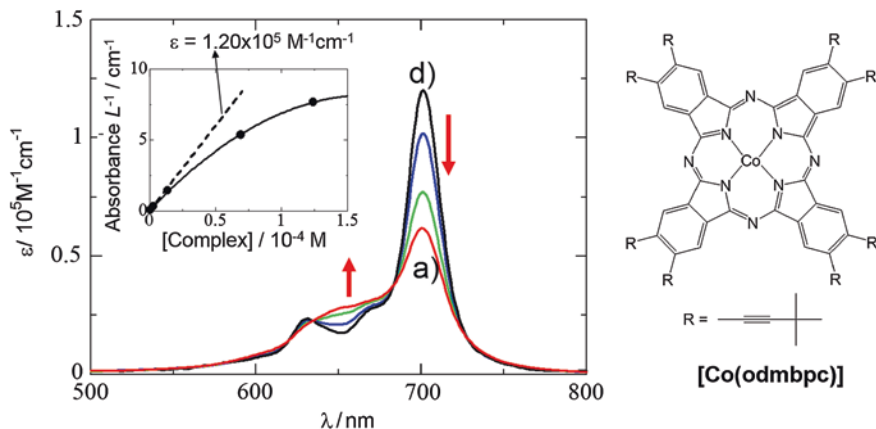


Fig. 3.14 Optical absorption spectra of Co^{II} complex of octakis(3,3-dimethyl-1-butynyl)-substituted phthalocyanine in dichloromethane at various concentrations (*a* 1.24×10^{-4} M; *b* 6.93×10^{-5} M; *c* 1.39×10^{-5} M; *d* 2.77×10^{-6} M). The inset shows Beer's plots (absorbance at the monomer Q-band maximum wavelength), in which the slope of the broken line exhibits the molar extinction constant of the complex monomer. The red arrows indicate the changes in molar absorptivity with increasing concentration. Reprinted from Ref. [101], Copyright 1998, with permission from the Chemical Society of Japan

types of solvent can effectively induce aggregation even at very low concentrations ($\sim 10^{-6}$ M).¹⁸ In this case, the absorption band appears at the higher-energy side of the Q-band, and this manner of aggregation is referred to as “H-aggregation”. In H-aggregates, the macrocycles are aligned in a face-to-face manner (Fig. 3.15b) similarly to a pile of saucers. With respect to phthalocyanines, we most often encounter this type of aggregation because of their planar molecular structure.

In contrast, aggregates of some phthalocyanines show their absorption band on both sides of their Q-band (Fig. 3.16) [134] or occasionally, on the lower-energy side of their Q-band alone (Fig. 3.17) [6]. In these cases, the macrocycles are aligned in a “slipped face-to-face” manner (Fig. 3.15b, c). Such aggregates are

¹⁸The author has learned through his activities as a scientist and an article reviewer that a considerable number of people (including experts) believe that highly aggregating phthalocyanines are poorly soluble in common solvents or that highly soluble phthalocyanines are nonaggregating. However, this is not always true. For example, the octa(alkynyl)-substituted derivative in Fig. 3.14 is highly soluble (its solubility reaches almost 10^{-2} M) but it also aggregates even in dilute solutions (ca. 10^{-5} M) as illustrated above. On the other hand, the Sb^{V} complex of unsubstituted Pc is not very soluble (at most, 10^{-4} M) whereas its aggregation could not be detected by optical absorption spectroscopy using an optical cell of 1 mm path length up to the upper limit of the concentration range studied. Thus, having good solubility is one thing and being nonaggregating is another, at least with respect to phthalocyanines.

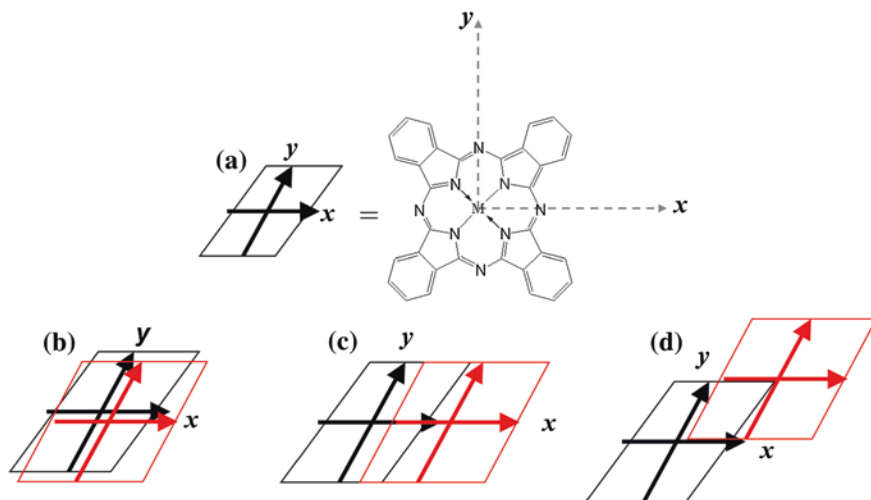


Fig. 3.15 Some common stacking manners observed for phthalocyanine derivatives: **a** monomer; **b** face-to-face stacking; **c** slipped face-to-face stacking (along x-axis); **d** slipped face-to-face stacking (along both axes). The two crossing *arrows* represent two orthogonal transition dipole moments

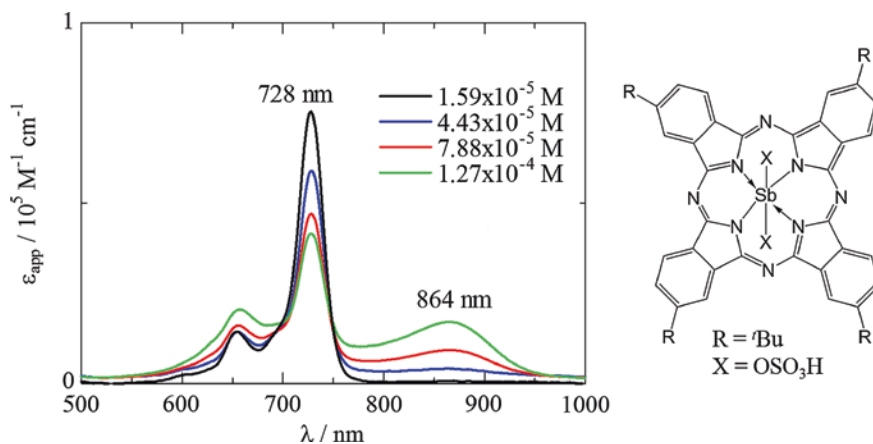


Fig. 3.16 Optical absorption spectra of $[\text{Sb}(\text{tbpc})(\text{SO}_4\text{H})_2]^+$ at various concentrations in water solutions containing Triton X-100 (2% w/v). Below $1.59 \times 10^{-5} \text{ M}$, the complex is free from aggregation under these conditions. Reprinted from Ref. [134], Copyright 2012, with permission from Elsevier

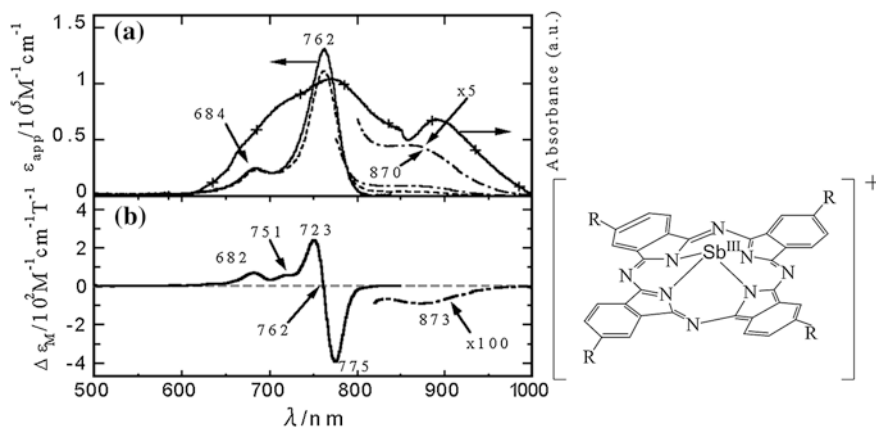


Fig. 3.17 Optical absorption (*top*) and MCD (*bottom*) spectra of Sb^{III} complex of tetra-*tert*-butyl phthalocyanine in dichloromethane at various concentrations. Reproduced from Ref. [6] with permission from The Royal Society of Chemistry

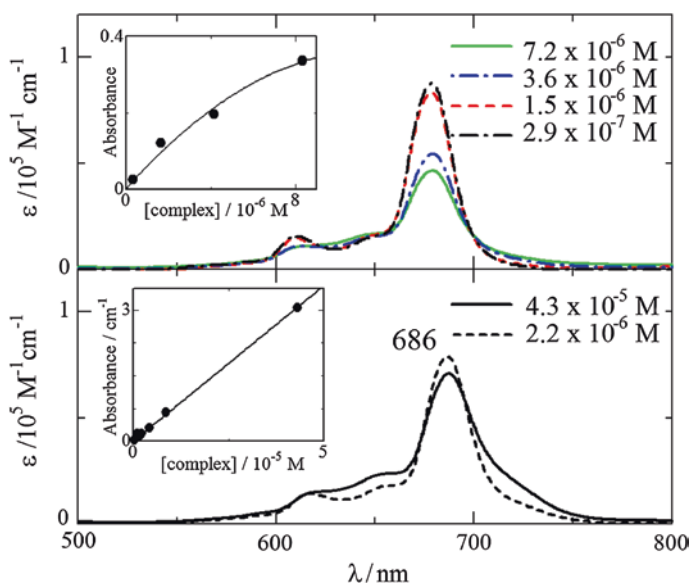


Fig. 3.18 Optical absorption spectra of $[\text{P}(\text{tppc})(\text{O})(\text{OH})]$ in acetonitrile (*top*), and dichloromethane solutions at various concentrations. The insets depict plots of absorbance at the Q-band maximum wavelength versus concentration. Reproduced from Ref. [59], Copyright 2013, with permission from World Scientific Publishing Company

referred to as J-aggregation.¹⁹ We have much less opportunity to observe this type of aggregation unless the metal ion of the macrocyclic ligand has axial ligands to sterically prevent H-aggregation or the peripheral substituents are capable of coordination to the central metal ion in the cavity of another macrocycle.

The relationship between the spectra of the aggregates and the alignment of the chromophores can be understood in terms of exciton coupling theory [135], as described in the next subsection (Sect. 3.2.4.2).

Note that the linear concentration dependence of the Q-band intensity is not necessarily sufficient to show that a given compound is free from aggregation in the solvent. The author has reviewed articles for a number of journals and has seen many researchers concluding that their compounds were free from aggregation in some specific solvents on the basis of a linear Lambert-Beer plot alone.²⁰ This may be true for some cases because the linear dependence indicates an insignificant contribution from aggregated species in the concentration range studied. Here, an example is given of a case where a linear Lambert-Beer plot was obtained for a specific phthalocyanine dye, even though it aggregates in the same solvent. Figure 3.18 shows the optical absorption spectra of a P^V complex (the same compound as that shown in Fig. 3.3) in acetonitrile and dichloromethane solutions at various concentrations. In acetonitrile, clear spectral changes are observed in a narrow concentration range, and the absorbance-concentration correlation gives a convex curve (top inset of Fig. 3.18). Therefore, one can easily conclude that the compound aggregates in the solvent. On the other hand, in dichloromethane, the Lambert-Beer plot appears linear up to 4.3×10^{-5} M (bottom inset of Fig. 3.18). Nevertheless, a careful comparison of the absorption spectra at 4.3×10^{-5} M and a much more dilute solution shows a clear spectral difference: i.e., the apparent Q-band intensity decreases and the absorbances at both flanks of the Q-band intensify [59], as is the case for J-aggregation. Thus, it is risky to exclude the possibility of aggregation on the basis of the linear Lambert-Beer plots alone. This can happen when the dimerization constant of the dye of interest is relatively small because the deviation from the linear regression line due to aggregation is comparable to the scatter deviation of the data owing to experimental errors generated during the preparation of the solutions. Even if a linear correlation is obtained, a few (several, if possible) spectra should be compared with each other in terms of molar absorptivity, as shown in Figs. 3.14, 3.16, 3.17,

¹⁹J-aggregates show their main band at a red flank of the monomer band, but the converse is not necessarily true. A number of phthalocyanines show an additional band at a wavelength longer than that of the monomer Q-band owing to acid-base equilibria involving the macrocycle (Sect. 3.2.5.2), electron transfer (Sect. 3.2.6.1), etc. Special care has to be taken when assigning such extra bands at longer wavelengths as “J-aggregates” particularly in the case of nondonor solvents (Sect. 3.2.5.2).

²⁰Readers are reminded that the Lambert-Beer plot must include the zero point because the absorbance attributed to the compound must be zero when its concentration is zero. Nevertheless, a number of authors have concluded a lack of aggregation of their compounds on the basis of the linear Lambert-Beer plot within a narrow concentration range excluding the zero point. The same plot including the zero point could be nonlinear.

and 3.18, but not in terms of absorbance (those of the highest and lowest concentrations inclusive). In addition, the concentration range to be studied should be as wide as possible (two orders of magnitude if the other conditions allow).

3.2.4.2 Exciton Coupling of Nondegenerate Transitions

First of all, we consider the interaction between two rodlike dye molecules in close proximity ($>3.4 \text{ \AA}$ so that the effects of the overlap of π -clouds between the two molecules are negligible) for simplicity. We assume that the transition dipole is generated along the long axis of the molecule [recall that an optically excited molecule has a vector (Sect. 2.2.1)]. In this model, we do not need to consider the degeneracy of their transitions. Figure 3.19 shows a schematic diagram of exciton coupling between the two excited molecules aligned in various manners. When the two rods are parallel to each other, the two transition dipoles can be parallel or antiparallel (Fig. 3.19a). In this arrangement, the parallel configuration gives rise to the destabilization of the excited state ($S_{2'}$) relative to that of the monomer (S_1) owing to the repulsion between the dipoles (similarly to that between two magnets). This excited state is allowed because the dipole moment is nonzero (in fact, it is doubled); hence, intense optical absorption is expected to be observed on the higher-energy side of the monomer band. In contrast, the antiparallel configuration leads to a forbidden excited state because the two dipoles offset each other. This state is stabilized ($S_{1'}$) relative to that of the monomer because of the attractive interaction between the two dipoles. Hence, no intense absorption band is expected to be observed on the red side of the monomer band. Thus, two chromophores in this arrangement show their new absorption band only on the blue flank of their monomer band. This type of assembly is referred to as the H-aggregate (Cf. Sect. 3.2.4.1).

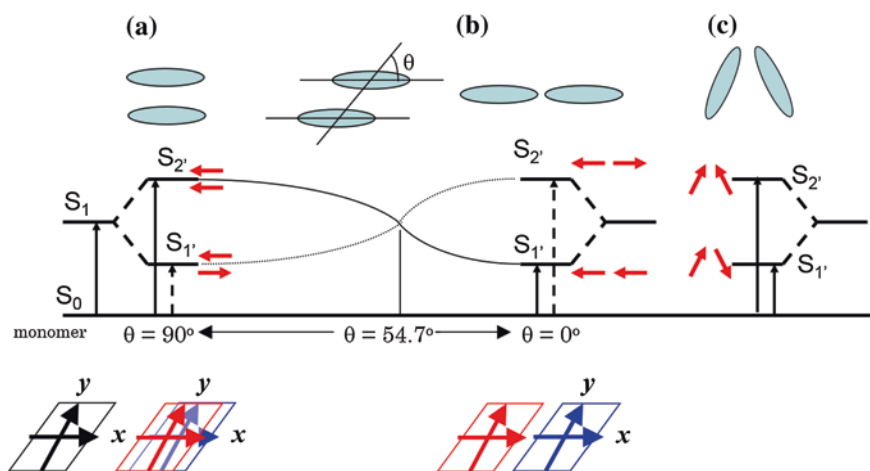


Fig. 3.19 Schematic diagram of exciton coupling between two chromophores stacked in various manners. *Source* NIMS eSciDoc—IMEJI. © Hiroaki Isago with CC-BY-NC 3.0 license

When two dye molecules are aligned in a head-to-tail manner (Fig. 3.19b), parallel and antiparallel configurations likewise generate dipole-allowed and dipole-forbidden excited states, respectively. However, in this case, the parallel and antiparallel configurations give rise to stabilization ($S_{1'}$, due to their attractive interaction) and destabilization ($S_{2'}$, due to repulsion) of the excited states, respectively, relative to that of the monomer. Consequently, only the $S_{1'}$ state is allowed; hence, the absorption band of the aggregated species appears at the red flank of the monomer band. This type of assembly is referred to as the J-aggregate.

Coplanar inclined transition dipoles lead to the exciton energy diagram shown between Fig. 3.19a, b, which continuously covers the variation of angle θ between the polarization axis and the line passing through the molecule centers from $\theta = 0^\circ$ (corresponding to Fig. 3.19b) to $\theta = 90^\circ$ (corresponding to Fig. 3.19a). The exciton band splitting ΔE in this case is given by the formula

$$\Delta E = \frac{2M^2(1 - 3\cos^2\theta)}{r^3} \quad (3.1)$$

M and r denote the magnitude of the transition moment for the singlet-singlet transition in the monomer (i.e., S_0 - S_1) and the center-to-center distance between the molecules, respectively. ΔE becomes zero for $\theta = 54.7^\circ$, where $\cos^2\theta = 0$, i.e., the dipole-dipole interaction is zero for this orientation of transition moments in the aggregate, regardless of the intermolecular distance. That is, the two molecules behave as an H-aggregate above 54.7° and as a J-aggregate below this angle.

Oblique transition dipoles in a dimer lead to the energy diagram shown in Fig. 3.19c. In this case, the antiparallel (along the vertical direction) arrangement of transition dipoles for the monomer is attractive and leads to the stabilization of the excited state ($S_{1'}$) relative to that of the monomer, and the parallel arrangement is repulsive and causes the destabilization of the excited state ($S_{2'}$). The transition moments from the ground state to the excited states of the dimer are both non-vanishing: their moments are nonzero along the vertical direction in the $S_{2'}$ state and along the horizontal direction in the $S_{1'}$ state.

As the description of exciton coupling theory in this monograph is superficial, readers who are interested in this theory should refer to Kasha's original paper [135].

3.2.4.3 Cofacial Dimers of Phthalocyanine and Degeneracy of Their Transitions

In the previous subsection, the interaction between nondegenerate electronic transitions was described. However, the transitions of interest in phthalocyanines or porphyrins (Q and Soret bands) are doubly degenerate. Therefore, we need to consider two orthogonal dipole moments instead of a single dipole moment. Here again, we take the C_4 axis as the z-axis and hence the molecular plane as the xy plane. With this convention, the optical absorption around the Q-band (as well as the Soret band) leads to x- and y-polarized dipoles in the S_1 state (Fig. 3.15a) in the monomer.

When two macrocycles aggregate in a face-to-face manner (i.e., H-aggregation), both the x- and y-polarized dipoles are aligned in a parallel arrangement (Fig. 3.15b). Consequently, both the allowed excited states are destabilized; hence, the Q-band of the dimer is blue-shifted, in common with the case for the nondegenerate transition. Although many phthalocyanines are known to form H-aggregates, probably because of their planar structure [40, 117, 131–133, 136], only a limited number of examples of phthalocyanine H-aggregates, in which the relative conformation is known, have been reported. Kobayashi and Lever have revealed that the species exhibiting the blue-shifted Q-band are composed of two macrocycles stacked in a cofacial manner through elegant experiments using phthalocyanines bearing crown ethers as peripheral substituents (Fig. 3.20a) [136]. Figure 3.20b shows the optical absorption spectra of the Co^{II} complex of the crown-ether-substituted phthalocyanine in the presence of various concentrations of CH_3COOK . In the absence of the K^+ ion, the spectrum is characteristic of the monomer, but the Q-band apparent intensity decreased with increasing $[\text{K}^+]$ until two equivalents of K^+ (i.e., four K^+ ions for two macrocycles) were added and a new band appeared at the blue flank of the Q-band. This clearly indicates that the two macrocycles cofacially stacked via the four K^+ ions in the cavity of the crown-ether substituents. This has further been evidenced by ESR works on the Cu^{II} analogue [136].

As discussed in Sect. 2.2.9, the Q-band transition for metal complexes of the normal phthalocyanine monomer is doubly degenerate. When two molecules form a cofacial dimer, both the x- and y-polarized dipoles are parallel (or antiparallel) as mentioned above (Fig. 3.15b); hence, the excited state of the dimer is also doubly degenerate. This has been exemplified by Gasyna et al. [137] on the basis of the

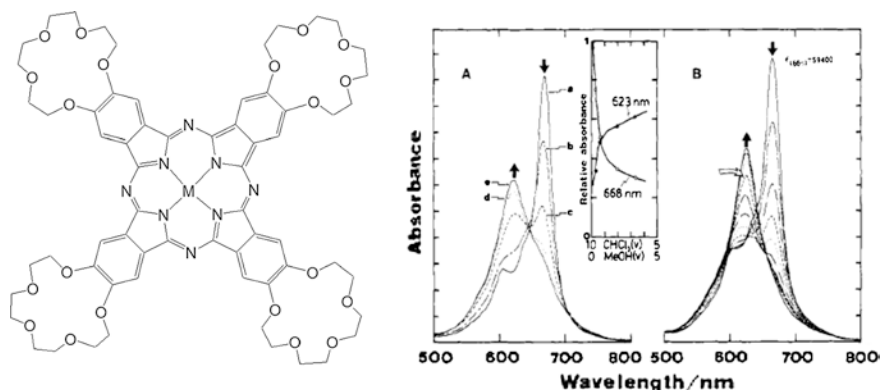
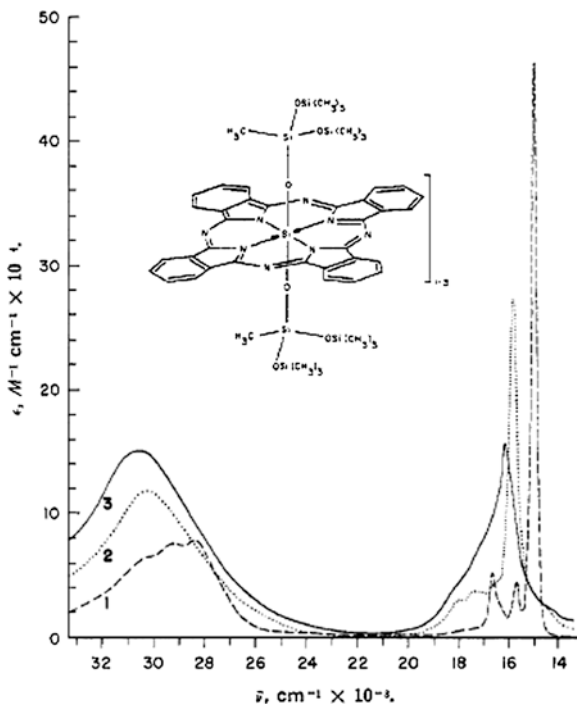


Fig. 3.20 Crown-ether-substituted phthalocyanines (*left*) and optical absorption spectra of Co^{II} complex ($\text{M} = \text{Co}^{\text{II}}$) in chloroform/methanol mixed solvent systems at various mixing ratios (A) and in chloroform solutions containing various concentrations of CH_3COOK dissolved in chloroform/methanol (95:5 v/v). Reprinted from Ref. [136], Copyright 1987, with permission from the American Chemical Society

Fig. 3.21 Optical absorption spectra of monomeric Si^{IV} phthalocyanine and μ -oxo oligomers (1 one macrocyclic ring, 2 two rings, and 3 three rings in cyclohexane. Reprinted from Ref. [34], Copyright 1970, with permission from the American Chemical Society



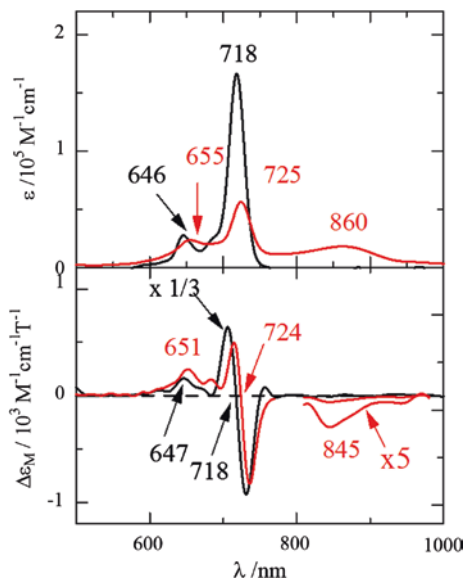
appearance of the Faraday A-term in the MCD spectra associated with the blue-shifted Q-band of the aforementioned crown-ether-substituted phthalocyanines.

The optical absorption spectra of μ -oxo dimers of the Si^{IV} complex of phthalocyanine derivatives in cyclohexane (Fig. 3.21) also show that both the Q- and Soret bands blue-shift with an increase in the number of stacked macrocycles [34, 138]. A similar blue shift of the Q-band has also been reported for Al^{III} [47, 139], Ge^{IV} [34], Fe^{III} [140], Mn^{III} [49], and Cr^{III} [141] derivatives. The degeneracy of the Q-transition has been evidenced by MCD spectroscopy for the μ -oxo dimer of the Si^{IV} complex of the phthalocyanine derivative [142]. A similar blue shift of the Q-band and the appearance of the Faraday A-term in the spectral range have been reported for a μ -oxo Si^{IV} complex heterodimer composed of phthalocyanine and naphthalocyanine [143].

3.2.4.4 J-Aggregation of Phthalocyanines and Degeneracy of Their Transitions

J-aggregates of phthalocyanines are much less common. Many of them have been reported for water-soluble derivatives [134, 143, 144], such as cationic porphyrin derivatives that are relatively well known [145]. In the last decade, J-aggregation in nonaqueous media has been reported [6, 146]. This type of aggregate has a

Fig. 3.22 Optical absorption (*top*) and MCD (*bottom*) spectra of [Sb(tbpc)(SO₄H)₂]⁺ (the compound shown in Fig. 3.16) in ethanol (*black solid lines*) and water containing surfactant (2 % w/v Triton X-100). Reprinted from Ref. [134], Copyright 2013, with permission from Elsevier



slipped cofacial conformation between macrocycles, as shown in Fig. 3.15c, d. In the former case, one macrocycle has slipped relative to another one along only the x -axis. Hence, with respect to dipole-allowed excited states, y -polarized dipoles are parallel to each other, while x -polarized dipoles are aligned in a head-to-tail manner. Therefore, the x -polarized excited state is stabilized relative to that of the monomer (redshifted) whereas the y -polarized excited state is destabilized (blue-shifted). Consequently, two bands are observed (e.g., Fig. 3.16). In another case, one macrocycle has slipped along both axes. Hence, both the x - and y -polarized dipoles are aligned in a head-to-tail manner. Therefore, as both the x - and y -polarized excited states are stabilized, only the redshift of the Q-band is observed (Fig. 3.17) [6]. Unlike cofacial dimers, the new chromophore loses the C_4 symmetry upon J-aggregation that the monomers used to have. As the excited states are no longer degenerate, the observed MCD spectra are dominated by Faraday B-terms (Figs. 3.17 and 3.22).

3.2.4.5 Oblique Dimer of Phthalocyanines

Split Q-bands have been observed in the optical absorption spectra (Fig. 3.23a) of clamshell-type phthalocyanine dimers that are bridged via a peripheral substituent (Fig. 3.23b) [131, 147–149]. Some absorption bands are concentration-dependent owing to intermolecular aggregation, whereas others are unchanged regardless of concentration and hence are attributed to intramolecular exciton coupling [147–149]. As the split Q-bands are observed even in sufficiently dilute solutions, the

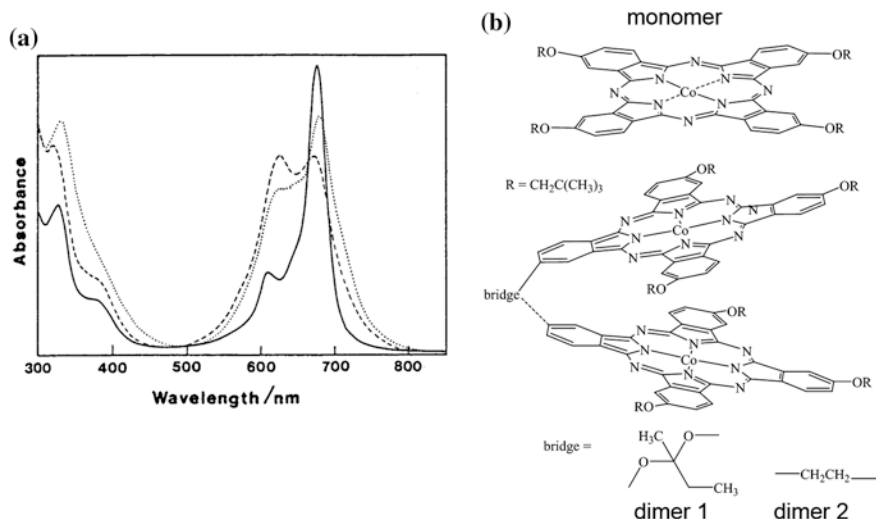


Fig. 3.23 Optical absorption spectra of Co^{II} complex of monomer (*solid line*) and bridged-dimer phthalocyanines 1 (*dashed line*) and 2 (*dotted line*) in 1,2-dichlorobenzene. Reprinted from Ref. [147], Copyright 1987, with permission from the American Chemical Society

splitting has been attributed to exciton coupling between macrocycles aligned in an oblique arrangement, as shown in Fig. 3.19c [149]. Similar splitting of Q-bands has also been reported for phthalocyanine dimers bridged via a more rigid aromatic ring such as 1,8-naphthyl groups as a spacer [150].

3.2.4.6 π - π Interaction Between Macrocycles

When two macrocycles in a cofacial dimer are much closer ($<3.4 \text{ \AA}$), their π -clouds can overlap with each other; hence, the ground-state electronic structure of individual macrocycles can no longer be considered independently. The molecular structure of the Sn^{IV} complex of the double-decker phthalocyanine in a cofacial manner, $[\text{Sn}(\text{pc})_2]$, has been crystallographically determined (Fig. 3.24a), and the distance between the two macrocyclic ligands²¹ (2.61 \AA) has been found to be shorter than the sum of the van der Waals distances (3.4 \AA) [151]. Therefore, the π - π interaction between the two macrocycles needs to be taken into consideration [152]. Its optical absorption spectrum in solution shows split Q-bands and a single Soret band (Fig. 3.24b) [153]. The appearance of Faraday A-terms in the MCD spectra for both the split Q-bands indicates that both transitions are degenerate. Similar split Q-bands have been reported for derivatives of lanthanoids (III/IV)

²¹Actually, this is the distance between the planes composed of the four pyrrole nitrogen atoms in each macrocyclic ligand.

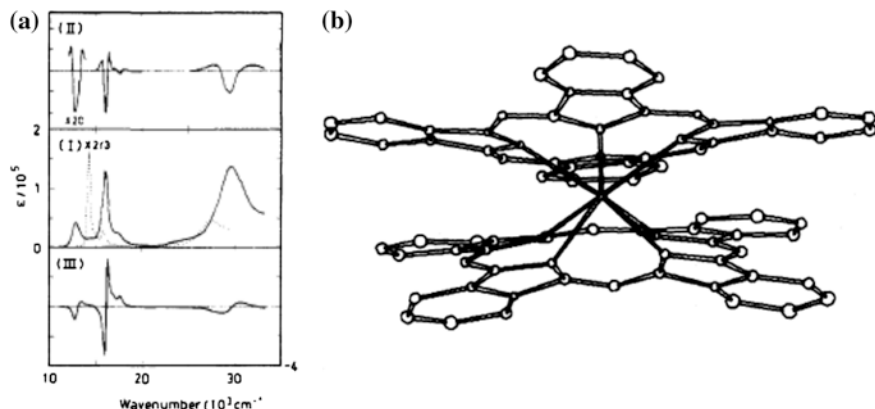


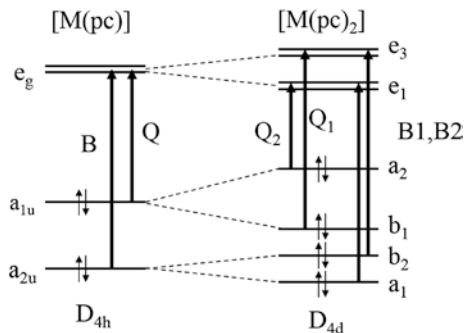
Fig. 3.24 **a** Optical absorption (*middle*), second-derivative absorption (*top*), and MCD (*bottom*) spectra of double-decker Sn^{IV} -diphthalocyanine $[\text{Sn}(\text{pc})_2]$ in toluene (Reprinted from Ref. [152], Copyright 1989, with permission from the American Chemical Society) and **b** crystal structure of $[\text{Sn}(\text{pc})_2]$ (Reprinted from Ref. [151], Copyright 1973, with permission from the American Chemical Society)

[154–156], actinoids (III/IV) [157–160], Zr^{IV} and Hf^{IV} [161–164], In^{III} [165], Bi^{III} [166], and Sb^{III} [167]. In particular, in the series of double-decker rare-earth (III) derivatives, $[\text{M}(\text{pc})_2]^-$ (where $\text{M} = \text{Sc}^{\text{III}}$, Y^{III} , and lanthanoid (III)), the magnitude of the splitting significantly increases with decreasing ionic radius of the central metal ion [154], indicating that the π - π interaction between the macrocycles becomes stronger with decreasing interplanar distance. Similar split Q-bands have been reported for triple-decker $[\text{M}_2(\text{pc})_3]$ (where $\text{M} = \text{lanthanoid (III)}$) [168] and quadruple-decker derivatives (two double deckers bridged via a Hg^{II} ion) [169].

To explain the splitting of the Q-band and the strong effect of the ionic radius of the central elements on the magnitude of the splitting,²² the overlapping of π -conjugation systems between the two macrocycles has been proposed [170]. As shown in Fig. 3.24a, the two macrocycles in double-decker phthalocyanine dimers are cofacial but staggered by ca. 45° . Konami et al. have reported that the overlapping of the following four frontier orbitals (LUMO (doubly degenerate), HOMO, and next-HOMO) between the two macrocycles is important for understanding the properties of double-decker phthalocyanine dimers and, in particular, that the overlap integral between HOMOs ($\pi(a_{1u})$ in monomer) is much larger than those between next-HOMO ($\pi(a_{2u})$) and LUMO ($\pi(e_g)$) [170]. Therefore, their MOs should be considered not in D_{4h} symmetry for two independent monomers, but in D_{4d} for one conjugation system composed of two macrocycles (Fig. 3.25).

²²The splitting of the Q-band can be explained by exciton coupling (one is assigned as an allowed transition and the other weaker one is due to the forbidden transition that borrowed intensity from vibronic transition). However, the increase in the magnitude of the splitting with decreasing ionic radius is much steeper than expected from the change in the interplanar distance (Eq. 3.1).

Fig. 3.25 Schematic diagrams of frontier orbitals in single-decker (left) and double-decker phthalocyanines (right). The large and small arrows denote dipole-allowed electronic transitions and electrons, respectively



Because of the overlap of π -clouds, each of the MOs in a single-decker macrocycle will be split in the new conjugation system owing to bonding and antibonding interactions. The magnitude of the splitting becomes larger with a decrease in distance between the two macrocycles because the magnitude of the overlap integral of their π -clouds decreases with increasing distance [170]. The $\pi(a_{1u})$ HOMO in a single-decker phthalocyanine will be split into antibonding $\pi(a_2)$ and bonding $\pi(b_1)$ orbitals in the new MOs [153]. Likewise, the $\pi(a_{2u})$ and $\pi(e_g)$ in a monomer will be reorganized to a set of bonding $\pi(a_1)$ and antibonding $\pi(b_2)$ orbitals and a set of bonding $\pi(e_1)$ and antibonding $\pi(e_3)$ orbitals, respectively [153], although the magnitude of splitting between these MOs is much smaller than that between the MOs derived from the monomer HOMOs. Therefore, it is easily understood that the Q-band for the monomer will be split into two bands, which are both degenerate, in the double-decker dimer: That is, of the four possible transitions derived from a_{1u} -to- e_g (Q-band) transitions, $a_2 \rightarrow e_1$ and $b_1 \rightarrow e_3$ transitions are dipole-allowed. Furthermore, as the π - π interaction becomes stronger with decreasing interplanar distance, the energy gap between the b_1 and a_2 MOs increases; hence, the magnitude of the Q-band splitting becomes larger. In contrast, as the overlapping between $\pi(a_{2u})$ MOs and that between $\pi(e_g)$ MOs are small, the Soret band is observed as a single band. Thus, this MO model successfully explains the optical absorption spectra of double-decker phthalocyanines and the effects of ionic radius of the central metal on the splitting of the Q-band.²³

Optical absorption spectra of metal complex dimers linked by a direct M-M bond, i.e., $(pc)M-M(pc)$, ($d(M-M \text{ distance}) = 2.89 \text{ \AA}$ for $M = Ir$ [171], $d = 2.827 \text{ \AA}$ for $M = Rh$ [172], and $d = 3.14 \text{ \AA}$ for $M = Re$ [173]) also show split Q-bands²⁴ of essentially the same intensity. Interestingly, those of Si^{IV} -

²³This model also successfully explains the spectral properties of a series of lanthanoid(III) derivatives of neutral double-decker phthalocyanines $[M(pc^{2-})(pc^-)]$ and $[M(pc^-)]_2$ as well as their redox potentials.

²⁴In these works, the authors have tried to explain the splitting on the basis of the exciton coupling alone.

phthalocyanine cofacial dimers linked by a direct Si–Si bond show a single Q-band despite the much shorter Si–Si distance (2.576 Å)²⁵ [138].

Readers who are interested in syntheses, structures, and other properties as well as spectral properties of phthalocyanine dimers should refer to Kobayashi's excellent review paper [154].

3.2.5 Effects of Acid-Base Equilibria Involving Phthalocyanine Macrocycle

As one phthalocyanine molecule has a nitrogen atom in each of the four pyrrole units and four aza nitrogen atoms bridging the units, each of them can be involved in an acid-base reaction (as a base). In addition, metal-free phthalocyanines, such as H₂pc, can dissociate one or two of the pyrrole N-H protons under appropriate conditions. Therefore, they can act as acids. Since these nitrogen atoms are members of the innermost 16-membered ring that dictates the spectral properties of the macrocycle (Sect. 2.2.6), any small changes may give rise to a significant spectral change.

3.2.5.1 Metal-Free Phthalocyanines as Acids

Figure 3.26a shows the optical absorption spectra of a water-soluble metal-free phthalocyanine in ethanolic solutions at various NaOH concentrations [174]. In ethanol alone, its spectrum shows twin Q-bands, which are characteristic of metal-free phthalocyanines (Sect. 2.1.1), but they coalesce with increasing [NaOH] and only one peak appears in the final solution. Quantitative analyses of the Q-band intensity as a function of [NaOH] have revealed that the spectral changes involve two Na⁺ ions per chromophore [174]; hence, the final product is the doubly deprotonated species Pc²⁻. The final spectrum is very close to those of metal complexes of phthalocyanine, which is understandable because their spectra have been successfully interpreted by employing the dianion of phthalocyanine as a model (Chap. 2). Similar spectral changes have been observed in aqueous solutions containing the same compound (Fig. 3.26b) and surfactant to prevent molecular aggregation. However, the dissociation of only one of the two protons (pK_a = 12.5) has been found to be involved in this spectral change on the basis of quantitative analyses of the Q-band intensity as a function of pH [174]. It is noteworthy that a tetraazaporphyrin that has eight *N*-methyl-pyridinium groups, which are strongly electron-withdrawing, on its periphery releases its imino protons more easily in water (pK_{a1} = 6.3 and pK_{a2} = 8.8) and shows a single Q-band [175]. These findings clearly indicate that the spectra of Pc²⁻ and HPC⁻ are close to each other.

²⁵The authors reported that the absorption spectra of the Si–Si dimers are very similar to those of tetrabenzotriazacorroles (Sect. 3.3.3).

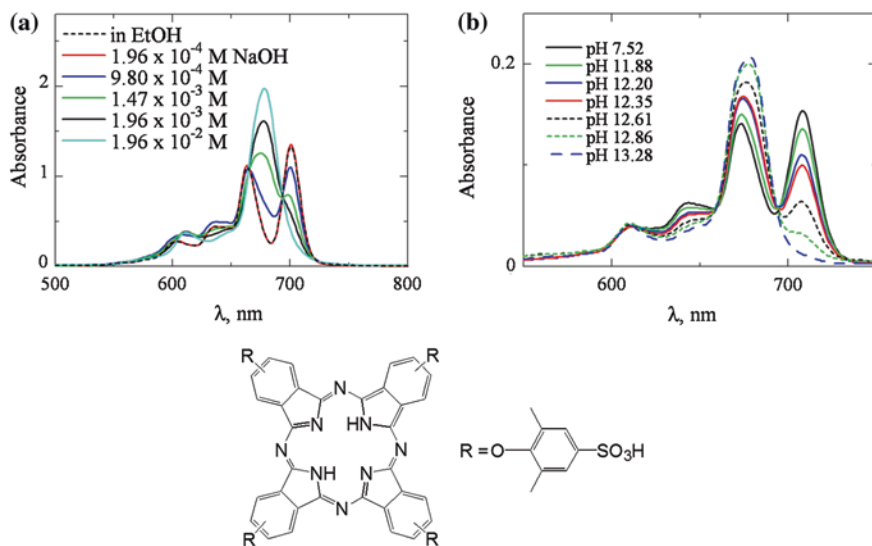


Fig. 3.26 **a** Optical absorption spectra of H₆tppc in EtOH in the presence of various concentrations of NaOH and **b** in aqueous solutions containing Triton X-100 (1.2 %) under various pH conditions ([NaCl] + [NaOH] = 0.8 M). Reproduced from Ref. [174], Copyright 2013, with permission from World Scientific Publishing Company

Actually, Homborg and Kalz have isolated both [Li₂(pc)] and [Li(Hpc)], which show similar absorption spectra [43]. It appears strange that the singly deprotonated species show a single Q-band because one proton remains on a pyrrole-nitrogen atom, but this is understandable if we assume the presence of a proton and a Na⁺ (or Li⁺) ion not in the cavity of the macrocycle but above and below the macrocycle, respectively, as proposed by Stillman and coworkers [12, 176].

3.2.5.2 Phthalocyanines as Multicentered Bases

On the other hand, when both metallated and metal-free phthalocyanines react with acids, considerable four-step five-stage spectral changes are observed (Fig. 3.27a, b) [177, 178].²⁶ These changes are interpreted in terms of the stepwise protonation at the four meso nitrogen atoms (Fig. 3.27c) [177–184]. As a general trend, protonation gives rise to a shift of the Q-band position to longer wavelengths in the order of unprotonated < singly < doubly < triply < quadruply protonated species. The redshift at each protonation step is ascribable to the

²⁶We do not consider protonation at peripheral substituents or axial ligands because they are far from the innermost 16-membered ring, and detectable spectral changes are unlikely to be observed. An example of spectral changes associated with protonation at the axial ligand has been described elsewhere (Sect. 3.2.1; Fig. 3.3).

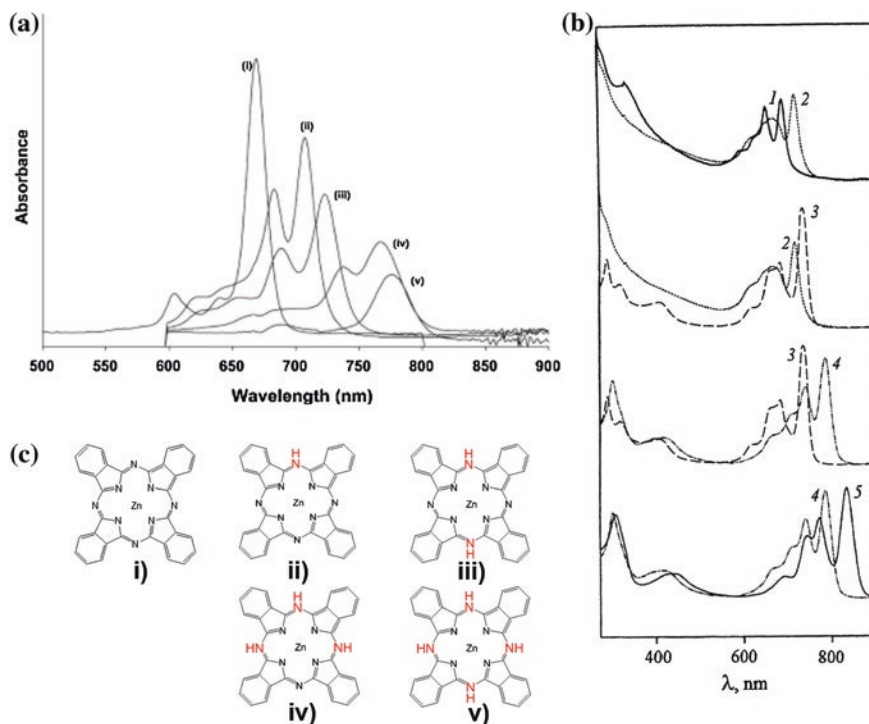


Fig. 3.27 **a** Changes in absorption spectrum observed upon addition of sulfuric acid (98 %) to [Zn(pc)] in DMF. Spectrum (i) is for [Zn(pc)] before acid addition, (ii) first, (iii) second, (iv) third, and (v) fourth protonations. Reprinted from Ref. [177], Copyright 2004, with permission from Elsevier. **b** Changes in optical absorption spectra, which are associated with protonation of H₂pc at meso nitrogen atoms: 1 in CH₃COOH, 2 monoprotated form (in 50 % CF₃COOH/CH₃COOH), 3 diprotated form (in CF₃COOH), 4 triprotonated form (in 10 % H₂SO₄/CF₃COOH), 5 tetraprotated form (in H₂SO₄). Reproduced from Ref. [178] with permission from John Wiley & Sons Ltd. **c** (i) Unprotonated, (ii) singly, (iii) doubly, (iv) triply, and (v) quadruply protonated phthalocyanines (Zn^{II} complex)

stabilization of the LUMO of the macrocycle that has a large coefficient of the wavefunction on nitrogen atoms relative to the HOMO that has nodal planes on all the nitrogen atoms (Sect. 2.2.3) [178, 179] owing to the elevated electronegativity of the nitrogen atom(s) upon protonation. That is, the protonation effectively reduces the HOMO-LUMO energy gap of the chromophore. Another important profile with respect to metal complexes is the reduction in the molecular symmetry upon protonation. Evidently, the spectra of singly, doubly, and triply protonated species exhibit split Q-bands (Fig. 3.27a). We have discussed the effects of the expansion of the π -conjugate system in Sect. 3.2.3.2. In a similar way, the singly, doubly, and triply protonated species (Fig. 3.27c(ii–iv)) have a lower symmetry (C_2) than the initial unprotonated species (C_4). Consequently, the LUMO of the chromophore that used to be doubly degenerate before protonation is split into two nondegenerate orbitals, resulting in the splitting of the doubly degenerate

HOMO-LUMO transition (Q-band) into two nondegenerate transitions [178–180]. The magnitude of splitting is largest for doubly protonated species, suggesting that the two protonated nitrogen atoms are in *trans* positions (Fig. 3.27c(iii)) [180]. It is noteworthy that the quadruply protonated phthalocyanine (Fig. 3.27c(v)) has a single Q-band in common with the unprotonated analogue (Fig. 3.27c(i)). This is because all four meso nitrogen atoms are protonated; hence, the chromophore regains the C_4 symmetry. Occasionally, the Q-band of singly protonated species has been observed as a single but considerably broadened band envelope [178–180]. This broadening may be attributed to the presence of more than one absorption band, although the possibility of the aggregation of the macrocycles upon protonation has been proposed [180].

Reaction with strong Lewis acids, such as $AlCl_3$ [185] and $TeCl_4$ [90], as well as the alkylation of the meso nitrogen atom [186], gives rise to a similar spectral change.

3.2.6 Electron Transfer Reactions Involving Phthalocyanine Macrocycle

As phthalocyanines (actually, their dianion, $Pc(2-)^{27}$) have a nondegenerate HOMO and a doubly degenerate LUMO (Sect. 2.2.3), they can release up to two electrons and accept up to four electrons. Therefore, their oxidation states can diverge from $Pc(0)$ (doubly oxidized species) to $Pc(6-)$ (quadruply reduced species) [187]. The macrocyclic dye in each oxidation state exhibits a characteristic optical absorption spectrum because these electron transfer reactions involve significant changes in the innermost 16-membered ring that dictates their spectral properties.

3.2.6.1 Absorption Spectra of Oxidized Phthalocyanines

Conventional phthalocyanines are well known as stable p-type organic semiconductors because they readily (chemically, electrochemically, or photochemically) release an electron in their π -conjugation system to form singly oxidized species, $Pc(1-)$ [188]. As the majority of conventional $Pc(2-)$ species are neutral (e.g., $[Cu(Pc)]$, $[Al(Pc)Cl]$, or $[Sn(Pc)Cl_2]$), their singly oxidized species (e.g., $[Cu(Pc(1-))]^+$) are referred to as “radical cations”. Even when “ $Pc(2-)$ ” species ($[Li_2(Pc)]$, in particular) are being manipulated in the laboratory, they can occasionally be air-oxidized under aerobic conditions and show a reddish violet color instead of their initial blue color. Thus, we have relatively many opportunities to observe “radical cations”. The appearance of a reddish violet color is attributed to

²⁷See Sect. 1.2.2 for the representation of $Pc(2-)$.

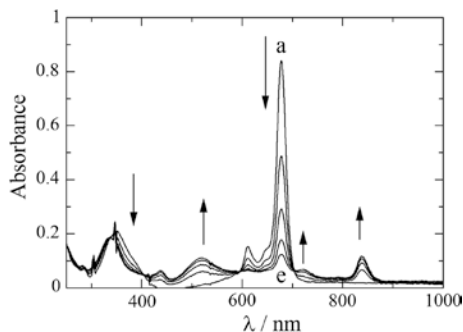


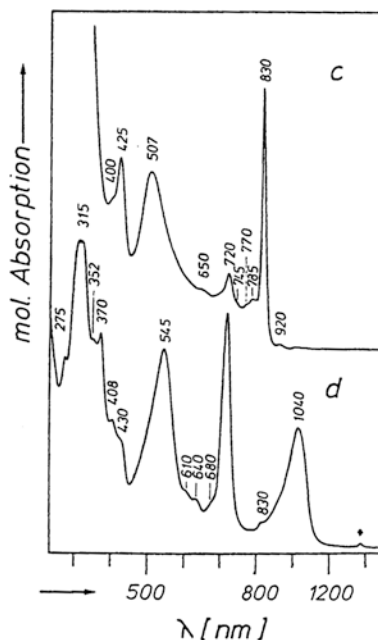
Fig. 3.28 Typical spectral changes in a dichloromethane solution containing a Zn^{II} complex and 0.1 M tetrabutylammonium hexafluorophosphate as the supporting electrolyte during the electrochemical oxidation at 0.88 V versus AgCl/Ag. Reproduced from Ref. [189], Copyright 2006, with permission from World Scientific Publishing Company

the presence of an intense extra absorption band around the 400–500 nm region, which is characteristic of “radical cation” species [188], as described below.

Figure 3.28 shows spectral changes observed in a dichloromethane solution containing the Zn^{II} complex of tetra-*tert*-butyl-substituted phthalocyanine (see Fig. 2.2b for its structure) during electrochemical oxidation around its first oxidation potential [189]. As the electrolysis proceeds, the characteristic Q-band disappears and simultaneously some new absorption bands grow at approximately 522, 722, and 837 nm in the spectral range, which were “window regions” before the oxidation. The reduction of the Q-band intensity and the growth of the extra band at approximately 500 nm make the solution reddish violet. Similar spectral changes have been reported for $[\text{Mg}(\text{pc})]$ [190], H_2pc [191], $[\text{Zn}(\text{pc})]$ [192], $[\text{Cu}(\text{pc})]$ [191], and $[\text{Li}_2(\text{pc})]$ [193]. Temperature [190] and solvent [191] studies have revealed that the oxidation product is an equilibrium mixture of monomers and dimers of singly oxidized phthalocyanines.²⁸ Homborg and Kalz have reported typical optical absorption spectra of the monomer and dimer (Fig. 3.29 top and bottom, respectively) of a singly oxidized phthalocyanine as a Mg^{II} complex [193]. Spectra of monomers alone will be discussed in this subsection because those of dimers should be discussed in the context of double-decker phthalocyanines (Sect. 3.2.6.2). Stillman and coworkers have elucidated that the electronic transition of the lowest energy in the spectra of monomers (e.g., the 830 nm band in Fig. 3.29 top) is degenerate on the basis of MCD studies and hence have assigned this absorption band as the Q-band of singly oxidized phthalocyanine [188, 190, 192]. They have likewise assigned the absorption bands observed in the near-ultraviolet region in line with those in the Soret region for unoxidized phthalocyanines. Nevertheless, no clear assignment has yet been given to the broad band at approximately 500 nm, which is the most characteristic band in the spectra

²⁸Singly oxidized phthalocyanines are more prone to molecular aggregation than unoxidized species [101, 128, 193].

Fig. 3.29 Optical absorption spectra of singly oxidized [Mg(pc)] in 1-chloronaphthalene (*top*) and ethanol (*bottom*). Reproduced from Ref. [191] with permission from John Wiley & Sons Ltd.



of singly oxidized phthalocyanines (hereafter, this band will be referred to as a “fingerprint marker band” or simply as a “marker band” in accordance with Stillman’s naming [188, 190, 192]). An earlier theoretical work on singly oxidized species has predicted the presence of a dipole-allowed electronic transition, which involves a transition from a lower-lying π orbital to the SOMO²⁹ between the Q- and Soret-band envelopes, which must be orbitally doubly degenerate [194]. On the other hand, Stillman and coworkers have assigned this marker band as a transition from the nonbonding orbital composed of lone-pair orbitals of pyrrole nitrogen atoms to the π^* orbital (i.e., $n \rightarrow \pi^*$ transition) on the basis of the lack of the Faraday A-term in the MCD spectra [195, 196]. Although this proposal well explains the observed MCD spectra, it has some problems because the marker band is too intense and must be observed for Pc(2-) species if the assignment is assumed to be correct. Ishikawa and Kaizu have found a set of two low-lying $\pi(e_g) \rightarrow \pi(a_{1u})$ (SOMO) transitions with magnetic dipole moments of essentially the same magnitude but of opposite signs between Q- and Soret-band envelopes of the singly oxidized monomer. They assigned the “marker band” as a mixture of such transitions and successfully explained the disappearance of the Faraday A-term in the MCD spectra [197].

²⁹SOMO = singly occupied molecular orbital. In this context, this means the HOMO from which one electron has been removed by oxidation.

In common with Pc(2-) species, the spectra of Zn^{II} , Mg^{II} , and Li^I complexes are of the prototype because their central metals have a closed shell; hence, d electrons do not take part in their electronic transitions. In contrast, those of $Fe^{II/III}$ [187], $Co^{II/III}$ [46, 157, 158], and Ru^{II} derivatives [198] can show one or more additional absorption bands assignable to CT transitions.

Spectral data of doubly oxidized phthalocyanine, Pc(0) species, are much less common and have been reported with respect to the Co^{III} complex [147].

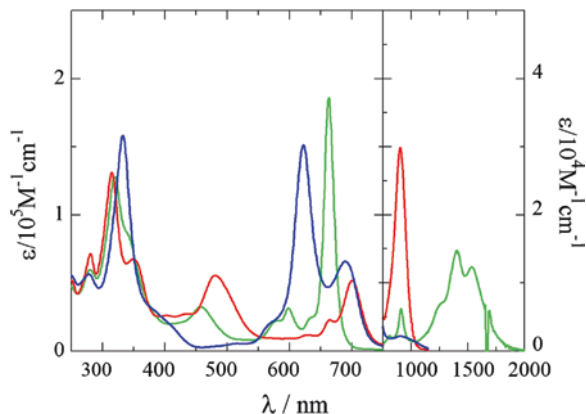
3.2.6.2 Oxidized Double-Decker Phthalocyanines

Although double-decker phthalocyanines have already been mentioned above (Sect. 3.2.4.6), we have to revisit these compounds again. This is firstly because they undergo facile oxidation involving the macrocyclic ligand(s) and show multiple colors according to their oxidation state and hence are interesting from the viewpoint of their application to electrochromic displays [199]. As described in Sect. 3.2.4.6, the HOMO of double-decker phthalocyanines is destabilized relative to that of single-decker species owing to the strong π - π interaction between the two macrocycles. Therefore, the two electrons in the HOMO of the antibonding character can be readily removed. Secondly, they form a stable organic radical species, in which the unpaired electron is delocalized over the macrocycles [200]. In particular, complexes of trivalent metal ions, such as Sc^{III} , Y^{III} , lanthanides (e.g., La^{III} , Pr^{III} , etc.) [155, 201–204], bismuth [205], and indium [202], have been isolated as neutral organic radical species $[M(pc(2-))(pc(1-))]$.³⁰

Figure 3.30 shows optical absorption spectra of the Y^{III} complex in various oxidation states. The spectrum of $[Y(pc(2-))_2]^-$ is characteristic of double-decker phthalocyanines (Sect. 3.2.4.6) and shows twin peaks. The appearance of a strong absorption band at approximately 620 nm makes this compound blue-colored. That of $[Y(pc(1-))_2]^+$ is similar to that of the dimer of singly oxidized phthalocyanine (Fig. 3.29 bottom); hence, this species looks reddish orange owing to the appearance of a “marker band” at approximately 480 nm [203]. In contrast, the mixed-valence compound $[Y(pc(2-))(pc(1-))]$ shows a green color owing to the presence of an intense band at approximately 660 nm and a less intense band at approximately 457 nm. Although its spectrum appears to be a superposition of the spectra of unoxidized and singly oxidized phthalocyanines (i.e., pc(2-) and pc(1-)), its electronic structure is not so straightforward. Ishikawa et al. have reported the optical absorption spectra of Lu^{III} complexes of homoleptic double-decker phthalocyanines $[Lu(pc(2-))(pc(1-))]$, double-decker naphthalocyanines $[Lu(nc(2-))(nc(1-))]$, and a heteroleptic dimer of the two different macrocycles (represented as $[Lu(pc)(nc)]$ for convenience) [204, 206]. The homoleptic pc dimer and its nc

³⁰Note that the formal representation, pc(2-) and pc(-), used to denote oxidation states of the macrocyclic ligands is not appropriate in this case because their π conjugation systems are not independent of each other (Sect. 3.2.4.6). However, we adopt this conventional formulation instead of $pc_2(3-)$ to avoid unnecessary confusion.

Fig. 3.30 Optical absorption spectra of Y^{III} complex of double-decker phthalocyanine in various oxidation states (dichloromethane solutions); *green* $[Y(pc(2-))(pc(1-))]$; *blue* $[Y(pc(2-))_2]^-$; *red* $[Y(pc(1-))_2]^+$

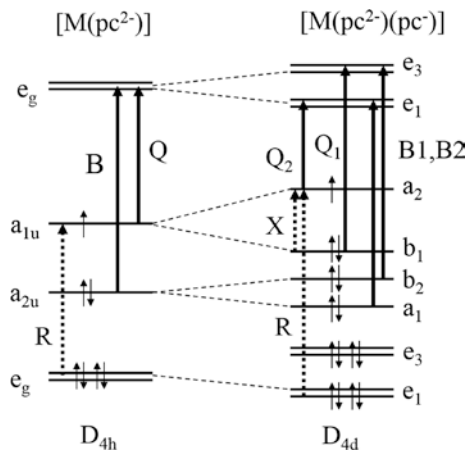


analogue show similar spectra, although the Q-band position of the latter is largely redshifted (ca. 760 nm in chloroform) relative to the former one (660 nm). Interestingly, the Q-band position of the heteroleptic dimer $[Lu(pc)(nc)]$ is located at the midpoint of those of the other two.³¹ That is, the spectrum of the heteroleptic dimer is neither a superposition of spectra of $pc(2-)$ and $nc(1-)$ nor that of $pc(1-)$ and $nc(2-)$, indicating that the unpaired electron is delocalized over the two different macrocycles. As discussed in Sect. 3.2.4.6, the optical absorption spectra of double-decker phthalocyanines (and also those of triple- and quadruple-decker phthalocyanines) need to be assigned on the basis of the whole π -conjugation system over the macrocycles. According to the schematic diagram of the MO model proposed for double-decker phthalocyanines [206], the 663 and 912 nm bands are assignable to Q_1 and Q_2 bands (Fig. 3.31), respectively. The radical “marker band” at approximately 457 nm may be assigned as a mixture of two sets of low-lying $\pi \rightarrow \pi^*$ ($e_1 \rightarrow a_2$) transitions (the R-band in Fig. 3.31), as suggested by Ishikawa et al. [206]. The broad band in the NIR region (1000–2000 nm) can be attributed to a $b_1 \rightarrow a_2$ transition (the X-band in Fig. 3.31) [207]. This assignment has been experimentally supported by the strong dependence of the peak position on the ionic radius of the central element [201, 208].³² The removal of another electron from $[Y(pc(2-))(pc(1-))]$ produces diamagnetic $[Y(pc(1-))_2]^+$ [201], the spectrum of which is similar to those of dimers of singly oxidized phthalocyanines (Sect. 3.2.6.1). This seems reasonable because the singly oxidized lithium phthalocyanine $[Li(pc(1-))]$ has a crystal structure similar to those of double-decker phthalocyanines (interplanar distance = 3.245 Å; staggered angle between the two macrocycles = 38.7°) [209]. On the basis of an MCD study [201] and the strong dependence of each absorption band on the ionic radius of the central metal [201,

³¹The Q-band of the heteroleptic dimer has been found to be degenerate on the basis of an MCD study [206, 208].

³²Decreasing interplanar distance gives rise to stronger π - π interaction between the two macrocycles and hence the splitting between b_1 and a_2 orbitals (Sect. 3.2.4.6).

Fig. 3.31 Schematic molecular orbital diagrams for single-decker (*left*) and singly oxidized double-decker (*right*) Pcs and assignments of the R-, Q-, and X-bands



210], the 701, 481, and 905 nm bands are assignable to Q₁, R, and X bands in Fig. 3.31, respectively [201]. The strong metal dependence has excluded the possibility of the $n \rightarrow \pi^*$ transition as a character of the X-band [201]. It is noteworthy that the X-bands observed for $[M(\text{pc}(1-))_2]^+$ species are significantly blue-shifted relative to those for $[M(\text{pc}(2-))(\text{pc}(1-))]$. This is reasonable because the removal of one electron from the a_2 HOMO of the antibonding character enhances the π - π interaction between the two macrocycles and hence enlarges the splitting between a_2 and b_1 , both of which are derived from a_{1u} HOMOs in the monomer. Note a broad X-band is observed for oxidized quadruple-decker phthalocyanines in the IR (not NIR!) region [211].

3.2.6.3 Absorption Spectra of Reduced Phthalocyanines

Although the optical absorption spectra of reduced phthalocyanines are not as common as those of oxidized species, several research groups have reported spectral data of good quality [4, 9, 74, 212–218]. Among them, spectra of up to quadruply reduced species have been reported for Zn^{II} , Al^{III} , Ni^{II} , and Mg^{II} complexes [212]. As their spectra are essentially the same regardless of the nature of the central metal at each reduction stage (Fig. 3.32), the spectral changes have been found to involve electron transfer occurring at the macrocyclic ligand (i.e., formation of $\text{pc}(3-)$ — $\text{pc}(6-)$ species). Stillman and coworkers have assigned optical absorption bands with respect to Zn^{II} [213] and Mg^{II} [214] complexes of singly reduced phthalocyanine ($\text{pc}(3-)$),³³ which were generated in donor solvents, on the basis of an MCD study. It is of interest whether the ground state of the singly reduced species is doubly degenerate because the LUMO (e_g) accepts the additional electron in the

³³The $\text{pc}(3-)$ species are referred to as radical anions for the same reason as in the case of singly oxidized phthalocyanine $\text{pc}(1-)$.

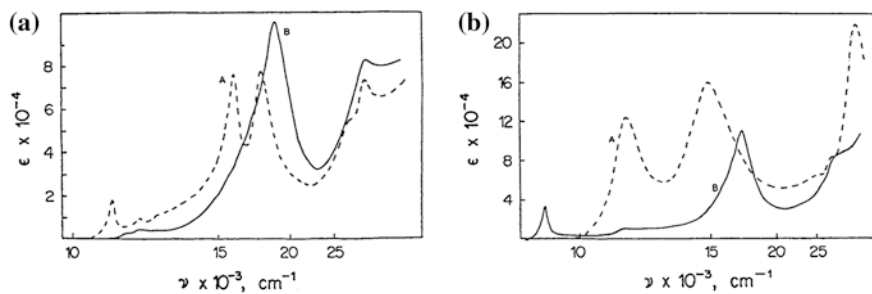


Fig. 3.32 Optical absorption spectra of reduced [Ni(pc)] in THF: **a** singly (dashed line) and doubly reduced (solid line) species and **b** triply (dashed line) and quadruply reduced species. Reprinted from Ref. [212], Copyright 1972, with permission from the American Chemical Society

degenerate orbital, which may give rise to a significant Jahn-Teller distortion of the macrocycle. Stillman and coworkers have elucidated that the ground state is nondegenerate on the basis of the little temperature dependence of their MCD spectra (i.e., lack of Faraday C-term; see Sect. 2.2.2 for C-term) [213, 214]. They concluded that the lifting of degeneracy upon reduction is attributable to the unsymmetrical solvation to the central metal ion as well as the Jahn-Teller distortion. Recently, the crystal structure of a singly reduced phthalocyanine prepared in a donor solvent has been determined by X-ray diffraction, and a significant distortion of the macrocyclic ligand has been exemplified [217]. Stillman and coworkers have assigned the NIR band (approximately 960 nm) and twin peaks in the visible region (500–700 nm) characteristic of pc(3-) species as the Q-band of singly reduced phthalocyanine and electronic transitions from the SOMO to higher π^* orbitals, respectively, on the basis of computational MO calculations [195, 213, 214]. On the other hand, Isago and coworkers have electrochemically generated pc(3-) species of Sb^{V} [216, 218] and As^{V} [9] complexes in nondonor solvents and reported that their absorption spectra, unlike those of Zn^{II} or Mg^{II} complexes, show a sharp single band in the 500–700 nm region instead of twin bands. They attributed their simple spectra to a much less significant Jahn-Teller distortion upon reduction. They have also found that a sharp absorption band appears at approximately 1050 nm, the position of which is significantly redshifted as compared with those of the Zn^{II} and Mg^{II} derivatives. As the Q-band of Pc(2-) complexes of Sb^{V} and As^{V} appears at a wavelength longer than those of the normal metal complexes, these findings also support the assignment of Stillman and coworkers.

The doubly reduced phthalocyanine, pc(4-) species, has been similarly investigated by optical absorption and MCD spectroscopies [215]. Likewise, the lowest transition and the most intense band at approximately 500 nm have been assigned as the Q-band of doubly reduced phthalocyanine and a transition from SOMO to a higher π^* orbital, respectively, both of which are nondegenerate.

Assignments of the optical absorption spectra of triply and quadruply reduced phthalocyanines (pc(5-) and pc(6-)) have been made on the basis of computational MO calculations by Mack and Stillman [195].

3.2.7 Solvent Effects

The solvent effects on the optical absorption spectra of phthalocyanines are generally complicated and hence are not clear-cut [219] because some solvents can induce chemical reactions involving the solutes (coordination of donor solvent molecule(s) to the central metal ion, aggregation, etc.) as described below. In addition, the purity of the solvents used for the spectral measurements sometimes affects their spectra (Sect. 3.2.7.4). Apart from such chemical reaction(s), the solvent dependence of optical absorption spectra of phthalocyanines is very small and can be interpreted in terms of a very simple physical interaction.

3.2.7.1 Physical Interaction

It is generally known that the optical absorption spectra of phthalocyanines show their Q-band at a longer wavelength in aromatic solvents (1-chloronaphthalene or pyridine) than in nonaromatic solvents (DMSO, dichloromethane, etc.). For example, the Q-band of the Cu^{II} complex of tetra-*tert*-butyl-phthalocyanine (see Fig. 2.4a for its structure) appears at 684 nm in 1-chloronaphthalene and 683 nm in nitrobenzene but at 675 nm in DMSO and 671 nm in *n*-pentane [107]. Although Co^{II} and Zn^{II} complexes behave similarly, this trend is not always straightforward because the Q-band position can be affected by the coordination to the central metal ion in donor solvents. Isago et al. have elucidated that the Q-band position of a specific phthalocyanine in a given solvent is governed by the refractive index alone, by using metal complexes of octahedral coordination geometry [220]. For example, the [Co^{III}(pc)(CN)₂]⁻ complex³⁴ shows essentially the same spectra in all the solvents studied except for its Q-band position, which regularly changes from MeOH (665 nm) to 1-chloronaphthalene (676 nm) in the order of increasing refractive index. Figure 3.33a clearly shows that there is a fairly good linear

³⁴As this complex has a six-coordinate, octahedral geometry (the two cyanide ions are in *trans* positions above and below the phthalocyanine macrocyclic ligand) [223], it is convenient for investigating the effects of the solvent on the electronic transition in the macrocyclic ligand alone for the following reasons: (1) donor-solvent molecules are unlikely to coordinate to the central metal ion because of the crowded coordination geometry around the metal ion; (2) ligand substitution is unlikely to occur because of strong Co–CN and Co–N(phthalocyanine) bonding; (3) the presence of the axial ligands and the net negative charge of the complex itself should prevent the aggregation of the macrocyclic ligands owing to steric hindrance and electrostatic repulsion, respectively; (4) it has no axial ligand or peripheral substituent that can be involved in the chemical interaction, such as hydrogen bonding, with the surrounding solvent molecules.

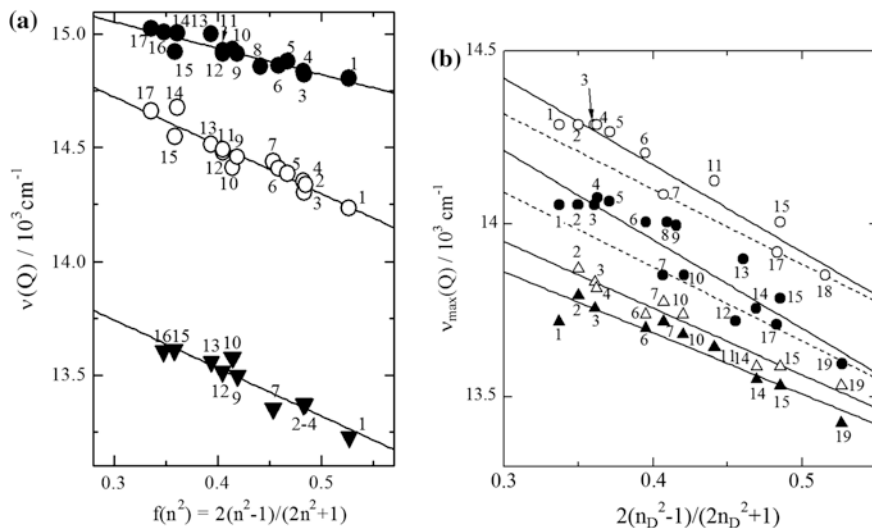


Fig. 3.33 Solvatochromic shifts in the Q-band position of **a** phthalocyanines incapable of chemical interaction with solvents: $[\text{Co}(\text{pc})(\text{CN})_2]^-$ (closed circles), $[\text{Sn}(\text{pc})\text{Cl}_2]^+$ (open circles), and $[\text{Sb}(\text{tbp})\text{Cl}_2]^+$ (closed triangles) as a function of refractive index of solvents. Reprinted from Ref. [220], Copyright 2004, with permission from the Chemical Society of Japan. **b** Same plots for phthalocyanines capable of chemical interaction: $[\text{Sb}(\text{pc})(\text{OH})_2]^+$ (closed circles) and $[\text{Sb}(\text{tbp})(\text{OH})_2]^+$ (open circles). Plots for $[\text{Sb}(\text{pc})\text{Cl}_2]^+$ (open triangles) and $[\text{Sb}(\text{pc})\text{Br}_2]^+$ (closed triangles), which are incapable of chemical interaction, are also shown in **b** for comparison. Reproduced from Ref. [69], Copyright 2009, with permission from the World Scientific Publishing Company. The integers near the plots represent the solvent studied: **a** 1 1-chloronaphthalene, 2 1,2,4-trichlorobenzene, 3 nitrobenzene, 4 1,2-dichlorobenzene, 5 chlorobenzene, 6 pyridine, 7 benzene, 8 DMSO, 9 chloroform, 10 DMA, 11 DMF, 12 dichloromethane, 13 THF, 14 ethanol, 15 acetone, 16 acetonitrile, 17 methanol. **b** 1 methanol, 2 acetonitrile, 3 acetone, 4 ethanol, 5 ethyl acetate, 6 THF, 7 dichloromethane, 8 DMF, 9 DMA, 10 chloroform, 11 DMSO, 12 benzene, 13 pyridine, 14 chlorobenzene, 15 nitrobenzene, 16 1,2,4-trichlorobenzene, 17 1,2-dichlorobenzene, 18 1,2-dibromobenzene, 19 1-chloronaphthalene. The dashed lines denote the regression lines derived from the analysis of Q-band positions in the nondonor solvent only

correlation between the Q-band positions and refractive indices in the form of Onsager's optical solvent polarity function [222]. Note that there is no clear correlation between the Q-band position and the other common solvent parameters, such as the donor number, acceptor number, permanent electric dipole moment, dielectric constant, or E_T value, that are commonly used to explain the solvatochromism. This finding undoubtedly indicates that the solvatochromic shift of the phthalocyanine Q-band is simply governed by the physical interaction between the electronic transition dipole and the induced dipole generated in the surrounding solvent molecules. As mentioned in Sect. 1.1.3, when a solute molecule (a phthalocyanine complex in this case) absorbs light, the molecule is polarized; hence, an electric dipole is generated within the molecule (within the molecular plane of the macrocyclic ligand in this case). At the same time, the surrounding solvent molecules are rearranged so as to minimize the effects of the excited

molecule. However, as the optical absorption occurs very rapidly (within a few femtoseconds), the orientation of the solvent molecules involving the movement of atomic nuclei cannot catch up with the electronic transition. Therefore, the movements of electrons (polarization), which are much quicker than those of nuclei, are predominant. That is, a more polarizable molecule, such as an aromatic compound with more mobile electrons, can more effectively stabilize the Franck-Condon excited state of the solute molecule. Similar trends can be expected for the other metal complexes unless the chemical interaction between the dye molecule and the solvent molecules is significant. Actually, similar solvatochromic shifts have been reported for complexes of As^V [9], Sb^V [1, 69, 220], and Sn^{IV} [220].

3.2.7.2 Chemical Interaction

In contrast, with respect to complexes bearing ligands capable of chemical interaction, such as hydroxides, plots for donor solvents result in a considerable deviation from the linear correlation (Fig. 3.33b) [1, 69, 223], suggesting the presence of chemical interaction (maybe hydrogen bonding) with solvent molecules.³⁵

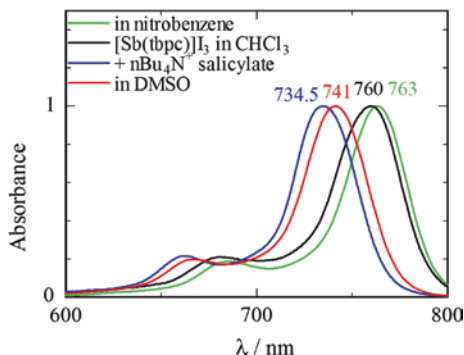
When a vacant coordination site is available on the central metal ion, a donor character of a specific solvent can give rise to a more significant change in the Q-band position. The optical absorption spectrum of the Sb^{III} complex of tetra-*tert*-butyl phthalocyanine (see Fig. 3.17 for its structure), which has no axial ligand, more strongly depends on the solvent. The Q-band maximum wavelengths are above 760 nm in nondonor solvents such as chloroform (760 nm) and nitrobenzene (763 nm), as shown in Fig. 3.34. Essentially, the same spectra have been observed in dichloromethane (762 nm), benzene (762 nm), and 1-chloronaphthalene (769 nm). In contrast, the Q-band maximum appears at a much shorter wavelength in DMSO (741 nm) despite its larger refractive index (1.47754) than that of chloroform (1.4453) or dichloromethane (1.42416). This phenomenon is attributable to the coordination of donor solvent molecules to the central metal ion because the Q-band in chloroform is immediately blue-shifted upon the addition of salicylate (Fig. 3.34) [224].³⁶ The Q-band appears in the same spectral region for the other donor solvents, such as THF (742 nm) and acetonitrile (746 nm). Therefore, these phenomena should be considered as chemical reactions involving solvent molecules rather than solvent effects.

The coordination of donor solvent molecules to a metal complex increases the electron density of the metal ion (Mn^{II}, Fe^{II}, Co^{II}, for example) in the cavity of the macrocyclic ligand, which stabilizes their higher oxidation states in donor solvents relative to those in nondonor solvents [187]. Therefore, some metal complexes in lower oxidation states can be air-oxidized to higher oxidation states in aerated

³⁵Plots of the Q-band position only in nondonor solvents exhibit a fairly good linear correlation.

³⁶Note that the addition of salicylic acid did not change the Q-band position [224].

Fig. 3.34 Optical absorption spectra of Sb^{III} complex in various solvents: in chloroform (*black*), in the same solvent but upon addition of tetrabutylammonium salicylate (*blue*), in nitrobenzene (*green*), and in DMSO (*red*). All the spectra are shown with their Q-band intensity normalized



donor solvents. For example, a colorful chemistry has been reported for Mn^{II} complexes. In a strong donor solvent such as DMA, $[\text{Mn}^{\text{II}}(\text{pc})]$ is oxidized by molecular oxygen to form $[\text{Mn}^{\text{III}}(\text{pc})(\text{O}_2^-)]$ ³⁷ [49, 225], which is further converted to the μ -oxo dimer $[\text{Mn}^{\text{III}}(\text{pc})]_2\text{O}$ in the presence of water [225]. As each species shows a characteristic absorption spectrum, manganese derivatives behave as if they were strongly solvatochromic.

3.2.7.3 Other Effects

Some solvents can induce the molecular aggregation of phthalocyanines [136, 226]. In general, more polar solvents tend to facilitate the aggregation of hydrophobic phthalocyanines. Nolte's group has reported that crown-ether-substituted phthalocyanines are more subject to molecular aggregation in the order of increasing solvent polarity (as measured on the basis of the dielectric constant or E_{T}^{N} value) [226]. On the other hand, the molecular aggregation of hydrophilic phthalocyanines can be facilitated by less polar solvents. Figure 3.35 (left) shows optical absorption spectra of the amphiphilic Sb^{V} complex of tetra-*n*-butoxy-substituted phthalocyanine (Fig. 3.35 right) in various ethanol-dichloromethane mixed solvent systems [134]. The spectrum in the Q-band region is broad in dichloromethane alone and hence indicates the occurrence of molecular aggregation. However, the Q-band becomes sharper with increasing ethanol ratio, indicating that ethanol plays a crucial role in disaggregating the amphiphilic phthalocyanine.

Highly solvatochromic behaviors have been reported for μ -oxo dimers of Si^{IV} phthalocyanines but not for the corresponding monomers [227–230]. In aromatic solvents such as benzene or toluene, their optical absorption spectra show a sharp, single Q-band at approximately 640 nm, which is characteristic of μ -oxo dimers (see Sect. 3.2.4.2), whereas more than five bands with comparable intensities are observed at 560–760 nm in nonaromatic solvents, such as dichloromethane and THF (Fig. 3.36) [227]. It seems that the molar extinction constant at the 640 nm

³⁷The Mn^{II} species fails to react with oxygen when dissolved in highly purified dry pyridine [49].

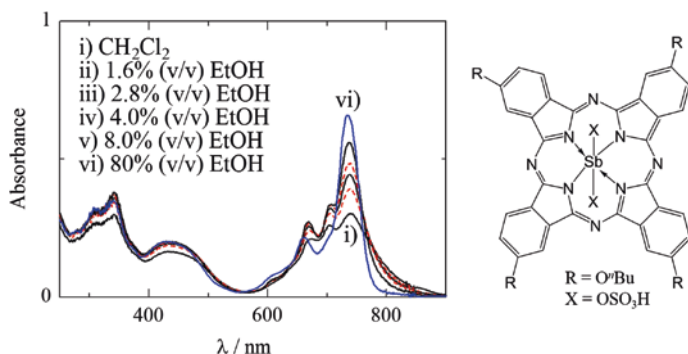
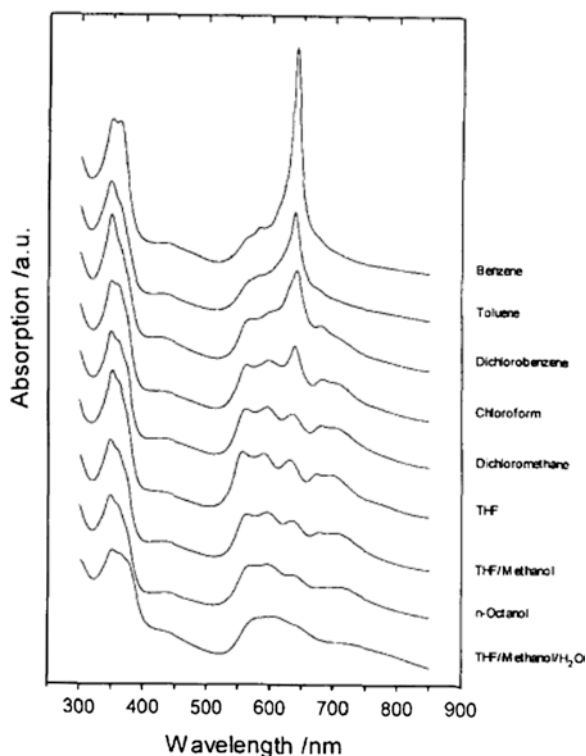


Fig. 3.35 *Left* Optical absorption spectra of amphiphilic phthalocyanine complex of Sb^{V} as a function of ethanol/dichloromethane ratio; *i* dichloromethane (alone); *ii–vi* CH_2Cl_2 solutions containing 1.6 % (v/v), 2.8 %, 4.0 %, 8.0 %, and 20 % ethanol. Reprinted from Ref. [134], Copyright 2012, with permission from Elsevier. *Right* Structure of the Sb^{V} complex

Fig. 3.36 Optical absorption spectra of μ -oxo Si^{IV} -phthalocyanine dimer in various solvent systems. Reprinted from Ref. [227], Copyright 1995, with permission from Elsevier



band decreases with increasing polarity of the solvent. Similar changes have been observed in aromatic solvents by changing the temperature of the solutions [228, 229]. Note that the solvatochromism has not yet been sufficiently elucidated to date. It has been attributed to the molecular aggregation (as mentioned above)

[228] or the stabilization of a specific rotational isomer³⁸ in aromatic solvents [229]. In addition, the multiple bands observed in nonaromatic solvents can be attributed to the tilting angle³⁹ between the two macrocyclic ligands [231].

3.2.7.4 Effect of Impurities in Solvents

In a strict sense, the effect of impurities in solvents on the optical absorption spectra cannot be considered as a “solvent effect”. However, this subject has to be incorporated into this subsection because we may encounter this problem whenever we study solvent effects on absorption spectra, particularly those of phthalocyanines. Because of their high molar extinction coefficients in general (on the order of $10^5 \text{ M}^{-1} \text{ cm}^{-1}$), measurements of optical absorption spectra are normally performed using very dilute solutions (ca. 10^{-6} M). Therefore, even a trace amount of impurity/impurities can consume a considerable portion of the dye stuff in the solution as a result of the chemical reaction(s) between them. For example, the absorption spectra of methanolic solutions containing a P^{V} complex⁴⁰ at various concentrations are shown in Fig. 3.37a. The apparent Q-band intensity becomes larger and closer to that in ethanol (ca. $1.6 \times 10^5 \text{ M}^{-1} \text{ cm}^{-1}$; Fig. 3.3 [30, 31]) at higher concentrations. The Lambert-Beer plot gives a concave curve; hence, this concentration dependence cannot be attributed to the aggregation of the macrocycles.⁴¹ This indicates that the P^{V} complex is degraded by unknown impurity/impurities in the solvent used to generate a colorless product. Because the amount of impurity/impurities in the solvent used is limited, the lower the concentration of the sample, the more significant the effect of the degradation becomes. This phenomenon is, however, not very misleading in this case because the degradation product is colorless. Let us consider another example, in which a reaction with an impurity generates a product that absorbs light in the same spectral region. Figure 3.37b shows the optical absorption spectra of metal-free octa-*n*-butoxyphthalocyanine (substituted at α positions) in dichloromethane and DMF solutions. Both spectra appear essentially the same but an additional band in the NIR region (around 870 nm) is observed in dichloromethane, which disappears upon the addition of an appropriate base such as pyridine or triethylamine. Similar phenomena are also observed for its metal complexes. We frequently encounter this type of phenomenon in nondonor solvents, particularly for phthalocyanines bearing substituents such as alkoxy, phenoxy, thioalkyl, thiophenyl, and other related groups

³⁸Because of the free rotation around the Si–O–Si axis, there can be more than one rotational isomer based on the difference in the torsion angle between the macrocyclic ligands.

³⁹The tilted stacking of the phthalocyanine rings with respect to the Si–O–Si axis gives rise to an oblique conformation between the two macrocyclic ligands (Fig. 3.19c).

⁴⁰The same compound is shown in Fig. 3.3 and has been found to be free from aggregation in ethanolic solution [30, 31].

⁴¹An aggregation phenomenon would give a convex curve (see Fig. 3.14 inset, for example) in the Lambert-Beer plot.

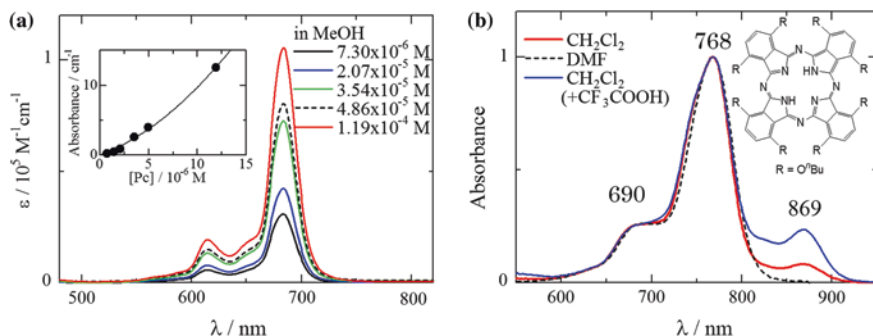


Fig. 3.37 **a** Optical absorption spectra of [P(tppc)(O)(OH)] in methanol (around the Q-band region) at various concentrations. The inset depicts the Lambert-Beer plot for the Q-band peak intensity. **b** Optical absorption spectra (normalized to the Q-band maximum intensity) of octabutoxyphthalocyanine in dichloromethane (red solid line), DMF (black broken line), and dichloromethane upon the addition of CF_3COOH (blue solid line). Isago and Fujita, unpublished result

at α positions. We have opportunities to see an extra band at the red flank of the Q-band, which is attributable to various known reasons, such as CT (MLCT, LMCT; Sect. 3.2.1), J-aggregation (Sect. 3.2.4.1), protonation at one or more meso nitrogen atoms (Sect. 3.2.5.2), and oxidation of the macrocycle (Sect. 3.2.6.1). In this case, the possibility of the CT band is unlikely because there is no metal ion in the cavity. The possibility of J-aggregation is also easily excluded on the basis of a concentration study of the spectra; the Lambert-Beer plot provides a concave curve for the Q-band intensity in common with Fig. 3.37a (inset), whereas it provides a convex curve for the extra band intensity. Hence, the appearance of the extra band is ascribable to the reaction with impurities in the solvent. Nondonor solvents, particularly chlorinated solvents, have more or less acidic impurities (e.g., HCl), which are capable of generating protonated phthalocyanines. As a matter of fact, the addition of CF_3COOH in the dichloromethane solution resulted in the growth of a similar extra band (Fig. 3.37b).

As mentioned above, similar phenomena are observed for metal complexes, particularly for Zn^{II} complexes, which are electron donors [80]. In this case, this type of solvent dependence is misleading to researchers, especially to those who are interested in J-aggregation. When the macrocyclic dye molecule of interest has one or more substituent groups capable of chemically interacting with a metal ion in the cavity of another macrocycle, the chemical interaction (e.g., coordination) allows the two molecules to align in a “head-to-tail” fashion (Fig. 3.15c or d). Thus, the possibility of J-aggregation cannot be completely excluded. Actually, Kameyama et al. have reported rigid J-type dimers of a Zn^{II} complex bearing a peripheral substituent containing an imidazole group [146]. A number of research groups have attempted to publish articles reporting on the possibility of J-aggregation on Zn^{II} complexes of phthalocyanines bearing peripheral substituents capable of coordinating with a metal ion. Among them, some authors have ascribed the extra band to J-aggregation without a sufficient concentration study

but mostly on the basis of its disappearance upon the addition of donors, such as pyridine, DMF, or triethylamine, which are capable of coordinating with the central metal ion. They attributed the disappearance of the extra band in the presence of donor molecules to the replacement of the ligated peripheral substituent by the annexed donor molecule(s) and hence to the disaggregation of the macrocycles. However, this is not convincing evidence because the donor molecule can also act as a proton acceptor. Therefore, readers encountering similar phenomena should remember the possibility of the “mischief” of impurity/impurities (protonation in this case). The likelihood of reaching an incorrect conclusion may be reduced by first carrying out a proper concentration study.

3.3 Spectra of Related Macrocyclic Compounds

In this section, the optical absorption spectra of macrocyclic compounds relevant to phthalocyanine, such as subphthalocyanines, superphthalocyanines, and tetrabenzocorrolazines (tetrabenzotriazacorroles), are shown.

3.3.1 *Subphthalocyanines*

Subphthalocyanines, which are composed of three isoindole units (unlike phthalocyanine, which is composed of four units), are only known to exist as compounds of trivalent boron (B^{III}) (Fig. 3.38a) [232–234]. No derivatives of other elements is known. A typical optical absorption spectrum (for the *tert*-butyl derivative) shows an intense band at approximately 550 nm (Q-band) and less intense bands in the Soret region (Fig. 3.38b) [232, 233]. The appearance of the 550 nm band makes this compound reddish violet. In common with the series of tetraazaporphyrin, phthalocyanine, and naphthalocyanine (Sect. 3.2.3.1), the Q-band is redshifted in the order of subtriaza porphyrin, subphthalocyanine, and subnaphthalocyanine. As each chromophore has a C_3 symmetry around the B-X axis, its LUMO is doubly degenerate and hence its HOMO-LUMO transition (Q-band) is also degenerate [232], as has been exemplified by an MCD study [232].

3.3.2 *Superphthalocyanines*

Superphthalocyanines, which are composed of five isoindole units (Fig. 3.39a) are only known to exist as uranyl ($U^{VI}O_2$) complexes [235–237]. Both their Q-band (900–1000 nm) and Soret bands are significantly redshifted (400–450 nm) relative to the corresponding phthalocyanines and are considerably broadened (Fig. 3.39b).

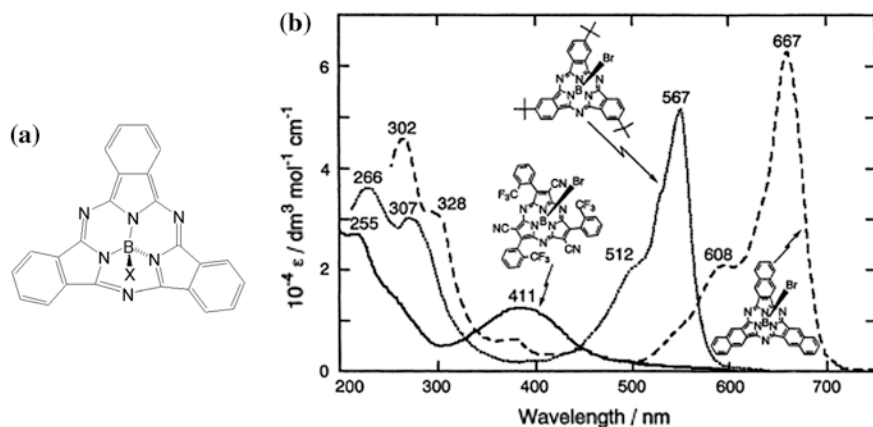


Fig. 3.38 a Subphthalocyanine. b Optical absorption spectra of subzaporphyrin (*solid line*), subphthalocyanine (*dotted line*), and subnaphthalocyanine derivatives (*broken line*) in chloroform. Reprinted from Ref. [233], Copyright 2002, with permission from the Chemical Society of Japan

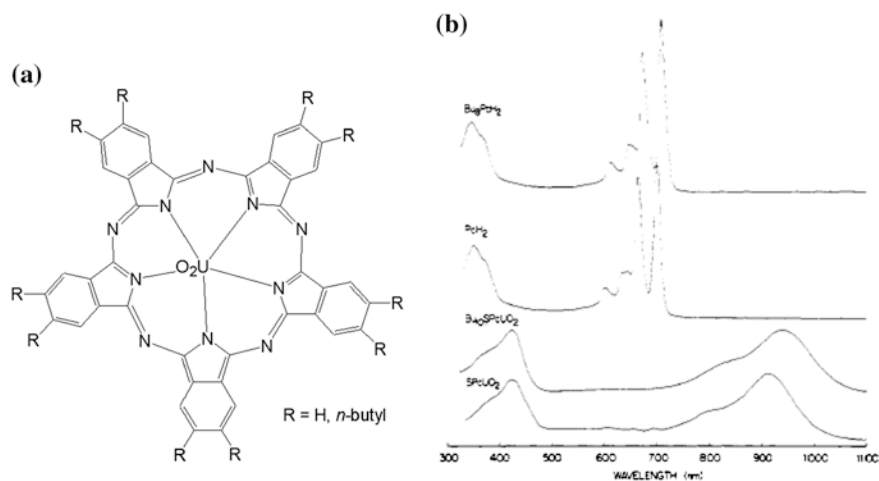


Fig. 3.39 a Superphthalocyanine and b optical absorption spectra of unsubstituted (*bottommost*) and deca-butyl-substituted superphthalocyanines (*second from bottom*) in 1-chloronaphthalene (the upper two spectra are of the corresponding metal-free phthalocyanines in the same solvent). Reprinted from Ref. [235], Copyright 1981, with permission from the American Chemical Society

The chromophore has a fivefold axis around the O-U-O bond; hence, its LUMO is doubly degenerate. Therefore, HOMO-LUMO transitions in superphthalocyanines are degenerate, as has been demonstrated by the appearance of the Faraday A-term in the MCD spectra in the Q-band envelope [237].

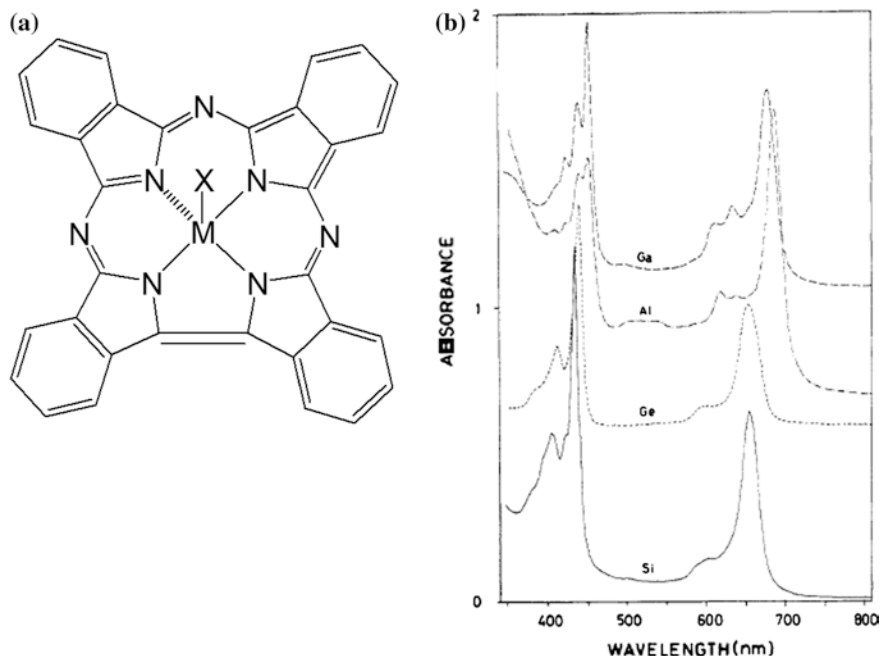


Fig. 3.40 **a** Structure of tetrabenzocorrolazine (tetrabenzotriazacorrole) and **b** optical absorption spectra of Ga^{III}, Al^{III}, Ge^{IV}, and Si^{IV} complexes in isopropyl alcohol. Reprinted from Ref. [238], Copyright 1986, with permission from the American Chemical Society

3.3.3 Tetrabenzocorrolazines (Tetrabenzotriazacorroles)

Tetrabenzocorrolazines have a molecular structure similar to that of phthalocyanines except that one nitrogen atom at a meso position is missing (Fig. 3.40a). To date, metal complexes of the main group elements, such as Al^{III} [238], Si^{IV} [142, 238–241], P^{III/IV} [10, 57, 242], Ga^{III} [238], and Ge^{IV} [238], are known.⁴² The optical absorption spectra of tetrabenzocorrolazines (Fig. 3.40b) show a characteristic sharp band at approximately 450 nm in addition to a slightly less intense band in the range of 650–700 nm [238]. The former and latter absorption bands are assigned as the Soret band and Q-band of corrolazines, respectively, on the basis of computational MO calculations [240, 241, 243]. Clearly, as a corrolazine moiety does not have a symmetry element higher than the threefold axis, no electronic transition can be degenerate. Therefore, it is reasonable that the MCD spectra of corrolazines are dominated by Faraday B-terms [240, 241, 243].

⁴²The metal-free triazacorrole derivatives (corrolazines) and their transition metal complexes are known [for example, 245, 246]. Note that the phosphorus complexes of tetrabenzocorrolazine used to be considered as P^{III} derivatives of phthalocyanines (which are still unknown).

3.4 Absorption Spectra in Solid State

Generally, absorption spectra of phthalocyanines in solid state are quite different from their corresponding solution spectra (crystallochromy) [245] and never provide solvent-free envelope (e.g. see Fig. 3.17). This is because chromophores are much closer to each other in solid state than in solution; hence exciton coupling mainly determines solid-state spectra. Therefore, the absorption bands, particularly in the Q-band region, are considerably broadened and/or split; the spectra are similar to those of aggregated phthalocyanines rather than those of monomeric species (Sect. 3.2.4).

It is well known that phthalocyanines are polymorphic. For example, crystals of copper phthalocyanine [Cu(pc)] have α -, β -, γ -, δ -, ϵ -, π -, τ -, χ - and *M*-polymorphs [246 and references cited herein], each of which shows a characteristic spectrum. In general α phase phthalocyanines show an absorption spectrum extending from 800 to below 200 nm in which the Q band (625 nm) is characterized by the presence of a shoulder at the red flank (694 nm) of the main band. The β -polymorph shows a similar spectrum, although the shoulder lies on the blue flank (645 nm) of the main band (720 nm). The χ -polymorph shows a much more resolved set of bands with essentially the same intensity (624 and 782 nm) in the Q-region [247]. Amongst the polymorphs, crystal structures of α - and β -polymorphs, which are the most important in industry, have been determined by X-ray crystallography [248, 249]. In both cases, the planar and almost square molecules are arranged in one dimensional molecular columns, where the dye molecules are stacked in a manner as shown in Fig. 3.15c. The α -polymorph has stacking of chromophores with a longer interplanar distance ($r = 3.42 \text{ \AA}$) and a larger angle between the polarization axis (actually, the molecular plane of phthalocyanine) and the line passing through the molecule centers ($\theta = 65.1^\circ$) than those of the β -modification ($r = 3.34 \text{ \AA}$ and $\theta = 44.2^\circ$; see Fig. 3.11 and Eq. 3.1 for the meaning of the r and θ values). Therefore, solid-state spectra of phthalocyanines are mainly interpreted in terms of exciton coupling as discussed in Sect. 3.2.4.

Mizuguchi and coworkers have demonstrated that some phthalocyanines are distorted in crystals which exhibit multiple intense bands in the Q-band envelope [250–252]. Significant molecular distortion gives rise to lowering in symmetry of the π conjugation system, which makes degenerate transitions such as Q-band non-degenerate (Sect. 3.2.3). They attributed the splitting to the lowering of symmetry of the molecules that had belonged to C_{4v} in solution [250–252]. Readers who are interested in spectra of phthalocyanines in crystals should be referred to an excellent review written by Mizuguchi [253].

A few years later, Kobayashi and coworkers have investigated optical absorption spectra of titanyl phthalocyanine in crystal that exhibits an intense NIR absorption [254]. They took contribution of intermolecular CT transition between neighboring chromophores (e.g., an electronic transition from the HOMO in one molecule to the LUMO in another molecule nearby) into consideration in addition

to effects of exciton coupling and molecular distortion and successfully reproduced the experimental spectra on the basis of computational calculation.

In solvent-cast films or spin-coated films, absorption spectra are also similar to those of aggregated species [e.g., 5, 6, 255] because of exciton coupling (Sect. 3.2.4). However, Shirota and coworkers have demonstrated that phthalocyanines bearing 4-(*N*-2-naphthyl-*N*-phenylamino)phenoxy groups as peripheral substituents exhibit a monomer-like Q-band in spin-coated thin films [255]. This is because the very bulky and flexible peripheral groups allow the macrocyclic compounds to form stable amorphous glasses with high glass transition temperatures.

References

1. H. Isago, Y. Kagaya, H. Fujita, T. Sugimori, *Dyes Pigm* **88**, 187–194 (2011)
2. H. Isago, Y. Kagaya, *Bull. Chem. Soc. Jpn.* **67**, 383–389 (1994)
3. H. Isago, Y. Kagaya, *Bull. Chem. Soc. Jpn.* **67**, 3212–3215 (1994)
4. Y. Kagaya, H. Isago, *Chem. Lett.* 1957–1960 (1994)
5. H. Isago, Y. Kagaya, S.-I. Nakajima, *Chem. Lett.* **32**, 112–113 (2003)
6. H. Isago, *Chem. Commun.* 1864–1865 (2003)
7. G. Knör, *Inorg. Chem.* **35**, 7916–7918 (1996)
8. D.K. Modibane, T. Nyokong, *Polyhedron* **28**, 479–484 (2009)
9. H. Isago, Y. Kagaya, *Inorg. Chem.* **51**, 8447–8454 (2012)
10. J.P. Fox, D.P. Goldberg, *Inorg. Chem.* **42**, 8181–8191 (2003)
11. N. Kobayashi, T. Furuyama, K. Satoh, *J. Am. Chem. Soc.* **133**, 19642–19645 (2011)
12. M.J. Stillman, T. Nyokong, in *Phthalocyanines: Properties and Applications*, vol. 1, ed. by C.C. Leznoff, A.B.P. Lever (VCH, New York, 1989), pp. 133–289
13. H. Isago, in *Phthalocyanines as Functional Dyes (in Japanese)*, ed. by R. Hirohashi, K. Sakamoto, E. Okumura (IPC, Tokyo, 2004), pp. 141–198
14. N. Kobayashi, T. Fukuda, in *Handbook of Porphyrin Science*, vol. 9, ed. by K.M. Kadish, K.M. Smith, R. Guilard (World Science Publishing, USA, 2010), p. 1
15. M. Gorsch, A. Kienast, H. Hückstädt, H. Homborg, *Z. Anorg. Allg. Chem.* **623**, 1433–1440 (1998)
16. M.J. Stillman, A.J. Thomson, *J. Chem. Soc., Faraday Trans. II* **70**, 805–814 (1974)
17. H. Homborg, K.S. Murray, *Z. Anorg. Allg. Chem.* **517**, 149–160 (1984)
18. A. MacCragh, W.S. Koski, *J. Am. Chem. Soc.* **85**, 2375–2376 (1963)
19. G. Fu, Y. Fu, K. Jayaraj, A.B.P. Lever, *Inorg. Chem.* **29**, 4090–4095 (1990)
20. A.B.P. Lever, *Adv. Inorg. Chem. Radiochem.* **7**, 27–114 (1965)
21. J.S. Anderson, E.F. Bradbrook, A.H. Cook, R.P. Linstead, *J. Chem. Soc.* 1151–1156
22. L. Edwards, M. Gouterman, *J. Mol. Spectrosc.* **33**, 292–310 (1970)
23. M.J. Stillman, A.J. Thomson, *J. Chem. Soc., Faraday Trans. II* **70**, 790–804 (1974)
24. H. Homborg, W. Kalz, *Z. Naturforsch. Sect. B* **39**, 1478–1489 (1984)
25. H. Homborg, W. Kalz, *Z. Naturforsch. Sect. B* **39**, 1490–1499 (1984)
26. J.A. Elvidge, A.B.P. Lever, *J. Chem. Soc.* 1257–1265 (1961)
27. S. Sievertsen, H. Grunewald, H. Homborg, *Z. Anorg. Allg. Chem.* **622**, 1573–1580 (1996)
28. H. Sugimoto, T. Higashi, M. Mori, *Chem. Lett.* 801 (1982)
29. A.B.P. Lever, J.P. Wilshire, *Inorg. Chem.* **17**, 1145–1151 (1978)
30. E.A. Ough, M.J. Stillman, *Inorg. Chem.* **33**, 573–583 (1994)
31. E.A. Ough, M.J. Stillman, *Inorg. Chem.* **34**, 4317–4325 (1995)
32. L.-K. Chau, C.D. England, S. Chen, N.R. Armstrong, *J. Phys. Chem.* **97**, 2699–2706 (1993)
33. R.L. Stover, C.L. Thrall, R.D. Joyner, *Inorg. Chem.* **10**, 2335–2337 (1971)

34. A.R. Kane, J.F. Sullivan, D.H. Kenny, M.E. Kenny, *Inorg. Chem.* **9**, 1445–1448 (1970)
35. K. Schweiger, H. Hückstädt, H. Homborg, *Z. Anorg. Allg. Chem.* **624**, 1298–1302 (1998)
36. P. Clare, F. Glockling, *Inorg. Chim. Acta* **14**, L12 (1975)
37. R.D. George, A.W. Snow, P.F. McMillan, V.A. Burrows, *J. Am. Chem. Soc.* **114**, 8286–8287 (1992)
38. B. Außmann, G. Ostendorp, H. Homborg, *Z. Anorg. Allg. Chem.* **621**, 1708–1714 (1995)
39. K. Schweiger, H. Hückstädt, H. Homborg, *Z. Anorg. Allg. Chem.* **624**, 44–50 (1998)
40. H. Hückstädt, H. Homborg, *Z. Anorg. Allg. Chem.* **624**, 715–720 (1998)
41. H. Hückstädt, H. Homborg, *Z. Anorg. Allg. Chem.* **623**, 292–298 (1997)
42. D.L. Ledson, M.V. Twigg, *Inorg. Chim. Acta* **13**, 43–46 (1975)
43. H. Homborg, W. Kalz, *Z. Anorg. Allg. Chem.* **514**, 115–119 (1984)
44. N.B. Subbon, L.G. Tomilova, N.A. Kostromina, E.A. Lu'kyanets, *J. Gen. Chem. USSR* **56**, 345–348 (1986)
45. N.B. Subbon, L.G. Tomilova, N.A. Kostromina, E.A. Lu'kyanets, *Zh. Obshch. Chem.* **56**, 397–400 (1986)
46. E. Ough, T. Nyokong, K.A.M. Creber, M.J. Stillman, *Inorg. Chem.* **27**, 2724–2732 (1988)
47. A.B.P. Lever, S.R. Pickens, P.C. Minor, S. Licoccia, B.S. Ramaswamy, K. Magnell, *J. Am. Chem. Soc.* **103**, 6800–6806 (1981)
48. S. Sievertsen, H. Grunewald, H. Homborg, *Z. Anorg. Allg. Chem.* **619**, 1279–1737 (1993)
49. A.B.P. Lever, J.P. Wilshire, S.K. Quan, *Inorg. Chem.* **20**, 761–768 (1981)
50. M. Gorsch, H. Homborg, *Z. Anorg. Allg. Chem.* **624**, 634–641 (1998)
51. S.J. Edmondson, P.C.H. Mitchell, *Polyhedron* **5**, 315–317 (1986)
52. T. Nyokong, *Polyhedron* **13**, 215–220 (1994)
53. S. Omiya, M. Tsutsui, E.F. Meyer Jr, I. Bernal, D. Cullen, *Inorg. Chem.* **19**, 134–142 (1980)
54. M. Hanack, P. Vermehren, *Inorg. Chem.* **29**, 134–136 (1990)
55. H. Schlehahn, H. Homborg, *Z. Anorg. Allg. Chem.* **621**, 1558–1566 (1995)
56. S. Sievertsen, H. Schlehahn, H. Homborg, *Z. Anorg. Allg. Chem.* **619**, 1064–1072 (1993)
57. K. Kasuga, L. Lin, M. Handa, T. Sugimori, K. Isa, K. Matsuura, Y. Takinami, *Inorg. Chem.* **38**, 4174–4176 (1999)
58. J. Li, R. Subramanian, M. Hanack, *Eur. J. Org. Chem.* **1998**, 2759–2767 (1998)
59. H. Isago, H. Fujita, M. Hirota, T. Sugimori, Y. Kagaya, *J. Porphyrins Phthalocyanines* **17**, 763–771 (2013)
60. B.D. Berezin, *Russ. J. Phys. Chem.* **36**, 258–261 (1962)
61. M. Whalley, *J. Chem. Soc.* 866–869 (1961)
62. M. Göldner, H. Hückstädt, H. Homborg, *Z. Anorg. Allg. Chem.* **624**, 897–901 (1998)
63. S. Sievertsen, H. Homborg, *Z. Anorg. Allg. Chem.* **620**, 1439–1442 (1994)
64. X. Münz, M. Hanack, *Chem. Ber.* **121**, 235–238 (1988)
65. G. Ostendorp, S. Sievertsen, H. Homborg, *Z. Anorg. Allg. Chem.* **620**, 279–289 (1994)
66. S. Muralidharan, G. Ferraudi, K. Schmatz, *Inorg. Chem.* **21**, 2961–2967 (1982)
67. D. Dolphin, B.R. James, A.L. Murray, J.R. Thornback, *Can. J. Chem.* **58**, 1125–1132 (1980)
68. W. Kobel, M. Hanack, *Inorg. Chem.* **25**, 103–107 (1986)
69. H. Isago, Y. Kagaya, *J. Porphyrins Phthalocyanines* **13**, 382–389 (2009)
70. H. Isago, Y. Kagaya, to be submitted
71. H. Isago, Y. Kagaya, *Chem. Lett.* **35**, 8–9 (2005)
72. E. Cilibert, K.A. Doris, W.J. Pietro, G.M. Reisner, D.E. Ellis, I. Fragala, F.H. Herbstein, M.A. Ratner, T.J. Marks, *J. Am. Chem. Soc.* **106**, 7748–7761 (1984)
73. H. Isago, N. Ishikawa, unpublished results
74. R. Guilard, A. Dormond, M. Belkalem, J.E. Anderson, Y.H. Liu, K.M. Kadish, *Inorg. Chem.* **26**, 1410–1414 (1987)
75. K. Schweiger, M. Göldner, H. Hückstädt, H. Homborg, *Z. Anorg. Allg. Chem.* **625**, 1693–1699 (1999)
76. K. Frick, S. Verma, J. Sundermeyer, M. Hanack, *Eur. J. Inorg. Chem.* 1025–1030 (2000)
77. A. Tutaß, M. Göldner, H. Hückstädt, H. Homborg, *Z. Anorg. Allg. Chem.* **627**, 2323–2336 (2001)

78. D. Eastwood, L. Edwards, M. Gouterman, J. Steinfeld, *J. Mol. Spectrosc.* **20**, 381–390 (1966)
79. T. Nyokong, Z. Gasyna, M.J. Stillman, *Inorg. Chem.* **26**, 1087–1095 (1987)
80. D. Wöhrle, V. Schmidt, *J. Chem. Soc., Dalton Trans.* 549–551 (1988)
81. M. Gorsch, A. Franken, S. Sievertsen, H. Homborg, *Z. Anorg. Allg. Chem.* **621**, 607–616 (1995)
82. N. Kobayashi, A. Muranaka, K. Ishii, *Inorg. Chem.* **39**, 2256–2257 (2000)
83. T. Nyokong, M.J. Stillman, unpublished results
84. P. Sayer, M. Gouterman, C.R. Connell, *Acc. Chem. Res.* **15**, 73–79 (1982)
85. M. Gouterman, P. Sayer, E. Shankland, J.P. Smith, *Inorg. Chem.* **20**, 87–92 (1981)
86. C.C. Leznoff, in *Phthalocyanines: Properties and Applications*, vol. 1, ed. by A.B.P. Lever, C.C. Leznoff (VCH, New York, 1989), pp. 1–54
87. E.A. Luk'yanets, *Electronic Spectra of Phthalocyanines and Related Compounds (in Russian)* (NIOPIK, Moscow, 1989)
88. Y. Ikeda, H. Konami, M. Hatano, K. Mochizuki, *Chem. Lett.* 763–766 (1992)
89. N. Kobayashi, N. Sasaki, Y. Higashi, T. Osa, *Inorg. Chem.* **34**, 1636–1637 (1995)
90. Y. Kagaya, H. Isago, *J. Porphyrins Phthalocyanines* **3**, 537–543 (1999)
91. S.A. Mikhailenko, S.V. Barkanova, O.L. Lebedev, E.A. Luk'yanets, *Zh. Obshch. Khim.* **41**, 2735–2738 (1971)
92. S.A. Mikhailenko, S.V. Barkanova, O.L. Lebedev, E.A. Luk'yanets, *J. Gen. Chem. USSR* **41**, 2770–2773 (1974)
93. S.A. Mikhailenko, E.A. Luk'yanets, *Zh. Obshch. Khim.* **39**, 2129–2136 (1969)
94. S.A. Mikhailenko, E.A. Luk'yanets, *J. Gen. Chem. USSR* **39**, 2081–2086 (1969)
95. N. Kobayashi, H. Ogata, N. Nonaka, E.A. Lukyanets, *Chem. Eur. J.* **9**, 5123–5134 (2003)
96. V.M. Derkacheva, O.L. Kaliya, E.A. Luk'yanets, *Zh. Obshch. Khim.* **53**, 188–192 (1983)
97. V.M. Derkacheva, O.L. Kaliya, E.A. Luk'yanets, *J. Gen. Chem. USSR* **53**, 163–167 (1983)
98. V.M. Derkacheva, E.A. Luk'yanets, *Zh. Obshch. Khim.* **50**, 2313–2318 (1980)
99. V.M. Derkacheva, E.A. Luk'yanets, *J. Gen. Chem. USSR* **50**, 1874–1878 (1980)
100. D. Wöhrle, G. Meyer, *Makromol. Chem.* **181**, 2127–2135 (1980)
101. H. Isago, C.C. Leznoff, F.R. Ryan, R.A. Metcalfe, R. Davids, A.B.P. Lever, *Bull. Chem. Soc. Jpn.* **71**, 1039–1047 (1998)
102. J. Mets, O. Schneider, M. Hanack, *Inorg. Chem.* **23**, 1065–1071 (1984)
103. T. Nyokong, Z. Gasyna, M.J. Stillman, *ACS Symp. Ser.* **321**, 309–327 (1986)
104. V.M. Negrinovskii, V.M. Derkacheva, O.L. Kaliya, E.A. Luk'yanets, *Zh. Obshch. Khim.* **61**, 460–470 (1991)
105. V.M. Negrinovskii, V.M. Derkacheva, O.L. Kaliya, E.A. Luk'yanets, *J. Gen. Chem. USSR* **61**, 419–428 (1991)
106. H. Isago, unpublished data
107. W. Freyer, L.Q. Minh, *Monatsh. Chem.* **117**, 475–489 (1986)
108. P.A. Barrett, E.F. Bradbrook, C.E. Dent, R.P. Linstead, *J. Chem. Soc.* 1820–1828 (1939)
109. I.G. Oksengendler, N.V. Kondratenko, E.A. Luk'yanets, L.M. Yagupol'skii, *Zh. Org. Khim.* **14**, 1046–1051 (1978)
110. I.G. Oksengendler, N.V. Kondratenko, E.A. Luk'yanets, L.M. Yagupol'skii, *J. Org. Chem. USSR* **14**, 976–980 (1978)
111. S.A. Mikhailenko, V.M. Derkacheva, E.A. Luk'yanets, *Zh. Obshch. Khim.* **51**, 1650–1656 (1981)
112. S.A. Mikhailenko, V.M. Derkacheva, E.A. Luk'yanets, *J. Gen. Chem. USSR* **51**, 1405–1411 (1981)
113. L.D. Rollman, R.T. Iwamoto, *J. Am. Chem. Soc.* **90**, 1455–1463 (1968)
114. L.I. Solov'eva, S.A. Mikhailenko, E.A. Chernykh, E.A. Luk'yanets, *Zh. Obshch. Khim.* **52**, 90–101 (1982)
115. L.I. Solov'eva, S.A. Mikhailenko, E.A. Chernykh, E.A. Luk'yanets, *J. Gen. Chem. USSR* **52**, 83–92 (1982)

116. M. Sommerauer, C. Rager, M. Hanack, *J. Am. Chem. Soc.* **118**, 10085–10093 (1996)
117. D.S. Terekhov, K.J.M. Nolan, C.R. McArthur, C.C. Leznoff, *J. Org. Chem.* **61**, 3034–3040 (1996)
118. C.C. Leznoff, Z. Li, H. Isago, A.M.D. D'ascanio, D.S. Terekhov, *J. Porphyrins Phthalocyanines* **3**, 406–416 (1999)
119. J.O. Morley, M.H. Charlton, *J. Phys. Chem.* **99**, 1928–1934 (1995)
120. T. Sugimori, S. Okamoto, N. Kotoh, M. Handa, K. Kasuga, *Chem. Lett.* 1200–1201 (2000)
121. H. Konami, M. Hatano, *Chem. Lett.* 1359–1362 (1988)
122. I. Chambrier, M.J. Cook, M.T. Wood, *Chem. Commun.* 2133–2134 (2000)
123. N. Kobayashi, T. Fukuda, K. Ueno, H. Ogino, *J. Am. Chem. Soc.* **123**, 10740–10741 (2001)
124. T. Fukuda, K. Ono, S. Homma, N. Kobayashi, *Chem. Lett.* 735–736 (2003)
125. N. Kobayashi, S.-I. Nakajima, T. Osa, *Inorg. Chim. Acta* **210**, 131–133 (1993)
126. N. Kobayashi, S.-I. Nakajima, H. Ogata, T. Fukuda, *Chem. Eur. J.* **10**, 6294–6312 (2004)
127. H. Konami, Y. Ikeda, M. Hatano, K. Mochizuki, *Mol. Phys.* **80**, 153–160 (1993)
128. N. Kobayashi, H. Miwa, H. Isago, T. Tomura, *Inorg. Chem.* **38**, 479–485 (1999)
129. N. Kobayashi, H. Konami, in *Phthalocyanines: Properties and Applications*, ed. by C.C. Leznoff, A.B.P. Lever (VCH, New York, 1996), pp. 343–404
130. N. Kobayashi, J. Mack, K. Ishii, M.J. Stillman, *Inorg. Chem.* **41**, 5350–5363 (2002)
131. W.A. Nevin, W. Liu, A.B.P. Lever, *Can. J. Chem.* **65**, 855–858 (1987)
132. A.R. Monahan, J.A. Brado, A.F. Deluca, *J. Phys. Chem.* **73**, 1994–1996 (1972)
133. A.R. Monahan, J.A. Brado, A.F. Deluca, *J. Phys. Chem.* **76**, 446–449 (1972)
134. H. Isago, Y. Kagaya, Y. Oyama, H. Fujita, T. Sugimori, *J. Inorg. Biochem.* **111**, 91–98 (2012)
135. M. Kasha, H.R. Rawls, M.A. El-Bayoumi, *Pure Appl. Chem.* **11**, 371–392 (1965)
136. N. Kobayashi, A.B.P. Lever, *J. Am. Chem. Soc.* **109**, 7433–7441 (1987)
137. Z. Gasyana, N. Kobayashi, M.J. Stillman, *J. Chem. Soc. Dalton Trans.* 2397–2405 (1989)
138. N. Kobayashi, F. Furuya, G.-C. Yug, H. Wakita, M. Yokomizo, N. Ishikawa, *Chem. Eur. J.* **8**, 1474–1484 (2002)
139. Z. Ou, J. Shen, K.M. Kadish, *Inorg. Chem.* **45**, 9569–9579 (2006)
140. L.A. Bottomley, C. Ercolani, J.-N. Gorce, G. Pennesi, G. Rossi, *Inorg. Chem.* **25**, 2338–2342 (1986)
141. S. Sievertsen, H. Homborg, *Z. Anorg. Allg. Chem.* **620**, 1601–1606 (1994)
142. K. Oniwa, S. Shimizu, Y. Shiina, T. Fukuda, N. Kobayashi, *Chem. Commun.* **49**, 8341–8343 (2013)
143. T. Kaneko, T. Arai, K. Tokumaru, D. Matsunaga, H. Sakuragi, *Chem. Lett.* 345–346 (1996)
144. M. Yoon, Y. Cheon, D. Kim, *Photochem. Photobiol.* **58**, 31–36 (1993)
145. A. Okada, H. Segawa, *J. Am. Chem. Soc.* **125**, 2792–2796 (2003). (and references therein)
146. K. Kameyama, M. Morisue, A. Satake, Y. Kobuke, *Angew. Chem. Int. Ed.* **44**, 4763–4766 (2005)
147. W.A. Nevin, M.R. Hemstead, W. Liu, C.C. Leznoff, A.B.P. Lever, *Inorg. Chem.* **26**, 570–577 (1987)
148. S.M. Marcuccio, P.I. Svirskaya, S. Greenberg, A.B.P. Lever, C.C. Leznoff, *Can. J. Chem.* **63**, 3057–3069 (1985)
149. E.S. Dodsworth, A.B.P. Lever, P. Seymour, C.C. Leznoff, *J. Phys. Chem.* **89**, 5698–5705 (1985)
150. H. Lam, S.M. Marcuccio, P.I. Svirskaya, S. Greenberg, A.B.P. Lever, C.C. Leznoff, R.L. Cerny, *Can. J. Chem.* **67**, 1087–1097 (1989)
151. W.E. Bennett, D.E. Broberg, N.C. Baenziger, *Inorg. Chem.* **12**, 930–936 (1973)
152. O. Ohno, N. Ishikawa, H. Matsuzawa, Y. Kaizu, H. Kobayashi, *J. Phys. Chem.* **93**, 1713–1718 (1989)
153. N. Ishikawa, O. Ohno, Y. Kaizu, H. Kobayashi, *J. Phys. Chem.* **96**, 8832–8839 (1992)
154. N. Kobayashi, *Coord. Chem. Rev.* **227**, 129–152 (2002)
155. H. Isago, M. Shimoda, *Chem. Lett.* 147–150 (1992)

156. M.S. Haghighi, C.L. Teske, H. Homborg, *Z. Anorg. Allg. Chem.* **608**, 73–80 (1992)
157. P.N. Moskalev, G.N. Shapkin, A.N. Darovskikh, *Russ. J. Inorg. Chem.* **24**, 188–192 (1979)
158. P.N. Moskalev, G.N. Shapkin, A.N. Darovskikh, *Zh Neorg. Khim* **24**, 340–346 (1979)
159. P.N. Moskalev, N.I. Alimova, *Russ. J. Inorg. Chem.* **20**, 1474–1477 (1975)
160. P.N. Moskalev, N.I. Alimova, *Zh Neorg. Khim* **20**, 2664–2668 (1975)
161. L.G. Tomilova, N.A. Ovchinnikova, E.A. Luk'yanets, *J. Gen. Chem. USSR* **57**, 1880–1883 (1987)
162. L.G. Tomilova, N.A. Ovchinnikova, E.A. Luk'yanets, *Zh. Obshch. Khim.* **57**, 2100–2104 (1987)
163. N.A. Ovchinnikova, L.G. Tomilova, N.B. Seregina, V.V. Minin, G.M. Larin, E.A. Luky'anets, *J Gen Chem. USSR* **62**, 1340–1345 (1992)
164. N.A. Ovchinnikova, L.G. Tomilova, N.B. Seregina, V.V. Minin, G.M. Larin, E.A. Luk'yanets, *Zh. Obshch. Khim.* **62**, 1631–1638 (1992)
165. G. Ostendorp, H. Homborg, *Z. Anorg. Allg. Chem.* **622**, 1358–1364 (1998)
166. G. Ostendorp, H. Homborg, *Z. Anorg. Allg. Chem.* **622**, 873–880 (1998)
167. H. Hückstädt, A. Tutaß, M. Göldner, U. Cornelissen, H. Homborg, *Z. Anorg. Allg. Chem.* **627**, 485–497 (2001)
168. K. Takahashi, J. Shimoda, M. Itoh, Y. Fuchita, H. Osawa, *Chem. Lett.* 173–174 (1998)
169. T. Fukuda, T. Biyajima, N. Kobayashi, *J. Am. Chem. Soc.* **132**, 6278–6279 (2010)
170. H. Konami, M. Hatano, A. Tajiri, *Chem. Phys. Lett.* **166**, 605–608 (1990)
171. H. Hückstädt, H. Homborg, *Z. Anorg. Allg. Chem.* **623**, 369–378 (1997)
172. H. Hückstädt, C. Bruhn, H. Homborg, *J. Porphyrins Phthalocyanines* **1**, 367–378 (1997)
173. M. Göldner, H. Hückstädt, K.S. Murray, B. Moubaraki, H. Homborg, *Z. Anorg. Allg. Chem.* **624**, 288–294 (1998)
174. H. Isago, H. Fujita, *J. Porphyrins Phthalocyanines* **17**, 447–453 (2013)
175. M.E. Anderson, A.G. Barrett, B.M. Hoffman, *Inorg. Chem.* **38**, 6143–6151 (1999)
176. K.A. Martin, M.J. Stillman, *Inorg. Chem.* **19**, 2473–2475 (1980)
177. A. Ogunsipe, T. Nyokong, *J. Mol. Struct.* **689**, 89–97 (2004)
178. P.A. Stuzhin, *J. Porphyrins Phthalocyanines* **3**, 500–513 (1999)
179. P.A. Stuzhin, in *Phthalocyanines—Properties and Applications*, vol. 4, ed. by C.C. Leznoff, A.B.P. Lever (VCH, New York, 1996) pp. 19–77
180. P.A. Bernstein, A.B.P. Lever, *Inorg. Chim. Acta* **198–200**, 543–555 (1992)
181. V.M. Derkacheva, S.S. Iodko, O.L. Kaliya, E.A. Luk'yanets, *J. Gen. Chem. USSR* **51**, 1998–2002 (1981)
182. V.M. Derkacheva, S.S. Iodko, O.L. Kaliya, E.A. Luk'yanets, *Zh. Obshch. Khim.* **51**, 2319–2324 (1981)
183. O.L. Levedev, E.A. Luk'yanets, V.A. Puchnova, *Opt. Spectrosc.* **30**, 347–349 (1971)
184. O.L. Levedev, E.A. Luk'yanets, V.A. Puchnova, *Opt. Spektrosc.* **30**, 640–643 (1971)
185. S. Gaspard, M. Verdager, G. Viovy, *J. Chem. Res. (S)* 271 (1979)
186. AKh Khanamiryan, N. Bhardwaj, C.C. Leznoff, *J. Porphyrins Phthalocyanines* **4**, 484–490 (2000)
187. A.B.P. Lever, E.R. Milaeva, G. Speier, in *Phthalocyanines—Properties and Applications*, vol. 3, ed. by Leznoff, C.C., Lever, A.B.P. (VCH, New York, 1993), pp. 1–69
188. M.J. Stillman, in *Phthalocyanines—Properties and Applications*, vol. 3, ed. by C.C. Leznoff, A.B.P. Lever (VCH, New York, 1993), pp. 227–296
189. H. Isago, *J. Porphyrins Phthalocyanines* **10**, 1125–1131 (2006)
190. E. Ough, Z. Gasyana, M.J. Stillman, *Inorg. Chem.* **30**, 2301–2310 (1991)
191. H. Homborg, *Z. Anorg. Allg. Chem.* **507**, 35–50 (1983)
192. T. Nyokong, Z. Gasyana, M.J. Stillman, *Inorg. Chem.* **26**, 548–553 (1987)
193. H. Homborg, Q. Kalz, *Z. Naturforsch. Sect. B* **33**, 1067–1071 (1978)
194. E. Orti, J.L. Bredas, C. Clarisse, *J. Chem. Phys.* **92**, 1228–1235 (1990)
195. J. Mack, M.J. Stillman, *J. Phys. Chem.* **99**, 7935–7945 (1995)
196. J. Mack, M.J. Stillman, *Coord. Chem. Rev.* **219–221**, 993–1032 (2001)

197. N. Ishikawa, Y. Kaizu, *Chem. Phys. Lett.* **339**, 125–132 (2001)
198. T. Nyokong, Z. Gasyna, M.J. Stillman, *Inorg. Chim. Acta* **112**, 11–15 (1986)
199. M.M. Nicholson, in *Phthalocyanines—Properties and Applications*, vol. 3, ed. by C.C. Leznoff, A.B.P. Lever (VCH, New York, 1993), pp. 71–118
200. P. Turek, P. Petit, J.J. Andre, R. Evan, B. Boudjema, G. Guillaud, M. Maitrot, *J. Am. Chem. Soc.* **109**, 5119–5122 (1987)
201. H. Isago, *J. Porphyrins Phthalocyanines* **12**, 861–869 (2012)
202. G. Ostendorp, H. Homborg, *Z. Anorg. Allg. Chem.* **622**, 1358–1364 (1996)
203. A. De Cian, M. Moussavi, J. Fischer, R. Weiss, *Inorg. Chem.* **24**, 3162–3167 (1985)
204. N. Ishikawa, O. Ohno, Y. Kaizu, *Chem. Phys. Lett.* **180**, 51–56 (1991)
205. G. Ostendorp, H. Homborg, *Z. Anorg. Allg. Chem.* **622**, 873–880 (1996)
206. N. Ishikawa, O. Ohno, Y. Kaizu, *J. Phys. Chem.* **97**, 1004–1010 (1993)
207. C.L. Dunford, B. Williamson, E. Krausz, *J. Phys. Chem. A* **104**, 3537–3543 (2000)
208. J.S. Shirk, J.R. Lindle, F.J. Bartoli, M.E. Boyle, *J. Phys. Chem.* **96**, 5847–5852 (1992)
209. H. Sugimoto, M. Mori, H. Masuda, T. Taga, *Chem. Commun.* 962–963 (1986)
210. G. Ostendorp, H.W. Rotter, H. Homborg, *Z. Anorg. Allg. Chem.* **622**, 235–244 (1996)
211. T. Fukuda, K. Hata, N. Ishikawa, *J. Am. Chem. Soc.* **134**, 14698–14701 (2012)
212. D.W. Clack, J.R. Yandle, *Inorg. Chem.* **11**, 1738–1742 (1972)
213. J. Mack, M.J. Stillman, *J. Am. Chem. Soc.* **116**, 1292–1304 (1994)
214. J. Mack, S. Kirkby, E.A. Ough, M.J. Stillman, *Inorg. Chem.* **31**, 1717–1719 (1992)
215. J. Mack, M.J. Stillman, *Inorg. Chem.* **36**, 413–425 (1997)
216. H. Isago, Y. Kagaya, *Bull. Chem. Soc. Jpn.* **69**, 1281–1288 (1996)
217. E.W.Y. Wong, D.B. Leznoff, *J. Porphyrins Phthalocyanines* **16**, 154–162 (2012)
218. MdH Zahir, Y. Kagaya, H. Isago, T. Furubayashi, *Inorg. Chim. Acta* **357**, 2755–2758 (2004)
219. T. Harazono, I. Takagishi, *Bull. Chem. Soc. Jpn.* **66**, 1016–1023 (1993)
220. H. Isago, Y. Kagaya, A. Matsushita, *Chem. Lett.* **33**, 862–863 (2004)
221. T. Inabe, Y. Maruyama, *Bull. Chem. Soc. Jpn.* **63**, 2273–2280 (1990)
222. P. Suppan, *J. Photochem. Photobiol. Sect. A* **50**, 293–330 (1990)
223. H. Isago, K. Miura, Y. Oyama, *J. Inorg. Biochem.* **102**, 380–387 (2008)
224. H. Isago, K. Miura, M. Kanesato, *J. Photochem. Photobiol. A* **197**, 313–320 (2008)
225. A.B.P. Lever, J.P. Wilshire, S.K. Quan, *J. Am. Chem. Soc.* **101**, 3868–3869 (1979)
226. O. E. Sielcken, M.M. van Tillborg, M.F.M. Roks, R. Hendricks, W. Drenth, R.J.M. Nolte, *J. Am. Chem. Soc.* **109**, 4261–4265 (1987)
227. A. Ferencz, D. Neher, M. Schulze, G. Wegner, L. Viaene, F.C. De Schryver, *Chem. Phys. Lett.* **245**, 23–29 (1995)
228. L. Oddos-Marcel, F. Madeore, A. Bock, D. Neher, A. Ferencz, H. Rengel, G. Wegner, C. Kryschi, H.P. Trommsdorff, *J. Phys. Chem.* **100**, 11850–11856 (1996)
229. J. Kleinwächter, M. Hanack, *J. Am. Chem. Soc.* **119**, 10684–10695 (1997)
230. Z. Li, M. Lieberman, *Inorg. Chem.* **40**, 932–939 (2001)
231. J. Ern, A. Bock, L. Oddos-Marcel, H. Rengel, G. Wegner, H.P. Trommsdorff, C. Kryschi, *J. Phys. Chem. A* **103**, 2446–2450 (1999)
232. N. Kobayashi, T. Ishizaki, K. Ishii, H. Konami, *J. Am. Chem. Soc.* **121**, 9096–9110 (1999)
233. N. Kobayashi, *Bull. Chem. Soc. Jpn.* **75**, 1–19 (2002)
234. C.G. Claessens, D. González-Rodríguez, T. Torres, *Chem. Rev.* **102**, 835–853 (2002)
235. E.A. Cuellar, T.J. Marks, *Inorg. Chem.* **20**, 3766–3770 (1981)
236. T.J. Marks, D.R. Stojakovic, *J. Am. Chem. Soc.* **100**, 1695–1705 (1978)
237. T. Furuyama, Y. Ogura, K. Yoza, N. Kobayashi, *Angew. Chem. Int. Ed.* **51**, 11110–11114 (2012)
238. M. Fujiki, H. Tabei, K. Isa, *J. Am. Chem. Soc.* **108**, 1532–1536 (1986)
239. J. Li, L. R. Subramanian, M. Hanack, *J. Chem. Soc. Chem. Commun.* 679–680 (1997)
240. J. Mack, N. Kobayashi, *Chem. Rev.* **111**, 281–321 (2011)
241. J. Mack, M. Bunya, D. Lansky, D.P. Goldberg, N. Kobayashi, *Heterocycles* **76**, 1369–1380 (2008)

242. J. Liu, F. Zhang, F. Zhao, Y. Tang, X. Song, G. Yao, J. Photochem. Photobiol. Sect. A **91**, 99–104 (1995)
243. W.D. Kerber, B. Ramdhanie, D.P. Goldberg, Angew. Chem. Int. Ed. **46**, 3718–3721 (2007)
244. N. Kobayashi, M. Yokoyama, A. Muranaka, A. Ceulemans, Tetrahedron Lett. **45**, 1755–1758 (2004)
245. T. Birnbaum, T. Hahn, C. Martin, J. Kortus, M. Fronk, F. Lungwitz, D.R.T. Zahn, G. Salvan, J. Phys. Condens. Matter **26**, 104201–104212 (2014)
246. F.H. Moser, A.L. Thomas, *The Phthalocyanines*, vol. 1 (CRC Press, Boca Raton, 1983)
247. J.H. Sharp, M. Abkowitz, J. Phys. Chem. **77**, 477–481 (1973)
248. A. Hoshino, Y. Takenaka, H. Miyaji, Acta Crystallogr. Sect. B **59**, 393–403 (2003)
249. A. Hoshino, Y. Takenaka, H. Miyaji, C.J. Brown, J. Chem. Soc. A 2488–2493 (1968)
250. J. Mizuguchi, G. Rihs, H.R. Karfunkel, J. Phys. Chem. **44**, 16217–16227 (1995)
251. J. Mizuguchi, S. Matsumoto, J. Phys. Chem. A **103**, 614–616 (1999)
252. A. Endo, S. Matsumoto, J. Mizuguchi, J. Phys. Chem. A **103**, 8193–8199 (1999)
253. J. Mizuguchi, Shikizai **72**, 510–514 (1999)
254. K. Nakai, K. Ishii, N. Kobayashi, H. Yonehara, C. Pac, J. Phys. Chem. B **107**, 9749–9755 (2003)
255. M. Ottmar, T. Ichisaka, L.R. Subramanian, M. Hanack, Y. Shirota, Chem. Lett. 788–789 (2001)

Chapter 4

Optical Emission Spectra of Phthalocyanines

4.1 Fluorescence: Optical Emission from the Lowest Singlet Excited States

As discussed in Chap. 1, optical absorption by a dye molecule occurs when the molecule is excited from its ground state (S_0) to a singlet excited state. In this monograph, attention will mostly be focused on emission from the S_1 state and other emissions will be briefly discussed in Sect. 4.2. This is because fluorescence spectroscopy is becoming increasingly popular and hence inexperienced scientists have greater access to such spectrometers in their laboratories. Since we are interested in fluorescence from the dye molecules, let us consider how an excited molecule in the lowest excited state behaves. A photoexcited dye molecule in its S_1 state can return to the S_0 ground state via various routes. Some molecules emit light with essentially the same but a slightly lower energy relative to the absorbed light (i.e., light with a slightly higher wavelength), some molecules convert the excess vibrational energy into heat and transfer the energy to neighboring molecules, such as, solvent molecules, through a collision process (nonradiative decay), and others undergo a transition (from singlet to triplet states) leading to phosphorescence, an energy transfer reaction with the other molecules (such as molecular oxygen (Sect. 4.2.3)). These processes are illustrated in Fig. 4.1, in a Jabłoński diagram.

4.1.1 How Does an Excited Molecule Emit Light?

We learned in Chap. 1 that methylene blue (MB) appears blue because it absorbs red light and thereby we see a blue color as its complementary color. Therefore, it is easily predicted that excited MB molecules emit red light when they return to

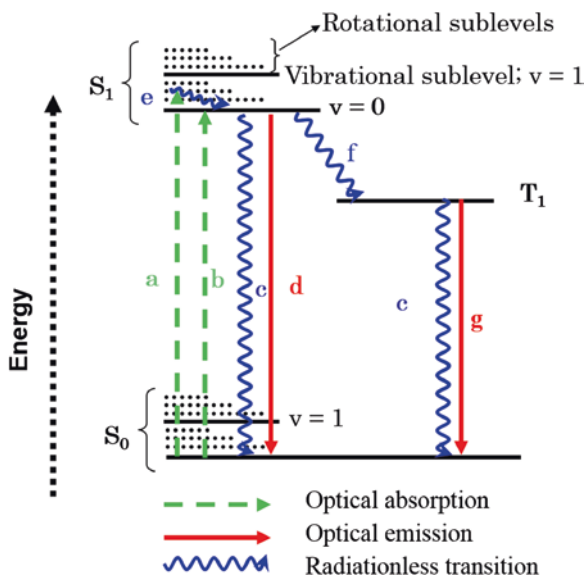


Fig. 4.1 Jablonski diagram: **a** optical absorption, **b** 0-0 transition (absorption), **c** radiationless transition, **d** fluorescence, **e** internal conversion, **f** intersystem crossing, **g** phosphorescence

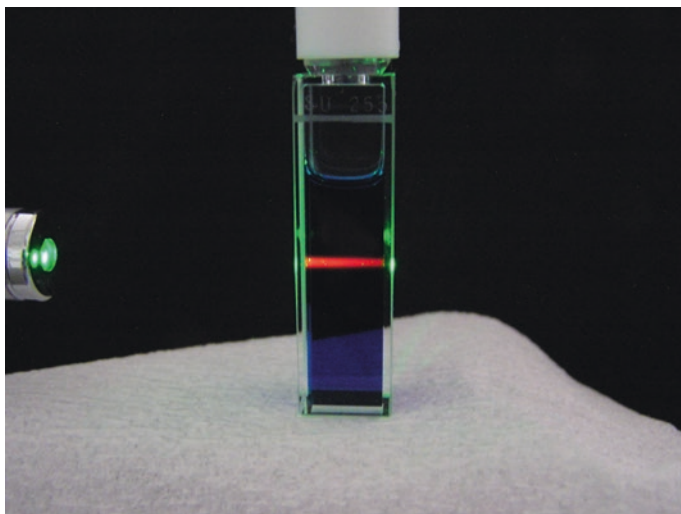
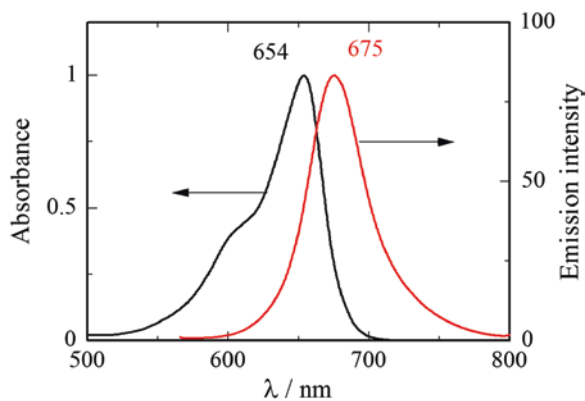


Fig. 4.2 Fluorescence from methylene blue in ethanolic solution (excited with 532 nm laser light). *Source* NIMS eSciDoc—IMEJI. © Hiroaki Isago with CC-BY-NC 3.0 license

the ground state (S_0). Figure 4.2 shows the emission of red light from MB excited by a green laser beam (532 nm). Figure 4.3 shows the optical absorption and emission spectra of MB in ethanol. The emission peak appears at a longer wavelength (675 nm) than the wavelength of maximum absorption (654 nm). This is attributed

Fig. 4.3 Optical absorption (black line) and emission (red line) spectra of methylene blue in ethanol. Source NIMS eSciDoc—IMEJI. © Hiroaki Isago with CC-BY-NC 3.0 license



to the general tendency for the structure of an excited molecule to be different from that in the ground state because of the stronger antibonding character in the excited states; i.e., a longer bonding distance and distortion, in the excited states). In the ground (S_0) state, the molecules are mostly at the lowest vibration level of the S_0 state; the higher vibrational levels are essentially empty at room temperature (<1 % on the basis of the Boltzmann distribution). Hence, most of the molecules will be excited from the lowest sublevel (Fig. 4.1a). The transition from S_0 ($v = 0$) to S_1 ($v = 0$) is referred to as a 0–0 transition (Fig. 4.1b). However, as mentioned in Sect. 1.1.3, not all of the molecules in the lowest level of S_0 are promoted to the lowest level in the S_1 state and some can be excited to higher levels of S_1 (each vibrational energy level has a number of rotational energy levels) because optical absorption occurs very rapidly (within femtoseconds).¹ Let us consider the behavior of the excited dye molecule in Fig. 4.1.

These photoexcited molecules are fully relaxed to the lowest vibrational level of S_1 within picoseconds by the emission of some energy as heat (internal conversion; Fig. 4.1e), whereby optical emission occurs in principle (Kasha's rule). As optical emission typically takes place after nanoseconds,² the fluorescence spectrum does not generally depend on the excitation wavelength. Thus, part of the energy gained by optical absorption has already been lost before the initiation of emission during the internal conversion process. The transition from S_1 to S_0 occurs simultaneously with optical emission (fluorescence; Fig. 4.1d). The energy difference between the 0–0 transitions³ in the optical absorption and emission is referred to as a Stokes shift. In the case of MB, the Stokes shift corresponds to the difference between the optical absorption and emission peaks (Fig. 4.3) and its magnitude is 480 cm^{-1} .

¹From the Frank-Condon principle (see Sect. 1.1.3).

²As the $S_1 \rightarrow S_0$ transition is an allowed process, the emission promptly occurs.

³The transition from S_1 ($v = 0$) to S_0 ($v = 0$) is referred to as a 0–0 transition, in common with optical absorption.

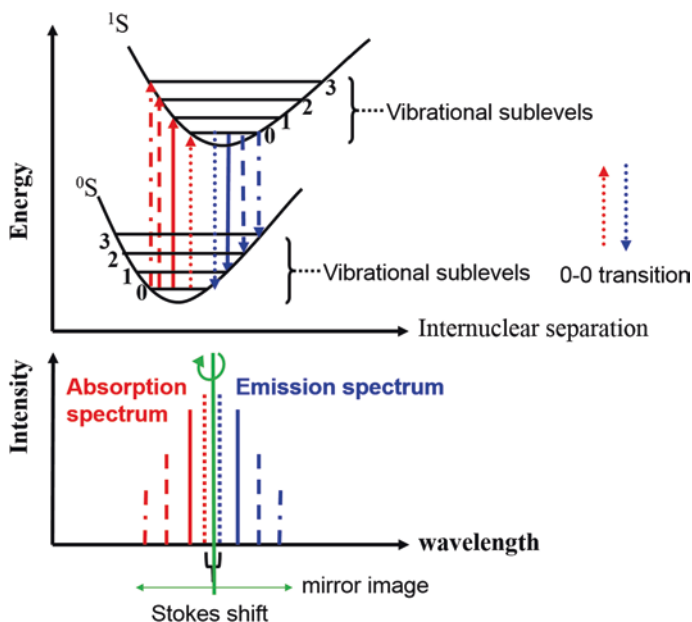


Fig. 4.4 (Top) Electronic transitions between S_0 and S_1 states, where red and blue arrows represent optical absorption and emission, respectively. (Bottom) Observed optical absorption (red) and emission (blue) spectra, which appear to be mirror images. Source NIMS eSciDoc—IMEJ. © Hiroaki Isago with CC-BY-NC 3.0 license

Another important aspect of the emission spectrum is that it appears to be a mirror image of the absorption spectrum. Let us consider the excitation and relaxation of a virtual dye molecule that has the electronic structure shown in Fig. 4.4 as a function of internuclear separation. As is the case for optical absorption, not all of the excited molecules in the lowest vibrational level of S_1 relax to the lowest vibrational level of S_0 . Some may return to a higher vibrational level of S_0 , from which they vibrationally relax to the lowest level. When the energy intervals between vibrational levels (e.g., the spacing between $v = 0$ and $v = 1$) in S_1 are close to those in S_0 , the optical absorption and emission spectra of dyes generally become symmetrical. Actually, the emission spectrum of MB appears to be a mirror image of the absorption spectrum in the same solvent (Fig. 4.3).

4.1.2 Appearance of Fluorescence Spectra

By analogy to the optical emission of MB, it is easily predicted that photoexcited phthalocyanines and their metal complexes should emit red light upon their relaxation to the ground state (if they are fluorescent⁴). Actually, both free-base tetra-*tert*-butyl-

⁴Not all metal complexes are fluorescent (Sect. 4.1.3.2).

substituted phthalocyanine (H_2tbc) and its P^V complex emit red light upon excitation with 532 nm laser light (Fig. 4.5) [1, 2]. Figure 4.6 shows the optical emission and absorption spectra of a P^V complex of tetra-(2', 6'-dimethylphenoxy)-substituted phthalocyanines (tppc) in ethanol as well as the corresponding excitation spectrum [3].

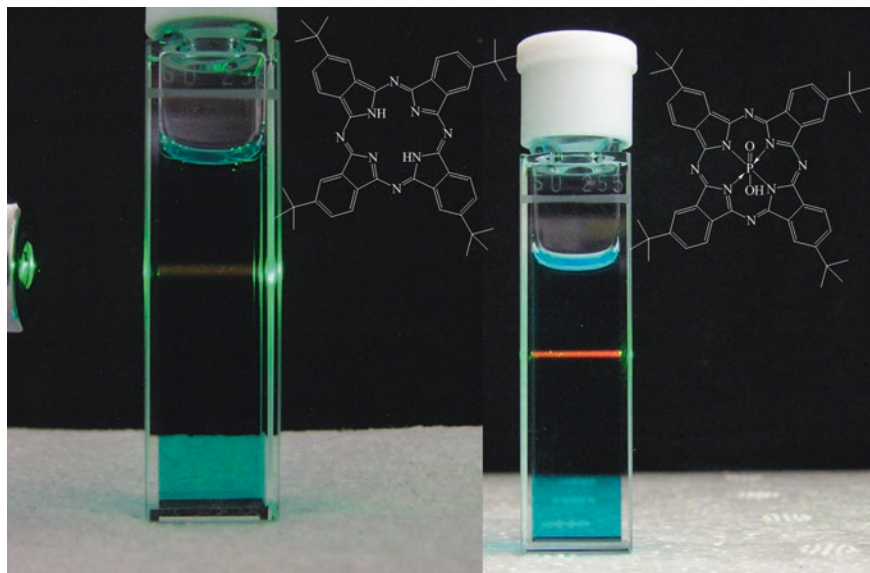


Fig. 4.5 Fluorescence from **a** H_2tbc in THF (emission peak; 708 nm [1]) and **b** its P^V complex, $[P(tbc)(O)(OH)]$, in ethanol (emission peak 686 nm [2]). Both dyes were excited with 532 nm laser light. *Source* NIMS eSciDoc—IMEJ. © Hiroaki Isago with CC-BY-NC 3.0 license

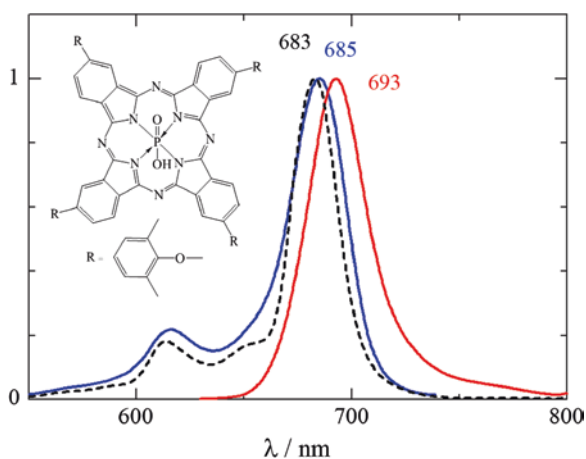
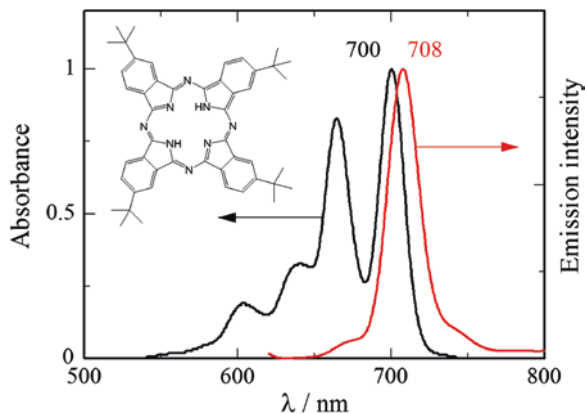


Fig. 4.6 Optical absorption (*black broken line*), emission (*red solid line*; excited at 614 nm) and excitation (*blue solid line*; monitored at 720 nm) spectra of P^V complex, $[P(tppc)(O)(OH)]$, (inset) in ethanol. Reproduced from Ref. [3], Copyright 2013, reproduced with permission from World Scientific Publishing Company

Fig. 4.7 Optical absorption (black solid line) and emission (red solid line) spectra of metal-free tetra-*tert*-butyl-substituted phthalocyanine (inset) in THF. Source NIMS eSciDoc—IMEJI. © Hiroaki Isago with CC-BY-NC 3.0 license



An excitation spectrum is measured with the emission light fixed at a constant wavelength, and the excitation light is scanned through many different wavelengths. Therefore, generally, excitation and optical absorption spectra are essentially the same, as shown by the black broken and blue solid lines in Fig. 4.6. In other words, the concordance of the two spectra proves that the emission is from the compound of interest.⁵ Here again the emission spectrum appears to be a mirror image of the absorption spectrum. However, in contrast to the spectra of MB, the overlap between the absorption and emission spectra of the P^V complex is quite large, and the difference between the peaks of the two spectra is quite small (the Stokes shift in this case is 169 cm⁻¹, about one-third of that of MB). This indicates insignificant rearrangement of the atomic coordinates of the phthalocyanine macrocycle upon photoexcitation, and hence the molecular skeleton of the macrocyclic ligand is much more rigid than that of MB. Symmetrical absorption and emission spectra and a small Stokes shift have been reported for many metal derivatives of phthalocyanines. An exception to this “mirror image rule” has been observed for the emission of metal-free derivatives. As an example, the optical absorption and emission spectra of the free base of the same phthalocyanine in THF are not symmetrical (Fig. 4.7). As described in Sect. 2.1.1, the most intense absorption of metal-free derivatives generally shows twin peaks with essentially the same intensity (Fig. 4.7) because of its C₂ symmetry due to the presence of central imino protons. Nevertheless, the emission spectrum of the same compound in the same solvent shows a single peak at a slightly longer wavelength than the absorption peak of the lowest transition (700 nm). This is because the lowest (S₁) and second lowest excited states (S₂) are so close in energy that the majority of those molecules excited to S₂ are rapidly (thermally) relaxed to S₁ (a radiationless process). Emission occurs predominantly from S₁ (Kasha’s rule), thus, little emission from S₂ is observed (appearing as a shoulder around 670 nm).⁶ Thus, the

⁵Otherwise, the emission is from another substance, such as an impurity (Sect. 4.1.5).

⁶The appearance of a single peak in the emission spectra of metal-free derivatives can occasionally give rise to a serious misinterpretation as mentioned later (Sect. 4.1.5).

emission spectrum in this case is almost the mirror image of the S_0 to S_1 absorption but not of the total absorption spectrum.

The emission of $H_2t\text{bpc}$ appears to be very weak (Fig. 4.5a) compared with that of the P^V complex of the same macrocyclic ligand (Fig. 4.5b) despite its comparable emission efficiency (0.85 [1]) to that of the latter (0.80 [2]). It is even weak compared with that of MB (Fig. 4.2), which has a much lower efficiency (0.02; [4]). This is simply because the sensitivity of our eyes to 708 nm light is much weaker than that to 686 nm light (P^V complex) or 675 nm (MB) light (Fig. 1.1). Such efficiency is quantitatively represented as a fluorescence quantum yield as described in the following subsection.

4.1.3 Fluorescence Quantum Yield

One of the most important quantitative data for fluorescence is the quantum yield (Φ_F). The value of 0.85 for $H_2t\text{bpc}$ [1] mentioned above means that out of 100 molecules that absorb incident light, 85 molecules emit fluorescence. Some of the other molecules thermally return to S_0 through a nonradiative process (Fig. 4.1c) or undergo an intersystem crossing transition to T_1 (Fig. 4.1f). Therefore, a fluorophore with a shorter fluorescence lifetime (i.e., a higher emission rate) has a larger quantum yield.

4.1.3.1 How to Determine Quantum Yield

Fluorescence quantum yields are generally determined by a relative method using an appropriate compound whose quantum yield is known as a standard (e.g., 0.85 for $H_2t\text{bpc}$ in THF [1]) in accordance with Eq. 4.1.⁷ The reference and sample solutions are irradiated at an appropriate wavelength at which the two spectra have the same absorbance. The quantum yield of the compound of interest is obtained using Eq. 4.1 from the areas (S) under the fluorescence spectra (on an energy scale but not on a wavelength scale), the refractive indices of the solvents used for the measurements (the n values), and the quantum yield of the standard ($\Phi_{\text{ref}F}$):

$$\Phi_{\text{sm}pF} = \Phi_{\text{ref}F} \times \frac{S_{\text{sm}p}}{S_{\text{ref}}} \times \frac{A_{\text{ref}}}{A_{\text{sm}p}} \times \frac{n_{\text{sm}p}^2}{n_{\text{ref}}^2} \quad (4.1)$$

As the excitation wavelength was chosen so that $A_{\text{ref}} = A_{\text{sm}p}$, this equation is simplified to

$$\Phi_{\text{sm}pF} = \Phi_{\text{ref}F} \times \frac{S_{\text{sm}p}}{S_{\text{ref}}} \times \frac{n_{\text{sm}p}^2}{n_{\text{ref}}^2} \quad (4.2)$$

⁷Some high-spec spectrometers can directly determine quantum yield values using an integrating sphere (also known as an Ulbricht sphere).

Therefore, if the same solvent can be used for both the sample and the standard, the quantum yield of the desired compound can be more easily determined by simply comparing the areas of the observed fluorescence.

4.1.3.2 Effects of Central Metal Element

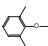
In general, quantum yield values are affected by various factors such as the temperature, molecular structure, solvent parameters (coordination ability, polarity, viscosity, and refractive index), and the presence of heavy atoms in the solvent and/or in the molecule itself. For phthalocyanines and related macrocyclic compounds, in particular, the nature of the central element plays a crucial role. Even with the same element included in the cavity, the emission characteristics depend on the oxidation state; for example, Sb^{V} derivatives are fluorescent (although weak) [5–7], whereas Sb^{III} derivative is not [8] (Table 4.1). Quantum yield data has been summarized in earlier reviews [9, 10]. Table 4.1 shows some quantum yield data for a limited

Table 4.1 Effects of central element and peripheral substituents on fluorescence characteristics of phthalocyanines

R ^a	P ^b	M ^c	L ^d	Solvent ^e	$\lambda_{\text{f}}^{\text{f}}$	$\Phi_{\text{f}}^{\text{g}}$	T/K ^h	Ref
H		H ₂		CLN	699	0.7	77	[11]
H		H ₂		CLN	704	0.6		[12]
H		Li ₂		AN	665	0.5		[13]
H		Mg		DMSO		0.6		[14]
H		Mg		CLN	683	0.6	77	[11]
H		Al	Cl	CLN	680	0.58		[15]
H		Al	Cl	CLN		0.58		[16]
H		Al	Cl	DMSO		0.67		[17]
H		V ^{IV}	O	QN	nd ⁱ	nd	77	[11]
H		Co ^{II}		CLN	nd	$<5 \times 10^{-5}$	77	[11]
H		Ni ^{II}		CLN	nd	$<5 \times 10^{-5}$	77	[11]
H		Cu ^{II}		CLN		$<10^{-4}$	77	[11]
H		Zn ^{II}		DMSO	682	0.32		[18]
H		Zn ^{II}		CLN	683	0.3	77	[11]
H		Ga ^{III}	Cl	CLN		0.31		[16]
H		Rh ^{III}	Cl	CLN	662	1×10^{-3}	2–4, 77	[19]
H		Ge ^{IV}	(OSiY ₃) ₂	TOL	673.7 ^k	0.6		[20]
H		Pd ^{II}		QN	664	5×10^{-4}	77	[11]
H		Cd ^{II}		QN	693	0.03–0.08	77	[11]
H		In ^{III}	Cl	CLN		0.031		[16]
H		Sn ^{IV}	(OSiY ₃) ₂	TOL	680.0 ^k	0.18		[20]
H		Sb ^V	OH ₂	EtOH	704	0.076		[21]
H		Ir ^{III}	Cl	CLN	nd	nd	2–4, 77	[19]

(continued)

Table 4.1 (continued)

R ^a	β ^b	M ^c	L ^d	Solvent ^e	λ _f ^f	Φ _f ^g	T/K ^h	Ref
H		Pt ^{II}		CLN	nd	nd	2–4, 77	[19]
H		Bi ^{III}	Cl	DMF	nd			[22]
^t Bu	β4	H ₂		BZ	708	0.77		[23]
^t Bu	β4	H ₂		THF	703	0.85		[1]
^t Bu	β4	H ₂		PY	704.6	0.54		[24]
^t Bu	β4	Mg ^{II}		BZ	700			[25]
^t Bu	β4	Al ^{III}	Cl	DMSO	693	0.64		[17]
^t Bu	β4	Si ^{IV}	OH ₂	TOL	682	0.57		[26]
^t Bu	β4	As ^V	F ₂	DCM		0.05		[27]
^t Bu	β4	Zn ^{II}		BZ	686	0.37		[23]
^t Bu	β4	Ru ^{II}	py ₂	DCM	nd			[28]
^t Bu	β4	Pd ^{II}		BZ	670	4.8 × 10 ⁻³		[23]
^t Bu	β4	Sb ^{III}		DCM	nd			[8]
^t Bu	β4	Sb ^V	OH ₂	DCM		0.01		[5]
^t Bu	β4	Sb ^V	Cl ₂	DCM		0.01		[6]
^t Bu	β4	Sb ^V	Br ₂	DCM		<0.001		[7]
^t Bu	β4	P ^V	OH/O	EtOH	686	0.80		[2]
	β4	P ^V	OH/O	EtOH		0.47		[3]
ⁿ BuO	α8	H ₂		THF	809	0.189		[12]
ⁿ BuO	α8	H ₂		BZ	778			[29]
ⁿ BuO	α8	Zn ^{II}		THF	807.5	0.062		[30]
ⁿ BuO	α8	Zn ^{II}		BZ ^l	752			[29]
ⁿ BuO	α8	Al ^{III}	OSiEt ₃	BZ	787			[29]
ⁿ BuO	α8	Ga ^{III}	OSiEt ₃	BZ	786			[29]
ⁿ BuO	α8	Ge ^{IV}	(OSiEt ₃) ₂	BZ	775			[29]
ⁿ BuO	α8	Sn ^{IV}	(OSiEt ₃) ₂	BZ	798			[29]
ⁿ BuO	α8	Ni ^{II}		TOL	nd			[29]
ⁿ BuO	α8	Ru ^{II}		BZ	750 ^k			[29]
ⁿ BuO	α8	Pd ^{II}		BZ	756 ^m	0.0008		[32]
ⁿ BuO	α8	Pt ^{II}		BZ	749 ^m	0.002		[32]

^aperipheral substituent, ^bpositions and numbers of the substituents (for example, β4 means that each isoindole unit has one substituent at the β position; see Fig. 1.12), ^ccentral element, ^daxial ligands and their number (when the number is two, the ligands take the *trans* conformation unless otherwise noted), ^ethe uncommon abbreviations represent the following solvents: *AN* acetonitrile, *BZ* benzene, *CLN* 1-chloronaphthalene, *DCM* dichloromethane, *PY* pyridine, *QN* quinoline, *TOL* toluene, ^ffluorescence peak wavelength, ^gfluorescence quantum yield, ^hroom temperature unless otherwise noted, ⁱnd: not detected, ^jY = *n*-hexyl, ^kabsorption peak wavelength (fluorescence spectral data not provided), ^lcontaining 1 % pyridine, ^mExcitation spectral data not provided

number of phthalocyanine derivatives bearing some peripheral substituents (R) for the purpose of highlighting the effect of the central element on the fluorophores [11–32]. Derivatives with a closed-shell atom in their cavity generally emit fluorescence, whereas in the case of those with an open-shell atom, it depends on the characteristics of the central metal ion whether they emit fluorescence or not.

Among the complexes with a closed-shell atom, meta-free derivatives generally have the highest quantum yield. Metal complexes have lower Φ_F values, which are much smaller for those with heavier atoms. This is explained in terms of the enhanced intersystem crossing from S_1 to T_1 (triplet excited state) in their π system due to metal-induced spin-orbit coupling (SOC) [19]. Basically, the transition from S_1 to T_1 is forbidden because their electron-spin multiplicities are different (i.e., the transition involves spin inversion). Nevertheless, some of the excited molecules can transit into the T_1 state. This is because the rotation of the unpaired electron around the nucleus produces another magnetic moment, which can interact with the spin. As the former magnetic moment becomes larger with increasing atomic number, the presence of heavier atoms (i.e., atoms with a larger atomic number) causes the unpaired electron to be involved in SOC and hence enhances the intersystem crossing more effectively (heavy-atom effect). A good example of this is in complexes of group-13 elements: their quantum yields decrease in the order $Al > Ga > In$ (Table 4.1, R = H), that is, in order of increasing atomic number of the central metal.

The emission characteristics of open-shell metal complexes strongly depend on the nature of the central metal ion. Vincett and coworkers investigated the fluorescence and phosphorescence of a number of metal complexes and classified them into the following three groups [11]: (i) complexes of a diamagnetic metal ion in the second or third row of transition elements, such as Rh^{III} , Pd^{II} , and Pt^{II} complexes that emit intense phosphorescence; (ii) nonfluorescent (but phosphorescent) complexes of a paramagnetic metal ion of a first-row transition element (e.g., those of Cu^{II} , V^{IV} , etc.); and (iii) nonluminescent (nonfluorescent or nonphosphorescent) complexes of a metal ion (irrespective of its paramagnetism or diamagnetism) in the first row of transition elements, such as those of Fe^{II} , Co^{II} , and Ni^{II} .

The first group includes complexes of diamagnetic metal ions in the second and third rows, such as those of Rh^{III} [19], Pd^{II} [19, 32], and Pt^{II} [19, 32], which are known to fluoresce. It is understandable that those in the second group (Cu^{II} , etc.) are not fluorescent but phosphorescent because the presence of the unpaired electron(s) facilitates a rapid intersystem crossing transition from the singlet excited to triplet state (note that these spin multiplicities refer to those of π -electrons in the π -conjugation system of the macrocyclic ligand alone but not metal-based spin multiplicity). Regarding the third group, the lack of luminescence (neither fluorescence nor phosphorescence) is interpreted in terms of the presence of a low-lying empty 3d orbital (e.g., x^2-y^2 in the case of Ni^{II}) slightly below the LUMO [11, 31]. Millard and Greene reported that dye molecules (Fe^{II} , Co^{II} , and Ni^{II} complexes) excited to the S_1 state rapidly deactivate to the low-lying metal-based (d, d) state within a few picoseconds and then thermally return to S_0 on the basis of direct picosecond time-resolved absorption measurements [33].

Note that $[\text{Sb}^{\text{III}}(\text{tbpc})]^+$ does not emit fluorescence [8] while $[\text{Sb}^{\text{V}}(\text{tbpc})(\text{OH})_2]^+$ with the same counter anion (I_3^-) does, although the emission is very weak [5]. As $[\text{Sb}^{\text{III}}(\text{tbpc})]^+$ is capable of sensitizing singlet oxygen upon photoirradiation with red light [34], the lack of fluorescence is interpreted in terms of rapid intersystem crossing from its S_1 state to the T_1 state. The presence of lone-pair electrons of the Sb^{III} ion may facilitate the transition more effectively than the Sb^{V} analogue.

4.1.3.3 Effects of Peripheral Substituents

The effects of peripheral substituents (Rs) on Φ_{F} values are reasonably large (Table 4.1). There appears to be no clear correlation between the electronic nature of the substituents (irrespective of their electron-donating or electron-withdrawing characters, etc.) and Φ_{F} values. Substituents that give rise to a larger shift of the Q-band position to a longer wavelength tend to have a lower Φ_{F} value. For example, Φ_{F} is 0.7 for unsubstituted metal-free phthalocyanine (i.e., H_2pc) [11], 0.5–0.8 for the tetra-*tert*-butyl-substituted (at β positions)⁸ analogue [1, 23, 24], i.e., H_2tbpc , and 0.42 for the tetra-*n*-butoxy-substituted (at β positions) analogue [12]. Thus, the effects of the substituents are moderate. In contrast, Φ_{F} for an α substituted isomer of the tetra-*n*-butoxy-substituted derivative is very low (0.07) [12]. As it is known that the introduction of substituents, such as $-\text{OZ}$ and $-\text{SZ}$ (Z denotes an alkyl or aryl group), to α positions of the macrocyclic ring gives rise to a significant redshift of the Q-band (Sect. 3.2.2), it is not surprising that phthalocyanine derivatives showing maximum fluorescence at a longer wavelength have a lower quantum yield. A clear (almost linear) correlation has been reported between fluorescent peak wavenumbers and Φ_{F} values [24]. This finding is in line with the so-called “energy gap law” that the nonradiative decay rate decreases with increasing energy gap between the excited and ground states [35, 36]. The Q-band is assigned to an essentially pure HOMO-LUMO transition (Sect. 2.2.10) and the energy gap between the S_0 and S_1 states is directly linked to the HOMO-LUMO gap. As a result, the position of the substituents (α or β) appears to be more important than their electronic nature.

The magnitude of the Stokes shift is quite small ($100\text{--}200\text{ cm}^{-1}$) for most phthalocyanine derivatives, irrespective of the number or nature of the substituents. This can be attributed to the rigidity of the macrocyclic ring (Sect. 4.1.2). However large values (1000 cm^{-1}) have been reported for derivatives with eight substituents at the α position [24, 32]. The presence of bulky substituents at each α position is known to give rise to significant distortion in the skeleton of the macrocycle due to the steric repulsion between the substituents [37]. The large Stokes shift for the octa- α -substituted phthalocyanines may be indicative of the flexibility of their macrocycles.

⁸See Fig. 1.12 for the α and β positions.

4.1.3.4 Fluorescence of Conjugate Acids of Phthalocyanines

Phthalocyanine derivatives that are protonated at their nitrogen atom(s) at the meso positions are also known to emit fluorescence [38, 39] if the parent macrocycles are fluorescent although little attention has been paid to this phenomenon. As the protonation gives rise to a considerable redshift of the Q-band (Sect. 3.2.5.2), the emission peak of the conjugate acid also appears at a longer wavelength than those of the parent fluorophores. Protonation is also known to reduce the fluorescence efficiency [38, 39]. This appears to be consistent with the energy gap law mentioned above. As expected, this emission disappears upon the addition of an amine (e.g., pyridine or lutidine) or another Lewis base and another emission is observed, which is assigned to emission from the parent fluorophore. Note that a similar emission can unexpectedly occur for the parent phthalocyanine derivative (i.e., unprotonated species) depending on the nature (and purity) of the solvent used (particularly for nondonor solvents such as chloroform, benzene, and toluene) and/or the concentration of the dye compound. Therefore, the additional fluorescence observed in this spectral region has often been attributed to aggregation (in particular, J-aggregates; Sect. 4.1.4) without sufficient experimental evidence, and vice versa. The fluorescence that appears in the spectral region must be carefully assigned, in common with absorption spectroscopy (Sect. 3.2.4.4).

4.1.3.5 Fluorescence of Related Macrocyclic Compounds

Expansion of the π -conjugation system of the macrocycle causes a considerable red-shift of the fluorescence peak position as well as the absorption peak of the same compound. For example, the fluorescence peak of metal-free derivatives, which are all tetra-*tert*-butyl-substituted, is known to shift to a lower wavelength in the order tetraazaporphyrin (633 nm in pyridine [24]) < phthalocyanine (i.e., H₂tbp (703 nm in THF [1]; 704.6 nm in pyridine [24]) < naphthalocyanine⁹ (781 nm in THF [1]), as expected from their absorption peak positions (Fig. 3.12). A significant reduction in the fluorescence quantum yield from H₂tbp (0.85 in THF [1]; 0.54 in pyridine [24]) to the naphthalocyanine analogue (0.14 in THF [1]) is also expected on the basis of the energy gap law. According to this law, a higher quantum yield is predicted for the tetraazaporphyrin analogue than the H₂tbp, but surprisingly it is much lower (0.11 in pyridine [24]). Note that the Φ_F values for subphthalocyanine and its ring-expanded and -contracted derivatives (see Fig. 3.38 for their structures) are known and they show the same trend; 0.034 for subazaporphyrin, 0.61 for subphthalocyanine, and 0.094 for subnaphthalocyanine in

⁹Fluorescence data for the same naphthalocyanine derivative in pyridine are reported in the same reference [24]. However, these data are not cited in this work because of the dissimilarity of the excitation spectrum to the absorption spectrum in the same solvent and the appearance of the emission peak at a much shorter wavelength (749.8 nm) than absorption peak (783.6 nm); see Sect. 4.1.5.

chloroform [40, 41]. In this case, a large Stokes shift (5300 cm^{-1}) for the sub-azaporphyrin analogue suggests a flexible structure. However, a similar possibility may be ruled out on the basis of the comparable magnitude of the Stokes shift for tetraazaporphyrin (317 cm^{-1}) and H_2tbpc (135 cm^{-1}) [24]. No clear explanation has yet been given for this [24]. Emission from superphthalocyanine derivatives is unknown to the best of the author's knowledge, although very weak emission is expected (if any) because of the heavy-atom effect of the U^{IV} ion.

It should be noted that all these dyes (phthalocyanines inclusive) exhibit their most intense fluorescence near their most intense absorption band, in contrast to porphyrins, such as tetraphenylporphyrin, of which the most intense emission appears at the red flank of their weak Q-band but not near their Soret band [42].¹⁰

4.1.4 Effects of Interactions Between Fluorophores

Let us consider what will occur when two or more fluorophores are within a short distance ($3.4\text{--}5\text{ \AA}$) of each other. In common with chromophores (Sect. 3.2.4), exciton coupling occurs between the fluorophores and hence the emission from the ensemble should be markedly different from the sum of those from the individual fluorophores. The selection rule discussed in the previous chapter can also be applied in this case (Fig. 4.8, which is essentially the same as Fig. 3.19). Here again, we must take into account the fact that the S_1 state of the phthalocyanine monomer is doubly degenerate (S_{1x} and S_{1y} with the molecular plane taken as the x , y -plane). For example, let us consider two fluorophores aligned in a face-to-face manner (Fig. 4.8a, i.e., an H-aggregate). The S_{1x} state for the monomer is split into new $S_{1x'}$ and $S_{2x'}$ states (likewise, S_{1y} is split into $S_{1y'}$ and $S_{2y'}$) due to exciton coupling and $S_{1x/y'}$ states are forbidden while $S_{2x/y'}$ states are allowed as described in Sect. 3.2.4.2. Thus, is the fluorescence peak for the dimer blue-shifted relative to that of the monomer? The answer is generally "no" because the molecules excited to the S_2' state are rapidly (thermally) relaxed to the S_1' state through internal conversion and most of the excited molecules are vibrationally relaxed to the S_0 state through the forbidden S_1' state (Sect. 4.1.2). In general, no emission is

¹⁰Readers are reminded that Q band of porphyrins (an electronic transition to the lowest excited state) is weak not because the transition is forbidden but configuration interaction between the two kinds of one-electron transitions involving the nearly degenerate HOMOs and LUMO significantly reduced the magnitude of the electric dipole moment in the lowest excited state (Sect. 2.2.6). As optical emission is the most likely to occur from the lowest excited (S_1) state (Kasha' rule; Sect. 4.1.1), it is quite reasonable that the most intense fluorescence from porphyrins is observed near the Q band. Note that this is not saying that no emission is observed near their Soret band. Actually, weak emission can be observed at the red flank of Soret band under appropriate conditions [43, 44] [i.e., emission from the S_2 state; cf. see S_2 emission from metal-free phthalocyanines (Fig. 4.7)]. Unlike the violet emission from phthalocyanines (Sect. 4.2.4), the corresponding excitation spectrum is similar to the Soret band.

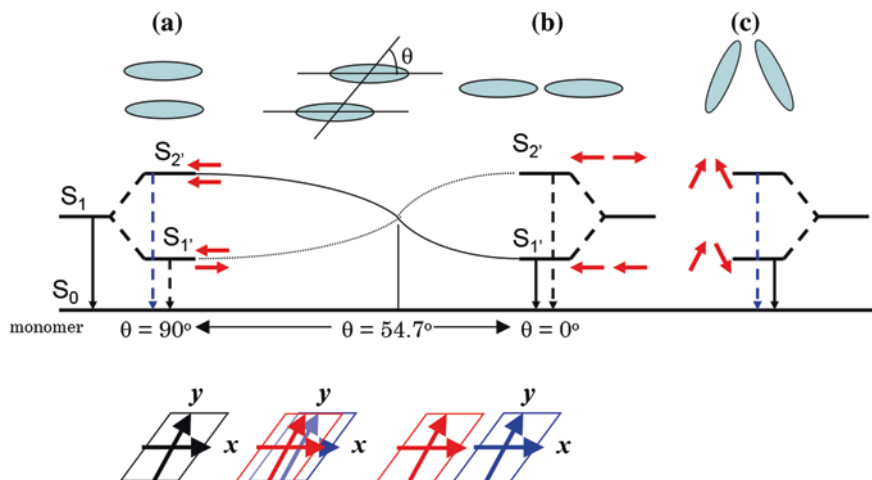


Fig. 4.8 Schematic diagram of exciton coupling between two fluorophores with various types of stacking. The *black solid* and *black dashed arrows* represent allowed and forbidden transitions, respectively. The transitions shown as *blue dashed arrows* are dipole-allowed, but emission is unlikely to be observed according to Kasha's rule. *Source* NIMS eSciDoc—IMEJI. © Hiroaki Isago with CC-BY-NC 3.0 license

expected for face-to-face dimers. Very weak emission has been observed for the μ -oxo dimer of the silicon phthalocyanine derivative in the near-infrared region (around 1000 nm in toluene) [45], although this is a rare case. On the basis of the low Φ_F value, which is three orders of magnitude smaller than that of the corresponding monomer, and the large gap between the absorption and emission peaks, the fluorescence is attributed to emission from the lower (S_1' , i.e., forbidden) excited state.

Double-decker phthalocyanine stacked in a face-to-face manner via a Sn^{IV} ion as the bridge ($[\text{Sn}(\text{pc})_2]$; see Fig. 3.24 for its structure) does not emit fluorescence, although the single-decker analogue, $[\text{Sn}(\text{pc})\text{Cl}_2]$, does [46]. As described in Sect. 3.2.4.6, this compound exhibits split Q-bands. This cannot be interpreted in terms of exciton coupling theory alone, which predicts emission from the lower excited state. As the interplanar distance between two macrocyclic ligands is shorter than the sum of the van der Waals radii of the two π -orbitals of the individual macrocycles, the two π -conjugation systems should not be considered independently but as a single conjugation system. Therefore, a total of four transitions involving the HOMOs and LUMOs (in the monomer) are possible, of which only two are allowed (Sect. 3.2.4.6) and the others are forbidden. The lack of emission for the double-decker form $[\text{Sn}(\text{pc})_2]$ is interpreted in terms of the presence of such low-lying forbidden excited states below the allowed excited states [46].

In the case of dimers aligned in a slipped-face-to-face manner (Fig. 4.8b; i.e., a J-aggregate), two transitions are allowed and hence two bands are observed in

the absorption spectrum at both the blue and red-flanks of the monomer Q-band (Sect. 3.2.4.4). However, only emission from the lower excited states alone is generally observed. As is the case for free-base derivatives, this is not surprising according to Kasha's rule. Actually, some research groups have reported the splitting of more than one Q-band peak due to the formation of J-type dimers with one fluorescent peak at a slightly longer wavelength than the lowest absorption band [47, 48]. In general, the emission from a dimer (formed by the van der Waals force) is weaker than that from the corresponding monomer [47, 48], but that from a dimer with a tight molecular structure (formed via coordination bonds) is rather intense ($\Phi_F = 0.26 - 0.76$ and essentially the same as that of the corresponding monomer) [49].

Readers are reminded that J-aggregates emit fluorescence (if the corresponding monomer does) at a longer wavelength than the monomer Q-band, but not all of the species with a fluorescence peak at a longer wavelength than the Q-band are J-aggregates. The fluorophore can be a protonated phthalocyanine (Sect. 4.1.3.2). Attention has to be paid to the purity of the solvent used.

Oblique face-to-face (i.e., clamshell type; Fig. 4.8c) dimers exhibit a split Q-band in their absorption spectra as mentioned in Sect. 3.2.4.5. They only emit fluorescence at the red flank of the lowest transition [50]. This is understandable because the emission is most likely to occur from the lower excited state of the two allowed transitions (Kasha's rule; Sect. 4.1.2).

4.1.5 Misleading Impurity Emission (Importance of Measuring the Excitation Spectra)

It should be noted here again that not all phthalocyanine derivatives exhibit luminescence, unlike optical absorption. Among even the luminescent derivatives, their emission efficiencies range considerably. In other words, the optical emission intensities of two species, whose other physical quantities (such as optical absorption and NMR signal intensity) show a similar relationship with their chemical quantities, are not necessarily comparable and vice versa. This is why the emission spectra of derivatives with low emission efficiency can be misleading when they are contaminated with a trace amount of a highly luminescent impurity. For example, Oddos-Marcel et al. [45] reported emission from the μ -oxo dimer of a silicon phthalocyanine derivative, as well as that from the corresponding monomers. Although the ratio of the monomer relative to the dimer is only 2 % (normally negligible in optical absorption, NMR spectroscopy, or elemental analysis), because the monomer is 1000 times as luminescent as the dimer, the emission intensities of both species are comparable. However, the problem is not serious in this case because their emission spectra are different from each other in both their shape and energy.

A more serious problem can arise when a metal complex of a given phthalocyanine derivative is contaminated with a trace amount of the corresponding free

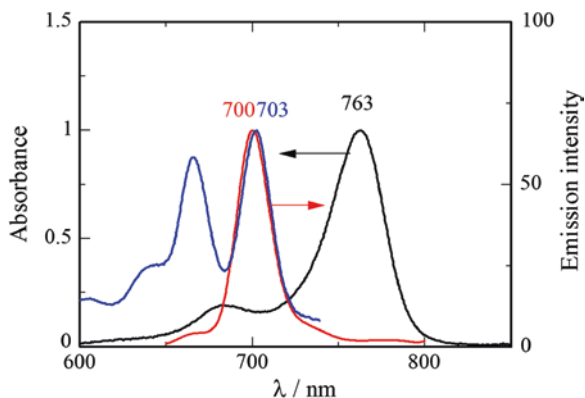


Fig. 4.9 Optical absorption (black line), emission (red line; excited at 670 nm), and excitation (blue line; monitored at 754 nm) spectra of a dichloromethane solution containing the Sb^{III} complex of tetra-(*tert*-butyl)-substituted phthalocyanine. The emission was assigned to the concomitant metal-free derivative on the basis of the excitation spectrum. Source NIMS eSciDoc—IMEJI. © Hiroaki Isago with CC-BY-NC 3.0 license

base.¹¹ This is because free bases generally have much higher quantum yields than their metal complexes (Table 4.1). When the metal complex of interest is sufficiently luminescent (e.g., Zn^{II} and Al^{III} complexes) for the emission from the contaminant to be negligible, the problem may not be serious. However, when the central metal ion significantly reduces the fluorescence efficiency of the macrocyclic ligand, as is the case for paramagnetic and heavy metal ions, the fluorescence spectra of the compound can be dominated by the emission of the free base. Furthermore, the fluorescence spectra of metal-free derivatives show a single peak (Fig. 4.7) close to the Q-band peak in the optical absorption spectra¹² of their metal complexes unless the metal ion significantly shifts the Q-band. Thus, the emission spectra of contaminated metal complexes can be misleading. In particular, when very weak emission is observed, we may need to consider the possibility of contamination with a trace amount of free base. Here, an example is given of the author almost making an erroneous conclusion when studying the spectral properties of the Sb^{III} complex $[\text{Sb}^{\text{III}}(\text{tbpc})]^+$ in dichloromethane solution. This compound shows a characteristic Q-band around 760 nm (Fig. 4.9; black), but very weak fluorescence was observed around 700 nm (Fig. 4.9; red).¹³ Fortunately, he realized that the emission was not from the Sb^{III} complex but from another species

¹¹This usually occurs when the metal ion is labile and hence liable to leave the cavity (e.g., the known Sb^{III} complex [8]) or when it is difficult to remove the unreacted free base from its metal complex through the synthetic procedure.

¹²Actually, the emission peak appears at a slightly longer wavelength, and the magnitude of the difference may be considered as being reasonably close to the Stokes shift.

¹³It was later found that emission could not be detected when the Sb^{III} complex was very carefully purified [8].

because the appearance of the fluorescence peak at a shorter wavelength than the absorption peak was rather unusual.¹⁴ As the excitation spectrum of the solution was very similar to the absorption spectrum of its corresponding metal-free derivative (Fig. 4.9; blue), it was easily confirmed that the observed emission was from H₂tbp. Because the emission quantum yield of H₂tbp is high ($\Phi_F = 0.85$ in THF [1]) while the Sb^{III} complex is essentially nonfluorescent, even a trace amount of the contaminant, which cannot be detected by other analytical methods, dominated the emission spectrum of the bulk solution. Conversely, emission from a free base contaminant can be a serious problem in the analysis of conventional metal complexes with their Q-band in the normal spectral range, particularly if the emission efficiency (Φ_F) is very low. For example, the complexes of a heavy atom, whose Q-band position is normal, emit very weak fluorescence (Table 4.1). It is difficult, therefore, to assign the emission from a metal complex of interest or from a trace amount of impurity without the excitation spectrum. Likewise, similar care has to be taken for complexes of open-shell metal ions (those of Cu^{II}, Co^{II}, Ni^{II}, etc.) for the same reason. This is why measuring the excitation spectrum is strongly recommended. When preparing papers, excitation spectra should be provided together with the emission spectra, even as supplementary information.¹⁵ Otherwise, it should be briefly mentioned in the text that, for example, the excitation spectrum was similar to the absorption spectrum in the same solvent.

4.2 Other Emission Phenomena

4.2.1 Phosphorescence

Phosphorescence is an emission phenomenon from the lowest triplet state of a photoexcited molecule. Although the transition from the S₁ to T₁ state is basically forbidden because their spin multiplicities are different, many compounds undergo this process as a result of spin-orbit coupling as mentioned above. Hence, a number of phthalocyanine derivatives are known to phosphoresce. Because the energy level of the lowest triplet state is much lower than that of S₁, phosphorescence emission is observed at much longer wavelengths. For example, the majority of phosphorescent phthalocyanine derivatives have an emission peak around 1100 nm (Table 4.2). Figure 4.10 (left; solid line) shows a typical phosphorescence

¹⁴Fortunately, the Q-band position of the Sb^{III} complex is significantly red shifted relative to those of the other metal complexes [8].

¹⁵Some authors have attempted to attribute the appearance of free-base-like excitation spectra to the demetallation of the photoexcited molecule followed by the protonation of the macrocyclic ligand in its cavity. Although this possibility cannot be completely excluded, it is unlikely because the two successive chemical steps must be completed within picoseconds before the initiation of the optical emission. If the assumed reactions do occur, continuous photoirradiation will increase the ratio of the corresponding free base to the bulk complex during irradiation.

Table 4.2 Effects of central element and peripheral substituents on phosphorescence characteristics of phthalocyanines

R ^a	p ^b	M ^c	L ^d	Solvent ^e	λ_f	$\Phi_p/10^{-4g}$	T/K ^h	Ref.
H		Mg ^{II}		CLN	1111	0.05	77	[11]
H		V ^{IV}	O	QN	1140	0.05	77	[11]
H		Cu ^{II}		CLN	1065	10	77	[11]
H		Cu ^{II}		CLN	1078	1	2.4	[11]
H		Zn ^{II}		CLN	1093	1	77	[11]
H		Zn ^{II}		CLN	1092	4	2.4	[11]
H		Rh ^{II}	Cl	CLN	987	20	77	[18]
H		Rh ^{III}	Cl	CLN	987	20	2–4	[18]
H		Pd ^{II}		QN	990	30	77	[11]
H		Cd ^{II}		QN	1097	2–4	77	[11]
H		Cd ^{II}		QN	1097	3–6	2–4	[11]
H		Ir ^{III}	Cl	CLN	957	80	77	[18]
H		Pt ^{II}		CLN	944	100	77	[18]
^t Bu	$\beta 4$	Zn ^{II}		MTHF	1100			[23]
^t Bu	$\beta 4$	Ru ^{II}	(pyridine) ₂	DCM	870	3		[28]
^t Bu	$\beta 4$	Pd ^{II}		BZ	1020			[52]
ⁿ BuO	$\alpha 8$	H ₂		MTHF	nd ⁱ		77	[29]
ⁿ BuO	$\alpha 8$	H ₂		BZ	nd			[29]
ⁿ BuO	$\alpha 8$	Zn ^{II}		MTHF	nd		77	[29]
ⁿ BuO	$\alpha 8$	Zn ^{II}		BZ	nd			[29]
ⁿ BuO	$\alpha 8$	Al ^{III}	OSiEt ₃	MTHF	nd		77	[29]
ⁿ BuO	$\alpha 8$	Al ^{III}	OSiEt ₃	BZ	nd			[29]
ⁿ BuO	$\alpha 8$	Ga ^{III}	OSiEt ₃	MTHF	nd		77	[29]
ⁿ BuO	$\alpha 8$	Ga ^{III}	OSiEt ₃	BZ	nd			[29]
ⁿ BuO	$\alpha 8$	Ge ^{IV}	(OSiEt ₃) ₂	MTHF	nd		77	[29]
ⁿ BuO	$\alpha 8$	Ge ^{IV}	(OSiEt ₃) ₂	BZ	nd			[29]
ⁿ BuO	$\alpha 8$	Sn ^{IV}	(OSiEt ₃) ₂	MTHF	nd		77	[29]
ⁿ BuO	$\alpha 8$	Sn ^{IV}	(OSiEt ₃) ₂	BZ	nd			[29]
ⁿ BuO	$\alpha 8$	Ni ^{II}		TOL	nd			[31]
ⁿ BuO	$\alpha 8$	Ru ^{II}	(pyridine) ₂	BZ	910			[29]
ⁿ BuO	$\alpha 8$	Pd ^{II}		BZ	1104 ^j			[32]
ⁿ BuO	$\alpha 8$	Pt ^{II}		BZ	1047 ^j			[32]

^aperipheral substituent, ^bpositions and numbers of the substituents (for example, $\beta 4$ means that each isoindole unit has one substituent at the β position; see Fig. 1.12), ^ccentral element, ^daxial ligands and their number (when the number is two, the ligands take the *trans* conformation unless otherwise noted), ^ethe uncommon abbreviations represent the following solvents: *BZ* benzene, *CLN* 1-chloronaphthalene, *DCM* dichloromethane, *MTHF* 2-methyltetrahydrofuran, *QN* quinoline, *TOL* toluene, ^fphosphorescence peak wavelength, ^gphosphorescence quantum yield, ^hroom temperature unless otherwise noted, ⁱnd: not detected, ^jExcitation spectral data not provided

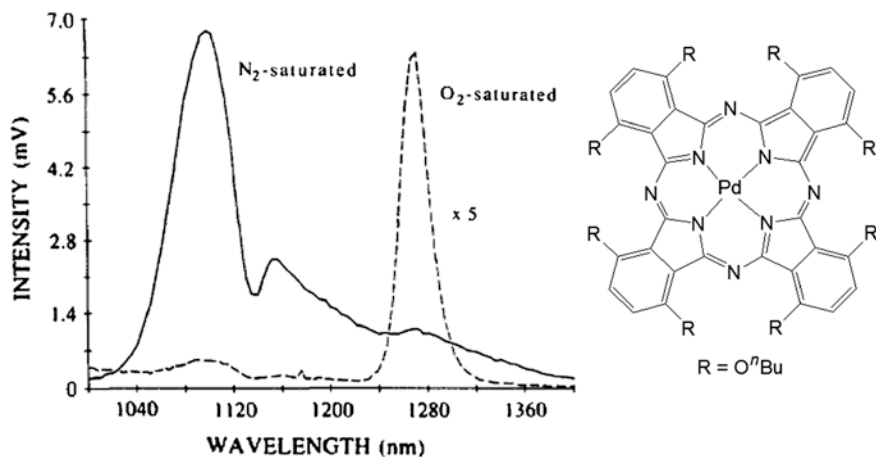


Fig. 4.10 Optical emission spectra of benzene solutions containing Pd^{II} complex of octa-butoxy-substituted phthalocyanine (right), saturated with nitrogen (solid line) and oxygen (broken line). The emission at 1270 nm in the oxygen-saturated solution is from singlet oxygen ¹O₂ (see Sect. 4.2.3). Reprinted with permission from Ref. [29]. Copyright 1990 American Chemical Society

spectrum of a Pd^{II} complex of octa-butoxy-substituted phthalocyanine (Fig. 4.10 inset) in nitrogen-saturated benzene solution [29]. It is noteworthy that the phosphorescence peak position appears around 1100 nm irrespective of the nature of the central metal ion in the cavity of the macrocycle or the substituents on its periphery. The lifetime of the phosphorescence is generally much longer (on the order of microseconds—milliseconds) than that of the fluorescence because the intersystem crossing is a forbidden process. Therefore, it takes the excited molecules more time until the initiation of luminescence. It is intriguing that phosphorescence has not been observed for metal-free phthalocyanines even at low temperatures [11, 29]. This has been attributed to the presence of imino protons in the cavity, which play a crucial role in tautomerization in the T₁ state [51].

The phosphorescence of complexes of a closed-shell metal ion is generally quite weak and can be observed only at low temperatures. Rodgers and co-workers investigated the phosphorescence of several main-group metal (M = H₂, Zn^{II},¹⁶ Al^{III}, Ga^{III}, Ge^{IV}, and Sn^{IV}) complexes of octa-*n*-butoxy-substituted (at α positions) phthalocyanine (see Fig. 4.10 (right) for the skeleton of the macrocyclic ligand) in benzene or 2-methyltetrahydrofuran at liquid-nitrogen temperature, but no detectable emission was observed [29]. An earlier work on unsubstituted phthalocyanine complexes was performed at a much lower temperature and in 1-chloronaphthalene, which contains a heavy atom (chlorine) [11].

¹⁶Phosphorescence of the zinc derivative had been reported in their earlier work [32], but this was later reassigned as an artifact by the same group [29].

Complexes of open-shell metal ions are categorized into three groups (Sect. 4.1.3.2). Those of Fe^{II} , Co^{II} , and Ni^{II} (i.e., the second group) do not phosphoresce for the same reason as given above.

Regarding the first group (i.e., Cu^{II} and V^{IV} complexes), their excited states are complicated owing to the presence of unpaired 3d electron(s). The singlet states in closed-shell metal complexes become doublets (^2S) while triplet states split into trip-doublets (^2T) and quartets (^4T) as a result of weak coupling between the unpaired 3d and π -electrons. The intersystem crossing from S_1 to T_1 (which is a forbidden process) therefore becomes spin-allowed and hence strong phosphorescence is observed [11]. In addition, the emission can be significantly temperature-dependent because the populations of the ^2T and ^4T states are functions of temperature (Boltzmann distribution). For example, $[\text{Cu}(\text{pc})]$ emits 1065 nm light above 77 K but 1078 nm light below 4 K. The former and latter emissions have been assigned to those from the ^2T and ^4T states, respectively (the energy gap between the two T states was evaluated to be approximately 100 cm^{-1}) [11].

Complexes of the third group, in particular those of Ru^{II} , Pd^{II} , and Pt^{II} , emit strong phosphorescence around 1100 nm, which can be observed even at room temperature [28, 29, 32, 52]. Phosphorescence from Ru^{II} complexes is known to appear at a much higher energy (emission peaks appear around 870 nm) and have a shorter lifetime (approximately 150 ns with a weak dependence on the solvent) than that from other phosphorescent metal complexes [28]. These findings suggest that the intersystem crossing occurs through an unusual conversion mechanism. On the basis of transient absorption spectral measurements [28] in addition to electrochemical and spectroelectrochemical studies [53], the emission is considered to be not from a conventional π -electron based triplet state but from a charge-transfer (CT) state involving a singly oxidized macrocyclic ligand (i.e., $\text{Pc}(1^-)$; see Sect. 3.2.6.1 for an explanation of this representation).

4.2.2 Delayed Fluorescence (DF)

Delayed fluorescence (DF) is the emission phenomenon that the spectral shape (and energy) is the same as that of the “prompt” (i.e., normal) fluorescence, as shown in Fig. 4.11, whereas its lifetime is much longer (as long as that of phosphorescence) [54 and references cited therein]. This phenomenon is interpreted in terms of the emission from an excited dye molecule in the S_1 state, which was somehow excited via the T_1 state.

Some possible mechanisms have been proposed for the DF phenomena, such as thermal excitation from T_1 to S_1 (E-type) or triplet-triplet annihilation, where an encounter between two T_1 states gives rise to S_1 and S_0 states (i.e., $2\text{T}_1 \rightarrow \text{S}_1 + \text{S}_0$; P-type) [54 and references cited therein]. In the case of phthalocyanines and related macrocyclic compounds, however, DF has been reported in the presence of molecular oxygen. As excited oxygen molecules ($^1\text{O}_2$; see

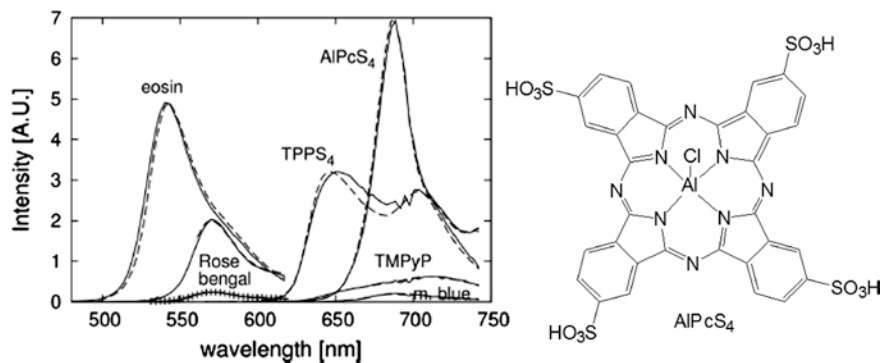


Fig. 4.11 Delayed (*solid line*) and prompt fluorescence (*dashed line*) spectra of aqueous solutions containing water-soluble dyes (10^{-5} M); AlPcS₄, TPPS₄, TMPyP, eosin, Rose bengal, and m-blue represent Al^{III} derivative of tetra-(sulfonic acid)-substituted phthalocyanine (structure shown to the right of the graph), meso-tetrakis(4-sulfonatophenyl)porphine, 5,10,15,20-tetrakis(1-methyl-e-pyridinio)porphine, eosin Y disodium salt, Rose bengal sodium salt, and methylene blue, respectively. The spectrum of Rose bengal with 10 mM NaN₃ is plotted with crosses. Reproduced from Ref. [54] with permission from the European Society for Photobiology, the European Photochemistry Association, and the Royal Society of Chemistry

Sect. 1.2.4.1), which are readily generated by organic dyes or other sensitizers upon visible-light irradiation [55], play a crucial role in the emission, such DF is referred to as singlet-oxygen-sensitized delayed fluorescence (SOSDF or SODF) [56–58]. Although two ¹O₂ molecules are involved in the emission from one fluorophore, the possibility of direct excitation of a fluorophore in the S₀ state by bimolecular ¹O₂ (i.e., the “dimol” mechanism) has been ruled out on the basis of kinetic studies of the DF and characteristic emission from ¹O₂¹⁷ [57, 58]. Furthermore, triplet phthalocyanine has been directly detected as an intermediate in the DF process by transient absorption spectroscopy, when H₂tbp_c is used as the fluorophore and C₆₀ is used as the ¹O₂ photosensitizer [59]. In the light of recent developments in this field, it appears that a stepwise excitation mechanism via the triplet state of the fluorophore (i.e., S₀ + ¹O₂ → T₁ + ³O₂ followed by T₁ + ¹O₂ → S₁ + ³O₂) underlies SOSDF phenomena involving phthalocyanines and other common ¹O₂ photosensitizers [54].

Scholz and coworkers have determined the SOSDF quantum yield to be ca. 4×10^{-4} for an Al^{III} complex of water-soluble phthalocyanine (see the right of Fig. 4.11 for its structure) in water [54]. Although this value is much smaller than that for normal fluorescence, it is greater than that for the ¹O₂ emission in the same solvent (ca. 6.5×10^{-7}) [55] by three orders of magnitude. In addition, the detection of visible-light fluorescence is much easier than that of near-infrared luminescence. Therefore, SOSDF can be used as a noninvasive probe for

¹⁷Emission from ¹O₂ around 1270 nm is mentioned in Sect. 4.2.3.

monitoring $^1\text{O}_2$ toward its application in photodynamic therapy (Sect. 1.2.4.1) and the photodegradation of pollutants in wastewater. Much attention has also been paid to DF from the viewpoint of its application to organic light-emitting diodes (OLEDs) and light-emitting polymers (OLEPs) as well¹⁸ [60 and references cited therein].

4.2.3 Emission at Approximately 1270 nm

Weak emission around 1270 nm can be observed in solutions containing some phthalocyanine derivatives upon photoirradiation. However, this emission is likely to be from singlet oxygen ($^1\text{O}_2$), which has been sensitized by the macrocyclic dye molecules, unless the solution is thoroughly deoxygenated. As mentioned in Sect. 1.2.4.1, organic dyes are capable of sensitizing $^1\text{O}_2$ upon visible-light irradiation. When $^1\text{O}_2$ molecules relax to their ground state ($^3\text{O}_2$), they emit characteristic light around 1270 nm [55]. Therefore, to study the emission from compounds of interest in this spectral region, their solutions must be sufficiently deoxygenated prior to their use. Otherwise, even though the emission from the dyes does not overlap with the 1270 nm emission, the macrocyclic molecules in the T_1 state will be rapidly deactivated to the S_0 state through an energy exchange reaction with the surrounding $^3\text{O}_2$ molecules and hence little emission will be observed (Fig. 4.10 broken line).

4.2.4 Emission from Upper Excited States

Some phthalocyanine derivatives are known to emit weak violet light (efficiency < 0.11) in the spectral range of 400–500 nm when irradiated with red laser light (695 nm) [61–63]. The excitation spectra of the emission are not the same as the absorption spectra in the Soret region. The intensity of this emission has been found to increase in proportion to the square of the incident laser intensity. This finding suggests that the violet emission is from a higher excited state that is promoted by two-photon absorption. No clear explanation has yet been provided for this phenomenon. The other possibility that this emission is from an impurity (a contaminant originally present in the macrocyclic compound or generated during the measurements) has not yet been completely excluded.

¹⁸As far as phthalocyanines and related macrocyclic compounds are concerned, their application to such devices appears to be unpromising because the energy gap between S_1 and T_1 is too large to thermally excite triplet molecules.

4.2.5 *Electrochemiluminescence (or Electrogenerated Chemiluminescence; ECL)*

Electrochemiluminescence (ECL) is a form of chemiluminescence in which electrochemically generated species are involved. In ECL phenomena, a highly exergonic reaction between the electrogenerated species (or one electrogenerated species and another species) produces an electronically excited species that emits light upon relaxation to a lower level (e.g., the ground state). The wavelength of the emitted light corresponds to the energy gap between the two states [64]. In other words, ECL is a form of chemiluminescence where at least one reactant is produced electrochemically on the electrodes. ECL is observed when a given potential (approximately 2–8 V) is applied between the electrodes of an electrochemical cell containing a solution of luminescent species (L), which can be an aromatic hydrocarbon, metal complex, or quantum dot, in an aprotic organic solvent. In organic media, both the oxidized and reduced forms (L^{n+} and L^{m-} , respectively) can be generated at different electrodes simultaneously or at the same electrode by sweeping the applied potential between the oxidation and reduction potentials of L. Annihilation between the two electrogenerated species (i.e., the recombination of L^{n+} and L^{m-}), produces an excited species, L^* , which emits light.

A number of phthalocyanine derivatives and related macrocyclic compounds are known as excellent illuminants that emit red or near-infrared light, as described above. In addition, they can be converted to their stable oxidized [Pc(1-)] and reduced [Pc(3-)] forms by electrochemical oxidation and reduction, respectively (Sect. 3.2.6). Therefore, these compounds may be intriguing targets of ECL research because there have been only a few systems that are capable of emitting light in such a spectral range [64–66]. Furthermore, only a limited number of papers have been published on ECL involving phthalocyanine derivatives. The first observation of ECL from a phthalocyanine derivative was reported four decades ago by Bard and coworkers, who detected very weak emission from metal-free unsubstituted phthalocyanine, H_2pc , in dichloromethane solution [67].¹⁹ Later, Bard and coworkers again investigated ECL from the much more soluble and much less aggregating derivatives [Si(pc)(OSiR₃)₂] and [Si(nc)(OSiR₃)₂] (where pc and nc denote unsubstituted phthalocyaninate and naphthalocyaninate ligands, respectively, and R = *n*-hexyl) [68]. The reaction enthalpies have been estimated to be about 1.8 and 1.5 eV for the pc and nc systems, respectively, on the basis of their first oxidation and the first reduction potentials; these values are close to their S₁ state energies (1.86 and 1.62 eV for the pc and nc derivatives, respectively) estimated from their wavelengths of maximum fluorescence. Hence, these systems have sufficient energy to populate the emitting state directly through the electron transfer reaction $L^+ + L^- \rightarrow L^* + L$. The ECL spectra of the pc and nc derivatives are shown in Fig. 4.12. The emission peak wavelengths appear to be

¹⁹The weak emission may have been due to poor solubility and strong aggregation of the macrocyclic compound in the solvent.

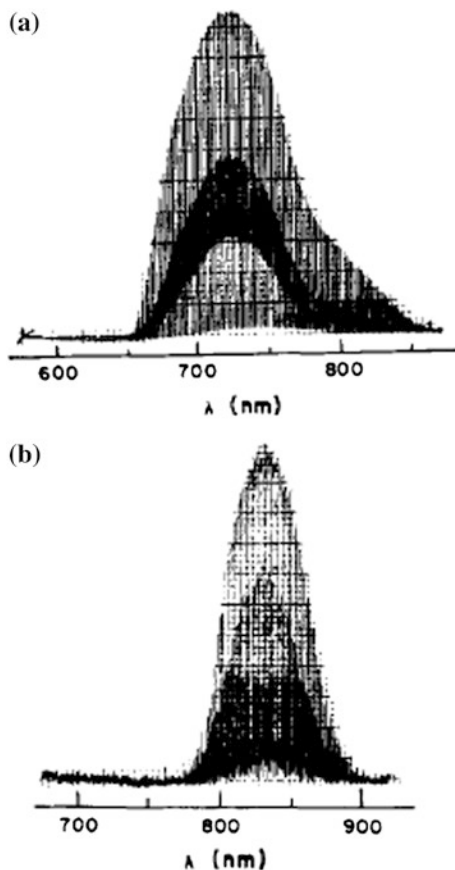


Fig. 4.12 ECL spectra of (*top*) pc derivative and (*bottom*) nc derivative in dichloromethane solution containing 0.1 M tetrabutylammonium perchlorate as the supporting electrolyte. The Pt electrode was subjected to pulses pulsed from +1.0 to -1.2 V (*top*) and +0.6 to -1.3 V (*bottom*) versus the reference Ag electrode for the pc and nc derivatives, respectively, at 0.5 Hz (see the original paper for the experimental details). Reprinted with permission from Ref. [68]. Copyright 1984 American Chemical Society

somewhat red shifted as compared with those in their fluorescence spectra (684 and 792 nm²⁰ for the pc and nc systems, respectively) because of self-absorption (Q-band) of the ECL emission by the illuminants themselves. In fact, the corrected ECL spectra with the self-absorption taken into account match their fluorescence spectra. No ECL was observed from the μ -oxo dimer of the pc system [Si(pc)(OSiR₃)₂O] [68], in line with the photophysical properties of face-to-face dimers and H-aggregates (Sect. 4.1.4).

²⁰It is noteworthy that only a few systems have been reported with the ECL peak position at a longer wavelength than the nc system despite more than three decades having passed since this work was published [62–64].

References

1. N. Kobayashi, Y. Higashi, T. Osa, *Chem. Lett.* 1813–1816 (1994)
2. H. Isago, H. Fujita, unpublished data
3. H. Isago, H. Fujita, M. Hirota, T. Sugimori, Y. Kagaya, *J. Porphyrins Phthalocyanines* **17**, 763–771 (2013)
4. S.J. Atherton, A. Hamiman, *J. Am. Chem. Soc.* **115**, 1816–1822 (1993)
5. H. Isago, K. Miura, Y. Oyama, J. Inorg. Biochem. **102**, 380–387 (2008)
6. H. Isago, Y. Kagaya, S.-I. Nakajima, *Chem. Lett.* **32**, 112–113 (2003)
7. H. Isago, Y. Kagaya, *Chem. Lett.* **35**, 8–9 (2005)
8. H. Isago, *Chem. Commun.* 1864–1865 (2003)
9. K. Ishii, N. Kobayashi, in *The Porphyrin Handbook*, vol. 16, ed. by K.M. Kadish, K.M. Smith, R. Guillard (Academic Press, San Diego, 2003), pp. 1–42
10. T. Nyokong, *Coord. Chem. Rev.* **251**, 1707–1722 (2007)
11. P.S. Vincett, E.M. Voigt, K.E. Rieckhoff, *J. Chem. Phys.* **55**, 4131–4140 (1971)
12. N. Kobayashi, N. Sasaki, Y. Higashi, T. Osa, *Inorg. Chem.* **34**, 1636–1638 (1995)
13. S.L. Gilat, T.W. Ebbesen, *J. Phys. Chem.* **97**, 3551–3554 (1993)
14. H. Ohtani, Y. Kobayashi, T. Ohno, S. Kato, T. Tanno, A. Yamada, *J. Phys. Chem.* **88**, 4431–4435 (1984)
15. R. Darwent, P. Douglas, A. Harriman, G. Ported, M.C. Richoux, *Coord. Chem. Rev.* **44**, 83–126 (1982)
16. J.H. Brannon, D. Magde, *J. Am. Chem. Soc.* **102**, 62–65 (1980)
17. W. Freyer, K. Teuchner, *J. Photochem. Photobiol. A* **45**, 117–121 (1988)
18. X.-F. Zhang, H.-J. Xu, *J. Chem. Soc. Faraday Trans.* **89**, 3347–3351 (1993)
19. E.R. Menzel, K.E. Rieckhoff, E.M. Voigt, *J. Chem. Phys.* **58**, 5726–5734 (1973)
20. A.P. Pelliccioli, K. Henbest, G. Kwag, T.R. Carvagno, M.E. Kenney, M.A.J. Rodgers, *J. Phys. Chem. A* **105**, 1757–1766 (2001)
21. G. Knör, *Inorg. Chem.* **35**, 7916–7918 (1996)
22. H. Isago, unpublished result
23. D.S. Laurence, D.G. Whinen, *Photochem. Photobiol.* **64**, 923–935 (1996)
24. N. Kobayashi, S.-I. Nakajima, H. Ogata, T. Fukuda, *Chem. Eur. J.* **10**, 6294–6312 (2004)
25. W. Freyer, S. Dahne, L. Q. Minh, K. Teuchner, *Z. Chem.* 334–336 (1986)
26. K. Ishi, Y. Hirose, M. Fujitsuka, O. Ito, N. Kobayashi, *J. Am. Chem. Soc.* **123**, 702–708 (2001)
27. H. Isago, Y. Kagaya, *Inorg. Chem.* **51**, 8447–8454 (2012)
28. D. Guez, D. Markovitsi, M. Sommerauer, M. Hanack, *Chem. Phys. Lett.* **249**, 309–313 (1996)
29. B.D. Richter, M.E. Kenny, W.E. Ford, M.A. Rodgers, *J. Am. Chem. Soc.* **112**, 8064–8070 (1990)
30. N. Kobayashi, H. Ogata, N. Nonaka, E.A. Luk'yanets, *Chem. Eur. J.* **9**, 5123–5134 (2003)
31. T.C. Gunaratne, A.V. Gusev, C. Rizzoli, X. Peng, A. Rosa, G. Ricciardi, E.J. Baerends, C. Rizzoli, M.E. Kenney, M.A.J. Rodgers, *J. Phys. Chem. A* **109**, 2078–2089 (2005)
32. A.V. Soldatova, J. Kim, C. Rizzoli, M.E. Kenney, M.A. Rodgers, A. Rosa, G. Ricciardi, *Inorg. Chem.* **50**, 1135–1149 (2011)
33. R.R. Millard, B.I. Greene, *J. Phys. Chem.* **89**, 2976–2978 (1985)
34. H. Isago, K. Miura, M. Kanetsato, *J. Photochem. Photobiol. A* **197**, 313–320 (2008)
35. E.M. Kober, J.V. Capsar, R.S. Lumpkin, T.J. Meyer, *J. Phys. Chem.* **90**, 3722–3734 (1986)
36. M. Bixon, J. Jortner, J. Cortes, H. Heitele, M.E. Michel-Beyerle, *J. Phys. Chem.* **98**, 7289–7299 (1994)
37. T. Fukuda, N. Kobayashi, K. Ueno, H. Ogino, *J. Am. Chem. Soc.* **123**, 10740–10741 (2001)
38. T. Nyokong, *J. Mol. Str.* **689**, 89–97 (2004)
39. A. Beeby, S. FitzGerald, C.F. Stanley, *J. Chem. Soc. Perkin Trans.* **2**, 1978–1982 (2001)
40. N. Kobayashi, T. Ishizaki, K. Ishi, H. Konami, *J. Am. Chem. Soc.* **121**, 9096–9110 (1999)

41. N. Kobayashi, *Bull. Chem. Soc. Jpn.* **75**, 1–19 (2002)
42. P.G. Seybold, M. Gouterman, *J. Mol. Spectrosc.* **31**, 1–13 (1969)
43. L. Bajema, M. Gouterman, C.B. Rose, *J. Mol. Spectrosc.* **39**, 421–431 (1971)
44. J. Karolczak, D. Kowalska, A. Lukaszewicz, A. Maciejewski, R.P. Steer, *J. Phys. Chem. A* **108**, 4570–4575 (2004)
45. L. Oddos-Marcel, F. Madeore, A. Bock, D. Neher, A. Ferencz, H. Rengel, G. Wegner, C. Kryschi, H.P. Trommsdorff, *J. Phys. Chem.* **100**, 11850–11856 (1996)
46. O. Ohno, N. Ishikawa, H. Matsuzawa, Y. Kaizu, H. Kobayashi, *J. Phys. Chem.* **93**, 1713–1718 (1989)
47. T. Kaneko, T. Arai, K. Tokumaru, D. Matsunaga, H. Sakuragi, *Chem. Lett.* 345–346 (1996)
48. X.-Y. Li, D.K.P. Ng, *Tetrahedron Lett.* **42**, 305–309 (2001)
49. K. Kameyama, M. Morisue, A. Satake, Y. Kobuke, *Angew. Chem.* **44**, 4763–4766 (2005)
50. E.S. Dodsworth, A.B.P. Lever, P. Seymour, C.C. Leznoff, *J. Phys. Chem.* **89**, 5698–5705 (1985)
51. W.E. Ford, B.D. Richter, M.E. Kenney, M.A.J. Rodgers, *Photochem. Photobiol.* **50**, 277–282 (1989)
52. W. Freyer, H. Stiel, M. Hild, K. Teuchner, D. Leupold, *Photochem. Photobiol.* **66**, 596–604 (1997)
53. D. Dolphin, B.R. James, A.L. Murray, J.R. Thornback, *Can. J. Chem.* **58**, 1125–1132 (1980)
54. M. Scholz, R. Dēdic, T. Breitenbach, J. Hála, *Photochem. Photobiol. Sci.* **12**, 1873–1884 (2013)
55. C. Schweitzer, R. Schmidt, *Chem. Rev.* **103**, 1685–1757 (2003)
56. A.A. Krasnovsky Jr, C.S. Foote, *J. Am. Chem. Soc.* **115**, 6013–6016 (1993)
57. A.A. Goman, I. Hamblett, T.J. Hill, *J. Am. Chem. Soc.* **117**, 10751–10752 (1995)
58. Y. Fu, A.A. Krasnovsky Jr, C.S. Foote, *J. Phys. Chem. A* **101**, 2552–2554 (1997)
59. S.T. Murphy, K. Kondo, C.S. Foote, *J. Am. Chem. Soc.* **121**, 3751–3755 (1999)
60. H. Uoyama, K. Goushi, K. Shizu, H. Nomura, C. Adachi, *Nature* **492**, 234–238 (2012)
61. S. Muralidharan, G. Ferraudi, *J. Phys. Chem.* **87**, 4877–4881 (1983)
62. S. Muralidharan, G. Ferraudi, L.K. Patterson, *Inorg. Chim. Acta* **65**, L235–L236 (1982)
63. Y. Kaneko, Y. Nishimura, N. Takane, T. Arai, H. Sakuragi, N. Kobayashi, D. Matsunaga, C. Pac, K. Tokumaru, *J. Photochem. Photobiol. A* **106**, 177–183 (1997)
64. M.M. Richter, *Chem. Rev.* **104**, 3003–3036 (2004)
65. L. Huab, G. Xu, *Chem. Soc. Rev.* **39**, 3275–3304 (2010)
66. W. Miao, *Chem. Rev.* **108**, 2506–2553 (2008)
67. N.E. Tokel, C.P. Keszthelyi, A.J. Bard, *J. Am. Chem. Soc.* **94**, 4872–4877 (1972)
68. B.L. Wheeler, G. Nagasubramanian, A.J. Bard, L.A. Schechtman, D.R. Dininny, M.E. Kenney, *J. Am. Chem. Soc.* **106**, 7404–7410 (1984)